Synthesis and Self-Assembly of Nucleobase-containing Polymers by RAFT Techniques

Yan Kang

Submitted for the degree of Doctor of Philosophy

Department of Chemistry

February 2015

Table of contents

List of figures

List of schemes

List of tables

Acknowledgements

Firstly, I must thank my supervisor and mentor prof. Rachel K. O'Reilly for not only giving me the great opportunity to study in the group and conduct this project, but more importantly for her invaluable advices, professional supervision and continued support. Without her trust and encouragement, none of this would be possible.

I also want to thank the University of Warwick for offer me the Chancellor International Scholarship, which has funded me for both my study and live.

I am also grateful to all O'Reilly group members, past and present, for their discussion, help, and advices. As an international student, their help and friendship make me feel at home. In particular, I thank Anaïs for carrying out and analyzing SAXS and SANS for me; I thank Anaïs, Daniel, and Marianne for DSC measurements; I also acknowledge Annhelen for analyzing Reactivity Ratio and Rebecca for reading and correcting my thesis; I also thank Mat, Dafni, Joe, Helen, Zan, Craig, Katie, Liang, Annie, Guillaume, Lewis, Alice, Victor, Anne, Robert, Maria, and Sean for their helps.

I thank all the university staff for help. In particular, Dr Ian Portman is thanked for performing Cryo-TEM. I also thank Dr Ana M. Sanchez for high resolution TEM and Dr Neil Wilson for demonstrating AFM.

Finally, I want to thank my parents Mr Zhongjian Kang and Mrs Jinfeng Jia for their support and encouragements. I also thank Yimeng for his encouragements all the time.

Declaration of authorship

This thesis is submitted to the University of Warwick in support of my application for the degree of Doctor of Philosophy. It has been composed by myself and has not been submitted in any previous application for any degree. The work presented (including data generated and data analysis) was carried out by the author except in the cases outlined below:

- The reactivity ratio in Chapter 2 was calculated by Dr Annhelen Lu (University of Warwick), who was using Contour program developed by Dr van Herk (Eindhoven University of Technology);
- The SAXS data throughout the thesis was collected and analyzed by Dr Anaïs Pitto-Barry (University of Warwick). The SANS data was collected by Dr Stephen King (Rutherford Appleton Laboratory, Oxford, UK) and analyzed by Dr Anaïs Pitto-Barry (University of Warwick);
- The high resolution TEM in Chapter 3 was obtained by Dr Ana M. Sanchez (University of Warwick);
- The DSC data in this thesis was collected and analyzed by Dr Anaïs Pitto-Barry, Daniel Wright, and Marianne Rolph (University of Warwick);
- The refractive index increment in Chapter 3 and Chapter 4 was measured by Daniel Wright (University of Warwick);
- The cryo-TEM in Chapter 5 was obtained by Dr Elizabeth Kelley (University of Delaware) and Dr Ian Portman (University of Warwick);
- Elemental analysis was performed by Warwick Analytical Service; HR Mass Spec was analyzed by mass spec group (University of Warwick).

Publications

Effect of complementary nucleobase interactions on the copolymer composition of RAFT copolymerizations, Y. Kang, A. Lu, A. Ellington, M.C. Jewett, R.K. O'Reilly, *ACS Macro Lett.*, 2013, 2, 581-586 (**Chapter 2**).

Exploiting nucleobase-containing materials – from monomers to complex morphologies using RAFT dispersion polymerization, Y. Kang, A. Pitto-Barry, H. Willcock, W-D Quan, N. Kirby, A. M. Sanchez and R. K. O'Reilly, *Polym. Chem.*, 2015, 6, 106-117 (**Chapter 3**).

Summary of thesis

This thesis explores the synthesis of nucleobase-containing polymers by both reversible addition-fragmentation chain transfer (RAFT) polymerization and RAFT dispersion polymerization. In addition, self-assembly behavior of nucleobase-containing polymers is also described.

Chapter 1 introduces main concepts and techniques used in this thesis. In addition, the study of nucleobase-containing materials is reviewed.

Chapter 2 describes the synthesis of nucleobase-containing monomers and the use of RAFT polymerization to prepare nucleobase-containing homopolymers and copolymers. Moreover, the effect of nucleobase-interactions on the resultant copolymer composition was investigated in chloroform and DMF.

Chapter 3 investigates RAFT dispersion polymerization of adenine-containing methacrylate monomer and a 1:1 mixture of adenine-containing and thymine-containing methacrylate monomers in both chloroform and 1,4-dioxane. Nucleobase-containing polymers with relatively good control were obtained and a range of nanostructures were observed that were solvent dependent.

Chapter 4 investigates RAFT dispersion polymerization of a thymine-containing methacrylate monomer, which displayed different self-assembly behavior to the observations in Chapter 3. A range of parameters affecting the resultant morphologies was additionally studied.

Chapter 5 investigates the self-assembly behavior of nucleobase-containing polymers in aqueous solution mainly using a solvent-switch method.

Chapter 6 provides a summary of the key findings of Chapters 2 – 5 and outlines the further work.

Abbreviations

A	5'-acryloyladenosine
A_2	second virial coefficient
AFM	atomic force microscopy
AIBN	azobisisobutylonitrile
AMA	2-(2-(adenine-9-yl)acetoxyl) ethyl methacrylate
ARGET	activators regeneration by electron transfer
ATRP	atom transfer radical polymerization
BCPs	block copolymers
br	broad (^{1}H NMR)
BzMA	benzyl methacrylate
c	concentration
CAC	critical aggregation concentration
CAL435	*Candida antarctica* lipase
$CDCl_3$	deuterated chloroform
$CHCl_3$	chloroform
COSY	correlated spectroscopy
CPDT	2-cyano-2-propyl dodecyl trithiocarbonate
CRP	controlled radical polymerization
cryo-TEM	cryogenic transmission electron microscopy
CTA	chain transfer agent
d	days/doublet

DCM	dichloromethane
DEPT	distortionless enhancement by polarization transfer
D_h	hydrodynamic diameters
DLS	dynamic light scattering
$Đ_M$	dispersity
DMF	dimethylformamide
DMF-d_7	deuterated dimethylformamide
DMSO	dimethyl sulfoxide
DMSO-d_6	deuterated dimethyl sulfoxide
dn/dc	the refractive index increment
DP	degree of polymerization
DSC	differential scanning calorimetry
D_t	translational diffusion coefficient
*e*ATRP	electrochemically mediated ATRP
EDX	energy-dispersive X-ray spectroscopy
EELS	electron energy loss spectroscopy
EGDMA	ethylene glycol dimethacrylate
eq	equivalents
EWR	exit wave reconstruction
f_1	initial mole fraction of monomer 1
F_1	mole fraction of monomer 1 in the copolymer
GO	graphene oxide

HAADF	the high angle annular dark field
HEMA	2-hydroxyethyl methacrylate
HMBC	heteronuclear multiple-bond correlation
HMQC	heteronuclear multiple-quantum coherence
HPMA	2-hydroxypropyl methacrylate
HR-MS	high resolution mass spectrometry
$I(q)$	scattering intensity
J	coupling constant
K_B	Boltzmann's constant
k_p	propagation rate constant
LCST	lower critical solution temperature
LUMO	lowest unoccupied molecular orbital
m	multiple
m/z	mass-to-charge ratio
macro-CTA	macromolecular chain transfer agent
MADIX	macromolecular design *via* the interchange of xanthates
MMA	methyl methacrylate
M_n	number average molecular weight
M_w	weight average molecular weight
n	refractive index
N_{agg}	aggregation number
NLLS	non-linear least squares

NMP	nitroxide-mediated radical polymerization/*N*-methyl-2-pyrrolidone
NMR	nuclear magnetic resonance
p	packing parameter
P4VP	poly(4-vinylpyridine)
PA	poly(5'-acryloyladenosine)
PAA	poly(acrylic acid)
PAMA	poly(2-(2-(adenine-9-yl)acetoxyl) ethyl methacrylate)
PBMA	poly(*n*-buty methacrylate)
PD	polydispersity
PEG	poly(ethylene glycol)
PEO	poly(ethylene oxide)
PFS	poly(ferrocenyldimethylsilane)
PGMA	poly(glycerol monomethacrylate)
PISA	polymerization-induced self-assembly
PITSA	polymerization-induced thermal self-assembly
PLA	polylactide
PLMA	poly(lauryl methacrylate)
PMMA	poly(methyl methacrylate)
PMPC	poly(2-(methacryloyloxy) ethylphosphorylcholine)
PNIPAm	poly(N-isopropylacrylamide)
POEGMA	poly(oligo(ethylene glycol) methyl ether methacrylate)

PS	poly(styrene)
PTMA	poly(2-(2-(thymin-1-yl)acetoxyl) ethyl methacrylate)
PU	poly(5'-acryloyuridine)
PVBT	poly(vinylbenzylthymine)
q	quartet
q	scattering vector
r	reactivity ratio
r.t.	room temperature
RAFT	reversible addition-fragmentation chain transfer
R_g	radius of gyration
R_H	hydrodynamic radius
RI	refractive index
ROMP	ring-opening metathesis polymerization
R_θ	Rayleigh ratio
SANS	small angle neutron scattering
SARA	supplemental activator and reducing agent
SAXS	small angle x-ray scattering
SCVs	spaced concentric vesicles
SEC	size exclusion chromatography
SEM	scanning electron microscopy
SET-LRP	Single-electron transfer living radical polymerization
SLD	scattering length density

SLS	static light scattering
STEM	scanning transmission electron microscopy
T	absolute temperature
t	triplet
TBAI	tetrabutylammonium iodide
TEA	triethylamine
TEM	transmission electron microscopy
TEMPO	2,2,6,6-tetramethyl-1-piperidinoxyl
T_g	glass transition temperature
THF	tetrahydrofuran
TMA	2-(2-(thymin-1-yl)acetoxyl) ethyl methacrylate
TMS	tetramethylsilane
U	5'-acryloyluridine
UV	ultraviolet
UV-vis	ultraviolet-visible
VBA	vinylbenzyladenine
w	weight fraction
δ	chemical shift
η	viscosity of solvent
θ	angle
λ	wavelength
ρ-ratio	R_g/R_H

Chapter 1. Introduction

1.1 Polymerization techniques

1.1.1 Controlled radical polymerizations

The synthesis of polymers, especially the polymerization of vinyl monomers, has benefited significantly from the development of controlled radical polymerizations (CRP). Compared to other living techniques,[1] such as living ionic polymerizations, CRP allows similar control of polymer structures, yet avoids extremely demanding experimental conditions and poor functional group tolerance. To this end, CRP has been readily applied towards synthesizing a wide range of vinyl polymers with well-defined structures and control over molecular weight, molecular weight distributions, chain architectures and compositions, which are not attainable by conventional free radical polymerizations.

Typically, a radical polymerization includes three main processes: initiation, propagation, and termination (Scheme 1.1).[2] Firstly, initiation is the generation of a reactive radical which then reacts with vinyl monomer. Secondly, propagation is the growth of polymer chains by addition of monomers to the chain end radical. The last step is termination by a combination of coupling and disproportionation of two chain end radicals to produce inactive polymers. Moreover, chain transfer reactions are always present, which can transfer the active radical between polymer chains or another species within the polymerization system. In a typical free radical polymerization, the propagating radicals are very short lived and tend to terminate readily as the termination rate constants are much greater than the propagation rate constant.[2,3] In addition, initiation is usually slower than propagation, which suggests that as the polymerization proceeds, some chains have grown significantly while others are still initiating.[2] Moreover, chain transfer reactions can also hinder control by moving radicals between or even within polymer chains. These are the kinetic

reasons that conventional free radical polymerization leads to ill-defined polymers with uncontrolled molecular weights, broad molecular weight distributions, and uncontrolled structures. Additionally, it is not attainable to make block copolymers using conventional radical polymerizations due to the absence of active chain ends on the final polymer. Based on these general considerations, CRP which can minimize irreversible bimolecular termination and prolong the lifetime of active sites was developed to prepare controlled polymers.

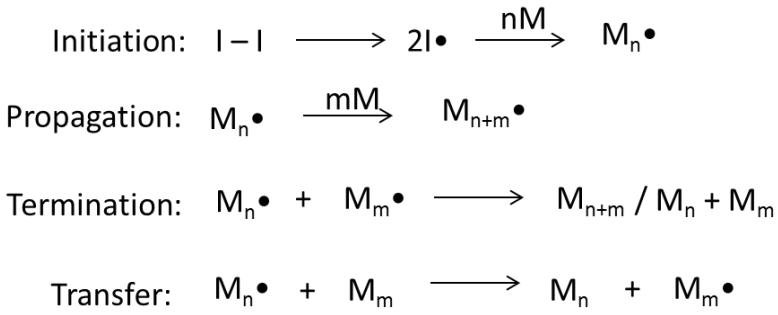

Scheme 1.1 A schematic representation of the steps of initiation, propagation, termination and transfer. I is the initiator and M is the monomer.[2]

The concept of CRP was originally introduced by Otsu in the 1980s through his investigation of iniferters.[4,5] The term *iniferters* is used to describe compounds that could *ini*tiate, trans*fer*, and *ter*minate a radical polymerization. To date, the major techniques of CRP are nitroxide-mediated polymerization (NMP),[6] atom transfer radical polymerization (ATRP),[7-10] single-electron transfer living radical polymerization (SET-LRP),[11,12] reversible addition-fragmentation chain transfer (RAFT) polymerization,[13,14] and macromolecular design *via* the interchange of xanthates (MADIX).[15,16] As ATRP and SET-LRP are both metal mediated polymerizations yet with different mechanism, they will be introduced together. In addition, RAFT polymerization and MADIX follow the same mechanism and differ only by the polymerization mediator and thus discussion on these two techniques will be combined in this Chapter.

1.1.1.1 Nitroxide-mediated polymerization

In NMP there is an equilibrium between dormant polymer chains and active radical chain ends, where nitroxide is used as the mediating or persistent radical (Scheme 1.2). As this equilibrium lies in favor of dormant species, the concentration of propagating radicals should be low and termination therefore can be minimized (Scheme 1.2).[6,17] Cyclic nitroxide radicals such as 2,2,6,6-tetramethyl-1-piperidinoxyl (TEMPO) have been widely studied.[3,6] By using NMP with TEMPO, styrene and 4-vinylpyridine can be polymerized with good control over molecular weight and molecular weight distribution. However, NMP with TEMPO generally needs high temperatures (125 – 145 °C) and long reaction times and moreover is only applicable to limited monomers (mainly styrenic).[3]

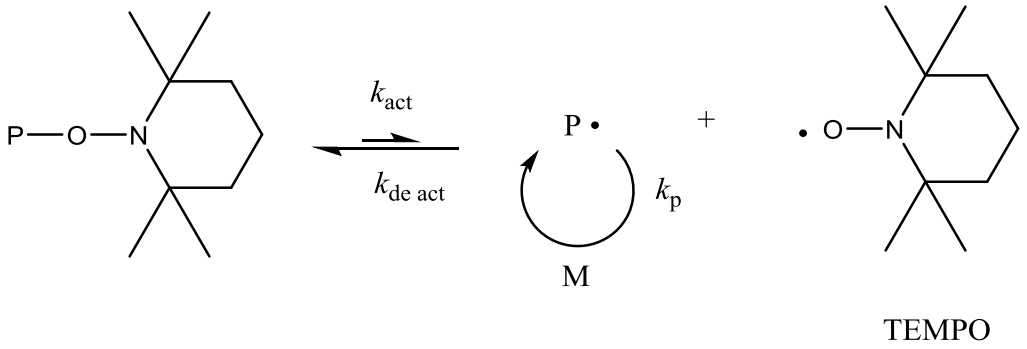

Scheme 1.2 Accepted mechanism of NMP using TEMPO.[18,19]

Many NMP initiators were designed to improve the feasibility and versatility of NMP. For example, *t*-butyl 2-methyl-1-phenylpropyl nitroxide (**a**) and *t*-butyl 1-diethylphosphono-2,2-dimethylpropyl nitroxide (**b**) can lead to faster but still controlled polymerizations (Scheme 1.3).[3,20,21] In addition, these nitroxides allow NMP to be performed at lower temperatures and expand NMP to a variety of monomers beyond styrenes to include acrylates, acrylamides, 1,3-dienes, and acrylonitriles. NMP used to be very challenging in the polymerization of

methacrylates,[3,22] however, recent work demonstrates the successful polymerization of methacrylates.[19,23,24]

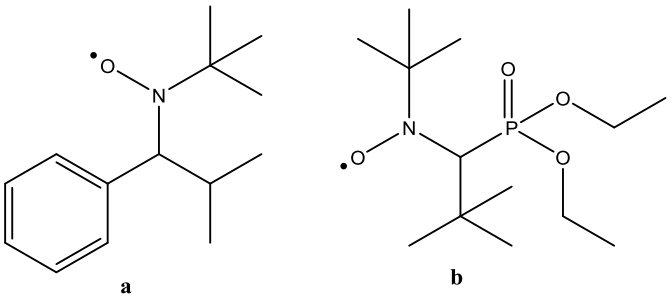

Scheme 1.3 Chemical structures of NMP nitroxides.[3]

1.1.1.2 Atom transfer radical polymerization

ATRP was firstly reported by Sawamoto[8] and Matyjaszewski[9] simultaneously in 1995. Radical generation in ATRP involves an organic halide undergoing a reversible redox process which is catalyzed by a transition metal compound. A well-accepted mechanism for Cu(I)-mediated ATRP is shown in Scheme 1.4.[25,26] The dormant species, the organic halide, is activated by a Cu(I) complex to form an active radical chain end that propagates and a Cu(II) complex. This process is reversible, therefore the active radical chain end can be deactivated, transforming it into a halide capped dormant species. As this equilibrium lies in favor of the dormant species (left), the amount of radicals should be low and thus termination of living polymers can be minimized. In addition, a successful ATRP needs fast and quantitative initiation so that all propagating species can begin propagating at the same time which yields polymers with narrow molecular weight distributions.[3]

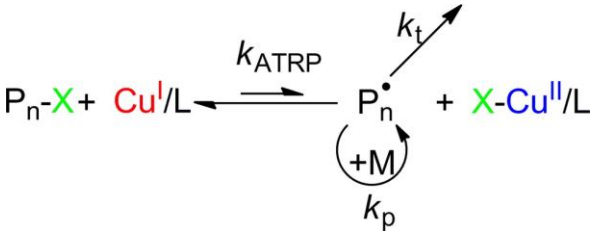

Scheme 1.4 Mechanism for ATRP (P_n is polymer chain; X is halide; L is ligand; M is monomer).[25,26]

ATRP is a robust technique which is applicable to a range of monomers and is tolerant of many functional groups. In addition, the experimental conditions and operations are not strict. However, the main drawback of ATRP is the use of relatively large amounts of Cu(I) activator which requires removal after the polymerization. Therefore, several variants of the ATRP system have been developed, such as activators regenerated by electron transfer (ARGET) ATRP,[27] electrochemically mediated ATRP (*e*ATRP),[28] and supplemental activator and reducing agent (SARA) ATRP,[29] which can reduce the amount of copper used to ppm levels.

SET-LRP is also a copper-mediated living polymerization, which employs Cu(0) as the activator and then utilizes the disproportionation reaction of *in situ* formed Cu(I) to generate 'nascent' Cu(0) and Cu(II). The mechanism of SET-LRP is shown in Scheme 1.5, which has been extensively studied by Percec *et al.*[11,30-32] However, it should be noted there is still a debate on the mechanism of SET-LRP in comparison to supplemental activator and reducing agent (SARA) ATRP.[33] Furthermore, the SET-LRP method has somewhat limited monomer versatility, and is well adapted for acrylate[11] and acrylamide[34] monomers.

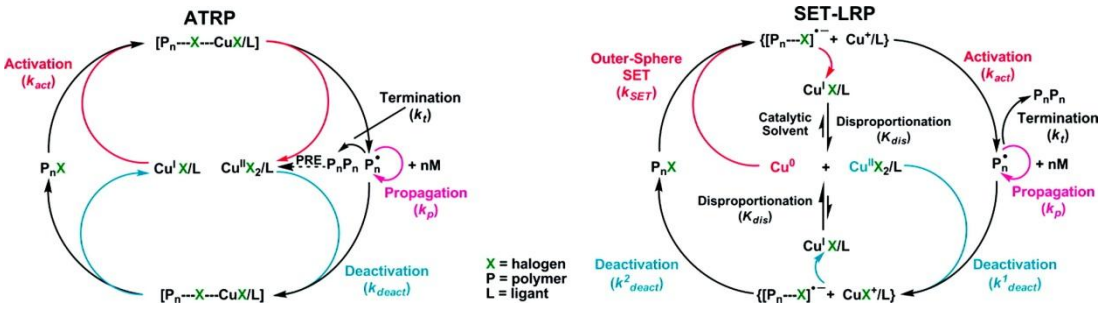

Scheme 1.5 Comparison of ATRP (left) and SET-LRP (right) mechanisms.[11,30]

1.1.1.3 Reversible addition-fragmentation chain transfer polymerization

RAFT polymerization was firstly reported and named in 1998 by Moad, Rizzardo, and Thang *et al.* in Australia.[13] A few months prior, a similar process called MADIX

was reported in France,[35] but MADIX is limited to the use of xanthates as chain transfer agents (CTA) and thus RAFT is still the most widely used term. The mechanism of RAFT polymerization differs from ATRP and NMP, where in RAFT polymerization control is not attained by equilibrium between a dormant species and its corresponding active radical chain end, but achieved by an equilibrium between polymer chains led by a reversible transfer reaction using a thiocarbonyl-thio as the CTA, which gives all polymer chains equal opportunities to grow and thus achieve a controlled system. A general mechanism of RAFT polymerization is shown in Scheme 1.6, which consists of the steps of free radical polymerization (initiation, propagation, and termination steps) and extra steps (chain transfer and equilibration steps).[14] More specifically, radical initiators decompose and then react with monomers to form radical polymer species (P_n•). This growing chain adds to the reactive C=S bond of the CTA (**1**) to generate a radical intermediate (**2**). This intermediate can undergo a reversible fragmentation reaction either toward starting species (P_n• and **1**) or to release the R group from the CTA (R•) and a macro-CTA (**3**). The R group then re-initiates and reacts with monomers to form a new growing chain (P_m•). Once all the initial CTA has been consumed, macro-CTA is only present in the reaction medium which enters the main equilibrium. This equilibrium is very important in the RAFT polymerization process and by a process of rapid exchange between active radical chain ends and dormant ends (thiocarbonyl-thio capped) all polymer chains have equal probability to grow which ensures the production of polymers with narrow molecular weight distributions. It should be noted that the intermediates (**2** and **4**) may be involved in a variety of side reactions during polymerization such as termination with growing polymer chains. The final step is termination by either combination or disproportionation which is minimized in

RAFT polymerization due to the presence of a CTA with high transfer efficiency, high ratio of CTA to initiator and the low concentration of radical initiator used.

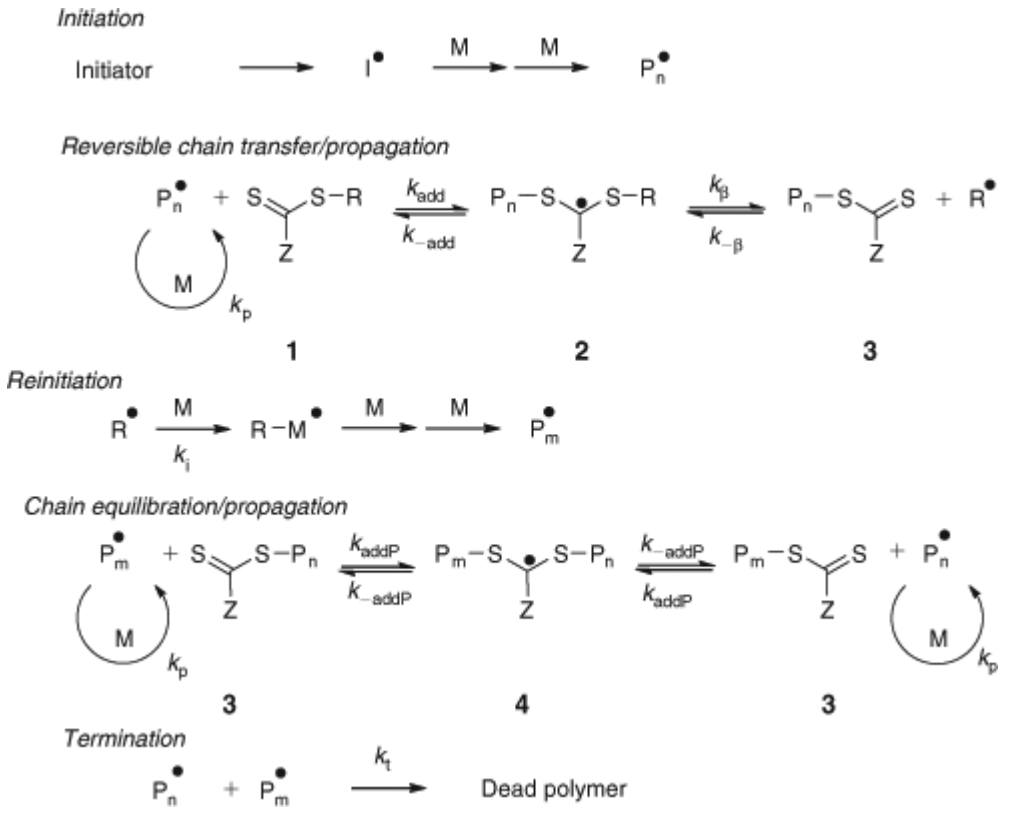

Scheme 1.6 Proposed general mechanism of RAFT/MADIX polymerization.[14]

In addition, there are some remarks drawn from the mechanism of RAFT polymerization:

(1) The amount of initiator should be low; otherwise it will increase the probability of chain termination (dead chains) and lead to broad molecular weight distributions.

(2) As termination is minimized, the majority of polymers consist of the re-initiating R group at one end and a thiocarbonyl-thio group at the other end.

(3) The molecular weight increases linearly with conversion and the theoretical molecular weight can be estimated by using Equation 1.1, where $M_{n,th}$ is the theoretical number-average molecular weight; [monomer]/[CTA] is the mole ratio between monomer and CTA; FW(M) is the molecular weight of monomer; c is the conversion; FW(CTA) is the molecular weight of CTA.

$$M_{n,th} = \frac{[Monomer]}{[CTA]} \times FW(M) \times c + FW(CTA) \qquad \text{Equation 1.1}^{36}$$

The choice of CTA is very important in RAFT as it has a significant effect on the polymerization kinetics and control. The common structure of a CTA is shown in Scheme 1.6 (**1**), where the identity of *Z* and *R* groups both affect the efficiency of the CTA.[14,36]

The Z group affects the activity of the C=S bond and stability of the radical intermediates. In other words, the Z group should be able to aid radical formation and stabilize the intermediate, however, the stability should be modest to favor its fragmentation which can free the reinitiating group R. Rankings for the Z group for a CTA are listed in Figure 1.1, where from left to right the addition rate decreases and fragmentation rate increases.

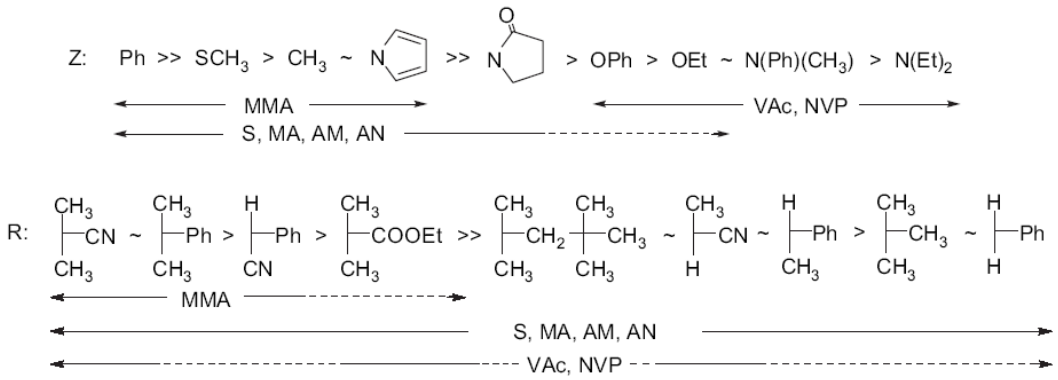

Figure 1.1 Guidelines for selection of RAFT agents for various polymerizations. For Z, addition rate decreases and fragmentation rates increases from left to right. For R, fragmentation rates decrease from left to right.[37]

The R group should be a good leaving group and also governs the re-initiation steps. It also contributes to stabilize the intermediates although is less important compared to the Z group. Rankings for R groups for a CTA are shown in Figure 1.1, where from left to right the fragmentation rates decrease.

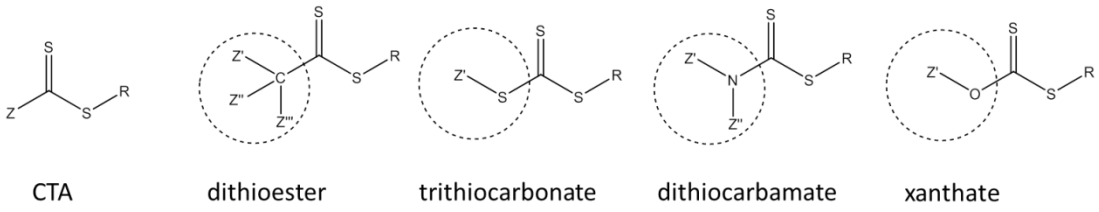

Figure 1.2 Types of RAFT chain transfer agent (CTA).[36]

By varying and combining different R and Z groups, a variety of CTAs can be synthesized. There are four types of CTA based on the identity of the Z group which are commonly used: dithioesters, trithiocarbonates, dithiocarbamates, and xanthates (Figure 1.2).[36] These CTAs can all be readily synthesized and more importantly have different properties, such as different transfer constants and tolerance towards functionalities, which make them suitable to mediate the polymerizations of different types of monomers. For monomers that form comparatively stable propagating radicals or possess high propagation rate constant, such as methacrylate, styrene, methacrylamide, acrylate, and acrylamide, dithioesters or trithiocarbonates are favored to prevent termination and broad distributions, as they possess high transfer constants.[37] In comparison, xanthates and dithiocarbamates are suitable for polymerization of monomers, such as *N*-vinyl pyrrolidone (NVP), vinyl acetate (VAc), and related vinyl monomers, where propagating radicals are poor homolytic leaving groups.[37] The lone pair of nitrogen or oxygen in the structure of dithiocarbamate and xanthate respectively is delocalized with the C=S bond, which results in their low reactivity and low transfer constants. Moreover, electron-withdrawing substituents on Z group can enhance the activity of dithiocarbamate and xanthate as delocalization between lone pair and C=S bond would be weakened.[36,37]

Among the controlled radical polymerization techniques, RAFT polymerization appears to be one of the most versatile processes in terms of the mild reaction conditions, the variety of monomers that can be polymerized and the feasibility for

the incorporation of various functionalities. The main disadvantages of RAFT polymerization are the use of toxic and odorous starting materials such as carbon disulfide and thiol-containing alkyls to make CTAs and the presence of RAFT polymerization end groups in the polymers that lead to colored polymers. The first drawback is hard to avoid although synthetic improvements have been achieved.[38] The second disadvantage can be solved as the CTA end groups are easy to remove or transform into other functionalities.[39,40] Given the advantages of RAFT polymerization and few reports on preparation of nucleobase-containing polymers by RAFT technique, in our work, RAFT polymerization was therefore investigated and used for the preparation of nucleobase-containing polymers.

1.1.2 Heterogeneous and dispersion polymerization

Heterogeneous polymerization reaction mixtures consist of two immiscible phases and are commonly used to prepare well-defined particles. There are four main types of heterogeneous polymerizations: precipitation, suspension, emulsion and dispersion.[41] These polymerizations are usually classified according to the solubility of the monomers, resulting polymers and initiators. Precipitation polymerizations begin as homogeneous polymerizations where both monomers and initiators are soluble in the reaction mixture, but convert to heterogeneous polymerizations as the polymerization progresses, as the resultant polymer is insoluble in the reaction medium. Polymerization proceeds after precipitation by absorption of monomers into the polymer precipitate. In addition, the final polymers are obtained in a powder or granular form.[3] In comparison, in suspension polymerizations both the monomers and initiators are insoluble in the reaction media but are stabilized by the presence of suspension stabilizers. Moreover, initiation and polymerization are performed within the droplets of monomer to produce insoluble polymers in the form of polymer

particles.[3,41,42] In emulsion polymerizations, the initiators are soluble, but monomers and resultant polymers are insoluble in the media which are stabilized by surfactants. The initiation of emulsion polymerizations occurs in the continuous medium and polymerization take place in the micelles formed by surfactants rather than monomer droplets. As polymerization proceeds, the micelles grow by addition of monomer from the continuous media which is replenished by dissolution of monomers from monomer droplets.[3,43] Polymer particles are obtained as a result of emulsion polymerization.[41,44]

Dispersion polymerizations are similar to precipitation polymerizations, which also start as homogeneous polymerizations with soluble monomers and initiators. However, in dispersion polymerizations the resultant insoluble polymers/growing chains are stabilized by additive stabilizers which are not present in precipitation polymerizations.[45] Dispersion polymerizations initiate in solution and the initial polymers remain in the solution until they reach a critical molecular weight. At that critical point, polymers begin to coagulate to form unstable particles, which further coagulate to form stabilized particles surrounded by stabilizers to avoid precipitation. Polymerization further proceeds in the stabilized polymer particles which absorb monomers from the continuous phase (Figure 1.3).[3,46] By taking advantage of dispersion polymerizations, particles with a range of morphologies can be achieved which will be discussed in Section 1.4.[47,48]

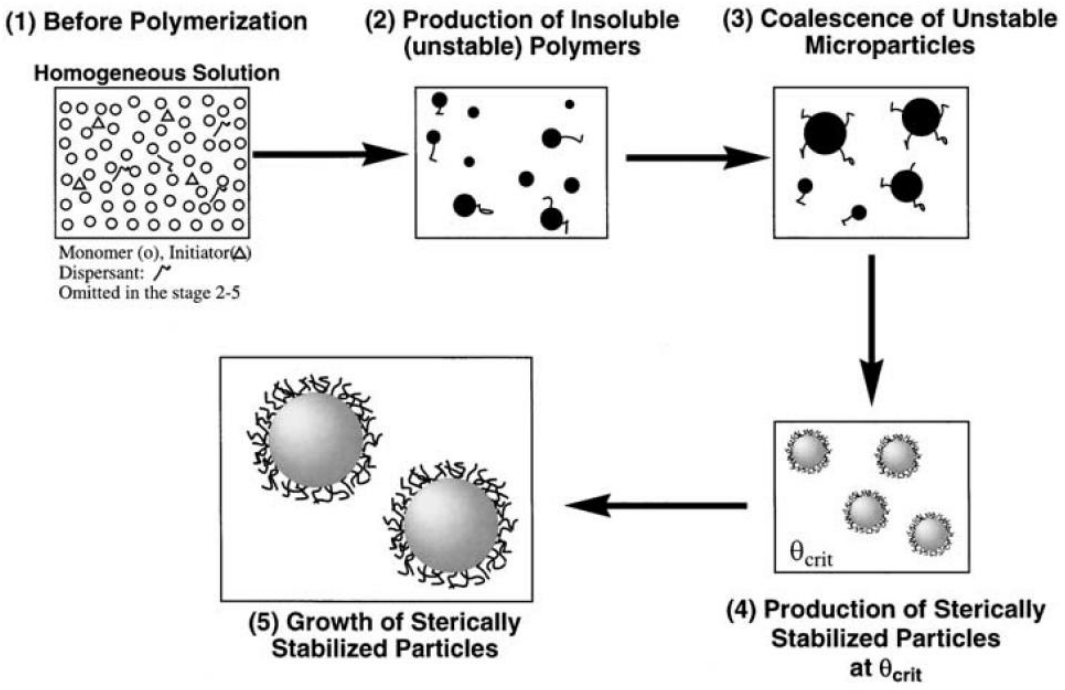

Figure 1.3 A representation of synthetic processes for dispersion polymerization.[46]

1.2 Copolymer composition of chain-growth polymerization

Chain-growth polymerizations can be carried out using only one monomer or mixtures of two or more monomers: the former produces homopolymers and the latter can generate copolymers. In a copolymerization, the overall amount of each monomer entering into the final copolymer is determined by their relative concentration and active species reactivity. However, it is found even if starting from the same monomer concentration, the composition of a copolymer cannot be simply determined by the homopolymerization rates of each monomer. Actually, different monomers have different tendencies towards copolymerization, which has been defined as the reactivity ratio (r_1 or r_2) of the monomer pairs (monomer 1 and 2, M_1 and M_2), reflecting the tendencies of an active species such as a radical to react with its own monomer relative to the comonomer (Scheme 1.7).[3] If $r_1 > 1$, then homopolymerization growth is preferred as the addition of the monomer 1 to the active chain end is preferred over addition of monomer 2. If $r_1 = 0$, then only reaction

with monomer 2 will occur. If $0 < r_1 < 1$, it means that cross-propagation is favored over self-propagation.[3]

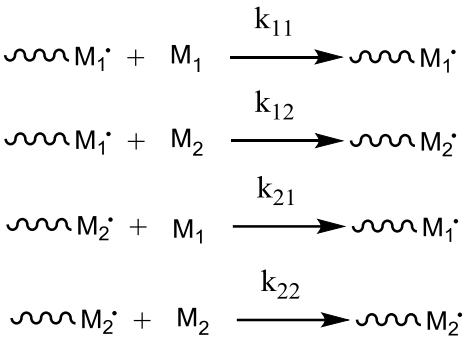

$r_1 = k_{11}/k_{12}$ $\quad$ $r_2 = k_{22}/k_{21}$

Scheme 1.7 The definition of reactivity ratios, r_1 and r_2, where k_{11} is the rate constant for a propagating chain ending in M_1 adding to monomer M_1, k_{12} that for a propagating chain ending in M_1 adding to monomer M_2, and so on.[3]

Different types of copolymerization behavior are observed depending on the values of reactivity ratios of monomers:[3]

(1) If $r_1 = r_2 >> 1$, this means the two monomers have no inclination to react with each other, leading to a mixture of two homopolymers;

(2) If $r_1 \times r_2 > 1$ with both reactivity ratios larger than 1, this indicates that both monomers prefer to react with themselves which gives rise to block copolymers;

(3) If $r_1 \times r_2 = 1$, the copolymerization is termed an ideal copolymerization where the two types of propagating species have the same preference for the same monomer relative to the other monomer and thus one monomer is more reactive than the other one towards both propagating species. One exception in this condition is that if $r_1 = r_2 = 1$, then monomer 1 will react with itself as fast as monomer 2 which results in random copolymers;

(4) If $r_1 \times r_2 = 0$ with neither reactivity ratio greater than 1, then alternating copolymerization occurs with two types of alternating behavior: extreme and

moderate alternating. For extreme alternating copolymerization, both r_1 and r_2 should be 0, which means one propagating species can only add the other monomer. Moderate alternating copolymerization occurs for two situations: (a) $r_1 \times r_2 \approx 0$ with both reactivity ratios around 0, which indicates that neither monomer wants to react *via* self-propagation and thus the resultant copolymer has an alternating composition. (b) $r_1 \times r_2 = 0$ where one ratio is 0 and the other is small, which indicates that one monomer cannot self-propagate while the other monomer prefers to cross-propagate.

Based on Equations 1.2 and 1.3 (the interpretation of these equations is introduced by Odian[3]), where f_1 is the feed ratio of monomer 1, M_1; F_1 is the mol fraction of M_1 in the copolymer; $[M_1]$ and $[M_2]$ are the concentrations of M_1 and M_2; $d[M_1]$ and $d[M_2]$ are the changes in concentration of M_1 and M_2, monomer reactivity ratios can be evaluated by experimental determination of the copolymer composition (F) for several different monomer compositions in the monomer feed (f). However, it should be noted that the conversions of copolymerizations should be kept as low as possible (< 10%) to minimize the error, as copolymer composition can change with increasing conversion. The copolymer composition can be determined by either directly analyzing the copolymer or indirectly by analyzing the change in monomer concentration. The values of r can be calculated manually by using either the Mayo and Lewis method[49] or the Fineman and Ross method.[50] More accurate results can be given by the Contour program developed by van Herk, which is based on a nonlinear least square method.[51] Values of reactivity ratios and plots of 95% joint confidence intervals can be given by this program directly.[52]

$$f_1 = 1 - f_2 = \frac{[M_1]}{[M_1] + [M_2]}$$ Equation 1.2

$$F_1 = 1 - F_2 = \frac{d[M_1]}{d[M_1] + d[M_2]} = \frac{r_1 f_1^2 + f_1 f_2}{r_1 f_1^2 + 2 f_1 f_2 + r_2 f_2^2}$$ Equation 1.3

By evaluating monomer reactivity ratios, information on polymer composition and even sequence can be obtained, which helps to understand and utilize the polymers' properties. Chain-growth polymerizations such as ionic or radical copolymerization are generally statistical processes leading to random structures.[53] However, in some particular cases, sequence can be controlled through manipulation of the reactivity of monomers with active chain ends. For example, the copolymerization of styrene and maleic anhydride or *N*-substituted maleimides is one of the most fascinating examples of monomer pairs. In this copolymerization system, cross-propagation between monomers is extremely favored. Thus, the copolymerization of these monomer pairs leads to alternating copolymers. Lutz's group have reported utilization of these reactivity ratios to allow for the preparation of sequence-defined copolymers by controlled sequential addition of various functional *N*-substituted maleimides into the bulk polymerization of styrene (Figure 1.4).[54] These well-defined copolymers were synthesized by ATRP of styrene with the addition of discrete amounts of *N*-substituted maleimide at precise polymerization times. Indeed, in further work this group were able to modify the system so that the polystyrene chains containing reactive alkyne functionalities could be reacted in a post-polymerization fashion with pendent azide groups, which was from the maleimide units, to form different types of covalently folded polymer chains.[55]

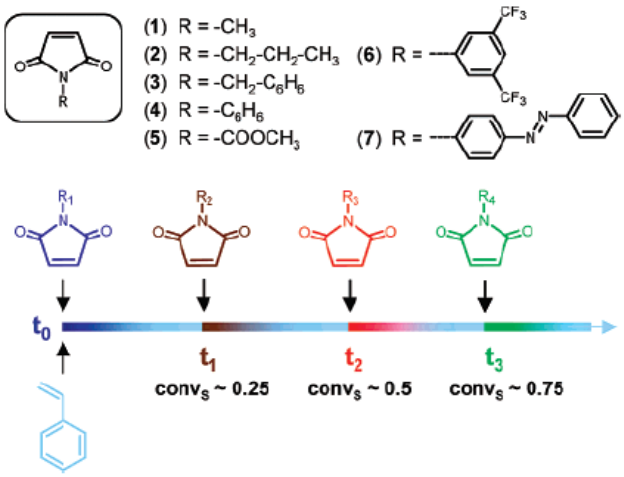

Figure 1.4 Concept of sequential atom transfer radical copolymerization of styrene and various *N*-substituted maleimides.[54]

1.3 Solution self-assembly of block copolymers

Solution self-assembly of amphiphilic block copolymers (BCPs) has attracted significant attention over the past decade as the resulting nanostructures have potential use in a variety of fields such as cosmetics, drug delivery, catalysis, separation, etc.[56,57] Similar to self-assembly of amphiphilic small-molecules, different aggregate morphologies can be achieved by self-assembly of amphiphilic BCPs, including spheres, cylinders, bicontinuous structures, lamellae and vesicles.[58] However, compared to the self-assembly of small-molecules, polymeric aggregates exhibit higher stability owing to their improved mechanical and physical properties.[57] Furthermore, the development of living polymerizations such as controlled radical polymerizations allows access to the preparation of polymers with various compositions and architectures, which contributes to the extensive study of the self-assembly of BCPs.[59]

Various morphologies can be seen through the self-assembly of BCPs. For example, Eisenberg and coworkers have shown the formation of a wide range of morphologies by self-assembly of a series of BCPs of poly(styrene)-*b*-poly(acrylic acid) (PS-*b*-PAA) (Figure 1.5).[57] In this example, the hydrophilic PAA block stabilizes the aggregates in

solution, behaving as the corona/shell of the structures. The hydrophobic PS block is hidden in the core of the structures to avoid energetically unfavorable hydrophobe-water interactions and thus lowers the total free energy of system. There are many factors affecting the formation of aggregates, such as copolymer composition, preparation methods or conditions and the nature of the polymers, which makes it difficult to predict the resultant morphologies. However, there are still a few general rules or considerations which help to predict the morphologies and understand their formation.

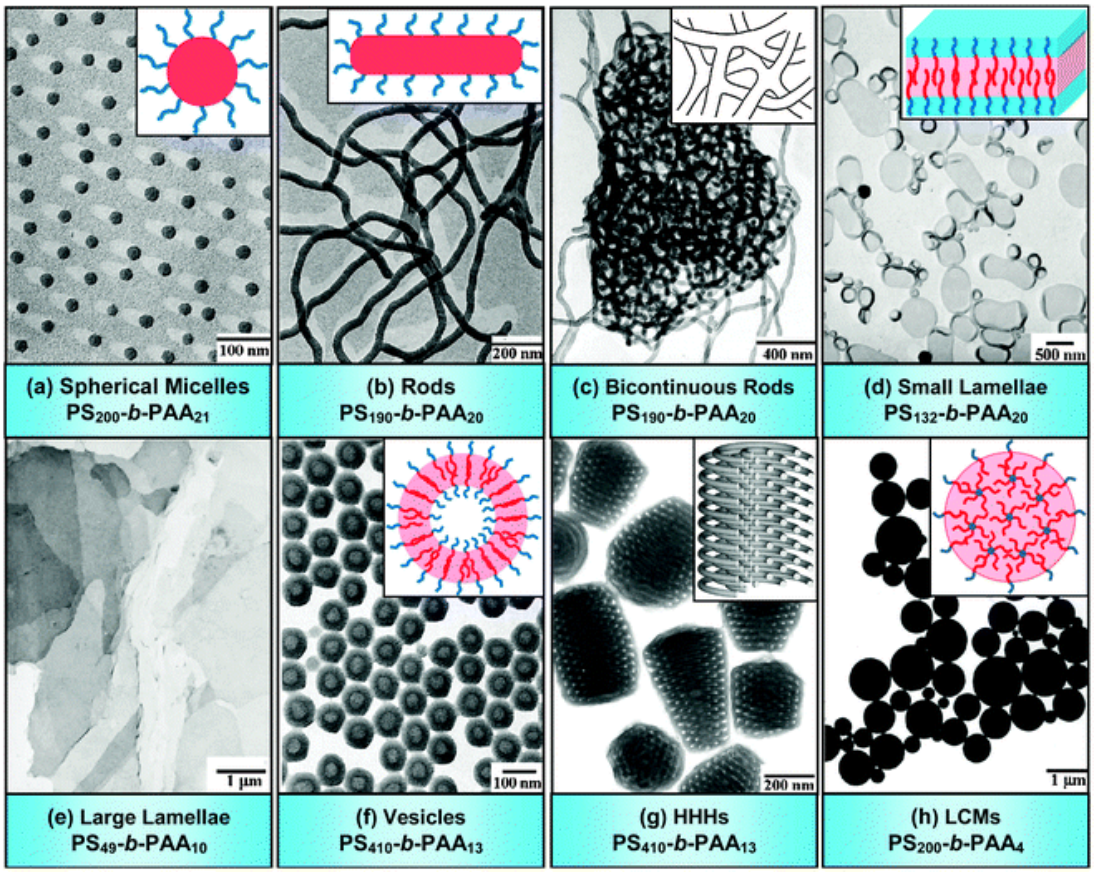

Figure 1.5 Transmission electron microscopy (TEM) micrographs and corresponding schematic diagrams of various morphologies formed from amphiphilic PS_m-*b*-PAA_n copolymers (note: m and n denote the degree of polymerization of PS and PAA, respectively). In the schematic diagrams, red represents hydrophobic PS parts, while blue denotes hydrophilic PAA segments. HHHs: hexagonally packed hollow hoops; LCMs: large compound micelles, in which inverse micelles consist of a PAA core surrounded by PS coronal chains.[57]

The different morphologies primarily result from the inherent curvature of the copolymer, which influences the packing of copolymer chains and can be defined by the packing parameter '*p*'.[60,61] In the equation for the packing parameter (Figure 1.6),

v is volume of the hydrophobic chain, a_o is the optimal area of the head group, and l_c is the length of hydrophobic tail. As a general rule, if $p \leq ⅓$, spherical micelles are most likely formed. If $⅓ \leq p \leq ½$, cylindrical micelles are favored. When $½ \leq p \leq 1$, vesicles (also named polymersomes) tend to form.[60] This serves as a useful guide, and it should be noted that any factors affecting v, a_o, and l_c will also have an effect on the resultant morphologies.

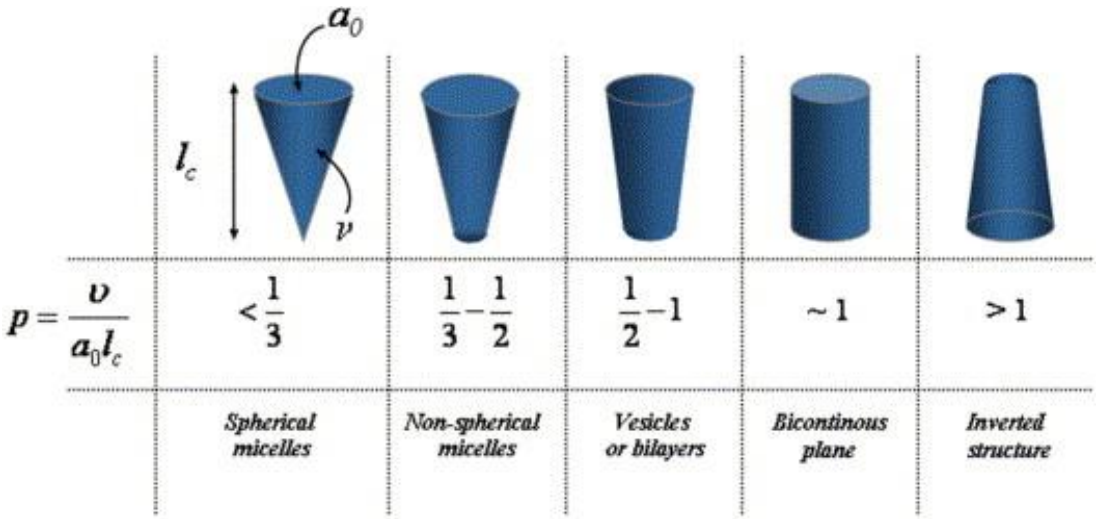

Figure 1.6 Relationship between polymer curvature, packing parameter, and expected morphologies of self-assembly.[61]

Many factors can influence the resultant morphologies, which can be divided into two main aspects according to their apparent sources: extraneous factors and the nature of the polymers. Major extraneous factors can be self-assembly method (*e.g.*, direct dissolution, solvent switch, thin-film hydration), polymer concentration, the nature and amount of common solvent, the amount and nature of selective solvent, temperature, presence of additives (ions, homopolymers), and so on.[56,57] In turn, these factors can affect polymer curvature in solution, polymer solubility, polymer interactions, mobility of polymer chains, the thermodynamics and kinetics of the formation of aggregates etc, which result in the formation of a wide range of morphologies. For instance, the nature of the common solvent plays a key role in the resultant morphologies.[62-64] Eisenberg and coworkers have shown that for self-

assembly of BCP PS_{200}-*b*-PAA_{18} spherical aggregates were formed when DMF was used as the common solvent, while large compound micelles were observed with THF as the common solvent.[63] The reason for this observation is that the nature of common solvent (solubility parameter) can affect polymer-solvent interactions and further change relative coil dimensions of both core and corona chains, which influence resultant morphologies in the same way as the packing parameter.[56,63] Similar observations were also seen by Holder and Sommerdijk, where by self-assembling poly(ethylene oxide)$_{52}$-*b*-poly(*n*-butyl methacrylate)$_{86}$ (PEO_{52}-*b*-$PBMA_{86}$), bicontinuous nanospheres were observed when using THF as a common solvent while multilamellar vesicles were obtained when 1,4-dioxane was employed (Figure 1.7).[64] This observation is also considered due to the different solubility parameter affecting the polymer curvatures.

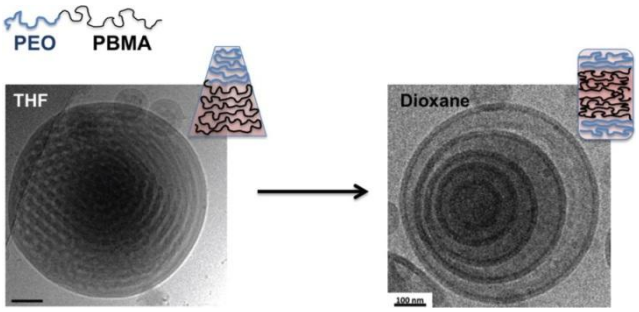

Figure 1.7 Cryo-TEM images of aggregates of PEO_{52}-*b*-$PBMA_{86}$ formed from THF-water mixes or dioxane-water mixes and a representation of the difference in the unimer segment in THF and dioxane.[64]

The nature of the polymer can also affect the resultant morphologies. Major factors include copolymer composition,[57,65-67] the presence of specific interactions between polymers (*e.g.*, hydrogen bonding,[68] π-π stacking[69]), thermal properties of polymers (*e.g.*, glass transition temperature (T_g)[70] and crystallinity[71,72]), and polydispersities.[73,74] For example, by taking advantage of the crystalline nature of a core forming polymer block, cylindrical micelles can be formed from polymers with a large hydrophilic block compared to the hydrophobic block, which would normally

form spherical micelles based on the packing parameter. Manners and coworkers demonstrated this with semicrystalline poly(ferrocenyldimethylsilane) (PFS),[72,75] while O'Reilly and Dove have investigated semicrystalline polylactide (PLA).[71,76] Additional morphologies such as bicontinuous nanospheres can also be obtained by the self-assembly of semicrystalline polymers. Holder, Sommerdijk and their coworkers reported that bicontinuous internal structures were formed from semicrystalline amphiphilic block copolymer PEO_{39}-*b*-poly(octadecyl methacrylate)$_{17}$ at 4 °C which was below the melting and crystallization point of the crystalline block.[77] In addition, these bicontinuous structures transitioned to planar oblate spheroids at elevated temperature (45 °C) as the crystallization was disturbed.[77] This could be further used for thermoresponsive controlled release.[78] The presence of specific interactions between polymers can also affect the resultant morphologies, for example, the presence of hydrogen bonding interactions. Hedrick and coworkers showed that spheres were formed from self-assembly of block copolymer PEO_{114}-*b*-poly(*L*-lactide)$_{32}$ (PLLA).[68] However, by incorporating rigid small-molecule hydrogen-bonding components at the block junction (urea-benzamide or thiourea-benzamide motifs), nanotubes were attained for polymers with the same block lengths. Additional examples show that specific interactions provided by nucleobases[79] or peptides[80,81] can affect the self-assembly structure. As the main topic of this thesis, the self-assembly of nucleobase-containing polymers will be reviewed separately in Section 1.6.

Self-assembly of BCPs is one of the important parts of this thesis. The above introduction on solution self-assembly of BCPs provides the basic knowledge of this area and moreover helps us to understand some phenomenon observed in this study.

1.4 Polymerization-induced self-assembly

Solution self-assembly of BCPs is generally prepared by post-polymerization methods, including direct dissolution, solvent switch, and thin-film hydration, where polymers are first prepared and then self-assembled by a second process. These methods are robust and lead to the formation of various self-assembled morphologies which were introduced in Section 1.3. However, this method of self-assembly has disadvantages: mainly the high dilution of the resultant nanostructures and the difficulties in large-scale preparation of self-assemblies. Therefore, a new strategy by which the synthesis of block copolymers and the preparation of well-defined self-assemblies could be performed simultaneously in high concentration is favored. In recent years, a strategy called polymerization-induced self-assembly (PISA) is of interest as it meets the above demands, where block copolymers are prepared in a selective solvent using soluble macroinitiator or macromolecular chain transfer agent (macro-CTA) and self-assembly is formed simultaneously during the polymerization as the growing block is insoluble in this selective solvent (Figure 1.8).[48]

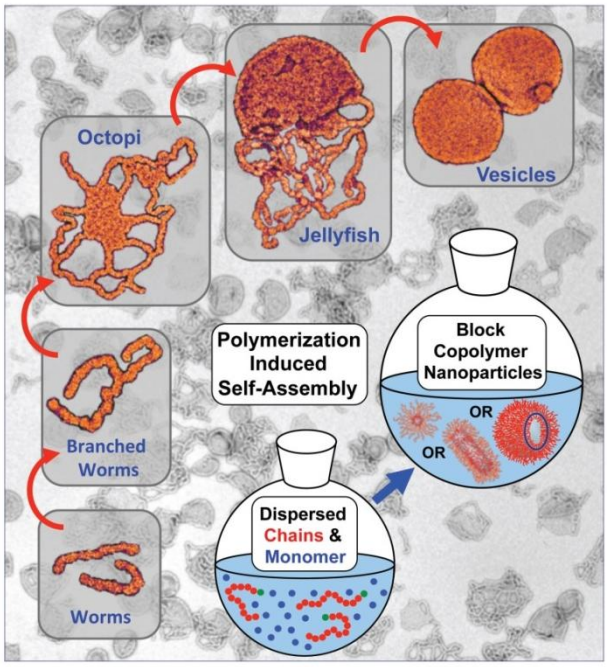

Figure 1.8 A representation of polymerization-induced self-assembly (PISA).[47]

PISA is now well established to allow access to different morphologies of self-assembly under both dispersion and emulsion polymerization conditions.[47,48,82-86] This approach has enormous advantages in the design of systematic morphologies, as these can be achieved by simply varying the polymerization conditions (*e.g.,* ratio of monomer to macro-CTA). Self-assemblies with controlled sizes and morphologies are formed during the polymerization process without any further assembly and purification steps. Controlled radical polymerization techniques such as NMP, ATRP, and RAFT polymerization have been broadly applied in this process,[87] although RAFT polymerization is still the most popular method due to its versatility.[48] Moreover, both dispersion polymerization and emulsion polymerization have been studied to polymerize soluble/insoluble monomers respectively in either aqueous or organic medium.[48] For example, RAFT dispersion polymerizations in aqueous solution have been utilized to grow a water-insoluble new block from the water-soluble/miscible monomers in the presence of a solvent-soluble macro-CTA *via* a PISA process. Armes and coworkers performed the RAFT aqueous dispersion polymerization of 2-hydroxypropyl methacrylate (HPMA) using a water-soluble macro-CTA poly(glycerol monomethacrylate) (PGMA), where spherical micelles, worm-like micelles, bilayer octopi-like micelles, jellyfish-like micelles and vesicles were obtained sequentially as the polymerization proceeded for a target $PGMA_{47}$-*b*-$PHPMA_{200}$ diblock copolymer (Figure 1.9). Similar morphologies and transitions were also observed from separate polymerizations at full conversion but with increasing the initial ratio of monomer to macro-CTA. In addition, the resultant block copolymers were well-controlled in terms of molecular weight and molecular weight distributions.[47]

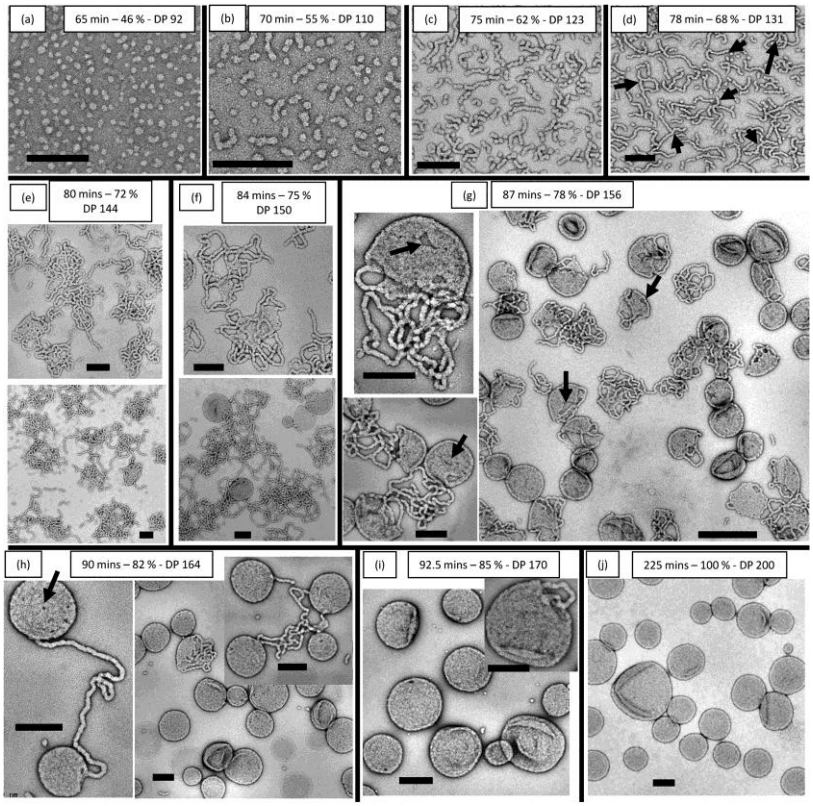

Figure 1.9 TEM images obtained for (a) spheres, (b) short worms, (c) long worms, (d) branched worms, (e,f) partially coalesced worms, (g) jellyfish, and (h–j) vesicles generated in situ after various reaction times for a target $PGMA_{47}$-*b*-$PHMA_{200}$ diblock copolymer prepared by RAFT aqueous dispersion polymerization at 70 °C and 10% w/v solids. Scale bars = 200 nm.[47]

Similar to solution self-assembly of BCPs prepared by post-polymerization processes, there are many factors affecting the resultant polymers, morphologies and morphology transitions of PISA. In general, the factors affecting solution self-assemblies prepared by post-polymerization processes should be also considered in the process of PISA. Additionally, according to previous literature on PISA, factors affecting the results of PISA mainly include the nature of the macro-CTA (*e.g.,* length, composition),[88,89] monomers,[48] core-forming polymer (*e.g.*, LCST),[90] and solvent,[48] total solid content,[91] feed ratio of polymerization components,[91] cross linker,[92] and the addition of monomers,[82,93] amongst others.[48]

The nature of macro-CTA/macroinitiator is very important to the resultant morphologies and morphology transitions. For example, Armes and coworkers

demonstrated RAFT dispersion polymerization of benzyl methacrylate (BzMA) using poly(lauryl methacrylate) (PLMA) as macro-CTA in non-polar solvents.[88] It was found that a sphere-cylinder-vesicle transition occurred when using PLMA with a DP of 17. However, if longer PLMA with a DP of 37 was used, only spheres were observed even when the studied polymer was $PLMA_{37}$-*b*-$PBzMA_{900}$, which was unexpected as in principle this system should form high order structures like vesicles due to the highly asymmetric chains. The proposed reason for this behaviour was that the longer PLMA block was sufficiently long to ensure effective steric stabilization and thus prevent the fusion of spheres to high order structures.

Another key parameter is the total solid content of the polymerization. Armes and coworkers showed that in the system of RAFT dispersion polymerization using HPMA as the monomer and poly(2-(methacryloyloxy) ethylphosphorylcholine) (PMPC) as the macro-CTA, different morphologies could be obtained from polymerizations with the same target polymer but at different solid contents (Figure 1.10, a-d, $PMPC_{25}$-*b*-$PHPMA_{400}$).[91] On the other hand, it was found that polymerizations with low solid content could only lead to the formation of spheres rather than high order structures like cylinders or vesicles (*e.g.*, only spheres were formed from $PMPC_{25}$-*b*-$PHPMA_x$ when the solid content was 10%, Figure 1.10). One possible reason for this, reported in the study, was that the nature of PMPC, which is sensitive to solvation resulted in different pervaded block volumes between in dilute solution and in concentrated solution.[91]

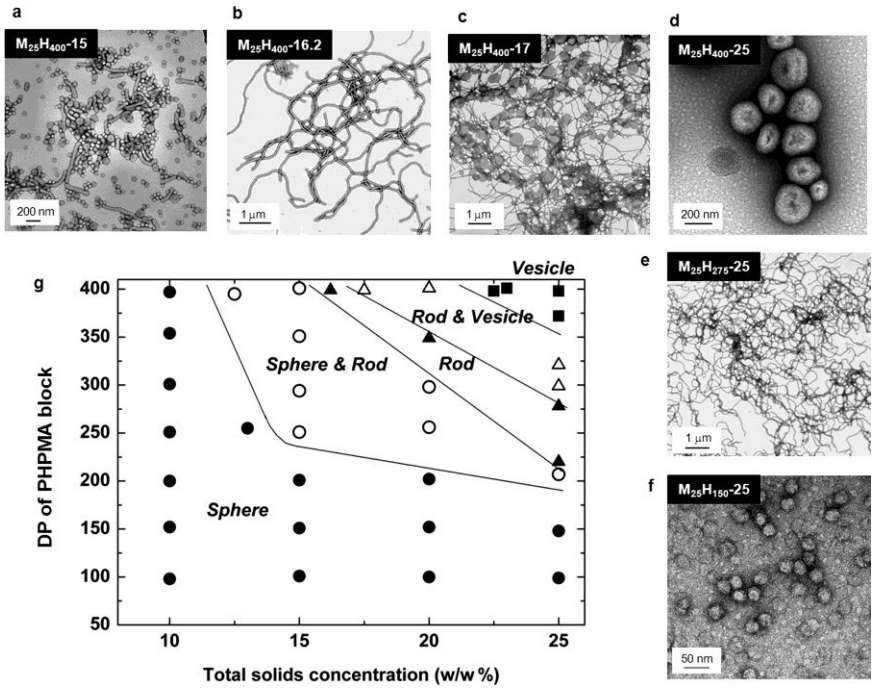

Figure 1.10 Detailed phase diagram constructed for the $PMPC_{25}$-*b*-$PHPMA_x$ system and TEM images for $PMPC_{25}$-*b*-$PHPMA_{400}$ at different solid contents and $PMPC_{25}$-*b*-$PHPMA_x$ at the same solid content (where M is PMPC, H is PHPMA, and x the DP of PHPMA).[91]

Besides common morphologies such as spheres, cylinders and vesicles, a few new morphologies can also be formed using PISA with the introduction of special monomers or polymerization conditions.[82,92,93] Armes and coworkers prepared polymeric vesicles from $PGMA_{58}$-*b*-$PHPMA_{350}$ through aqueous RAFT dispersion polymerization and then used it as a precursor to chain extend a third monomer.[82] Four different types of monomer were investigated. If HPMA was used, vesicles with thick membranes were observed. When water-immiscible monomer benzyl methacrylate (BzMA) was employed which contributed to a second hydrophobic block, a distinctive framboidal morphology was observed due to the phase separation between the PHPMA and PBzMA blocks. When using water-immiscible methyl methacrylate (MMA) as monomer, a similar yet less framboidal morphology was observed, suggesting weaker microphase separation between PMMA and PHPMA. The use of ethylene glycol dimethacrylate (EGDMA) led to the formation of highly cross-linked vesicles. In addition, Pan and coworkers showed the formation of

interesting unusual spaced concentric vesicles (SCVs) from poly(4-vinylpyridine)-*b*-polystyrene (P4VP-*b*-PS) by optimizing the conditions of RAFT dispersion polymerization in methanol. They showed that the concentration of the residual polymer chains in the lumen of nascent vesicles was a determining factor for the formation of SCVs.[93]

Recently, studies have also focused on introducing stimuli-responsive or functional polymers into PISA systems[90,94] and moving towards exploiting the potential applications of PISA.[94-96] For example, Sumerlin and coworkers demonstrated polymerization-induced thermal self-assembly (PITSA) using thermally responsive polymer, poly(*N*-isopropylacrylamide) (PNIPAm), as the growing core-forming block which induced the formation of self-assemblies above the lower critical solution temperature (LCST) of PNIPAm (Figure 1.11).[90] To characterize the resultant nanoparticles, the particles were crosslinked immediately following polymerization at elevated temperature. This approach expands the PISA system to allow for preparation of 'smart' polymeric nanoparticle delivery vehicles.[90] In addition, Davis and coworkers investigated guest molecule encapsulation through the PISA process.[95] In their study, a guest molecule (Nile Red) was encapsulated with high efficiency during PISA process, without disturbing the resultant morphology or kinetics of PISA system.[95] This study demonstrated that PISA has a significant potential for preparation of delivery vehicles in the medical or agricultural fields.[95] In this thesis, inspired by previous work, we have investigated the formation of nucleobase-containing self-assemblies *via* PISA.

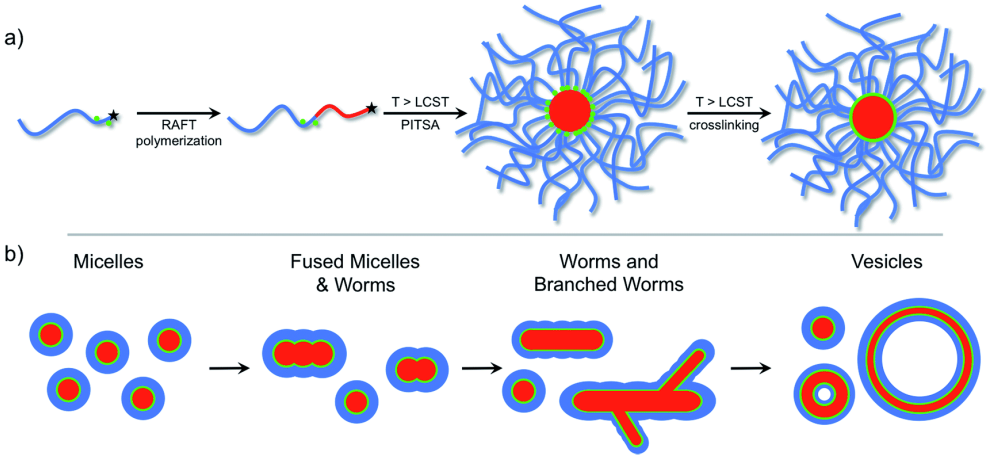

Figure 1.11 (a) A representation of a PITSA process using RAFT dispersion polymerization; (b) Progression of polymeric nanoparticle morphology with increasing the degree of polymerization of hydrophobic block.[90]

1.5 Analysis of polymer self-assemblies formed in solution

A range of self-assemblies can be prepared by both post-polymerization methods and polymerization-induced processes as mentioned above. It is of importance that the self-assembled structures can be characterized accurately. To date, the most common and robust techniques are based on microscopy and scattering.[97] Typically, microscopy can image samples directly and provide details on individual particles. However, there are disadvantages of microscopy. Microscopy is time-consuming if many samples or particles are subject to analysis. In addition, as almost all microscopy techniques require removing samples from their original state, artefacts may occur as a result of preparative and investigative processes. Moreover, some advanced microscopy techniques (cryogenic TEM (cryo-TEM),[97] *in situ* liquid TEM[98,99]) are only well-adapted to samples with limited conditions or structures. Scattering is a complementary technique to microscopy, where samples can be analyzed in solution which minimizes the occurrence of possible artefacts. However, analysis of scattering is often fitted to a model and the results only provide an overview of the sample, which means samples with multiple, complex or unusual

structures are difficult to analyze. Therefore, a combination of microscopy and scattering should be used to analyze self-assembly structures.

1.5.1 Microscopy techniques for polymer nanoparticles

Microscopy techniques can be generally divided into three categories: optical, electron and scanning probe.[97] Optical and electron microscopy use a beam of radiation (light or electrons) which is projected onto a sample to create images. As the wavelength of electrons can be 100,000 times shorter than light, the absolute resolution of electron microscopy is much higher than light optical microscopy (0.003 nm for 200 keV electrons, 150 nm for UV-light microscope λ = 200 nm).[97] Scanning microscopes utilize a probe to scan each point of the object serially to form an image. The resolution of scanning microscopes always depends on the size of the probe used and the degree in which a change in the probe (position or voltage) can be detected. Figure 1.12 shows different types of images obtained from different microscopy techniques for a spherical particle.[97]

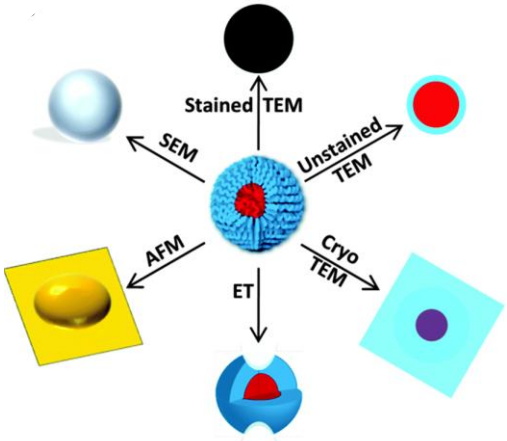

Figure 1.12 A schematic showing that the different types of images formed by different microscopy techniques for a spherical particle.[97]

1.5.1.1 Transmission electron microscopy

Transmission electron microscopy (TEM) is a microscopy technique in which a beam of electrons is transmitted through a thin specimen and interacts with the

specimen as it passes through. An image is then formed as a result of the interaction of electrons. Nowadays TEM can be used to image samples in both the dry-state and solvated state.

The dry-state TEM requires drying samples onto substrates before imaging, which may cause changes in particle size, morphology, crystallization or even damage the sample.[100] For example, solvated polymers such as the corona of micelles in solution will change their shape or length upon dehydration. However, given that dry-state TEM is relatively easy to perform and widely accessed, it is still commonly used in the research of polymer nanoparticles. In addition, the substrates on which the samples are dried are very important for gaining a better image contrast. In order to observe particles easily and clearly, samples should scatter more electrons than substrates. However, typical TEM grids use carbon based film which are about 40 nm in thickness and thus particles approaching similar sizes are always difficult to image.[97] To improve the contrast, staining techniques have been developed. A number of stains (*e.g.*, osmium tetroxide, ruthenium tetroxide, uranyl acetate, ammonium molybdate and phosphotungstic acid) are used, which selectively bind to the grid (negative staining) or particle (positive staining) to enhance the contrast. Staining appears to be a useful technique; however, stains sometimes can cause artefacts, limit resolution and obscure the internal structures of particles.[100,101] An alternative method has been developed, where thinner but inexpensive supports, graphene[102] and graphene oxide (GO)[103] are used as substrates to image low contrast materials without staining. Previously O'Reilly's group collaborated with Wilson's group to show that GO-coated grids are very useful for adhering polymer particles from both aqueous and organic solutions and imaging these particles with good contrast (Figure 1.13).[104] Moreover, Dyson and coworkers recently showed that a

combination of exit wave reconstruction (EWR) and GO-TEM grids can be used to produce extraordinary images where polymer chains within nanostructures can be observed.[105] In this thesis, all the dry-state TEM images were conducted using GO-coated TEM grids unless specified otherwise.

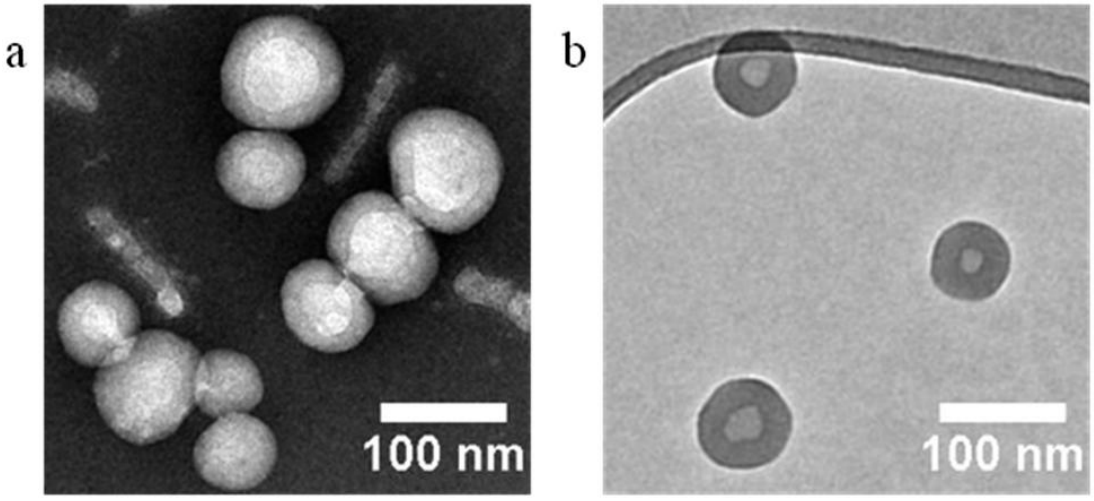

Figure 1.13 Vesicles prepared from PS_{250}-*b*-PAA_{11} imaged by (a) uranyl acetate staining and (b) unstained on a GO-TEM grid.[97,104]

As dry-state TEM cannot image solvated samples, cryo-TEM and *in situ* liquid TEM were developed to overcome this problem, by which samples could be kept in a solvated state while imaging. For the preparation of cryo-TEM grids, a small volume of sample solution is deposited on a lacey carbon grid, blotted to remove most of the solution and then rapidly plunged into a vitrification solvent (typically liquid ethane) to trap the particles in a solution-state. Once vitrified, the samples are kept, transferred, and imaged at liquid nitrogen temperature. Cryo-TEM is a powerful technique to show the structures of particles in their natural state, however, there are a few disadvantages of cryo-TEM. Cryo-TEM is only well-adapted to aqueous samples; samples in organic solvents are very difficult to image.[106] In addition, cryo-TEM requires significant time and proficient skills to prepare and analyze the samples. *In situ* liquid TEM is an exciting method, where liquid samples are injected into a sealed TEM chamber and then imaged in solution. This method is

ideal for observation of particle dynamics in real-time. However, currently this developing method is limited to metal-containing particles due to the poor contrast for polymeric particles.[98,99]

Electron tomography is a technique where a series of TEM images are taken at different tilt angles. These images are then reconstructed to provide a 3D representation of the studied particles. TEM images can be taken by both dry-state TEM[104] and cryo-TEM,[107] although for complex structures cryo-TEM is much better as there are minimized artefects. This method is invaluable in the study of particles with complex internal structures as it can provide internal details. For example, Figure 1.14, which is from Holder and Sommerdijk's work, shows TEM images of bicontinuous micelles obtained by both dry-state TEM and cryo-TEM and their corresponding 3D reconstructions.[80] However, ET is currently not widely used as it is rather challenging and hence requires expert skills in both computers and microscopy.

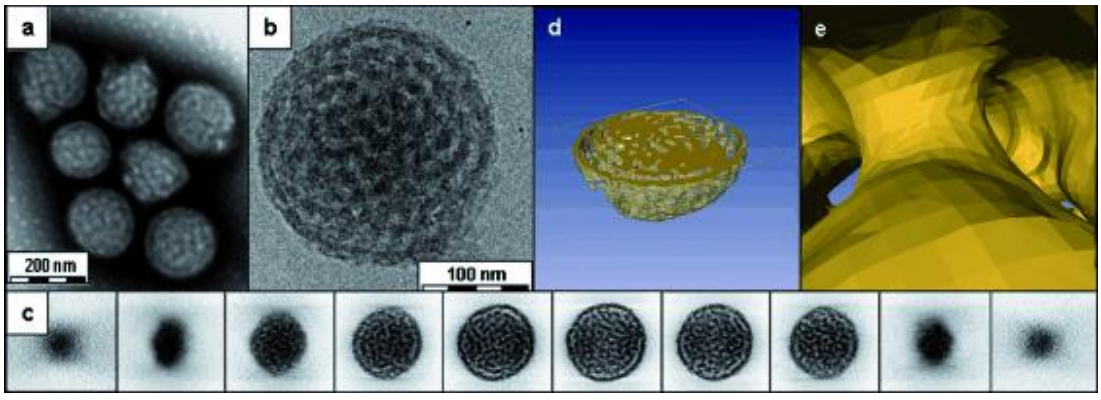

Figure 1.14 TEM analysis of bicontinuous micelles: a) Conventional TEM using negative staining; b) cryoTEM image of a vitrified film; c) gallery of *z* slices showing different cross sections of a 3D SIRT (simultaneous iterative reconstruction technique) of a tomographic series recorded from the vitrified film in (b); d,e) visualization of the segmented volume showing d) a cross section of the aggregate and e) a view from within the hydrated channels.[80]

1.5.1.2 Atomic force microscopy

Atomic force microscopy (AFM) is a scanning probe technique which utilizes a cantilever with a sharp tip at its end. When the tip is in close proximity of a sample surface, a deflection of the cantilever is formed resulting from the forces between the tip and sample. The deflection is then measured typically using a laser spot which is reflected by the top surface of the cantilever into an array of photodiodes. AFM can operate in different imaging modes with different feedback mechanisms: contact mode and tapping mode, where the gentle tapping mode is more suitable for soft polymeric materials. It should be noted the x resolution (horizon, see Figure 1.15) in AFM is always limited by the size of tip owing to convolution effects (Figure 1.15), while z resolution (height, see Figure 1.15) is always high and accurate.[97] Thus AFM is complementary to TEM as the height is hard to obtain using TEM unless changing the tilt angle. In addition, AFM is also capable of measuring extremely small particles and particles which have weak scattering in TEM and are therefore difficult to observe by TEM.[97,108] Moreover, it is also possible to characterize hydrated samples by using liquid AFM.[109] In this thesis, AFM is used to mainly measure the height of particles in a dry-state.

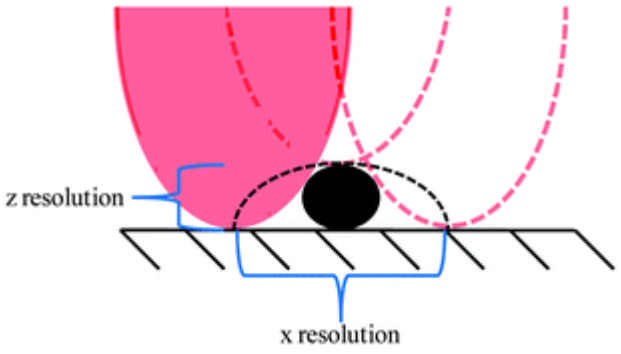

Figure 1.15 Schematic of an AFM tip measuring a spherical particle on a surface indicating how x resolution and z resolution.[97]

1.5.1.3 Other microscopy techniques

Other microscopy techniques such as scanning TEM (STEM) and scanning electron microscopy (SEM) are also used to analyze polymer nanoparticles although these techniques are less widely used than TEM and AFM.[97] In STEM, images are produced by a raster scan using a small beam of electrons. STEM mode is advantageous in chemical analysis by combining with energy-dispersive X-ray spectroscopy (EDX) and electron energy loss spectroscopy (EELS).[97,110] Moreover, STEM is able to image in the high angle annular dark field (HAADF), which means that the image contrast is directly related to the electron density and the specimen thickness.[104,111]

SEM is also conducted using a small beam of electrons; however, the electrons have lower energy (1 – 30 keV for SEM and 100 – 300 keV for STEM) and the beam sizes are larger than those used in STEM. Therefore the resolution in SEM is poorer than STEM. However, SEM provides information on surface or near surface rather than internal structures and is therefore complementary to TEM/STEM techniques. In addition, SEM also allows for chemical analysis of the surface. Typically samples are coated with Au or Pt to prevent charging the sample surface, which causes image distortion.[97]

1.5.2 Scattering techniques for polymer nanoparticles

The most common scattering techniques for analysis of polymer nanoparticles in solution are dynamic and static light scattering (DLS and SLS), small angle X-ray scattering (SAXS) and small angle neutron scattering (SANS). Typically, radiation of known wavelength (λ) is directed towards a sample solution and interacts with the scatterers within the solution which results in a deviation of trajectory (light

scattering).[97] The intensity of the scattered radiation is then detected at a given angle (θ). Changing θ and λ can alter the scattering vector (q) shown in Equation 1.4,

$$q = \frac{4\pi n}{\lambda} \sin\frac{\theta}{2} \qquad \text{Equation 1.4}^{97}$$

where n is the refractive index of solvent for light scattering and 1 for SANS and SAXS.[97] The reciprocal of q is proportional to the length scale at which the matter is detected; large q values are related to small length scales and vice versa. By interpreting scattering data, particle size, shape and molecular weight can be provided as in the case of SLS, SANS, and SAXS. In addition, if the data is collected as a function of time, particle dynamics can be analyzed, as by DLS. Figure 1.16 shows the information which is obtained by different scattering techniques for a spherical particle.[97]

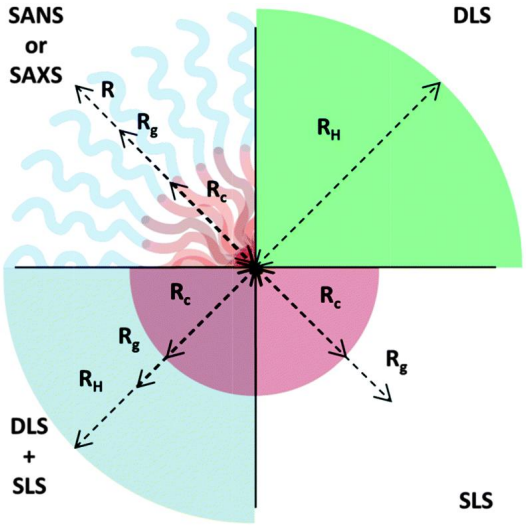

Figure 1.16 A schematic showing that the types of information which is obtained by different scattering techniques for a spherical particle, where R_c is the radius of core, R_H is the hydrodynamic radius and R_g is radius of gyration.[97]

1.5.2.1 Dynamic light scattering

Particles in solution undergo Brownian motion and thus the particle positions change with time. As a consequence of the changes in position, the scattered light from all particles undergoes either constructive or destructive interference and the resultant scattered intensity fluctuates with time at a given angle. This fluctuation can be

interpreted to give a time scale of the movement of particles, which can be described by the second order autocorrelation function generated from the intensity fluctuations as follows:

$$\boldsymbol{g_2\,(q,\tau)} = \frac{\boldsymbol{<I(q,t)I(q,t+\tau)>}}{\boldsymbol{<I(q,t)^2>}} \quad \text{Equation 1.5}^{112}$$

where $g_2(q,\tau)$ is the autocorrelation function at a particular wave vector q and correlation time τ and I is intensity. The angular brackets < > donates the average value.

For monodisperse particles, the relation between the second-order autocorrelation function $g_2(q,\tau)$ and first-order autocorrelation function $g_1(q,\tau)$ and the equation for $g_1(q,\tau)$ itself are as follows:

$$\boldsymbol{g_2\,(q,\tau) = 1 + [g_1\,(q,\tau)]^2} \quad \text{Equation 1.6}^{112}$$

$$\boldsymbol{g_1(q,\tau) = e^{-\Gamma\tau}} \quad \text{Equation 1.7}^{112}$$

where Γ is the decay rate and:

$$\Gamma = \boldsymbol{D_t\,q^2} \quad \text{Equation 1.8}^{112}$$

Where D_t is the translational diffusion coefficient at the given detection angle and sample concentration.

As the diffusion coefficient (D_t) is related to particles' hydrodynamic radius (R_H) by the Stokes-Einstein equation (Equation 1.9), R_H can be obtained:

$$\boldsymbol{R_H} = \frac{\boldsymbol{k_B T}}{\boldsymbol{6\pi\eta D_t}} \quad \text{Equation 1.9}^{112}$$

where K_B is Boltzmann's constant, T the absolute temperature, and η the viscosity of solvent.[112] It should be noted that in this method the scatterer is assumed to be a hard sphere and therefore the value of R_H obtained is not always equal to the radius of the particle unless it is spherical. In addition, given that polymer nanoparticles are never perfectly monodisperse, the cumulant method is routinely applied, which assumes a monomodal distribution of relaxation times. In the case of a multimodal system, the

CONTIN analysis is ideal, which fits the data with a constrained regularization method, which produces a continuous distribution of relaxation times and allows for analysis of disperse samples.[97,112] However, the R_H values obtained by these methods are still relative values due to the assumption that the particles are spherical, although the information on sample polydispersity is still valuable.[76]

1.5.2.2 Static light scattering

In contrast to DLS which monitors the change in scattering intensity over time, SLS measures the mean intensity of the scattered light averaged over time. The average molecular weight of a particle (M_w) and it's radius of gyration (R_g) can be calculated using the Zimm equation (Equation 1.10, q is scattering vector shown in Equation 1.4) when performing SLS measurements at multiple angles (θ) and concentrations (c). The average intensity scattered by the sample (I_{sample}) is measured in relation to the average intensity of a solvent ($I_{solvent}$) and a standard ($I_{standard}$), which is used to determine the Rayleigh ratio of the sample (R_θ) based on the known Rayleigh ratio of a standard ($R_{\theta,\,standard}$) (Equation 1.11). K is related to the wavelength of laser (λ), the refractive index of the solvent ($n_{solvent}$), the refractive index increment of sample (dn/dc) and Avogadro's number (N_A) (Equation 1.12). Plotting Kc/R_θ *vs* q^2 at multiple concentrations allows for determination of the weight average molecular weight of the scatterers and radius of gyration from the intercept and slope of the plot. In addition, by plotting each extrapolated Kc/R_θ *vs* concentration, the second virial coefficient (A_2) can be obtained from the slope. If A_2 is negative, it means there are attractive interactions between particles; if A_2 is positive, it shows repulsive interactions. Moreover, the aggregation number of a particle can be determined by comparing weight-average molecular weights of particles with those of polymers. It should be noted that use of the Zimm plot is only valid for $q \times R_g < 1$.

$$\frac{Kc}{R_\theta} = \left(\frac{q^2 {R_g}^2}{3} + 1\right)\left(\frac{1}{M_W} + 2A_2 c\right) \qquad \text{Equation 1.10}$$

$$R_\theta = \frac{I_{sample} - I_{solvent}}{I_{standard}} R_{\theta,\ standard} \qquad \text{Equation 1.11}^{97}$$

$$K = \frac{4\pi {n_{solvent}}^2 \left(\frac{dn}{dc}\right)^2}{N_A \lambda^4} \qquad \text{Equation 1.12}^{97}$$

By combining particle sizes determined from both DLS and SLS, information on particle topology can be obtained, namely the so-called ρ-ratio (R_g/R_H). In general, if the value of the ρ-ratio is 0.775, it indicates the formation of spheres. Hollow spheres are suggested to form if the value is 1, while cylinders or extended structures are most likely formed if the value is larger than 1 (Figure 1.17).[112]

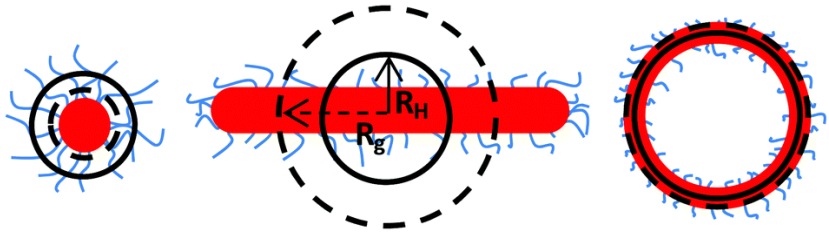

Figure 1.17 Schematic depicting how different morphologies would display a different R_g/R_H ratio.[97]

1.5.2.3 Small angle neutron and X-ray scattering

SANS and SAXS use neutrons and X-rays as the radiation source respectively, which possess much smaller wavelengths (typically 0.1 nm) and therefore they are able to probe much smaller length scales ($1/q$, where higher scattering vector q values as shown in Equation 1.4). As a consequence, information on the size, shape and organization of the amphiphilic blocks within the structure can be obtained. Thus SANS and SAXS measurements can probe the scatterers as a whole ($q \times R_g < 1$) as well as their interior structures ($q \times R_g > 1$). In addition, neutrons are scattered by the nuclei and the scattered intensity is related to the nuclear scattering length density (SLD), which is determined from the chemical formula of samples and density of the materials. As the SLD of hydrogen and deuterium-containing materials is different, good contrast can be obtained between materials containing hydrogen and

deuterium. Therefore, SANS is very suitable to measure deuterated materials or non-deuterated materials in deuterated solvents. In comparison, X-rays are scattered by the electron cloud and the scattered intensity is dependent on the atomic number squared; therefore, SAXS is sensitive to heavier elements.[113]

However, the main disadvantages of SANS and SAXS are that they are not widely accessible and the interpretation of the raw data requires fitting with suitable models. When fitting with a model, it is advisable to input some known parameters to make the fitting process easier. However, for complex and unknown structures, the fitting process is difficult and the information obtained would be limited.[97]

1.6 Nucleobase-containing synthetic polymers

Nature is an inexhaustible source of inspiration for synthetic chemistry. It is well-known that the specific interaction of corresponding nucleic acids plays a key role in nature for synthesizing biopolymers including DNA and RNA strands, by which a daughter biopolymer can be produced possessing the exact complementary sequence and the same length as the original template. Inspired by nature, nucleobases (thymine, uracil, adenine, cytosine and guanine) and nucleosides (thymidine, uridine, adenosine, cytidine and guanosine) have been employed in synthetic polymer chemistry.[79]

It has been demonstrated that synthetic polymers containing nucleobases can be prepared by the robust and broad convergence of synthetic and polymer chemistries.[114] A range of nucleobase-containing monomers including (meth)acrylate,[115-117] methacrylamide,[118] styrene,[119,120] and norbornene,[121-123] have been widely synthesized with reasonable yields. The main strategies for monomer synthesis are nucleophilic substitution at saturated carbon atoms[115] or Michael

addition reactions.[117] In addition to these chemical methods, Marsh and coworkers developed enzymatic synthesis, to modify nucleosides using oxime as the starting material and *Candida antarctica* lipase (CAL435 or Novozyme 435) as the catalyst and thus prepared a range of nucleoside-containing monomers.[124,125] Compared to typical chemical methods, this enzymatic synthesis has significant advantages particularly in synthesizing more challenging cytidine and guanosine based monomers.

The preparation of nucleobase-containing synthetic polymers has been reported by both conventional polymerization methods and living polymerization techniques. In the 1970s – 1990s, Takemoto and coworkers demonstrated the polymerizations of nucleobase-containing vinyl monomers using radical polymerizations.[126-128] With the more recent development of CRP, vinyl monomers have been successfully polymerized by these controlled techniques to obtain good control over molecular weight and molecular weight distributions. For example, nucleobase styrenic monomers can be polymerization by NMP,[129,130] while ATRP has been readily used to polymerize methacrylate and acrylate monomers, which have been studied mainly by Marsh and van Hest *et al*.[115,116,124,131,132] In the case of nucleobase-containing norbornene monomers, ring-opening metathesis polymerization (ROMP) is utilized.[121,122] However, there are few reports where reversible addition-fragmentation chain transfer (RAFT) polymerization has been used to prepare polymers containing nucleobases directly.[129] In order to expand the synthesis of nucleobase polymers, in this thesis a goal of ours is to study the synthesis of polymers containing nucleobase functionalities using RAFT polymerization techniques.

In polymer science, nucleobases can be used to control polymer structures.[127,133-137] Kamigaito's group used a thymine-containing compound to mediate the stereospecific radical polymerization of an acrylamide monomer *N*-(6-acetamidopyridin-2-yl)acrylamide) which contained hydrogen bonding sites complementary to thymine. It was found that the resultant polymers possessed high syndiotacticity which is attributed to the strong hydrogen-bonding interactions between the thymine-containing mediator and monomer.[137] Takemoto and coworkers studied the copolymerization behavior of adenine-containing and thymine-containing methacrylate monomers by free radical polymerization in solvents with different polarity. It was found in $CHCl_3$, a relatively non-polar solvent which allows hydrogen bonding, the copolymerization tended to be alternating due to the presence of nucleobase interactions.[127]

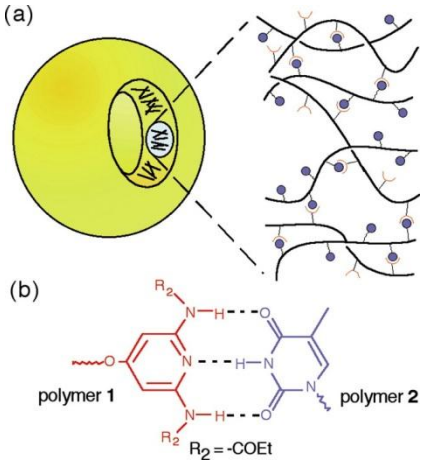

Figure 1.18 Schematic demonstration of vesicle formation between diaminopyridine-based polymer 1 and thymine-based polymer 2. (a) Illustration showing molecular recognition within vesicle wall. (b) The corresponding recognition groups.[138]

The self-assembly of nucleobase-containing polymers is also of interest. The Rotello group demonstrated the formation of giant vesicles by mixing thymine or uracil containing polystyrene or polynorbornene with diacyldiaminopyridine functionalized polymers in chloroform. The formation of giant vesicles was driven by the hydrogen bonding interactions between thymine/uracil and the

diacyldiaminopyridine functional group (Figure 1.18).[138,139] The same group also prepared microspheres using bis-thymine units to noncovalently cross-link a diamidopyridine containing copolymer. It was found that the microspheres were thermally-responsive as the hydrogen bonding interactions were temperature sensitive. The particles were reversibly formed at 25 °C and disassemble at 50 °C.[140] Sleiman and coworkers observed rod morphologies upon the self-assembly of adenine-containing norbornene polymers in THF, which was unexpected given the small ratio of DP between core and corona blocks (1:10). It was hypothesized that the presence of self-complementary hydrogen bonding interactions and the aromatic π-stacking behavior of adenine caused this observation.[122] In addition, van Hest and coworkers studied the aqueous self-assembly of poly(ethylene glycol)(PEG)-*b*-poly(adenine), PEG-*b*-poly(thymine) and a 1:1 mixture of these two polymers. It was found that the mixture exhibited different self-assembly behavior compared to the single polymers. The mixture possessed a higher critical aggregation concentration (CAC) and one population of self-assembled structures, while self-assembly of single the polymers revealed a bimodal distribution.[141] Besides solution self-assembly, self-assembly of nucleobase-containing polymers in the bulk/solid state is also well-studied.[130,142] These pioneering works suggest nucleobase interactions play a key role in the self-assembly of nucleobase-containing polymers. Based on these studies, in this thesis we have further exploited the solution self-assembly of nucleobase containing polymers by both polymerization-induced processes and post-polymerization methods.

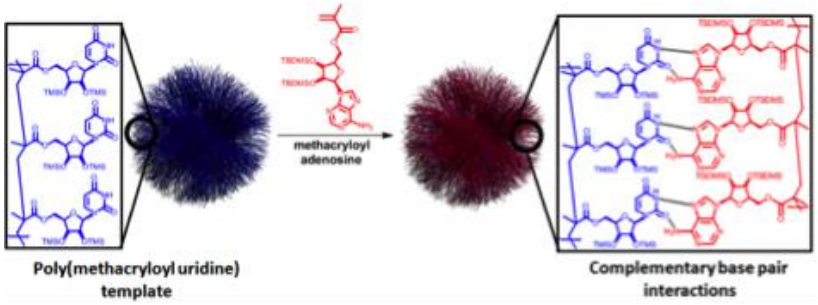

Figure 1.19 A representation of template polymerization on a solid support using poly(methacryloyl uridine) as a template and methacryloyl adenosine as a complementary monomer.[125]

Nucleobase interactions are also widely used in templated polymerizations. Over the past few years, chemical templating based on nucleobase-containing polymers has been studied by a number of research groups. Indeed in 1999, Marsh and co-workers used poly(5'-acryloyluridine) (PU) as a template to induce the polymerization of the complementary monomer 5'-acryloyladenosine (A) in the presence of non-complementary monomer 5'-acryloyluridine (U).[131] It was found that a complex of PU and poly(5'-acryloyladenosine) (PA) was formed during the templated polymerization of the adenosine monomer with a PU template, which was observed to possess a higher T_g than either single polymer (PA or PU). However, due to intramolecular association, PA did not template the polymerization of U. Recently, Marsh and co-workers also reported nucleoside templated polymerization from solid supports (Figure 1.19).[125] The templates were grown from solid support (Wang-type resin) by ATRP using uridine, adenosine, cytidine and guanosine based methacrylate monomers, followed by debromination of the end group. Polymerizations of complementary monomers were investigated in the presence and absence of the solid support templates. It was found that uridine derived templates exhibited good fidelity of templating even if from a mixture of monomers.[125] In addition to vinyl based polymers, Weck's group investigated similar templated polymerizations using a diaminopyridine functionalized norbornene polymer as the template, which was

synthesized *via* ROMP and designed to recognize norbornene-based thymine monomers. This chemical templating approach was also shown to enhance the rate of polymerization due to an increase in the local monomer concentration.[143] Furthermore, Sleiman and coworkers reported the construction of thymine-containing conjugated block copolymers using ROMP. These thymine-containing copolymers (with a DP of around 20) could further template the polymerization of the complementary adenine-containing monomers to afford a conjugated daughter polymer *via* metal-catalyzed coupling reactions. It was found that these daughter polymers possessed a similar degree of polymerization to the templates and narrow molecular weight distributions, indicating efficient templating occurred.[144] In O'Reilly's group, a biomimetic segregation/templating approach using nucleobase monomers was developed for application in affording polymers with good control.[129] Specifically, micelles were formed from a low molecular weight thymine-containing block copolymer poly(styrene)-*b*-poly(vinylbenzylthymine) (PSt-*b*-PVBT), which then acted as a confined environment for polymerization of the complementary monomer vinylbenzyladenine (VBA). It was found that the segregation of individual propagating chains resulted in single-chain daughter polymers per micelle with high molecular weight and extremely narrow polydispersity (Figure 1.20).

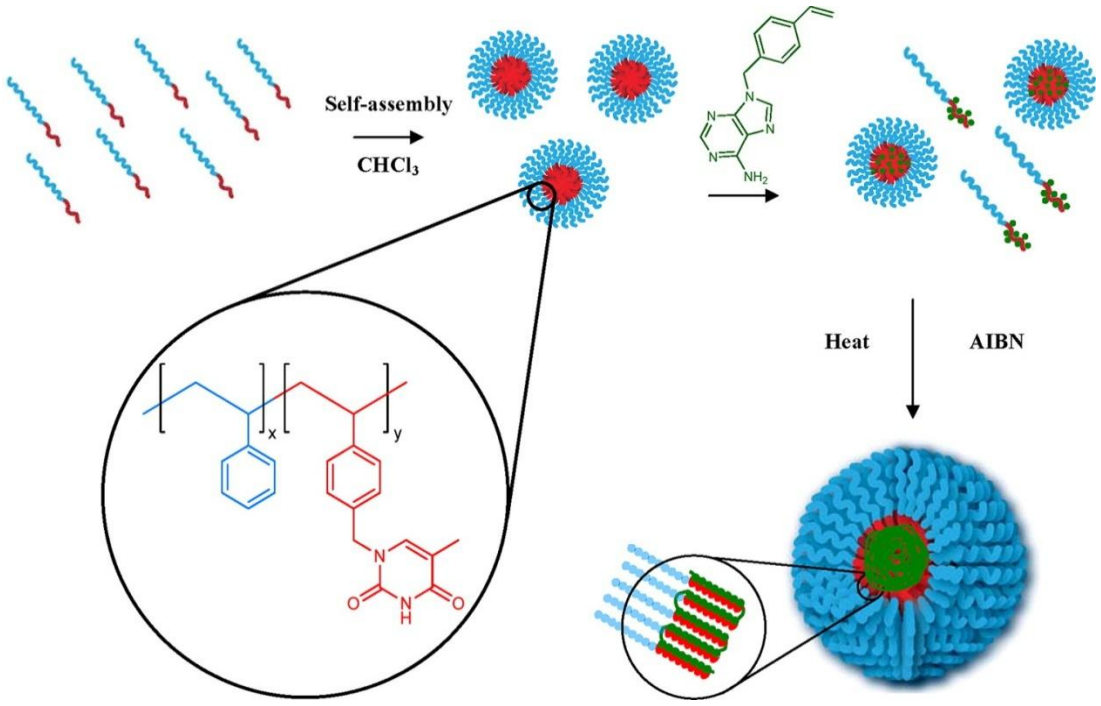

Figure 1.20 Self-assembly of template block copolymer PSt-*b*-PVBT in $CHCl_3$ yields a stable monodisperse micellar system with PVBT cores, which induced the polymerization of complementary adenine monomer VBA in the core of the micelles to give a daughter polymer with high molecular weight and low molecular weight distribution.[129]

This segregation/templating approach is very promising. However, there are still some aspects worthy of further investigation, such as tuning the molecular weight of the daughter polymer, expanding this approach to other types of polymers and performing the method in an aqueous environment. We assume that by changing the morphology, aggregation number or environment of the self-assembled templates, the molecular weight of the daughter polymer might be tunable. Beyond these pioneering studies, there is still very little research into the systemic study of the self-assembly of nucleobase polymers, which inspired us to further exploit this field.

1.7 Summary

In this Chapter, we have firstly introduced the basic knowledge and mechanisms of controlled radical polymerization techniques and heterogeneous polymerizations, among which RAFT has been chosen to prepare nucleobase-containing polymers throughout this thesis and RAFT dispersion polymerization has been employed in Chapter 3 and Chapter 4 to synthesize nucleobase functionalized polymers and nanostructures. Secondly, the concept of reactivity ratios has been introduced, which is a common parameter for copolymerizations and indicates the resultant copolymer compositions. In addition, self-assembly of block copolymers in solution has been outlined, which includes the general rules and considerations of self-assembly, as well as an introduction to polymerization-induced self-assembly and a brief description of microscopy and scattering techniques that are used to characterize nanostructures. Finally, the literature on nucleboase-containing synthetic polymers has been reviewed.

Based on the above knowledge and inspired by these pioneering work, in this thesis we have further explored the synthesis and self-assembly of nucleobase-containing materials. One goal of our work is to demonstrate the feasibility of preparing nucleobase polymers by RAFT techniques, which expands the synthesis of nucleobase materials. Another aim is to further discover and understand the self-assembly behavior of nucleobase polymers. The study in this thesis is expected to provide preliminary insights into understanding the polymerization and self-assembly behavior of nucleobase containing synthetic materials, which in the future can be applied to as a guideline for the preparation of nucleobase-containing materials and nanostructures.

1.8 References

(1) Szwarc, M. *Nature* **1956**, *178*, 1168.

(2) Colombani, D. *Prog. Polym. Sci.* **1997**, *22*, 1649.

(3) Odian, G. *Principles of Polymerization, Fourth Edition*, John Wiley & Sons, Inc., Hoboken, New Jersey, **2004**.

(4) Otsu, T.; Yoshida, M. *Makromol. Chem. Rapid Commun.* **1982**, *3*, 127.

(5) Otsu, T.; Yoshida, M.; Tazaki, T. *Makromol. Chem. Rapid Commun.* **1982**, *3*, 133.

(6) Hawker, C. J.; Bosman, A. W.; Harth, E. *Chem. Rev.* **2001**, *101*, 3661.

(7) Matyjaszewski, K.; Spanswick, J. *Mater. Today* **2005**, *8*, 26.

(8) Kato, M.; Kamigaito, M.; Sawamoto, M.; Higashimura, T. *Macromolecules* **1995**, *28*, 1721.

(9) Wang, J.-S.; Matyjaszewski, K. *J. Am. Chem. Soc.* **1995**, *117*, 5614.

(10) Matyjaszewski, K.; Patten, T. E.; Xia, J. *J. Am. Chem. Soc.* **1997**, *119*, 674.

(11) Rosen, B. M.; Percec, V. *Chem. Rev.* **2009**, *109*, 5069.

(12) Percec, V.; Barboiu, B. *Macromolecules* **1995**, *28*, 7970.

(13) Chiefari, J.; Chong, Y. K.; Ercole, F.; Krstina, J.; Jeffery, J.; Le, T. P. T.; Mayadunne, R. T. A.; Meijs, G. F.; Moad, C. L.; Moad, G.; Rizzardo, E.; Thang, S. H. *Macromolecules* **1998**, *31*, 5559.

(14) Moad, G.; Rizzardo, E.; Thang, S. H. *Aust. J. Chem.* **2012**, *65*, 985.

(15) Francis, R.; Ajayaghosh, A. *Macromolecules* **2000**, *33*, 4699.

(16) Charmot, D.; Corpart, P.; Adam, H.; Zard, S. Z.; Biadatti, T.; Bouhadir, G. *Macromol. Symp.* **2000**, *150*, 23.

(17) Hawker, C. J. *J. Am. Chem. Soc.* **1994**, *116*, 11185.

(18) Roy, D.; Semsarilar, M.; Guthrie, J. T.; Perrier, S. *Chem. Soc. Rev.* **2009**, *38*,

2046.

(19) Matyjaszewski, K. *Controlled/Living Radical Polymerization: Progress in RAFT, DT, NMP & OMRP*, American Chemical Society, **2009**.

(20) Benoit, D.; Chaplinski, V.; Braslau, R.; Hawker, C. J. *J. Am. Chem. Soc.* **1999**, *121*, 3904.

(21) Benoit, D.; Grimaldi, S.; Robin, S.; Finet, J.-P.; Tordo, P.; Gnanou, Y. *J. Am. Chem. Soc.* **2000**, *122*, 5929.

(22) Grubbs, R. B. *Polym. Rev.* **2011**, *51*, 104.

(23) Detrembleur, C.; Jerome, C.; De Winter, J.; Gerbaux, P.; Clement, J.-L.; Guillaneuf, Y.; Gigmes, D. *Polym. Chem.* **2014**, *5*, 335.

(24) Greene, A. C.; Grubbs, R. B. *Macromolecules* **2010**, *43*, 10320.

(25) Zhang, Q.; Wilson, P.; Li, Z.; McHale, R.; Godfrey, J.; Anastasaki, A.; Waldron, C.; Haddleton, D. M. *J. Am. Chem. Soc.* **2013**, *135*, 7355.

(26) Wang, Y.; Kwak, Y.; Buback, J.; Buback, M.; Matyjaszewski, K. *ACS Macro Lett.* **2012**, *1*, 1367.

(27) Jakubowski, W.; Matyjaszewski, K. *Angew. Chem. Int. Ed.* **2006**, *45*, 4482.

(28) Magenau, A. J. D.; Strandwitz, N. C.; Gennaro, A.; Matyjaszewski, K. *Science* **2011**, *332*, 81.

(29) Zhang, Y.; Wang, Y.; Peng, C.-h.; Zhong, M.; Zhu, W.; Konkolewicz, D.; Matyjaszewski, K. *Macromolecules* **2011**, *45*, 78.

(30) Guliashvili, T.; Percec, V. *J. Polym. Sci., Part A: Polym. Chem.* **2007**, *45*, 1607.

(31) Levere, M. E.; Nguyen, N. H.; Leng, X.; Percec, V. *Polym. Chem.* **2013**, *4*, 1635.

(32) Lligadas, G.; Rosen, B. M.; Monteiro, M. J.; Percec, V. *Macromolecules*

2008, *41*, 8360.

(33) Konkolewicz, D.; Wang, Y.; Krys, P.; Zhong, M.; Isse, A. A.; Gennaro, A.; Matyjaszewski, K. *Polym. Chem.* **2014**, *5*, 4396.

(34) Alsubaie, F.; Anastasaki, A.; Wilson, P.; Haddleton, D. M. *Polym. Chem.* **2015**, *6*, 406.

(35) Corpart, P.; Charmot, D.; Biadatti, T.; Zard, S.; Michelet, D. *Rhodia Chimie Int. Appl.* **1997**, WO 9858974.

(36) Perrier, S.; Takolpuckdee, P. *J. Polym. Sci., Part A: Polym. Chem.* **2005**, *43*, 5347.

(37) Moad, G.; Rizzardo, E.; Thang, S. H. *Polymer* **2008**, *49*, 1079.

(38) Wood, M. R.; Duncalf, D. J.; Rannard, S. P.; Perrier, S. *Org. Lett.* **2006**, *8*, 553.

(39) Perrier, S.; Takolpuckdee, P.; Mars, C. A. *Macromolecules* **2005**, *38*, 2033.

(40) Willcock, H.; O'Reilly, R. K. *Polym. Chem.* **2010**, *1*, 149.

(41) Arshady, R. *Colloid. Polym. Sci.* **1992**, *270*, 717.

(42) Hohenstein, W. P.; Mark, H. *J. Polym. Sci.* **1946**, *1*, 127.

(43) Harkins, W. D. *J. Am. Chem. Soc.* **1947**, *69*, 1428.

(44) Chern, C. S. *Prog. Polym. Sci.* **2006**, *31*, 443.

(45) Almog, Y.; Reich, S.; Levy, M. *Brit. Polym. J.* **1982**, *14*, 131.

(46) Kawaguchi, S.; Ito, K. *Polymer Particles*, Springer Berlin Heidelberg, 2005.

(47) Blanazs, A.; Madsen, J.; Battaglia, G.; Ryan, A. J.; Armes, S. P. *J. Am. Chem. Soc.* **2011**, *133*, 16581.

(48) Sun, J.-T.; Hong, C.-Y.; Pan, C.-Y. *Soft Matter* **2012**, *8*, 7753.

(49) Mayo, F. R.; Lewis, F. M. *J. Am. Chem. Soc.* **1944**, *66*, 1594.

(50) Fineman, M.; Ross, S. D. *J. Polym. Sci.* **1950**, *5*, 259.

(51) Van Herk, A. M.; Dröge, T. *Macromol. Theory Simul.* **1997**, *6*, 1263.

(52) Manders, B. G.; Smulders, W.; Aerdts, A. M.; van Herk, A. M. *Macromolecules* **1997**, *30*, 322.

(53) Badi, N.; Lutz, J.-F. *Chem. Soc. Rev.* **2009**, *38*, 3383.

(54) Pfeifer, S.; Lutz, J.-F. *J. Am. Chem. Soc.* **2007**, *129*, 9542.

(55) Schmidt, B. V. K. J.; Fechler, N.; Falkenhagen, J.; Lutz, J.-F. *Nature Chem.* **2011**, *3*, 234.

(56) Lim Soo, P.; Eisenberg, A. *J. Polym. Sci., Part B: Polym. Phys.* **2004**, *42*, 923.

(57) Mai, Y.; Eisenberg, A. *Chem. Soc. Rev.* **2012**, *41*, 5969.

(58) Fong, C.; Le, T.; Drummond, C. J. *Chem. Soc. Rev.* **2012**, *41*, 1297.

(59) Riess, G. *Prog. Polym. Sci.* **2003**, *28*, 1107.

(60) Blanazs, A.; Armes, S. P.; Ryan, A. J. *Macromol. Rapid Commun.* **2009**, *30*, 267.

(61) Rodríguez-Hernández, J.; Chécot, F.; Gnanou, Y.; Lecommandoux, S. *Prog. Polym. Sci.* **2005**, *30*, 691.

(62) Yu, Y.; Eisenberg, A. *J. Am. Chem. Soc.* **1997**, *119*, 8383.

(63) Yu, Y.; Zhang, L.; Eisenberg, A. *Macromolecules* **1998**, *31*, 1144.

(64) McKenzie, B. E.; de Visser, J. F.; Friedrich, H.; Wirix, M. J. M.; Bomans, P. H. H.; de With, G.; Holder, S. J.; Sommerdijk, N. A. J. M. *Macromolecules* **2013**, *46*, 9845.

(65) Discher, D. E.; Ahmed, F. *Annu. Rev. Biomed. Eng.* **2006**, *8*, 323.

(66) Discher, D. E.; Eisenberg, A. *Science* **2002**, *297*, 967.

(67) McKenzie, B. E.; Friedrich, H.; Wirix, M. J. M.; de Visser, J. F.; Monaghan, O. R.; Bomans, P. H. H.; Nudelman, F.; Holder, S. J.; Sommerdijk, N. A. J.

M. *Angew. Chem. Int. Ed.* **2015**, *54*, 2457.

(68) Kim, S. H.; Nederberg, F.; Jakobs, R.; Tan, J. P. K.; Fukushima, K.; Nelson, A.; Meijer, E. W.; Yang, Y. Y.; Hedrick, J. L. *Angew. Chem. Int. Ed.* **2009**, *48*, 4508.

(69) He, M.; Zhao, L.; Wang, J.; Han, W.; Yang, Y.; Qiu, F.; Lin, Z. *ACS Nano* **2010**, *4*, 3241.

(70) Nicolai, T.; Colombani, O.; Chassenieux, C. *Soft Matter* **2010**, *6*, 3111.

(71) Petzetakis, N.; Dove, A. P.; O'Reilly, R. K. *Chem. Sci.* **2011**, *2*, 955.

(72) Massey, J. A.; Temple, K.; Cao, L.; Rharbi, Y.; Raez, J.; Winnik, M. A.; Manners, I. *J. Am. Chem. Soc.* **2000**, *122*, 11577.

(73) Schmitt, A. L.; Repollet-Pedrosa, M. H.; Mahanthappa, M. K. *ACS Macro Lett.* **2012**, *1*, 300.

(74) Luo, L.; Eisenberg, A. *J. Am. Chem. Soc.* **2001**, *123*, 1012.

(75) Wang, X.; Guerin, G.; Wang, H.; Wang, Y.; Manners, I.; Winnik, M. A. *Science* **2007**, *317*, 644.

(76) Petzetakis, N.; Walker, D.; Dove, A. P.; O'Reilly, R. K. *Soft Matter* **2012**, *8*, 7408.

(77) McKenzie, B. E.; Nudelman, F.; Bomans, P. H. H.; Holder, S. J.; Sommerdijk, N. A. J. M. *J. Am. Chem. Soc.* **2010**, *132*, 10256.

(78) Holder, S. J.; Woodward, G.; McKenzie, B.; Sommerdijk, N. A. J. M. *RSC Adv.* **2014**, *4*, 26354.

(79) McHale, R.; O'Reilly, R. K. *Macromolecules* **2012**, *45*, 7665.

(80) Parry, A. L.; Bomans, P. H. H.; Holder, S. J.; Sommerdijk, N. A. J. M.; Biagini, S. C. G. *Angew. Chem. Int. Ed.* **2008**, *47*, 8859.

(81) Carlsen, A.; Lecommandoux, S. *Curr. Opin. Colloid Interface Sci.* **2009**, *14*,

329.

(82) Chambon, P.; Blanazs, A.; Battaglia, G.; Armes, S. P. *Macromolecules* **2012**, *45*, 5081.

(83) Huang, C.-Q.; Pan, C.-Y. *Polymer* **2010**, *51*, 5115.

(84) Zhang, X.; Boissé, S. P.; Zhang, W.; Beaunier, P.; D'Agosto, F.; Rieger, J.; Charleux, B. *Macromolecules* **2011**, *44*, 4149.

(85) Zhang, W.; D'Agosto, F.; Boyron, O.; Rieger, J.; Charleux, B. *Macromolecules* **2011**, *44*, 7584.

(86) Zhang, W.; D'Agosto, F.; Dugas, P.-Y.; Rieger, J.; Charleux, B. *Polymer* **2013**, *54*, 2011.

(87) Charleux, B.; Delaittre, G.; Rieger, J.; D'Agosto, F. *Macromolecules* **2012**, *45*, 6753.

(88) Fielding, L. A.; Derry, M. J.; Ladmiral, V.; Rosselgong, J.; Rodrigues, A. M.; Ratcliffe, L. P. D.; Sugihara, S.; Armes, S. P. *Chem. Sci.* **2013**, *4*, 2081.

(89) Semsarilar, M.; Jones, E. R.; Blanazs, A.; Armes, S. P. *Adv. Mater.* **2012**, *24*, 3378.

(90) Figg, C. A.; Simula, A.; Gebre, K. A.; Tucker, B. S.; Haddleton, D. M.; Sumerlin, B. S. *Chem. Sci.* **2015**, *6*, 1230.

(91) Sugihara, S.; Blanazs, A.; Armes, S. P.; Ryan, A. J.; Lewis, A. L. *J. Am. Chem. Soc.* **2011**, *133*, 15707.

(92) Sugihara, S.; Armes, S. P.; Blanazs, A.; Lewis, A. L. *Soft Matter* **2011**, *7*, 10787.

(93) Zhang, W.-J.; Hong, C.-Y.; Pan, C.-Y. *Macromolecules* **2014**, *47*, 1664.

(94) Ladmiral, V.; Semsarilar, M.; Canton, I.; Armes, S. P. *J. Am. Chem. Soc.* **2013**, *135*, 13574.

(95) Karagoz, B.; Boyer, C.; Davis, T. P. *Macromol. Rapid Commun.* **2014**, *35*, 417.

(96) Karagoz, B.; Esser, L.; Duong, H. T.; Basuki, J. S.; Boyer, C.; Davis, T. P. *Polym. Chem.* **2014**, *5*, 350.

(97) Patterson, J. P.; Robin, M. P.; Chassenieux, C.; Colombani, O.; O'Reilly, R. K. *Chem. Soc. Rev.* **2014**, *43*, 2412.

(98) Evans, J. E.; Jungjohann, K. L.; Browning, N. D.; Arslan, I. *Nano Lett.* **2011**, *11*, 2809.

(99) Proetto, M. T.; Rush, A. M.; Chien, M.-P.; Abellan Baeza, P.; Patterson, J. P.; Thompson, M. P.; Olson, N. H.; Moore, C. E.; Rheingold, A. L.; Andolina, C.; Millstone, J.; Howell, S. B.; Browning, N. D.; Evans, J. E.; Gianneschi, N. C. *J. Am. Chem. Soc.* **2014**, *136*, 1162.

(100) Talmon, Y. *J. Colloid Interface Sci.* **1983**, *93*, 366.

(101) Friedrich, H.; Frederik, P. M.; de With, G.; Sommerdijk, N. A. J. M. *Angew. Chem. Int. Ed.* **2010**, *49*, 7850.

(102) Meyer, J. C.; Girit, C. O.; Crommie, M. F.; Zettl, A. *Nature* **2008**, *454*, 319.

(103) Wilson, N. R.; Pandey, P. A.; Beanland, R.; Young, R. J.; Kinloch, I. A.; Gong, L.; Liu, Z.; Suenaga, K.; Rourke, J. P.; York, S. J.; Sloan, J. *ACS Nano* **2009**, *3*, 2547.

(104) Patterson, J. P.; Sanchez, A. M.; Petzetakis, N.; Smart, T. P.; Epps III, T. H.; Portman, I.; Wilson, N. R.; O'Reilly, R. K. *Soft Matter* **2012**, *8*, 3322.

(105) Dyson, M. A.; Sanchez, A. M.; Patterson, J. P.; O'Reilly, R. K.; Sloan, J.; Wilson, N. R. *Soft Matter* **2013**, *9*, 3741.

(106) Zhao, H.; Chen, Q.; Hong, L.; Zhao, L.; Wang, J.; Wu, C. *Macromol. Chem. Phys.* **2011**, *212*, 663.

(107) Holder, S. J.; Sommerdijk, N. A. J. M. *Polym. Chem.* **2011**, *2*, 1018.

(108) Appel, E. A.; Barrio, J. d.; Dyson, J.; Isaacs, L.; Scherman, O. A. *Chem. Sci.* **2012**, *3*, 2278.

(109) Rodríguez-Hernández, J.; Babin, J.; Zappone, B.; Lecommandoux, S. *Biomacromolecules* **2005**, *6*, 2213.

(110) Hickey, R. J.; Haynes, A. S.; Kikkawa, J. M.; Park, S.-J. *J. Am. Chem. Soc.* **2011**, *133*, 1517.

(111) Loos, J.; Sourty, E.; Lu, K.; de With, G.; v. Bavel, S. *Macromolecules* **2009**, *42*, 2581.

(112) Schärtl, W. *Light Scattering from Polymer Solutions and Nanoparticle Dispersions*, Springer Berlin Heidelberg, **2007**.

(113) Roe, R. J. *Methods of X-ray and Neutron Scattering in Polymer Science*, Oxford University Press, **2000**.

(114) Lutz, J.-F.; Börner, H. G. *Prog. Polym. Sci.* **2008**, *33*, 1.

(115) Spijker, H. J.; Dirks, A. J.; van Hest, J. C. M. *Polymer* **2005**, *46*, 8528.

(116) Spijker, H. J.; van Delft, F. L.; van Hest, J. C. M. *Macromolecules* **2007**, *40*, 12.

(117) Cheng, S.; Zhang, M.; Dixit, N.; Moore, R. B.; Long, T. E. *Macromolecules* **2012**, *45*, 805.

(118) Inaki, Y.; Ebisutani, K.; Takemoto, K. *J. Polym. Sci., Part A: Polym. Chem.* **1986**, *24*, 3249.

(119) Lutz, J.-F.; Thünemann, A. F.; Rurack, K. *Macromolecules* **2005**, *38*, 8124.

(120) Sedlák, M.; Šimůnek, P.; Antonietti, M. *J. Heterocycl. Chem.* **2003**, *40*, 671.

(121) Gibson, V. C.; Marshall, E. L.; North, M.; Robson, D. A.; Williams, P. J. *Chem. Commun.* **1997**, 1095.

(122) Bazzi, H. S.; Sleiman, H. F. *Macromolecules* **2002**, *35*, 9617.

(123) Burd, C.; Weck, M. *Macromolecules* **2005**, *38*, 7225.

(124) Marsh, A.; Khan, A.; Haddleton, D. M.; Hannon, M. J. *Macromolecules* **1999**, *32*, 8725.

(125) Garcia, M.; Kempe, K.; Haddleton, D. M.; Khan, A.; Marsh, A. *Polym. Chem.* **2015**, *6*, 1944.

(126) Takemoto, K.; Akashi, M.; Inaki, Y. *J. Polym. Sci., Polym. Chem. Ed.* **1974**, *12*, 1861.

(127) Akashi, M.; Kita, Y.; Inaki, Y.; Takemoto, K. *J. Polym. Sci., Polym. Chem. Ed.* **1979**, *17*, 301.

(128) Inaki, Y.; Sugita, S.-I.; Takahara, T.; Takemoto, K. *J. Polym. Sci., Part A: Polym. Chem.* **1986**, *24*, 3201.

(129) McHale, R.; Patterson, J. P.; Zetterlund, P. B.; O'Reilly, R. K. *Nature Chem.* **2012**, *4*, 491.

(130) Mather, B. D.; Baker, M. B.; Beyer, F. L.; Berg, M. A. G.; Green, M. D.; Long, T. E. *Macromolecules* **2007**, *40*, 6834.

(131) Khan, A.; Haddleton, D. M.; Hannon, M. J.; Kukulj, D.; Marsh, A. *Macromolecules* **1999**, *32*, 6560.

(132) Marsh, A.; Khan, A.; Garcia, M.; Haddleton, D. M. *Chem. Commun.* **2000**, 2083.

(133) Gulik-Krzywicki, T.; Fouquey, C.; Lehn, J. *Proc. Natl. Acad. Sci. U. S. A.* **1993**, *90*, 163.

(134) Sivakova, S.; Wu, J.; Campo, C. J.; Mather, P. T.; Rowan, S. J. *Chem. Eur. J.* **2006**, *12*, 446.

(135) Burke, K. A.; Sivakova, S.; McKenzie, B. M.; Mather, P. T.; Rowan, S. J. *J.*

Polym. Sci., Part A: Polym. Chem. **2006**, *44*, 5049.

(136) Sivakova, S.; Rowan, S. J. *Chem. Commun.* **2003**, 2428.

(137) Tao, Y.; Satoh, K.; Kamigaito, M. *Macromol. Rapid Commun.* **2011**, *32*, 226.

(138) Ilhan, F.; Galow, T. H.; Gray, M.; Clavier, G.; Rotello, V. M. *J. Am. Chem. Soc.* **2000**, *122*, 5895.

(139) Drechsler, U.; Thibault, R. J.; Rotello, V. M. *Macromolecules* **2002**, *35*, 9621.

(140) Thibault, R. J.; Hotchkiss, P. J.; Gray, M.; Rotello, V. M. *J. Am. Chem. Soc.* **2003**, *125*, 11249.

(141) Spijker, H. J.; Dirks, A. J.; van Hest, J. C. M. *J. Polym. Sci., Part A: Polym. Chem.* **2006**, *44*, 4242.

(142) Sivakova, S.; Bohnsack, D. A.; Mackay, M. E.; Suwanmala, P.; Rowan, S. J. *J. Am. Chem. Soc.* **2005**, *127*, 18202.

(143) South, C. R.; Weck, M. *Macromolecules* **2007**, *40*, 1386.

(144) Lo, P. K.; Sleiman, H. F. *J. Am. Chem. Soc.* **2009**, *131*, 4182.

Chapter 2. Effect of complementary nucleobase interactions on the copolymer composition of RAFT copolymerizations

2.1 Abstract

Methacryloyl-type monomers containing adenine and thymine have been successfully synthesized with reasonable yields (≥ 60%). The homopolymerization and copolymerization of these two new functional monomers were carried out using RAFT polymerization. The reactivity ratios of monomer pairs were measured and calculated using a non-linear least squares (NLLS) method and the results confirmed that the monomer reactivities were dependent on the solvent used for polymerization. The presence and absence of hydrogen-bonding in different solvents affected the resultant copolymer composition, where moderate alternating copolymers showed a tendency to form in $CHCl_3$, while in DMF statistical copolymers were formed. Furthermore, glass transition temperatures of copolymers synthesized in different solvents were investigated and the self-assembly of the various block copolymers made in solvents with different polarity was studied.

2.2 Introduction

It is known that chain-growth copolymerizations (*e.g.* ionic or radical polymerizations) are generally statistical processes leading to statistical polymer structures.[1,2] However, in some particular cases, composition can be controlled through manipulation of the reactivity of the active chain ends. One way to achieve this manipulation is to shorten the distance between a chain end and a monomer or between monomers by specific covalent[3] or noncovalent interactions, such as host-guest interactions,[4] donor-acceptor interactions,[5,6] coordination bonding[7] and hydrogen bonding of nucleobases.[8,9] Among these interactions, hydrogen bonding recognition interactions, as a fundamental property of nucleic acids, are of great interest.[10]

Hydrogen bonding interactions of corresponding nucleobases play a key role in nature for synthesizing biopolymer with an exact complementary sequence, which is the same length as the original template, and for mediating the self-assembly of biomacromolecules to fold into one or more specific spatial conformations.[10] Inspired by nature, synthetic nucleobase chemistry[11-13] has been developed to control the polymers' tacticity,[14] template polymerizations,[15-18] achieve a biomimetic segregation/templating approach to polymerizations,[19] drive self-assembly[20,21] and manipulate polymer composition.[8,9] This pioneering work has provided preliminary scope for further investigation into nucleobase materials.[12] However, to our knowledge, there has been little research into copolymer composition of polymerizations driven by complementary nucleobases. Previous reports from the 1970s' have indicated that methacryloyl-type monomers containing nucleobases (in this work uracil/thymine and adenine) can be polymerized using free radical polymerization to access alternating polymers.[8,9] Since these reports, no further work

has explored this observation. Given the recent advances in characterization, polymerization and monomer reactivity ratios, we have thus revisited this system.

Controlled radical polymerizations, such as nitroxide-mediated radical polymerization (NMP)[19,22] and atom transfer radical polymerization (ATRP),[18,23-26] have been employed to prepare well-defined nucleobase-containing polymers. However, there have been few reports where reversible addition-fragmentation chain transfer (RAFT) polymerization has been used to prepare polymers containing nucleobases directly.[14,19] As RAFT polymerization appears to be one of the most versatile process in terms of the mild reaction conditions, the variety of monomers that can be polymerized and the feasibility for the incorporation of various functionalities,[27-29] hence, in this Chapter, one goal is to study the synthesis of polymers containing nucleobase functionalities *via* RAFT technique, which can enrich the synthesis of nucleobase polymers. In addition, copolymerization behaviors of the nucleobase monomers were studied in solvents with different capabilities of hydrogen bonding tolerance ($CHCl_3$ and DMF). The reactivity ratios of the two monomers in both $CHCl_3$ and DMF were estimated. Moreover, the physical properties and the self-assembly behavior of the copolymers synthesized in different solvents were also investigated.

2.3 Results and discussions

2.3.1 Monomer synthesis

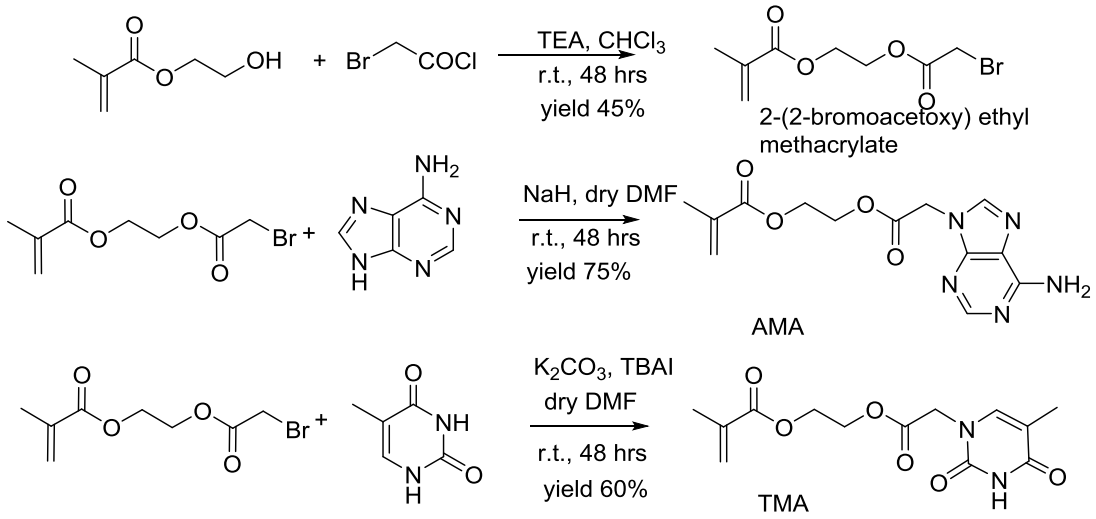

Scheme 2.1 Synthetic route for the monomers: adenine (AMA) and thymine (TMA) methacrylate.

The monomers were synthesized according to a modification of a previous report (Scheme 2.1).[25] These two monomers, 2-(2-(adenine-9-yl)acetoxyl) ethyl methacrylate (AMA) and 2-(2-(thymin-1-yl)acetoxyl) ethyl methacrylate (TMA), were obtained in a relatively high yield compared to previous literature (38% for thymine methacrylate and 69% for adenine methacrylate), which is due to the incorporation of the C=O bond that indeed makes the C-Br bond more reactive. More specifically, two low-energy empty orbitals (π* of the C=O bond and σ* of the C-Br bond) are combined to form a new molecular LUMO (π*+ σ*) which has lower energy than either.[30] Nucleophilic attack occurs easily and therefore yields are improved.

The monomers were firstly characterized by ^{1}H NMR and ^{13}C distortionless enhancement by polarization transfer (DEPT) spectroscopy (Figure 2.1 and Figure 2.2), where all the peaks were successfully assigned. Peaks at 6.13 ppm and 5.62 ppm corresponded to the protons of double bonds. In addition, the characteristic

peaks for both purine and pyrimidine were observed in the downfield area (between 6.50 ppm and 8.50 ppm). Elemental analysis, mass spectrometry, and two-dimensional NMR spectroscopy (correlated spectroscopy (COSY), heteronuclear multiple-bond correlation (HMBC), and heteronuclear multiple-quantum coherence (HMQC)) were also used to confirm the monomer structures, proving a successful synthesis.

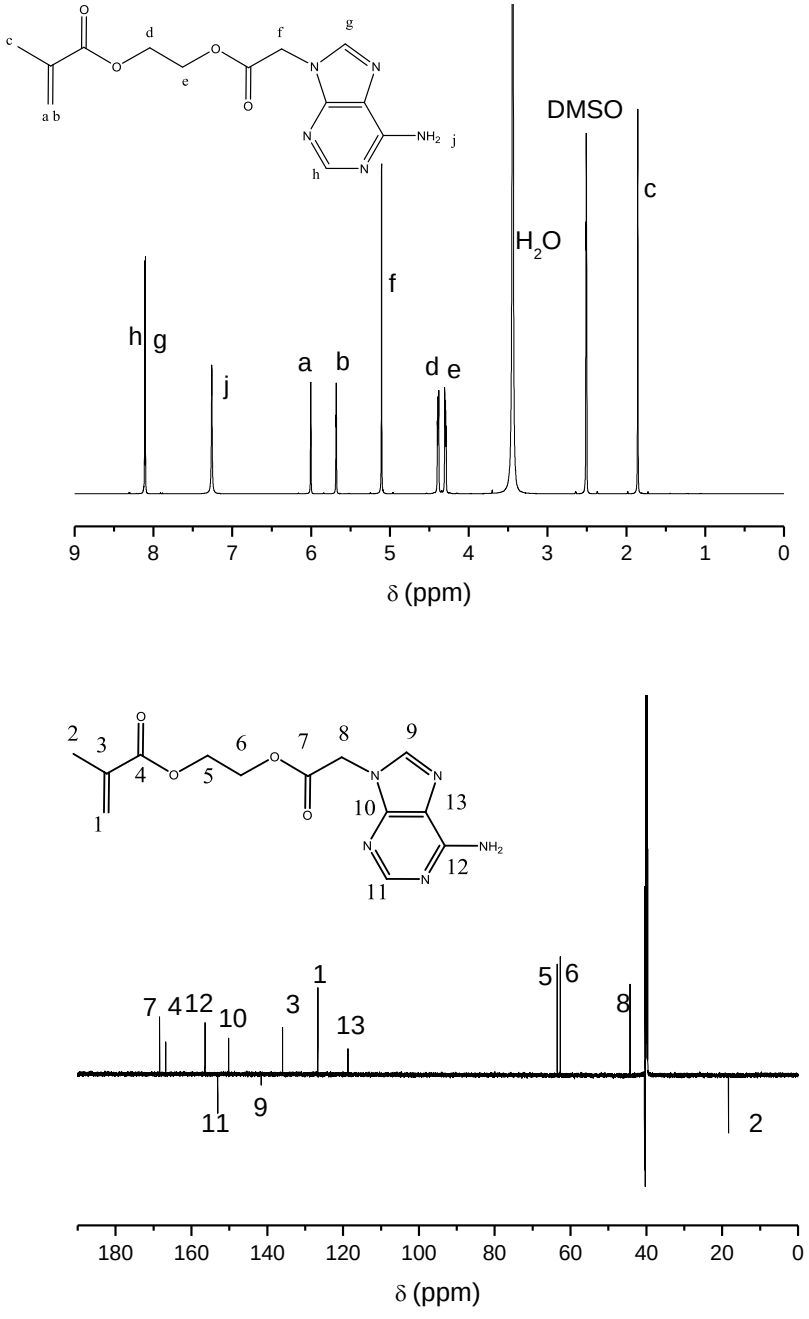

Figure 2.1 ^{1}H NMR and ^{13}C DEPT NMR spectra of AMA in DMSO-d_6.

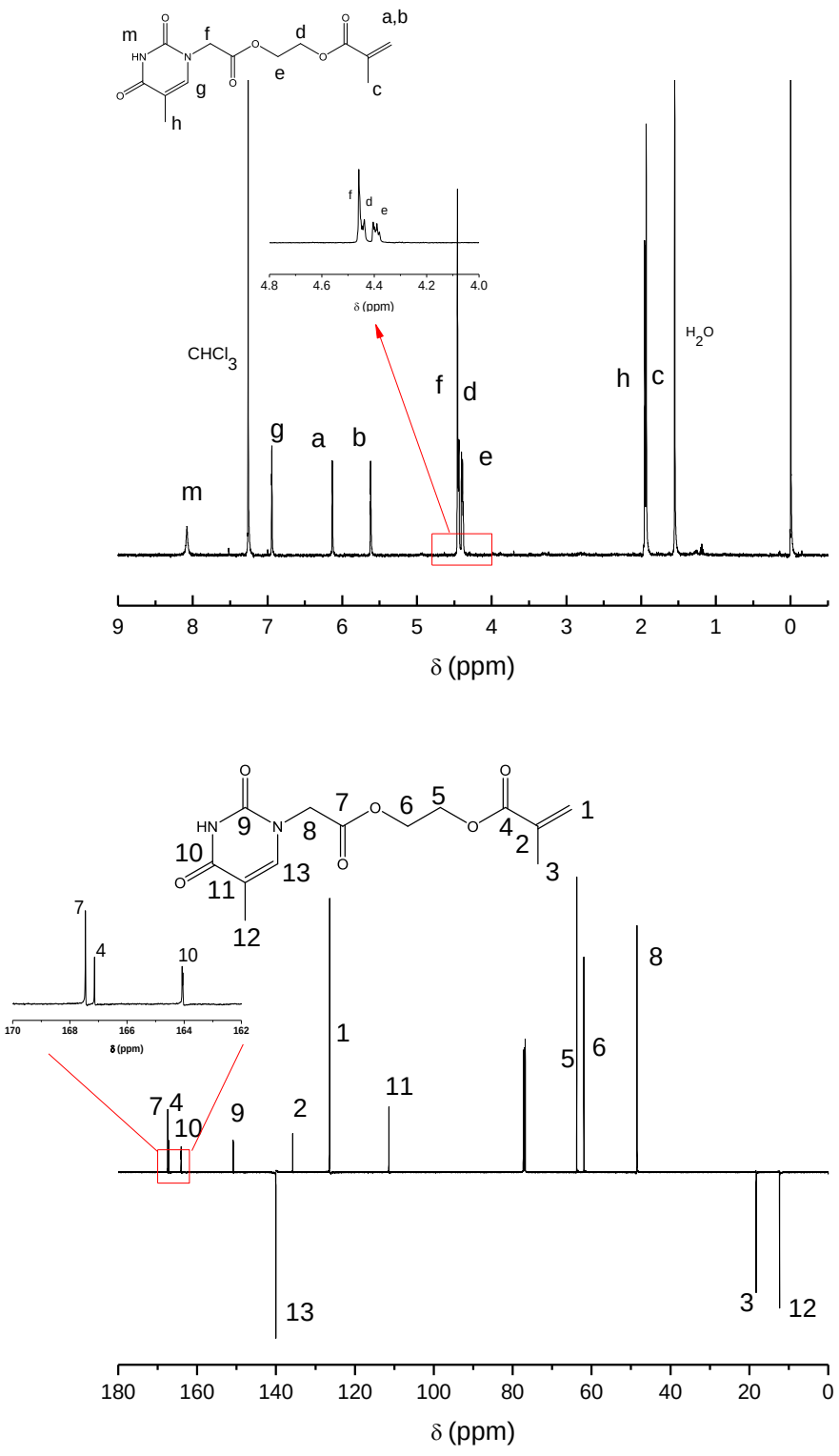

Figure 2.2 ^{1}H NMR and ^{13}C DEPT NMR spectra of TMA in $CDCl_3$.

2.3.2 Monomer interactions

One of the most important features of nucleobases is their ability to hydrogen bond to each other forming a base-base interaction pair.[10] For adenine and thymine this is

the result of hydrogen bonding interactions between the purine and pyrimidine functionalities (Figure 2.3, top). To investigate the hydrogen bonding interactions between the synthesized nucleobase monomers, AMA and TMA, mixtures at varying ratios of the two were studied by ^{1}H NMR spectroscopy at different temperatures. $CDCl_3$ and DMF-d_7 were selected as target solvents due to their different hydrogen-bonding parameters (hydrogen bonding acceptor ability, β, 0.8 for chloroform; 8.3 for amide (DMF); hydrogen bonding donor ability, α, 2.2 for chloroform and 2.9 for amide)[31] and the established differences in ability to suppress or promote hydrogen bonding interactions between nucleobases.[32] The ^{1}H NMR spectroscopic investigations were carried out at room temperature (25 °C) and at higher temperature (60 °C) to explore the strength of these interactions at the temperatures used for polymerization (Figure 2.3). In $CDCl_3$, it was observed that increasing the concentration of AMA resulted in a downfield shift of the imide proton of TMA (labelled * in Figure 2.3, from 8.28 ppm to 11.27 ppm at 25 °C, from 8.02 ppm to 9.80 ppm at 60 °C). The downfield shift at 25 °C was more prominent than at 60 °C, indicating that the hydrogen bonding interactions are weaker at elevated temperatures. Nevertheless, hydrogen bonding interactions still occur at elevated temperatures. In contrast, in DMF little or no shift of the imide proton of TMA was observed at 25 °C or 60 °C. This is indicative of the lack of nucleobase interactions even at room temperature. The weaker nucleobase interaction is expected as a result of the higher hydrogen bonding acceptor ability of DMF.[31-34]

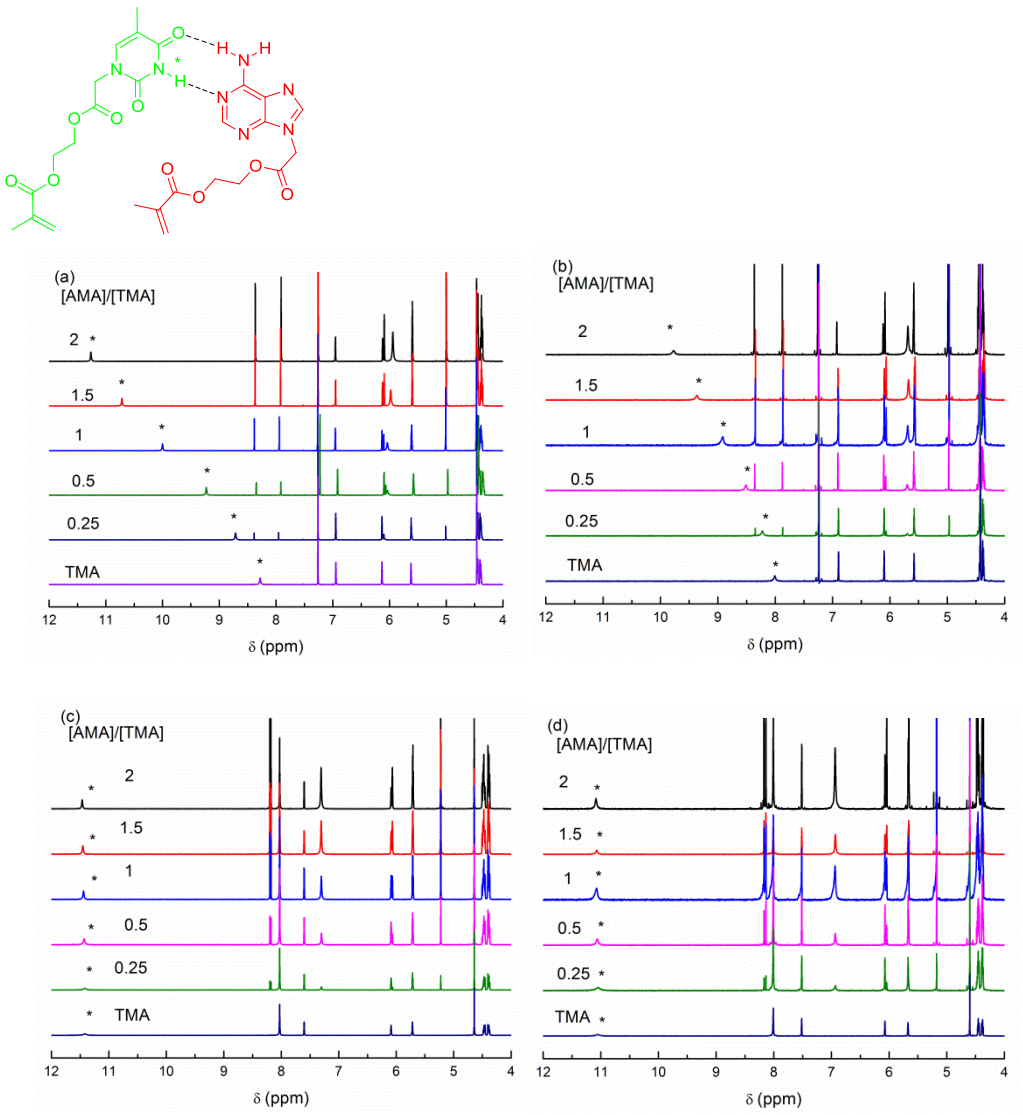

Figure 2.3 The expected hydrogen bonding interactions of the adenine-thymine pair is shown where the key imide signal used in the ^{1}H NMR spectroscopy study is indicated with a * (top); ^{1}H NMR spectra of the AMA and TMA mixtures with varying concentrations of AMA: [TMA] = 10 mM; [AMA] = 0, 2.5, 5, 10, 15, 20 mM. (a) $CDCl_3$, at 25 °C; (b) $CDCl_3$, at 60 °C; (c) DMF-d_7, at 25 °C; (d) DMF-d_7, at 60 °C.

The stoichiometry of the H-bonding complex was evaluated by Job's method under conditions similar to those for further copolymerizations (same monomer concentrations and temperature) (Figure 2.4). In this method, the total concentration of the two binding species was kept constant, but their mole fractions were varied. The signal that is proportional to the resultant complex (changes of chemical shift of imide proton of TMA × mole fraction of TMA ($\Delta\delta \times \chi_{TMA}$) in this study) is plotted against the mole fraction of the species. The results show the formation of a 1:1 complex between AMA and TMA in both $CDCl_3$ and DMF-d_7.[35]

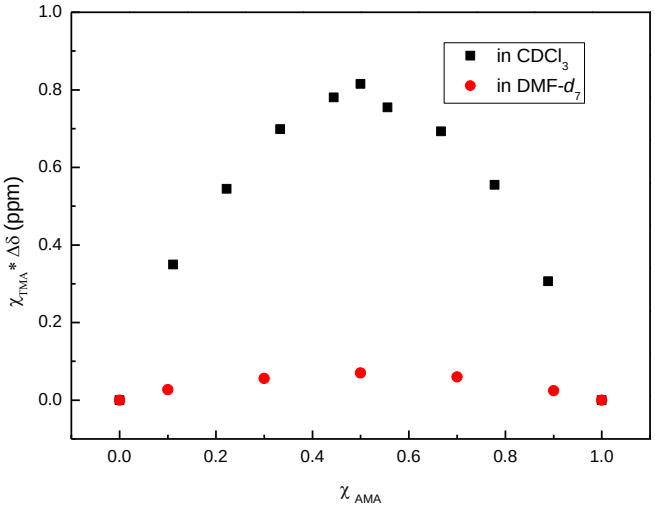

Figure 2.4 Job plots to determine the stoichiometry of complex of AMA and TMA in $CDCl_3$ ([AMA]+[TMA]= 40 mM) or DMF-d_7 ([AMA]+[TMA] = 200 mM) at 60 °C.

Moreover, the association constant between the two monomers was calculated using Hildebrand-Benesi model, where the inverse of changes of chemical shift is plotted again the inverse of mole fraction of AMA (Figure 2.5).[36,37] The measured association constants were 20 M^{-1}, which was consistent with the value in the literature[38] in $CDCl_3$ at 60 °C and *ca.* 0 M^{-1} in DMF-d_7 at 60 °C. It suggests that monomer interactions in $CDCl_3$ are much stronger than those in DMF-d_7. These studies further reveal that the hydrogen bonding interactions between the two monomers are solvent dependent.

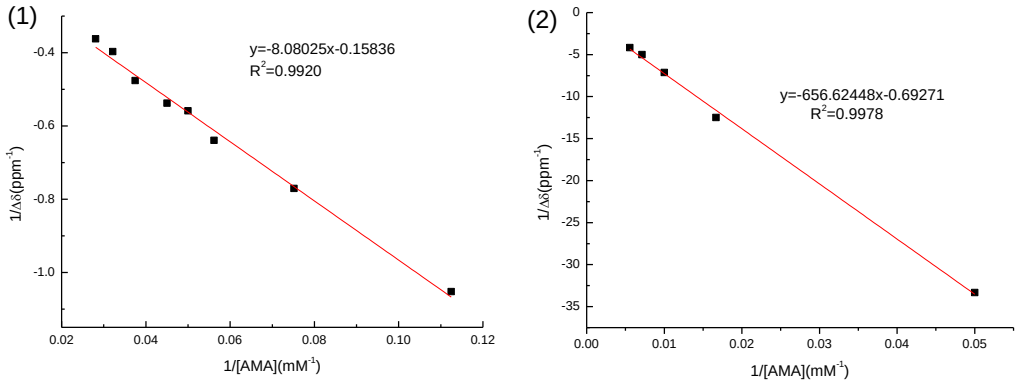

Figure 2.5 Hildebrand – Benesi plots based on 1:1 complex of AMA and TMA (1) in $CDCl_3$, (2) in DMF-d_7 at 60 °C. $1/\Delta\delta = 1/(K_a\Delta\delta_{max}[AMA]) + 1/\Delta\delta_{max}$. In $CDCl_3$, $1/\Delta\delta_{max}$ = -0.15836, $1/K_a\Delta\delta_{max}$ = -8.08025, K_a = 20 M^{-1}; In DMF-d_7, $1/\Delta\delta_{max}$ = -0.69271, $1/K_a\Delta\delta_{max}$ = -656.62448, $K_a \approx 0$ M^{-1}.

2.3.3 Homopolymerization

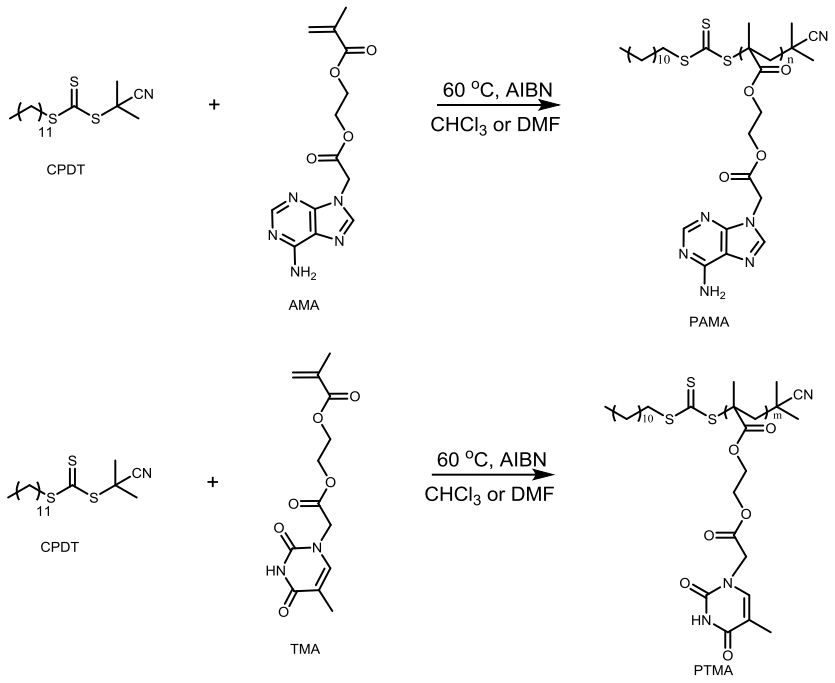

Scheme 2.2 Synthetic route for PAMA and PTMA homopolymers.

After the successful synthesis of the nucleobase monomers, the homopolymerizations of AMA and TMA with a target DP of 40 were explored using established RAFT methods.[19] RAFT polymerization was carried out using 2-cyano-2-propyl dodecyl trithiocarbonate (CPDT) as the chain transfer agent (CTA), DMF or $CHCl_3$ as the solvent, and AIBN as the initiator (Scheme 2.2). The polymerization in DMF was found to be homogeneous, suggesting a strong interaction between the nucloebase functionalities and the solvent exists. However, when $CHCl_3$ was used as the solvent, the polymerization was found to be heterogeneous due to the insolubility of the polymer, leading to relatively low monomer conversions (40% for AMA and 68% for TMA). The molecular weight of the resultant polymers were determined by ^{1}H NMR spectroscopy by comparing the integration of the backbone signals with those of the end group from the CTA. Furthermore, SEC (DMF as eluent, PMMA as standards) was used to determine the molecular weight and molecular weight distribution. It was observed that all the homopolymers were generally with narrow

molecular weight distributions (*ca.* 1.20) except thymine-containing polymer (PTMA) synthesized in chloroform that possessed high molecular weight distribution ($Đ_M$ = 1.86). RAFT polymerization of thymine-containing monomers would be further studied and discussed in Chapter 4.

Table 2.1 Characterization data for PAMA and PTMA homopolymers

Polymer	Solvent	Conv. (%)	$M_{n,\,th}$ (kDa)	$M_{n,\,NMR}$[a] (kDa)	$M_{n,SEC}$[b] (kDa)	$Đ_M$[c]
PAMA,**a**	DMF	90	11.0	12.2	15.0	1.19
PAMA,**b**	$CHCl_3$	40	4.9	9.8	14.4	1.21
PTMA,**c**	DMF	85	10.5	12.0	12.9	1.19
PTMA,**d**	$CHCl_3$	68	8.1	19.8	20.4	1.86

[a]determined by ^{1}H NMR spectroscopy in DMF-d_7; [b, c]determined by SEC analysis (DMF as eluent, PMMA as standards).

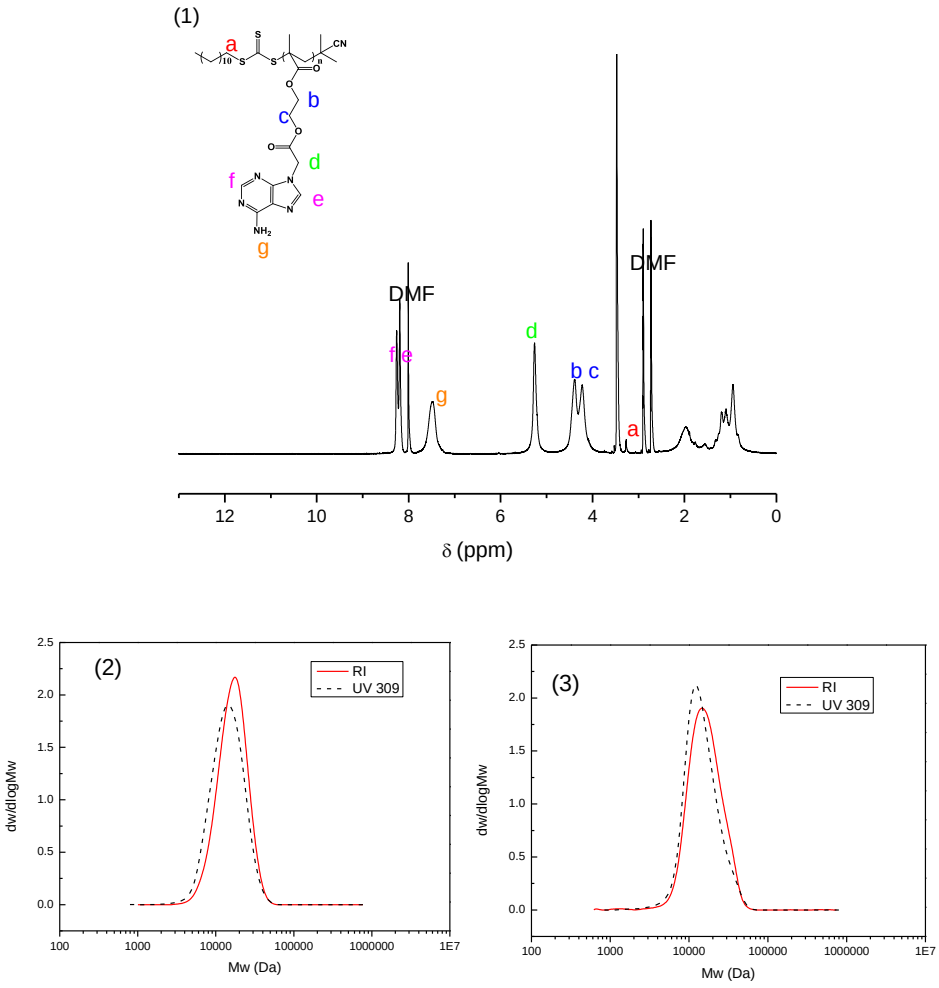

Figure 2.6 (1) ^{1}H NMR spectrum of PAMA, **a** in DMF-d_7; (2) SEC trace of PAMA, **a** synthesized in DMF (DMF eluent, PMMA standards); (3) SEC trace of PAMA, **b** synthesized in $CHCl_3$ (DMF eluent, PMMA standards).

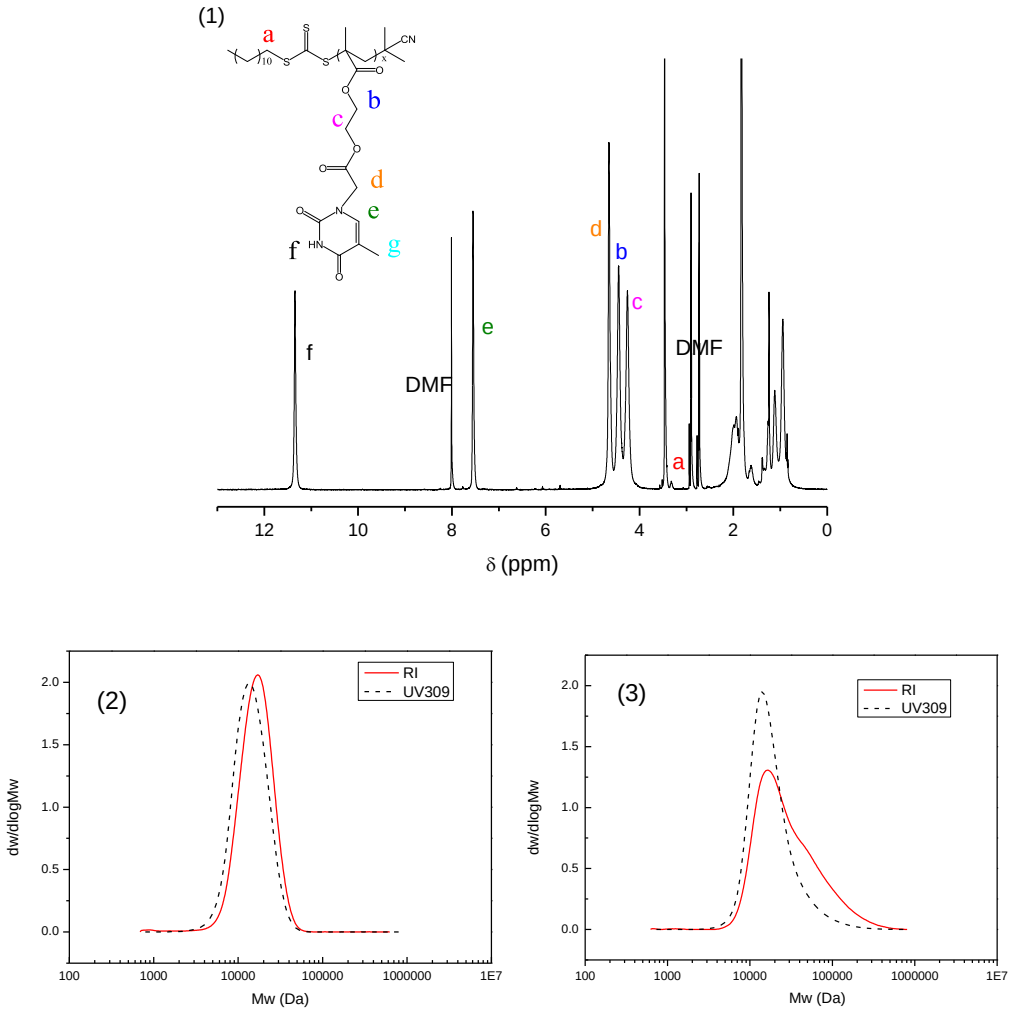

Figure 2.7 (1) ^{1}H NMR spectrum of PTMA, **c** in DMF-d_7; (2) SEC trace of PTMA, **c** synthesized in DMF (DMF eluent, PMMA standards); (3) SEC trace of PTMA, **d** synthesized in $CHCl_3$ (DMF eluent, PMMA standards).

Both homopolymerizations carried out in DMF were polymerized with good control over molecular weights and high conversions were obtained after 24 h (Table 2.1). The SEC traces for both homopolymers (PAMA and PTMA) were found to be narrow indicating a narrow molecular weight distribution. Additionally, RAFT chain end functionalities were quantified by ^{1}H NMR spectroscopy, where the peak at δ = 3.32 ppm corresponds to CH_2 group next to the trithiocarbonate (Table 2.1, Figure 2.6(1) and Figure 2.7(1)), confirming good RAFT group chain end fidelity. Polymerizations carried out in $CHCl_3$ on the other hand, were found to be less controlled due to polymer precipitation during the polymerization process (Table 2.1,

Figure 2.6(3) and Figure 2.7(3)). Nevertheless, the polymers were found to be more controlled than those synthesized *via* traditional free radical polymerization methods.[8,15]

It should be noted that the solubility of the resultant homopolymers is somewhat limited but were found to be soluble in DMF, DMSO, dimethylacetamide (DMAc), and *N*-methyl-2-pyrrolidone (NMP). An adenine containing methacrylate polymer, which had different polymer structure and was prepared by free radical polymerization, has previously been reported to be insoluble in DMF and pyridine,[8] but this study has shown that the PAMA prepared in our work is fully soluble in DMF at relatively low molecular weights (*i.e.* < 15 kDa).

2.3.4 Copolymerizations

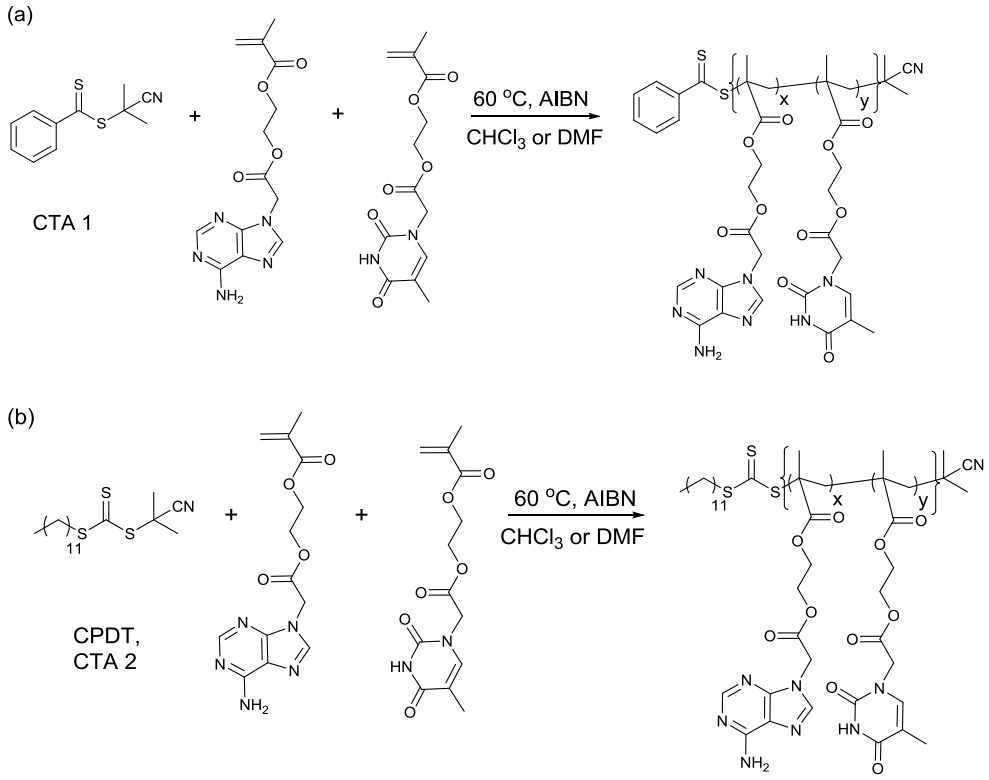

Scheme 2.3 Synthesis of (a) copolymers PAMA-*co*-PTMA using CTA 1; (b) copolymers PAMA-*co*-PTMA using CTA 2 in $CHCl_3$ or DMF.

To explore the effect of solvent on the composition of the resulting copolymers of AMA and TMA, further studies were carried out in both $CHCl_3$ and DMF. Two different CTAs, 2-cyano-2-propyl benzodithioate (CTA 1) and 2-cyano-2-propyl dodecyl trithiocarbonate (CPDT, CTA 2), were used for the copolymerizations of AMA/TMA (Scheme 2.3) to confirm the observed results were in fact related to the different solvents (DMF and $CHCl_3$) used in the polymerization and not an effect of the CTA. Copolymerizations were performed at 60 °C with AIBN as the radical initiator. Following the polymerization, the conversions of each monomer were determined using ^{1}H NMR spectroscopy. Furthermore, the final copolymers were dissolved in DMSO-d_6 or DMF-d_7 and the ratio of the two monomers in the resultant copolymer was calculated using ^{1}H NMR spectroscopy by comparing the integration of the backbone signals from PAMA with those from PTMA. All the characterization data for polymers **1** - **8** is summarized in Table 2.2 and Figures 2.8 and 2.9.

Table 2.2 Polymerization data for AMA/TMA copolymers

Polymer	CTA	Solvent	AMA:TMA (before)[a]	AMA:TMA (after)[b]	Conv. (%)[c]	$M_{n,\,th}$ (kDa)	$M_{n,NMR}$ (kDa)[d]	$M_{n,SEC}$ (kDa)[e]	$Đ_M$	Copolymer composition (PAMA:PTMA)
1	1	$CHCl_3$	1:1	1.1:1	48, 50	5.7	7.9	10.8	1.23	~ 1:1
2	1	$CHCl_3$	2:1	2.9:1	39, 58	6.3	9.6	11.4	1.26	1.25:1
3	1	DMF	1:1	1:1	43, 43	5.7	6.0	11.0	1.11	1:1
4	1	DMF	2:1	2:1	27, 27	3.7	5.4	10.7	1.12	2:1
5	2	$CHCl_3$	1:1	1.1:1	70, 75	10.0	13.2	16.1	1.37	~ 1:1
6	2	$CHCl_3$	1.9:1	2.9:1	51, 68	7.6	18.0	21.3	1.38	1.4:1
7	2	DMF	1:1	1:1	92, 92	12.7	14.1	17.0	1.22	1:1
8	2	DMF	2:1	2:1	60, 60	8.1	9.0	14.7	1.23	2:1

[a]the ratio of monomers in initial feed;
[b]the ratio of residual monomers after polymerization;
[c]the final conversion of AMA (first number) and the final conversion of TMA (second number);
[d]determined by ^{1}H NMR spectroscopy in DMSO-d_6 and DMF-d_7;
[e]determined by SEC analysis (DMF as eluent, PMMA as standards).

In the polymerizations using CTA 1, where the initial feed mol fraction of the two monomers was 1:1, the conversions of AMA and TMA monomers were the same in each condition. In addition, the resulting mole fraction in the copolymers (**1** and **3**) was very close to 1:1 regardless of the solvent used. However, when the mole fraction of the two monomers in the initial feed was changed to 2:1 (AMA:TMA, polymerizations **2** and **4**), a difference in the mole fraction in the resulting copolymers was observed. The final copolymer composition was found to be dependent on the solvent used in the polymerization. When the polymerization was carried out in DMF, the monomer conversions of AMA and TMA were the same and the final copolymer composition for **4** was found to be very close to 2:1. However, in $CHCl_3$, the conversion of AMA monomer (39%) was less than that of TMA (58%) and the ratio of the two monomers in the final copolymer **2** was found to be around 1.25:1. These results indicate copolymers with different microstructures can be synthesized when using the two different solvent systems.

Similar results were observed for the CTA 2, indicating the final polymer composition is independent of the type of CTA used. Hence, in $CHCl_3$, regardless of the initial monomer ratios the final polymer synthesized (**5** and **6**) tends to have a 1:1 composition of the two monomers. In contrast, in DMF the final polymer composition is the same as the initial monomer feed (for CTA 2, polymers **7** and **8**). As previously discussed, hydrogen bonding interactions were observed between AMA and TMA in $CHCl_3$ at 60 °C, while little or no interactions were observed in DMF at the same temperature. We propose that the presence or absence of such interactions between monomers during polymerization has an effect on the resulting copolymer composition. In addition, interactions between monomers and polymers can also affect the copolymer composition, which have been observed by Marsh and

coworkers in the previous literature.[15] In the literature, interactions between polymers and monomers can lead to the formation of polymer complexes with a 1:1 ratio of the two species.

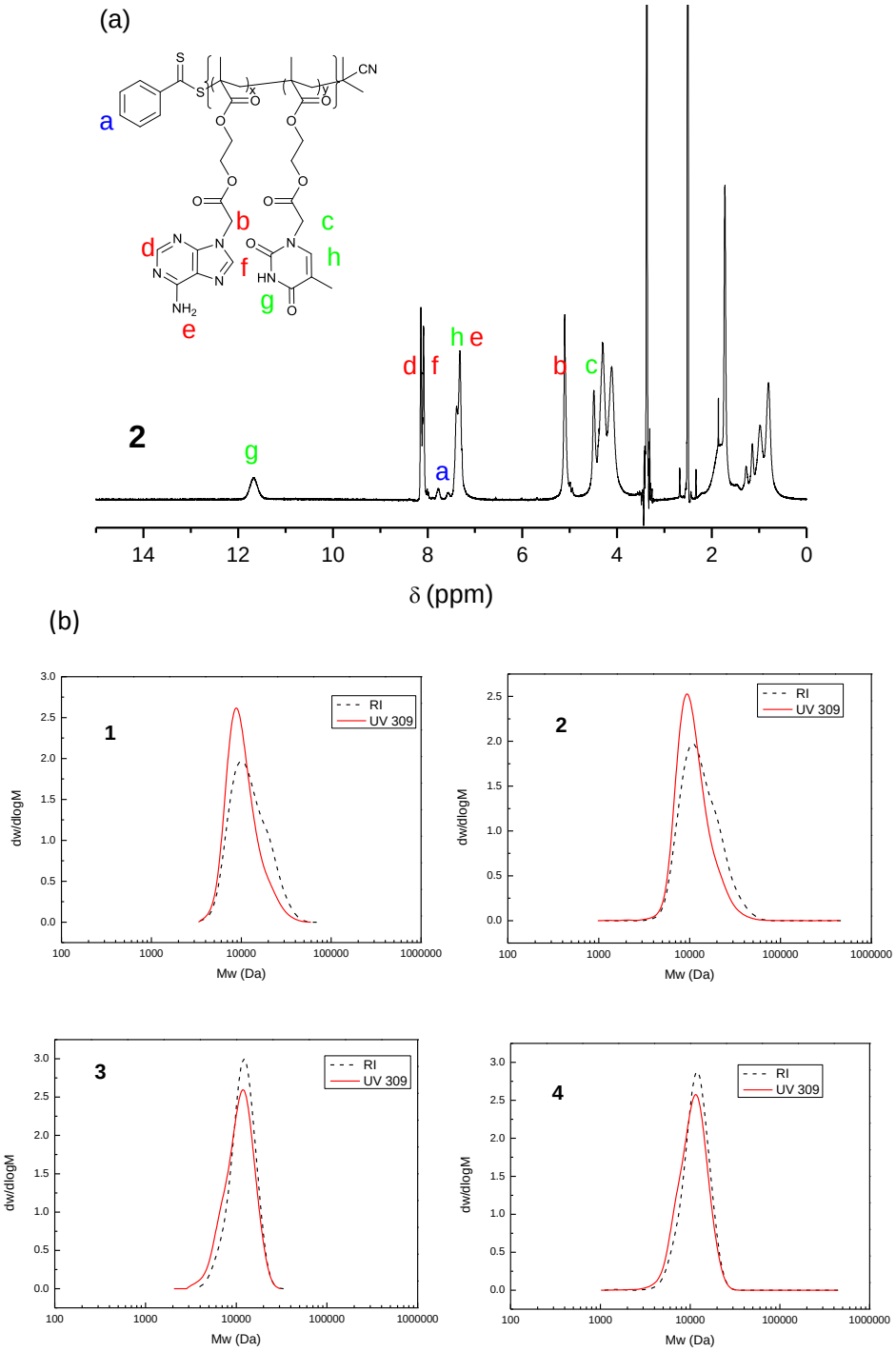

Figure 2.8 Structure of copolymer PAMA-*co*-PTMA and ^{1}H NMR spectra of copolymers (copolymer **2**) in DMSO-d_6 (a); SEC chromatograms of copolymers (copolymer **1** - **4**) (DMF eluent, PMMA standards) (b).

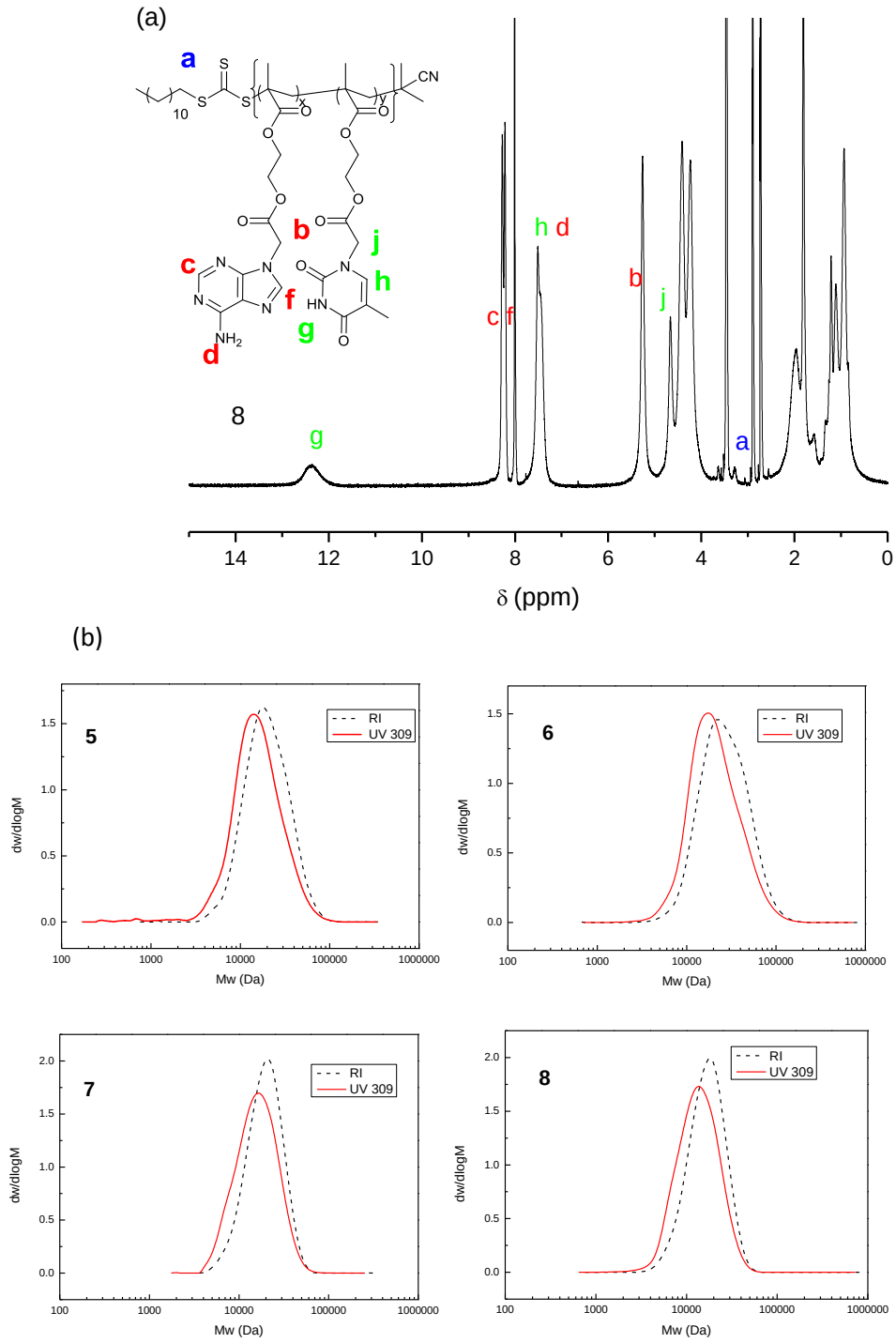

Figure 2.9 Structure of copolymer PAMA-*co*-PTMA and ^{1}H NMR spectra of copolymers (copolymer **8**) in DMF-d_7 (a); SEC chromatograms of copolymers (copolymer **5** - **8**) (DMF eluent, PMMA standards) (b).

CTA 1 was selected as it is a good CTA for the polymerization of methacrylate monomers. Furthermore, characteristic signals from the end group can be seen clearly by ^{1}H NMR spectroscopy and these can be used to determine the number

average molecular weight of polymers by ^{1}H NMR spectroscopy *via* the comparison between the backbones of the polymers and the end group. However, it was found that the conversions of polymerizations performed in DMF using CTA 1 were not readily reproduced. We assumed that CTA 1 was very sensitive to the quality of DMF. Sometimes the color of the CTA/DMF solution was observed to change from pink to orange after 1 day while the solution color always stayed pink in $CHCl_3$. Previous studies have reported that dithiobenzoates are more sensitive to hydrolysis and decomposition than trithiocarbonates.[39] In addition, trithiocarbonates are more preferred in the previous literature to polymerize monomers containing amine or amide functionalities.[14,40] Thus, although some insightful results have been obtained using CTA 1 in DMF, in order to eliminate the instability caused by CTA 1, further studies were carried out utilizing CTA 2 for polymerizations performed in DMF.

Copolymers were also analyzed by SEC analysis (DMF as eluent, PMMA as standards). In general, all the copolymers obtained were with narrow molecular weight distributions (< 1.40). However, due to polymer precipitation during the polymerization process in $CHCl_3$, the copolymers synthesized in $CHCl_3$ had broader dispersities than those prepared in DMF.

2.3.5 Reactivity ratios

In order to further explore the behavior of AMA and TMA copolymerizations, the monomer reactivity ratios were investigated. Mole fractions of the two monomers in the initial feed and in the final copolymers were obtained by ^{1}H NMR spectroscopic analysis. A representative ^{1}H NMR spectrum of a mixture of AMA and TMA is shown below in Figure 2.10. The mole fraction of the two monomers in the initial feed was obtained by comparing the integral of signal '1' and signal 'a' before polymerization. After polymerization, most of the signals (except double bonds)

became broader or shifted. Signals ‘f + g’ or ‘e’ comparing with ‘a’ were used to calculate the conversion of AMA, while conversion of TMA was determined by comparing signal ‘7’ with ‘1’ which is a common method in the reference as signals of TMA and polymer are overlapped except pyrimidine-*N*H ‘7’.[41] In addition, by comparing signal ‘1’ and ‘a’ before and after polymerizations, monomer conversions and copolymer compositions were also obtained, which were consistent with the conversions determined using pyrimidine-*N*H signals. All the data obtained is summarized in Tables 2.3 - 2.5.

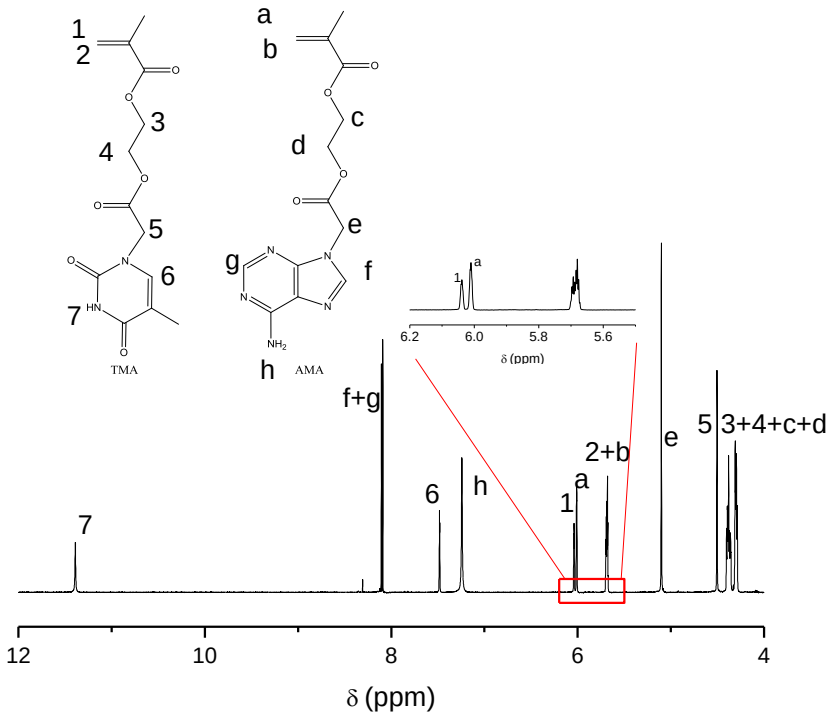

Figure 2.10 ^{1}H NMR spectrum of a mixture of AMA and TMA before polymerization in DMSO-d_6.

Table 2.3 Mole fraction of monomers in initial feed and copolymers using CTA 2 in DMF

Mole fraction in initial feed (TMA:AMA)	Mole fraction in copolymer (TMA:AMA)	Conv. (%)
10:90	13:87	10
20:80	18:82	13
32:68	34:66	11
40:60	40:60	7
49:51	49:51	5
59:41	59:41	13
69:31	70:30	4
79:21	79:21	5
90:10	92:8	8

Table 2.4 Mole fraction of monomers in initial feed and copolymers using CTA 2 in $CHCl_3$

Mole fraction in initial feed (TMA:AMA)	Mole fraction in copolymer (TMA:AMA)	Conv. (%)
10:90	32:68	5
20:80	36:64	5
31:69	40:60	4
39:61	52:48	13
51:49	55:45	11
59:41	56:44	8
69:31	60:40	6
80:20	66:34	7
89:11	67:33	9

Table 2.5 Mole fraction of monomers in initial feed and copolymers using CTA 1 in $CHCl_3$

Mole fraction in initial feed (TMA:AMA)	Mole fraction in copolymer (TMA:AMA)	Conv. (%)
12:88	31:69	4
21:79	38:62	6
30:70	42:58	11
41:59	55:45	6
50:50	52:48	9
60:40	59:41	11
69:31	62:38	9
78:22	63:37	11
89:11	64:36	7

Plots of f_1 (f_1 = initial mole fraction of monomer 1, M_1 = TMA) *vs* F_1 (F_1 = mole fraction of M_1 in the copolymer) are presented in Figure 2.11, highlighting the copolymer compositions. The reactivity ratios were calculated using Contour, a program based on a NLLS method developed by van Herk.[42-45] The calculated monomer reactivity ratios are shown in Table 2.6 and plots of 95% joint confidence intervals for the reactivity ratios are shown in Figure 2.12, which give an idea of the experimental error and the accuracy of the experimental data.[46] It should be noted that the joint confidence intervals are not always ellipsoidal or follow a normal distribution, depending on the linearity of the fitted equations.[45] In $CHCl_3$, regardless of the CTA used the reactivity ratios are comparable and close to zero (Table 2.6). The results suggest that the copolymerizations carried out in $CHCl_3$ tend to form alternating polymers, shown by the shape of the F_1 *vs* f_1 plot (Figure 2.11 (2) and (3)) and the reactivity ratios being close to zero. It should be noted that the investigated alternating behaviour of the copolymerization in $CHCl_3$ is not an extreme alternating behaviour (both r_1 and r_2 are zero in extreme alternating behavior) but a moderate alternating behaviour.[47] In DMF on the other hand, the reactivity ratios are close to one, suggesting statistical copolymers are most likely synthesized. This is supported by the shape of the F_1 *vs* f_1 plot (Figure 2.11(1)). The monomer reactivity ratio experiments further support that the presence and absence of nucleobase interactions have a strong influence on the final polymer composition which may be tuned by the choice of solvent.

In $CHCl_3$, the presence of hydrogen bonding interactions leads to alternating copolymers by holding complementary nucleobase pairs in close proximity to a propagation chain end. Both monomer-monomer interactions and a growing end unit-monomer interactions can be considered.[9] In comparison, in DMF, as there are

little interactions between nucleobase units, statistical polymerizations are most likely to occur. It should be noted that polymerization conversions were kept low in this reactivity study (< 15%), therefore, the interactions between polymers and monomers, which could lead to the formation of polymer complexes as mentioned above, should be not very obvious although still present and thus have a weak effect on the resulting copolymer composition. However, this effect should be considered for polymerizations with a high monomer conversion.

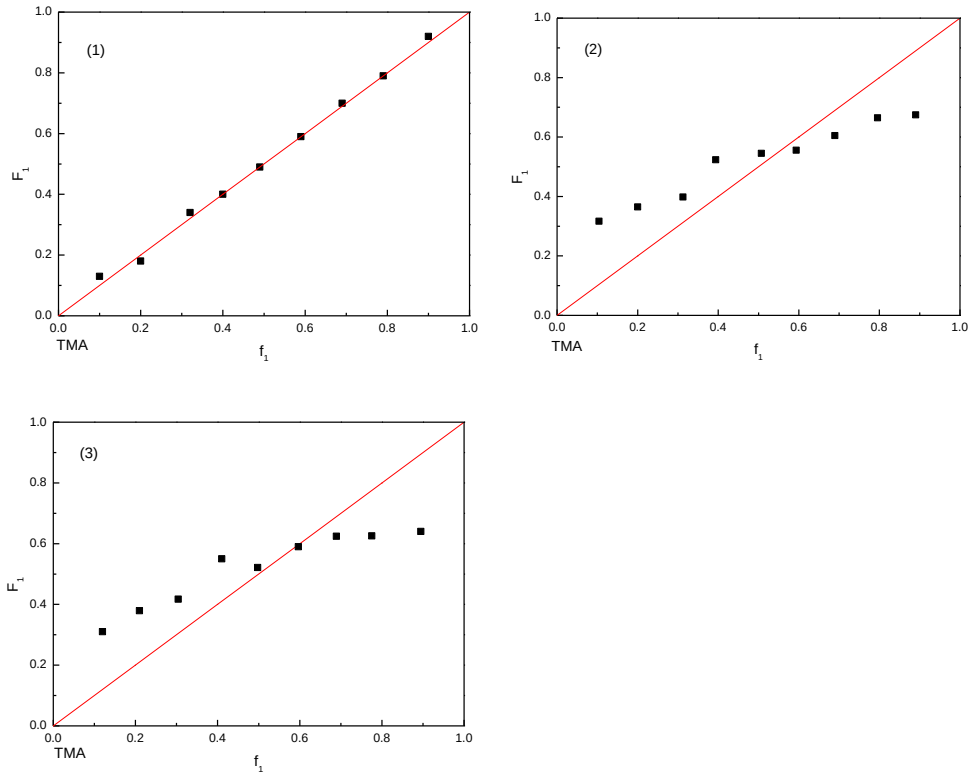

Figure 2.11 Plots of F_1 *vs* f_1 for the copolymerization of TMA and AMA using (1) CTA 2, in DMF; (2) CTA 2, in $CHCl_3$; (3) CTA 1, in $CHCl_3$ (the red line is the plot of F_1*vs* f_1 for an ideal polymerization, where $r_1 = r_2 = 1$).

Table 2.6 Calculated reactivity ratios (r_1 and r_2) using a non-linear least squares (NLLS) method.

CTA	solvent	M_1[a]	M_2[b]	r_1	r_2	r_1*r_2	error[c]
CTA 2	DMF	TMA	AMA	0.89	0.88	0.78	5%
CTA 2	$CHCl_3$	TMA	AMA	0.23	0.17	0.039	6%
CTA 1	$CHCl_3$	TMA	AMA	0.21	0.17	0.036	6%

[a]M_1 is monomer 1; [b]M_2 is monomer 2; [c]average relative error given by the Contour program.

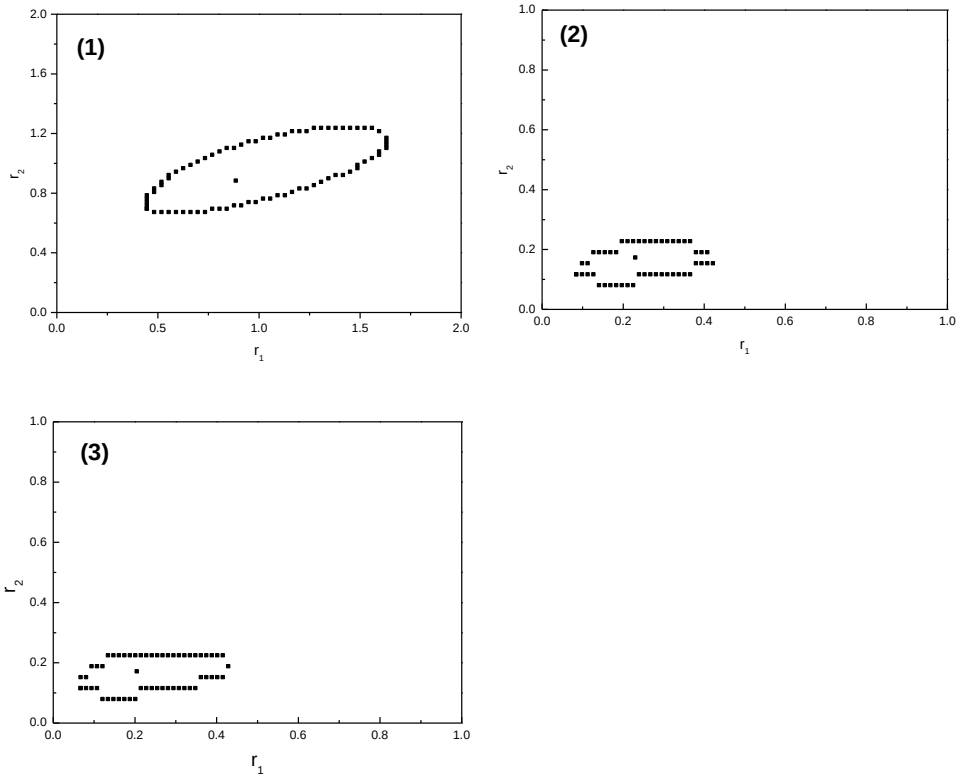

Figure 2.12 Plots of 95% joint confidence intervals for the reactivity ratios (1) CTA 2, in DMF; (2) CTA 2, in $CHCl_3$; (3) CTA 1, in $CHCl_3$.

2.3.6 Thermal properties

After the successful synthesis of adenine and thymine containing polymers, the thermal properties of the resultant polymers were also investigated. The glass transition temperature (T_g) of both homopolymers and copolymers were measured by differential scanning calorimetry (DSC) (Figure 2.13 and Table 2.7). In general, the T_g of a copolymer is between the T_g of the two mother polymers and can be predicted by the Fox equation (Equation 2.1):[48]

$$\frac{\mathbf{1}}{\boldsymbol{T_g}} = \frac{\boldsymbol{w_1}}{\boldsymbol{T_{g,1}}} + \frac{\boldsymbol{w_2}}{\boldsymbol{T_{g,2}}} \quad \text{Equation 2.1}$$

where w_1 and w_2 are the weight fractions of components 1 and 2, respectively; T_g, $T_{g,1}$ and $T_{g,2}$ are the glass transition temperatures of copolymer, components 1 and 2, respectively. However, in terms of specific interactions within a copolymer, such as hydrogen bonding interactions, higher T_g would be expected.[49] In this study,

compared to the PAMA and PTMA homopolymers prepared with CTA 2 (PAMA **a** T_g = 102 °C, PTMA **c** T_g = 87 °C), the AMA/TMA copolymers exhibit strong hydrogen bonding interactions and therefore higher values of T_g were observed as expected (Table 2.7). The identity of the CTA end group may also affect the polymers' T_g.[50] Copolymers with CTA 2 as the end group (**5** and **7**) exhibited lower values of T_g than copolymers with CTA 1 as the end group (**1** and **3**), as CTA 2 is more flexible than CTA 1. However, due to the different molecular weights and end group fidelity among the copolymers, the T_g's are not directly comparable.

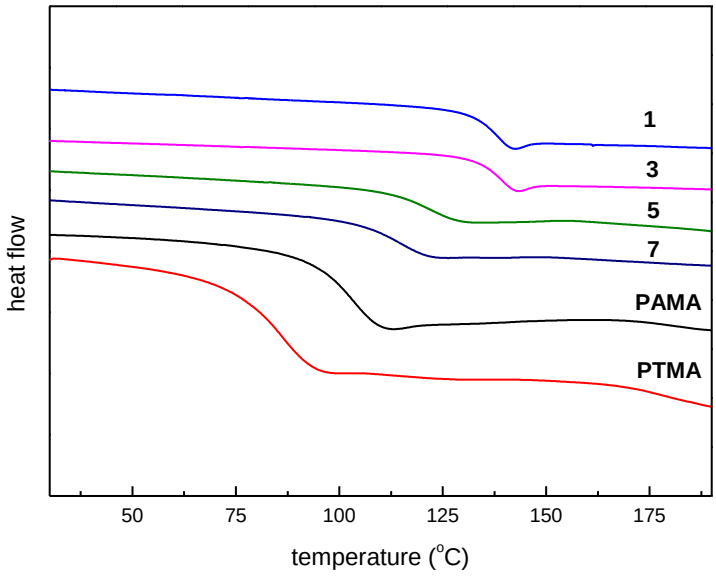

Figure 2.13 DSC second heating thermograms of homopolymers (**a** and **c**) and copolymers (**1**, **3**, **5** and **7**) with a heating rate of 5 °C/ min and cooling rate of 10 °C/min.

Table 2.7 T_g of nucleobase-containing polymers

Polymer	Nucleobase ratio (A:T)	Polymerization solvent	$M_{n,\,NMR}$ (kDa)	$M_{n,\,SEC}$ (kDa)	T_g (°C)
1	1:1	$CHCl_3$	7.9	10.8	137
3	1:1	DMF	6.0	11.0	138
5	1:1	$CHCl_3$	13.2	16.1	120
7	1:1	DMF	14.1	17.0	115
PAMA, **a**	1:0	DMF	12.2	15.0	102
PTMA, **c**	0:1	DMF	12.0	12.9	87

The effect on T_g of blending homopolymers PAMA (**a)** and PTMA (**c)** was also studied. Three blending methods were applied. The first one is called physical blending, where homopolymers PAMA (**a)** and PTMA (**c)** were mixed physically. The second method is solution - precipitation blending, where the two homopolymers were firstly both dissolved in DMF and then precipitated in methanol to obtain a resultant blended polymer. The last method is solution blending, where a 1:1 mixture of homopolymers PAMA and PTMA was dissolved in DMF and then the solvent was left to evaporate under a flow of compressed air. The resulting blended film was further dried in a vacuum oven at 40 °C. The DSC thermograms of the blended polymers are shown in Figure 2.14. The polymer mixture obtained by physical blending (T_g = 94 ^oC) had very broad bimodal peaks, implying that the blended polymer prepared by this method is less homogeneous. The other two methods gave very similar values of T_g (T_g = 105 ^oC), which is slightly higher than that of the blend prepared by physical blending. The possible reason for this observation is that by using solution assistant methods more homogeneous polymer complex can be formed and thus the interassociation interactions would be stronger. In addition, it should be noted that the blended polymers exhibited a single T_g, indicating the formation of miscible polymer complex.[51] It was also observed that the values of T_g of blended polymers prepared by solvent assistant methods are slightly higher than both PAMA and PTMA homopolymers, which is also higher than the value expected from Fox equation yet consistent with previous observations in the literatures.[15,49,51] In the literature, Marsh and coworker observed that owing to the presence of complementary hydrogen-bonding interactions, nucleobase complex prepared from a 1:1 mixture of adenine and thymine containing homopoloymers had higher T_g than both single components.[15] Finally, it should be note that the

copolymers (**5** and **7**) possess higher T_g than the blending mixtures as expected. This observation has been reported[15,49] and can be reasonably explained by differences in the degree of rotational freedom due to an intramolecular screening and spacing effect.[52,53]

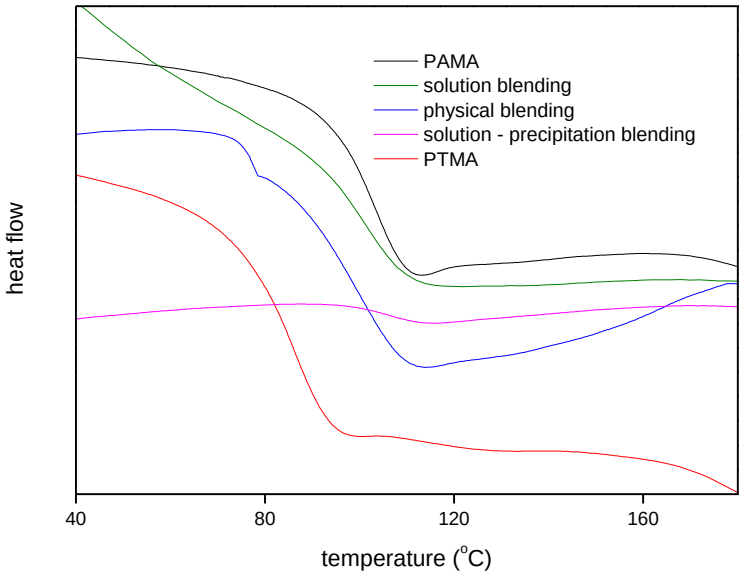

Figure 2.14 DSC second heating thermograms of mixtures of homopolymers (PAMA and PTMA) prepared by different methods, with a heating rate of 5 °C/ min and cooling rate of 10 °C/min.

2.3.7 Self-assembly behaviour

Polymers with different compositions usually allow access to different polymeric microstructures. To further study the properties of the functional copolymers prepared in this study, block copolymers were synthesized and self-assembled in $CHCl_3$. However, due to the heterogeneous character of the polymerization involving the two nucleobase monomers in $CHCl_3$ resulting in unreliable RAFT end group fidelity, chain extension starting from the functional copolymers was not ideal. Thus, the block copolymers were prepared by first synthesizing the non-functional block, in this case poly(methyl methacrylate) (PMMA) followed by chain extension with the functional block, a 1:1 mixture of AMA and TMA.

PMMA were firstly synthesized in toluene using CPDT as chain transfer agent (CTA) and AIBN as initiator (Scheme 2.4). The resulting polymers were characterized by a combination of ^{1}H NMR spectroscopy and SEC analysis (DMF as eluent, PMMA as standards), showing a successful synthesis with good end group fidelity. It was found that PMMA with different degrees of polymerization (DPs) could be successfully prepared (220 for polymer **9**, and 70 for polymer **12**). Block copolymers were then prepared in both $CHCl_3$ and DMF at 60 °C using PMMA as the macro-CTA and AIBN as the initiator. The ratio of monomer:PMMA:AIBN was kept to 50:1:0.1. The characterization data for the final block copolymers are shown in Table 2.8, polymers **9**-**14**. It is evident that well-defined block copolymers with comparable molecular weight were obtained for both polymerizations in $CHCl_3$ and DMF (Figure 2.15 - Figure 2.18). For instance, polymer **10** and polymer **11**, which were synthesized from the same macro-CTA, **9**, have the comparable molecular weights determined by both ^{1}H NMR spectroscopy and SEC analysis (DMF as eluent, PMMA as standards) and narrow molecular weight distributions by SEC analysis. Successful synthesis was also observed for the preparation of polymer **13** and **14**, which were prepared in different solvents but from the same macro-CTA, **12**.

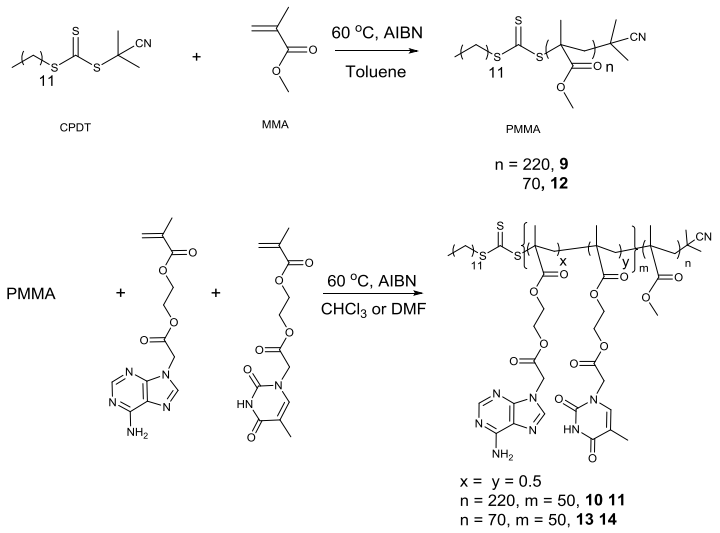

Scheme 2.4 Synthesis of block copolymers $PMMA_n$-*b*-$(PAMA_x$-*co*-$PTMA_y)_m$.

Table 2.8 Polymerization data for polymers **9-14**

Polymer	CTA	Solvent	AMA:TMA (before)[a]	AMA:TMA (after)[b]	Conv. (%)[c]	$M_{n,\,th}$ (kDa)	$M_{n,NMR}$ (kDa)[d]	$M_{n,SEC}$ (kDa)[e]	$Đ_M$	Copolymer composition (PAMA:PTMA)
9	CTA 2	--	--	--	57	22.6	22.0	22.1	1.20	--
10	**9**	$CHCl_3$	1:1	1:1	90, 90	35.5	35.8	34.9	1.33	1:1
11	**9**	DMF	1:1	1:1	99, 99	36.9	37.0	34.5	1.20	1:1
12	CTA 2	--	--	--	36	7.2	7.0	7.0	1.17	--
13	**12**	$CHCl_3$	1:1	1:1	95, 95	21.3	26.8	26.1	1.32	1:1
14	**12**	DMF	1:1	1:1	95, 95	21.3	22.0	21.5	1.14	1:1

[a]the ratio of monomers in initial feed;
[b]the ratio of residual monomers after polymerization;
[c]the final conversion of AMA (first number) and the final conversion of TMA (second number);
[d]determined by ^{1}H NMR spectroscopy in DMSO-d_6;
[e]determined by SEC analysis (DMF as eluent, PMMA as standards).

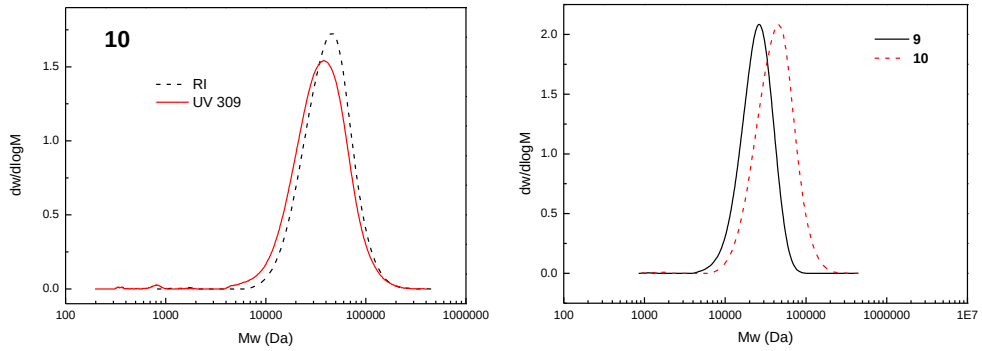

Figure 2.15 SEC chromatograms of polymer **10** (left) and overlay of RI traces of polymers **9** and **10** (right) (DMF eluent, PMMA as standards).

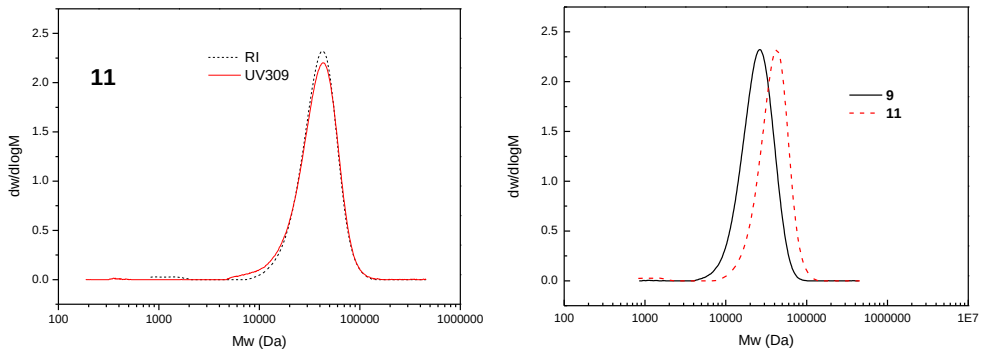

Figure 2.16 SEC chromatograms of polymer **11** (left) and overlay of RI traces of polymers **9** and **11** (right) (DMF eluent, PMMA as standards).

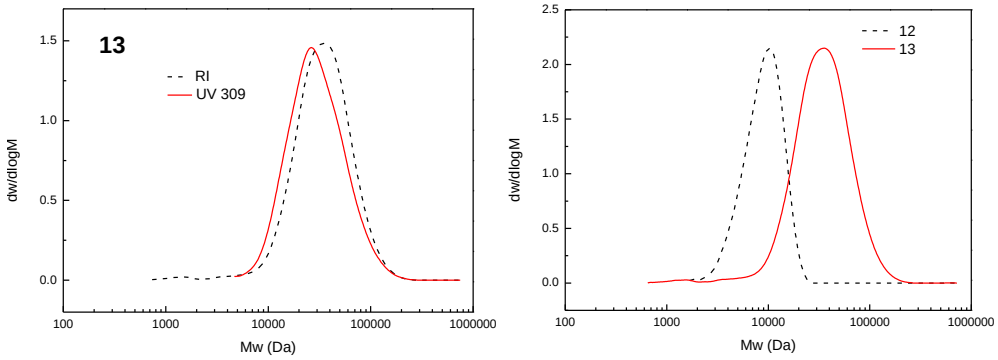

Figure 2.17 SEC chromatograms of polymer **13** (left) and overlay of RI traces of polymers **12** and **13** (right) (DMF eluent, PMMA as standards).

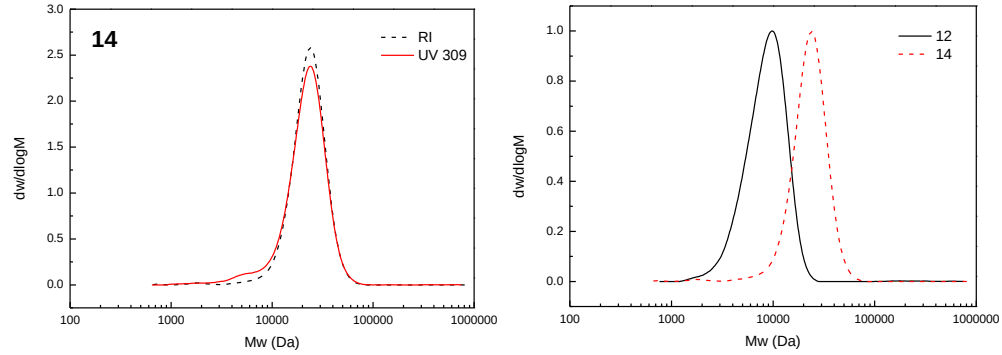

Figure 2.18 SEC chromatograms of polymer **14** (left) and overlay of RI traces of polymers **12** and **14** (right) (DMF eluent, PMMA as standards).

Comparable polymers (**10** and **11**, **13** and **14**) were then self-assembled in $CHCl_3$ and the morphologies were characterized by transmission electron microscopy (TEM) and dynamic light scattering (DLS) analysis. Polymer solutions in $CHCl_3$ with a concentration of 10 mg/mL were firstly stirred at 60 °C for 1 hour and then further stirred at room temperature for 2 days. The solution was diluted to 0.5 or 0.1 mg/mL for TEM and DLS analysis.

Close to spherical structures of around 40 nm were observed for polymer **10** (prepared in $CHCl_3$) assembled in $CHCl_3$ by unstained TEM on graphene oxide (Figure 2.19a). By comparison, a mixture of spherical micelles and elongated worm-like structures was observed by TEM (Figure 2.19b) under the same conditions when polymer **11** (prepared in DMF) was assembled in $CHCl_3$. The size distributions were

narrow determined by DLS (0.086 and 0.096, for **10** and **11** respectively, see Figure 2.20). Compared to polymer **10** and **11**, polymers **13** and **14** have a shorter PMMA block. Larger and close to spherical micelles with a diameter of 90 nm by TEM analysis were observed for polymer **13** (prepared in $CHCl_3$) assembled in $CHCl_3$ (Figure 2.19c), while obvious cylinder-like micelles were observed from the self-assembly of polymer **14** (prepared in DMF) (Figure 2.19d). We hypothesize that the different tendency of monomer composition in the functional block for block copolymers prepared in $CHCl_3$ and DMF, affecting the solubility and polymer curvature of resulting block copolymer, is responsible for the different morphologies observed. As infrared spectroscopy is a useful tool to investigate hydrogen bonding interactions between nucleobases,[38,54,55] polymers **13** and **14** were further characterized by infrared spectroscopy (Figure 2.21). However, due to the complex nature of polymer structures, no obvious differences were observed for these two polymers, **13** and **14**, synthesized in different solvents. Therefore, the exact cause for this behavior remains unclear.

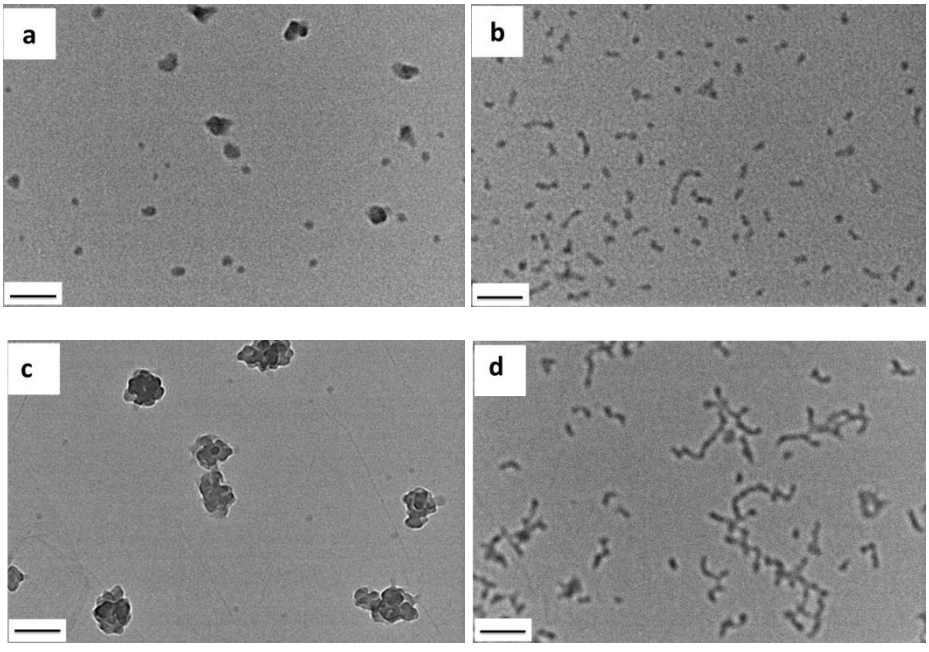

Figure 2.19 TEM images of self-assembled polymers (a) **10**, (b) **11**, (c) **13**, and (d) **14**, scale bar 100 nm.

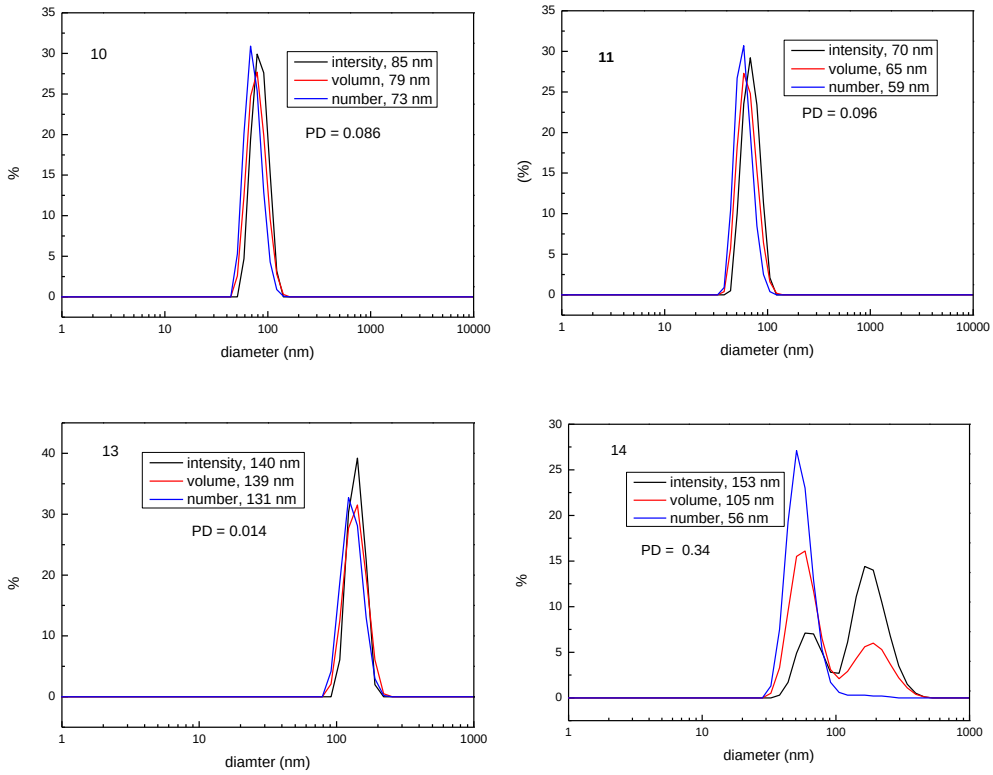

Figure 2.20 DLS of self-assemblies prepared by polymers **10**, **11**, **13** and **14** in $CHCl_3$.

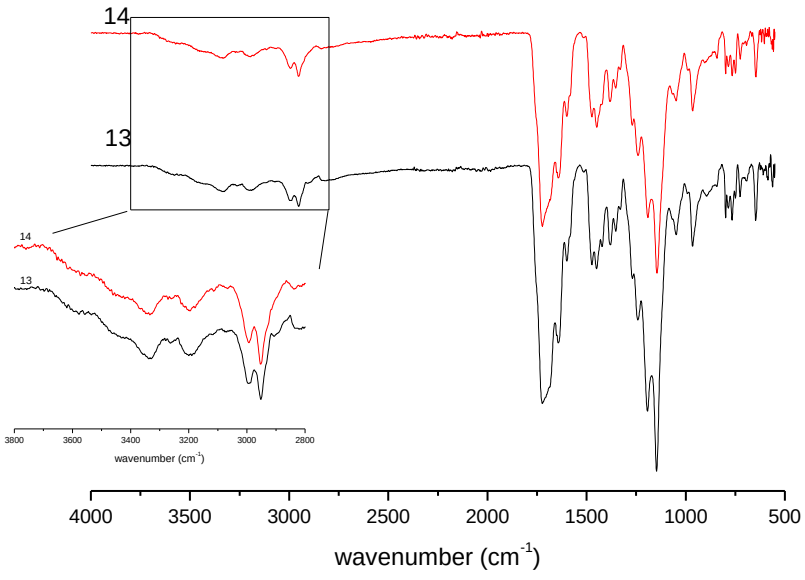

Figure 2.21 Infrared spectra of polymers **13** and **14**.

2.4 Conclusion

In conclusion, methacryloyl-type monomers containing adenine and thymine functionalities have been successfully synthesized. RAFT polymerizations were used to prepare homopolymers and copolymers using these monomers with good control over molecular weight and end group fidelity. The difference in reactivity of the two monomers during copolymerizations in DMF and $CHCl_3$ was investigated. The results indicate polymerizations carried out in $CHCl_3$, a solvent that promotes hydrogen bonding interactions between the nucleobase based monomers, tend to give moderate alternating copolymers. However, polymerizations in DMF, a solvent that suppresses the interactions, tend to give statistical copolymers. These hydrogen bonding interactions between two monomers may be used to access copolymers with different copolymer compositions. Moreover, properties of the copolymers such as self-assembly behavior were investigated and were found to be greatly influenced by the presence or absence of hydrogen bonding between the two nucleobases.

2.5 Experimental section

2.5.1 Materials and instrumentation

2-Hydroxyethyl methacrylate (HEMA), 2-cyano-2-propyl benzodithioate (CTA 1), 2-cyano-2-propyl dodecyl trithiocarbonate (CPDT, CTA 2), bromoacetyl chloride, sodium hydride (NaH) (60% in dispersion mineral oil), and tetrabutylammonium iodide (TBAI) were purchased from Sigma-Aldrich and used as received. Adenine and thymine were purchased from Sigma-Aldrich and Acros respectively. 2,2'-Azo-bis(isobutyronitrile) (AIBN) was purchased from Molekula, recrystallized from methanol and stored in the dark at 4 °C. Triethylamine (TEA), anhydrous potassium carbonate (K_2CO_3), anhydrous magnesium sulfate ($MgSO_4$), ammonium chloride (NH_4Cl), sodium hydrogen carbonate ($NaHCO_3$), *N*,*N*-dimethylformamide (DMF), chloroform ($CHCl_3$), and other solvents were used as received from Fisher Chemical. Dry solvents were obtained by passing them over a column of activated alumina using an Innovative Technologies solvent purification system.

^{1}H NMR and ^{13}C NMR spectra were recorded on a Bruker DPX-300 or DPX-400 spectrometer using deuterated solvents. Chemical shifts are reported as δ in parts per million (ppm) relative to DMSO-d_6 (2.50 ppm), DMF-d_7 (8.01 ppm) or $CDCl_3$ with tetramethylsilane (TMS, δ = 0 ppm) as the internal standard. Size exclusion chromatography (SEC) data were obtained in HPLC grade DMF containing 5 mM NH_4BF_4 at 50 °C, with a flow rate of 1.0 mL/min, on a set of two PLgel 5 μm Mixed-D columns, plus one guard column. SEC data was analyzed using Cirrus SEC software using poly(methyl methacrylate) (PMMA) standards. High resolution mass spectrometry (HR-MS) was conducted on a Bruker UHR-Q-TOF MaXis with electrospray ionization. DSC measurements were performed on a Mettler Toledo HP DSC827 from 0 to 200 °C with a heating rate of 5 °C/min. Data was analyzed using

Mettler Toledo STARe software v9.20. Glass transition temperatures (T_g) were taken as the midpoint of the inflection tangent. Elemental analysis was performed in duplicate by Warwick Analytical Service. Hydrodynamic diameters (D_h) and size distributions of the self-assemblies was determined by dynamic light scattering (DLS). The DLS instrumentation consisted of a Malvern Zetasizer NanoS instrument operating at 25 °C with a 4 mW He-Ne 633 nm laser module. Measurements were made at a detection angle of 173 ° (back scattering), and Malvern Zetasizer 7.03 software was used to analyze the data. Transmission electron microscopy (TEM) observation was performed on JEOL 2000FX electron microscopy at an acceleration voltage of 200 kV. All TEM samples were prepared either on graphene oxide (GO) – coated carbon grids which can acquire high contrast TEM images without staining.[56] Generally, a drop of sample (20 μL) was deposited onto a grid which was placed on a filter paper and left to air dry. Infrared spectroscopy was recorded on a Perkin Elmer Spectrum 100 FT-IR Spectrometer.

2.5.2 Synthesis of 2-(2-bromoacetoxyl) ethyl methacrylate

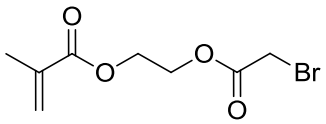

To a solution of HEMA (13 g, 0.1 mol) and TEA (15 mL, 0.107 mol) in $CHCl_3$ (300 mL), bromoacetyl chloride (8.3 mL, 0.1 mol) was added dropwise in an ice bath. After stirring for 2 days, the unreacted bromoacetyl chloride was quenched *via* the addition of methanol (5 mL). The solution was stirred for 30 min and then poured into saturated aqueous $NaHCO_3$ (100 mL). The solution was washed with water twice (2 × 100 mL). The organic layer was collected and dried with anhydrous $MgSO_4$, filtered and concentrated *in vacuo* to give a brown oil. The product was

further purified by column chromatography (silica, 20% ethyl acetate in hexane) to give a colorless oil (12 g, 45%).

^{1}H NMR (400 MHz, $CDCl_3$, ppm): δ = 6.13 (quintet, 1H, CH_A=C(CH_3)-COO, $^{2}J_{H-H}$ = 1.2 Hz), δ = 5.61 (quintet, 1H, CH_B=C(CH_3)-COO, $^{2}J_{H-H}$ = 1.6 Hz), δ = 4.45 (m, 2H, C=CCOO-CH_2-CH_2, $^{3}J_{H-H}$ = 6.7 Hz), δ = 4.39 (m, 2H, C=CCOO-CH_2-CH_2, $^{3}J_{H-H}$ = 7.1 Hz), δ = 4.09 (s, 2H, OOC-CH_2-Br), δ = 1.95 (q, 3H, OOC-C(CH_3)=CH_2).

^{13}C NMR (100 MHz, $CDCl_3$, ppm): δ = 167.2 (CH_2=C(CH_3)*C*OO), δ = 167.0 (O*C*OCH_2Br), δ = 135.8 (CH_2=*C*(CH_3)COO), δ = 126.3 (*C*H_2=C(CH_3)COO), δ = 64.9 (CH_2=C(CH_3)COO*C*$H_2$$CH_2$), δ = 62.0 (CH_2=C(CH_3)COOCH_2*C*H_2), δ = 40.7 (OCOCH_2Br), δ = 18.3 (CH_2=C(*C*H_3)COO).

HR-MS (MaXis): m/z $[M+Na]^+$ found 272.9733, expected 272.9733.

2.5.3 Synthesis of 2-(2-(adenine-9-yl)acetoxyl) ethyl methacrylate (AMA)

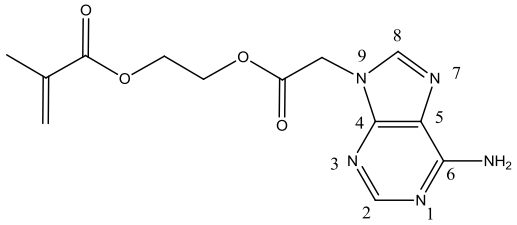

To a suspension of adenine (2.6 g, 19.2 mmol) in dry DMF (125 mL), NaH (0.764 g, 19.2 mmol) was added slowly. The mixture was stirred for 1 h until no more gas was produced. The white slurry was immersed into an ice bath and 2-(2-bromoacetoxyl) ethyl methacrylate (4 g, 15.9 mmol) was added dropwise. A yellow and less viscous mixture resulted and was stirred for 2 days at room temperature. The reaction was then quenched via the addition of saturated aqueous NH_4Cl (5 mL). The resulting suspension was filtered and concentrated in *vacuo*. The solid was extracted by 200 mL dichloromethane (DCM) and concentrated. The mixture was further purified by column chromatography (silica, 7% methanol in DCM) to give an off-white solid.

The product was further washed with hexane to remove excess DMF yielding a pale solid, AMA (3.5 g, 75%).

^{1}H NMR (400 MHz, DMSO-d_6, ppm): δ = 8.10 (s, 1H, purine *H*-2), δ = 8.09 (s, 1H, purine *H*-8), δ = 7.25 (s, 2H, NH_2), δ = 6.00 (quintet, 1H, CH_A=C(CH$_3$)-COO, $^{2}J_{H-H}$ = 1.1 Hz,), δ = 5.68 (quintet, 1H, CH_B=C(CH$_3$)-COO, $^{2}J_{H-H}$ = 1.6 Hz), δ = 5.10 (s, 2H, OOC-CH_2-purine), δ = 4.38 (m, 2H, CH$_2$=C(CH$_3$)COO-CH_2-CH$_2$, $^{3}J_{H-H}$ = 6.6 Hz), δ = 4.31 (m, 2H, CH$_2$=C(CH$_3$)COO-CH$_2$-CH_2, $^{3}J_{H-H}$ = 6.6 Hz), δ = 1.86 (q, 3H, OOC-C(CH_3)=CH$_2$).

^{13}C NMR (100 MHz, DMSO-d_6, ppm): δ = 168.4 (O*C*OCH$_2$-purine), δ = 166.8 (CH$_2$=C(CH$_3$)*C*OO), δ = 156.4 (purine *C*-6), δ = 153.1 (purine *C*-2), δ = 150.2 (purine *C*-4), δ = 141.6 (purine *C*-8), δ = 135.9 (CH$_2$=*C*(CH$_3$)COO), δ = 126.7 (CH_2=C(CH$_3$)COO), δ = 118.7 (purine *C*-5), δ = 63.5 (CH$_2$=C(CH$_3$)COO*C*H$_2$CH$_2$), δ = 62.7 (CH$_2$=C(CH$_3$)COOCH$_2$*C*H$_2$), δ = 44.3 (OCO*C*H$_2$-purine), δ = 18.3 (CH$_2$=C(*C*H$_3$)COO).

IR, ν_{max} (solid): 3335, 3155, 2970, 2934, 1749, 1715, 1666, 1604, 1429, 1428, 1310, 1210, 1156 cm^{-1}.

HR-MS (MaXis): m/z [M+Na]$^{+}$ found 328.1017, expected 328.1016.

Elemental analysis found: C 51.02, H 4.88, N 22.58; expected (C$_{13}$H$_{15}$N$_5$O$_4$): C 51.14, H 4.95, N 22.94.

mp: 175 – 178 °C

2.5.4 Synthesis of 2-(2-(thymin-1-yl)acetoxyl) ethyl methacrylate (TMA)

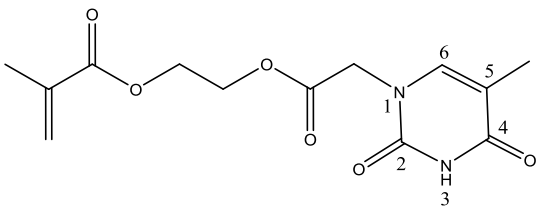

To a solution of thymine (2 g, 14.2 mmol) in dry DMF (100 mL), anhydrous K_2CO_3 (2.21 g, 14.2 mmol) was added and stirred for 30 min, followed by addition of TBAI (0.33 g, 0.9 mmol). The mixture was put into an ice bath and 2-(2-bromoacetoxy) ethyl methacrylate (2 g, 8 mmol) was added slowly. After stirring at room temperature for 2 days, the mixture was filtered and concentrated *in vacuo*. The resulting solid was extracted by 200 mL DCM, filtered and concentrated. The yellow liquid was further purified by column chromatography (silica, 2% methanol in DCM) yielding a viscous liquid. The liquid was dried *in vacuo* to remove DMF. The resulting solid was further washed with hexane to remove excess DMF to give a white solid, TMA (1.4 g, 60%).

^{1}H NMR (400 MHz, $CDCl_3$, ppm): δ = 8.20 (br s, 1H, pyrimidine N*H*), δ = 6.94 (q, 1H, pyrimidine *H*-6), δ = 6.13 (quintet, 1H, CH_A=C(CH_3)-COO, $^2J_{H-H}$ = 1.0 Hz), δ = 5.62 (quintet, 1H, CH_B=C(CH_3)-COO, $^2J_{H-H}$ = 1.5 Hz), δ = 4.46 (s, 2H, OCO-CH_2-pyrimidine), δ = 4.44 (m, 2H, COO-CH_2-CH_2, $^3J_{H-H}$ = 6.7 Hz), δ = 4.41 (m, 2H, COO-CH_2-CH_2, $^3J_{H-H}$ = 6.8 Hz), δ = 1.95 (q, 3H, OOC-C(CH_3)=CH_2), δ = 1.86 (d, 3H, pyrimidine-CH_3).

^{13}C NMR (100 MHz, $CDCl_3$, ppm): δ = 167.4 (O*C*OCH_2-pyrimidine), δ = 167.1 (CH_2=C(CH_3)*C*OO), δ = 163.6 (pyrimidine *C*-4), δ = 150.5 (pyrimidine *C*-2), δ = 140.0 (pyrimidine *C*-6), δ = 135.8 (CH_2=*C*(CH_3)COO), δ = 126.4 (CH_2=C(CH_3)COO), δ = 111.4 (pyrimidine *C*-5), δ = 63.8 (CH_2=C(CH_3)COO*C*$H_2$$CH_2$), δ = 61.9 (CH_2=C(CH_3)COOCH_2*C*H_2), δ = 48.5 (OCO*C*H_2-pyrimidine), δ = 18.3 (CH_2=C(*C*H_3)COO), δ = 12.3 (pyrimidine-*C*H_3).

IR, ν_{max} (solid): 3162, 3040, 2962, 2830, 1738, 1690, 1461, 1350, 1215, 1160 cm^{-1}.

HR-MS (MaXis): m/z $[M+Na]^+$ found 319.0895, expected 319.0901.

Elemental analysis found: C 52.62, H 5.33, N 9.38; expected ($C_{13}H_{16}N_2O_6$): C 52.70, H 5.44, N 9.46.

mp: 97 – 99 °C.

2.5.5 Monomer interaction studies

TMA (12 mg, 0.04 mmol) was dissolved in $CDCl_3$ (2 mL) or DMF-d_7 (2 mL) giving a monomer concentration of 20 mM (solution T). AMA (24 mg, 0.08 mmol) was dissolved in $CDCl_3$ (2 mL) or DMF-d_7 (2 mL) giving a monomer concentration of 40 mM (solution A). Different ratios of the two solutions (A and T) were mixed and the resulting mixture studied by ^{1}H NMR spectroscopy at 25 °C and 60 °C.

Table 2.9 Preparation of the mixtures of AMA and TMA for the interaction study

Samples	Solution AMA/μL	$CDCl_3$/DMF-d_7/ μL	Solution TMA/ μL	[AMA]/[TMA]
1	300	0	300	2
2	225	75	300	1.5
3	150	150	300	1
4	75	225	300	0.5
5	37.5	262.5	300	0.25
6	0	300	300	0

2.5.6 Homopolymerization of AMA and TMA

A typical procedure for the RAFT homopolymerization of AMA or TMA (polymers **a**, **b**, **c**, **d**) was as follows: AMA or TMA (120 mg, 0.4 mmol), CPDT (3.5 mg, 0.01 mmol), and AIBN (0.2 mg, 0.0012 mmol) were dissolved in DMF (2 mL) or $CHCl_3$ (10 mL). The polymerization mixture was thoroughly degassed *via* four freeze-pump-thaw cycles, back-filled with nitrogen and immersed into an oil bath at 60 °C for 24 h. The reaction was quenched *via* cooling in liquid nitrogen and exposure to air. The polymer was precipitated in methanol and further washed with methanol.

The light yellow polymer was dried in a vacuum oven overnight and characterized by ^{1}H NMR spectroscopy and SEC (DMF, PMMA standards).

^{1}H NMR (400 MHz, DMF-d_7, ppm) of PAMA: δ = 8.38 – 8.11 (d, 2H$_{\text{backbone-PAMA}}$, purine *H*-2+8), δ = 7.76 – 7.30 (br s, 2H$_{\text{backbone-PAMA}}$, NH_2 of purine), δ = 5.47 – 5.08 (br s, 2H$_{\text{backbone-PAMA}}$, NCH_2COO), δ = 4.57 – 4.05 (d, 4H$_{\text{backbone-PAMA}}$, OCH_2CH_2O), δ = 3.36 – 3.28 (t, 2H$_{\text{end-group}}$, CH_2SC=S), δ = 2.38 – 1.50 (m, 2H$_{\text{backbone-PAMA}}$, CH_2CCH$_3$; 20H$_{\text{end-group}}$, SCH$_2$(CH_2)$_{10}$CH$_3$), δ = 1.30 – 0.50 (m, 3H$_{\text{backbone-PAMA}}$, CH$_2$CCH_3). IR, ν_{max} (solid): 3322, 3183, 2997, 2951, 1726, 1643, 1599, 1472, 1419, 1244, 1202, 1152, 1043, 965, 800, 723, 647 cm^{-1}.

^{1}H NMR (400 MHz, DMF-d_7, ppm) of PTMA: δ = 11.31 (br, 1H$_{\text{backbone-PTMA}}$, N*H*CO of pyrimidine), δ = 7.52 (br s, 1H$_{\text{backbone-PTMA}}$, NC*H*=CCH$_3$ of pyrimidine), δ = 4.65–4.26 (t, 6H$_{\text{backbone-PTMA}}$, OCH_2CH_2OCOCH_2), δ = 3.36 – 3.28 (t, 2H$_{\text{end-group}}$, CH_2SC=S), δ = 2.30 – 1.27 (m, 5H$_{\text{backbone-PTMA}}$, CH_2CCH$_3$ and NCH=CCH_3 of pyrimidine; 20H$_{\text{end-group}}$, SCH$_2$(CH_2)$_{10}$CH$_3$), δ = 1.30 – 0.75 (m, 3H$_{\text{backbone-PTMA}}$, CH$_2$CCH_3). IR, ν_{max} (solid): 3187, 3068, 2999, 293, 1745, 1682, 1459, 1380, 1347, 1200, 1150, 1043, 962, 762 cm^{-1}.

2.5.7 Copolymerization of AMA and TMA

A typical procedure for the RAFT copolymerization of AMA and TMA (copolymers **1 - 8**) was as follows: AMA (x), TMA (y), CTA 1 or CTA 2 (1 eq), and AIBN (0.1 eq) were dissolved in DMF or $CHCl_3$. The total concentration of monomers was 0.2 M in DMF and 0.04 M in $CHCl_3$. The polymerization mixture was thoroughly degassed *via* four freeze-pump-thaw cycles, back-filled with nitrogen and immersed into an oil bath at 60 °C. The reaction was quenched *via* cooling in liquid nitrogen and exposure to air. The copolymer was precipitated in methanol and further washed with

methanol. The light yellow polymer was dried in a vacuum oven overnight and characterized by ^{1}H NMR spectroscopy and SEC (DMF, PMMA standards).

^{1}H NMR (400 MHz, DMSO-d_6, ppm) of copolymer using CTA 1:δ = 11.76 – 11.52 (br s, 1H$_{\text{backbone-PTMA}}$, N*H*CO), δ = 8.23 – 8.01 (d, 2H$_{\text{backbone-PAMA}}$, two NC*H*N of purine), δ = 7.85 – 7.70 (br, 1H$_{\text{end-group}}$, Ar-*H*(*o*)), δ = 7.49 – 7.14 (d, 3H$_{\text{backbone-PAMA+PTMA}}$, N$H_2$ of purine and NC*H*=CCH$_3$ of pyrimidine), δ = 5.22 – 5.20 (br, 2H$_{\text{backbone-PAMA}}$, NCH_2COO), δ = 4.63 – 3.92 (m, 10H$_{\text{backbone-PAMA+PTMA}}$, OC$H_2CH_2$O of PAMA and OC$H_2CH_2$OCOC$H_2$ of PTMA), δ = 2.20 – 1.50 (m, 2H$_{\text{backbone}}$, CH_2CCH$_3$; 3H$_{\text{backbone-PTMA}}$, NCH=CCH_3 of pyrimidine), δ = 1.30 – 0.50 (m, 3H$_{\text{backbone}}$, CH$_2$CCH_3). IR, ν_{max} (solid): 3343, 3194, 2993, 2960, 1700, 1639, 1596, 1477, 1241, 1203, 1148, 1051, 969, 873, 649 cm^{-1}.

^{1}H NMR (400 MHz, DMF-d_7, ppm) of copolymer using CTA 2: δ = 13.00 – 12.00 (br s, 1H$_{\text{backbone-PTMA}}$, N*H*CO), δ = 8.59 – 8.30 (d, 2H$_{\text{backbone-PAMA}}$, two NC*H*N of purine), δ = 7.92 – 7.47 (d, 3H$_{\text{backbone-PAMA+PTMA}}$, N$H_2$ of purine and NC*H*=CCH$_3$ of pyrimidine), δ = 5.65 – 5.27 (br, 2H$_{\text{backbone-PAMA}}$, NCH_2COO), δ = 5.00 – 4.20 (m, 10H$_{\text{backbone-PAMA+PTMA}}$, OC$H_2CH_2$O of PAMA and OC$H_2CH_2$OCOC$H_2$ of PTMA), δ = 3.53 – 3.42 (s, 2H$_{\text{end-group}}$, CH_2SC=S), δ = 2.60 – 1.85 (m, 2H$_{\text{backbone}}$, CH_2CCH$_3$; 20H$_{\text{end-group}}$, SCH$_2$(CH_2)$_{10}$CH$_3$; 3H$_{\text{backbone-PTMA}}$, NCH=CCH_3 of pyrimidine), δ = 1.50 – 0.80 (m, 3H$_{\text{backbone}}$, CH$_2$CCH_3). IR, ν_{max} (solid): 3338, 3193, 2994, 2953, 1703, 1643, 1601, 1473, 1419, 1250, 1202, 1148, 1045, 969, 800, 646 cm^{-1}.

2.5.8 Polymerization of methyl methacrylate (MMA)

The typical procedure for RAFT homopolymerization of MMA (**9** and **12**) was as follows: MMA (4 g, 40 mmol), CTA 2 (35 mg, 0.1 mmol), and AIBN (1.7 mg, 0.01 mmol) were dissolved into toluene. The mixture was thoroughly degassed *via* 4

freeze-pump-thaw cycles, back-filled with nitrogen and then immersed into an oil bath at 60 °C for 9 h/6 h. The reaction was quenched *via* cooling in liquid nitrogen and exposure to air. The mixture was precipitated in methanol and filtered. The solid was dissolved in $CHCl_3$ and precipitated in methanol again. The precipitation procedure was repeated twice. The light yellow polymers, poly(methyl methacrylate) (PMMA) were dried in a vacuum oven overnight and characterized by ^{1}H NMR spectroscopy and SEC (both THF and DMF, PMMA standards).

^{1}H NMR (400 MHz, $CDCl_3$, ppm): δ = 3.60 (s, $3H_{backbone\text{-}PMMA}$, OCH_3), δ = 3.25 – 3.22 (t, $2H_{end\text{-}group}$, $CH_2SC{=}S$), δ = 1.96 – 1.81 (m, $2H_{backbone\text{-}PMMA}$, CH_2CCH_3), δ = 1.51 – 1.33 (m, $18H_{end\text{-}group}$, $SCH_2CH_2(CH_2)_9CH_3$), δ = 1.30 – 0.75 (m, $3H_{backbone\text{-}PMMA}$, CH_2CCH_3).

2.5.9 Synthesis of block polymers using PMMA as macro-CTA

The typical procedure for diblock copolymers **10**, **11**, **13** and **14** as follows: PMMA (112 mg, 0.005 mmol), AMA (38 mg, 0.125 mmol), TMA (37 mg, 0.125 mmol), and AIBN (0.1 mg, 0.0005 mmol) were dissolved in DMF (2 mL) or $CHCl_3$ (6 mL). The mixture was thoroughly degassed *via* 4 freeze-pump-thaw cycles, back-filled with nitrogen and then immersed into an oil bath at 60 °C. The reaction was quenched *via* cooling in liquid nitrogen and exposure to air. The mixture was precipitated in methanol and washed with methanol several times. The light yellow polymers were dried in a vacuum oven overnight and characterized by ^{1}H NMR spectroscopy and DMF SEC (PMMA standards).

^{1}H NMR (400 MHz, DMSO-d_6, ppm):δ = 11.73 – 11.58 (br, $1H_{backbone\text{-}PTMA}$, $NHCO$), δ = 8.23 – 8.05 (d, $2H_{backbone\text{-}PAMA}$, two $NCHN$ of purine), δ = 7.64 – 7.28 (d, $3H_{backbone\text{-}PAMA+PTMA}$, NH_2 of purine and $NCH{=}CCH_3$ of pyrimidine), δ = 5.27 – 4.85

(br, $2H_{backbone\text{-}PAMA}$, NC*H*2COO), δ = 4.80 – 3.80 (m, $10H_{backbone\text{-}PAMA+PTMA}$, OCH_2CH_2O of PAMA and $OCH_2CH_2OCOCH_2$ of PTMA), δ = 3.70 – 3.40 (s, $3H_{backbone\text{-}PMMA}$, OCH_3), δ = 2.12 – 1.50 (m, $3H_{backbone\text{-}PTMA}$, $CH{=}C(CH_3)$ of pyrimidine; $2H_{backbone}$, CH_2CCH_3 of backbone; $20H_{end\text{-}group}$, $SCH_2(CH_2)_{10}CH_3$), δ = 1.30 – 0.50 (m, $3H_{backbone}$, CH_2CCH_3). IR, ν_{max} (solid): 3341, 3191, 2999, 2956, 1728, 1638, 1604, 1470, 1446, 1377, 1246, 1187, 1142, 1046, 962 cm^{-1}.

2.5.10 Determination of monomer reactivity ratios

AMA and TMA at different ratios (90:10, 80:20, 70:30, 60:40, 50:50, 40:60, 30:70, 20:80, and 10:90), CTA (CTA 1 or CTA 2) and AIBN were dissolved in DMF or $CHCl_3$. The ratio of monomers: CTA: AIBN was 88: 1: 0.2 or 92: 1: 0.2. The polymerization mixture was thoroughly degassed *via* four freeze-pump-thaw cycles, back-filled with nitrogen and immersed into an oil bath at 60 °C. The conversion was kept to less than 10% and the reaction was quenched *via* cooling in liquid nitrogen. $CHCl_3$ and DMF were removed over a flow of compressed air and the polymer residues were dissolved in a small amount of DMSO-d_6 and characterized by ^1H NMR spectroscopy.

2.5.11 Self-assembly

A typical procedure for self-assembly was as follows: block copolymer (10 mg) was added into $CHCl_3$ (1mL). The mixtures were heated at 60 °C for 1 hour and then stirred at room temperature for 2 days. Before carrying out TEM and DLS measurements, the solutions were diluted to 0.5 or 0.1 mg/mL. For TEM preparation, a drop of sample (20 μL) was deposited onto a grid which was placed on a filter paper and left to air dry.

2.5.12 Mixtures of homopolymers

Physical blending: PAMA (10 mg, solid) and PTMA (10 mg, solid) were mixed and stirred using a spatula.

Solution-precipitation blending: PAMA (10 mg, solid) and PTMA (10 mg, solid) were mixed. DMF (2 mL) was added into the mixture and the resultant solution mixture was stirred overnight. The mixture was concentrated under a flow of compressed air and then precipitated in methanol.

Solution blending: PAMA (10 mg, solid) and PTMA (10 mg, solid) were mixed. DMF (2 mL) was added into the mixture and the resultant solution mixture was stirred overnight. DMF was then left to evaporate under a flow of compressed air. The resultant blended film was further dried in a vacuum oven at 40 °C.

2.6 References

(1) Badi, N.; Lutz, J.-F. *Chem. Soc. Rev.* **2009**, *38*, 3383.

(2) Matyjaszewski, K. *Prog. Polym. Sci.* **2005**, *30*, 858.

(3) Hibi, Y.; Tokuoka, S.; Terashima, T.; Ouchi, M.; Sawamoto, M. *Polym. Chem.* **2011**, *2*, 341.

(4) Ida, S.; Ouchi, M.; Sawamoto, M. *J. Am. Chem. Soc.* **2010**, *132*, 14748.

(5) Pfeifer, S.; Lutz, J.-F. *J. Am. Chem. Soc.* **2007**, *129*, 9542.

(6) Davies, M. C.; Dawkins, J. V.; Hourston, D. J. *Polymer* **2005**, *46*, 1739.

(7) Hibi, Y.; Ouchi, M.; Sawamoto, M. *Angew. Chem. Int. Ed.* **2011**, *50*, 7434.

(8) Takemoto, K.; Akashi, M.; Inaki, Y. *J. Polym. Sci. Polym. Chem. Ed.* **1974**, *12*, 1861.

(9) Akashi, M.; Kita, Y.; Inaki, Y.; Takemoto, K. *J. Polym. Sci., Polym. Chem. Ed.* **1979**, *17*, 301.

(10) Watson, J. D.; Crick, F. H. C. *Nature* **1953**, *171*, 737.

(11) Inaki, Y. *Prog. Polym. Sci.* **1992**, *17*, 515.

(12) McHale, R.; O'Reilly, R. K. *Macromolecules* **2012**, *45*, 7665.

(13) Smith Jr, W. T. *Prog. Polym. Sci.* **1996**, *21*, 209.

(14) Tao, Y.; Satoh, K.; Kamigaito, M. *Macromol. Rapid Commun.* **2011**, *32*, 226.

(15) Khan, A.; Haddleton, D. M.; Hannon, M. J.; Kukulj, D.; Marsh, A. *Macromolecules* **1999**, *32*, 6560.

(16) South, C. R.; Weck, M. *Macromolecules* **2007**, *40*, 1386.

(17) Lo, P. K.; Sleiman, H. F. *J. Am. Chem. Soc.* **2009**, *131*, 4182.

(18) Garcia, M.; Kempe, K.; Haddleton, D. M.; Khan, A.; Marsh, A. *Polym. Chem.* **2015**, *6*, 1944.

(19) McHale, R.; Patterson, J. P.; Zetterlund, P. B.; O'Reilly, R. K. *Nature Chem.*

2012, *4*, 491.

(20) Tang, H.; Radosz, M.; Shen, Y. *J. Polym. Sci., Part A: Polym. Chem.* **2006**, *44*, 5995.

(21) Lutz, J.-F.; Thünemann, A. F.; Nehring, R. *J. Polym. Sci., Part A: Polym. Chem.* **2005**, *43*, 4805.

(22) Mather, B. D.; Baker, M. B.; Beyer, F. L.; Berg, M. A. G.; Green, M. D.; Long, T. E. *Macromolecules* **2007**, *40*, 6834.

(23) Marsh, A.; Khan, A.; Haddleton, D. M.; Hannon, M. J. *Macromolecules* **1999**, *32*, 8725.

(24) Marsh, A.; Khan, A.; Garcia, M.; Haddleton, D. M. *Chem. Commun.* **2000**, 2083.

(25) Spijker, H. J.; van Delft, F. L.; van Hest, J. C. M. *Macromolecules* **2007**, *40*, 12.

(26) Spijker, H. J.; Dirks, A. J.; van Hest, J. C. M. *Polymer* **2005**, *46*, 8528.

(27) Perrier, S.; Takolpuckdee, P. *J. Polym. Sci., Part A: Polym. Chem.* **2005**, *43*, 5347.

(28) Keddie, D. J.; Moad, G.; Rizzardo, E.; Thang, S. H. *Macromolecules* **2012**, *45*, 5321.

(29) Moad, G.; Rizzardo, E.; Thang, S. H. *Aust. J. Chem.* **2012**, *65*, 985.

(30) Clayden, J.; Greeves, N.; Warren, S. *Organic Chemistry*, OUP Oxford, **2012**.

(31) Hunter, C. A. *Angew. Chem. Int. Ed.* **2004**, *43*, 5310.

(32) Yan, X.; Liu, G.; Hu, J.; Willson, C. G. *Macromolecules* **2006**, *39*, 1906.

(33) Schmuck, C.; Wienand, W. *J. Am. Chem. Soc.* **2002**, *125*, 452.

(34) Gellman, S. H. *Chem. Rev.* **1997**, *97*, 1231.

(35) Wan, D.; Satoh, K.; Kamigaito, M. *Macromolecules* **2006**, *39*, 6882.

(36) Benesi, H. A.; Hildebrand, J. H. *J. Am. Chem. Soc.* **1949**, *71*, 2703.

(37) Lu, J.; Hu, J.; Liu, C.; Gao, H.; Ju, Y. *Soft Matter* **2012**, *8*, 9576.

(38) Kyogoku, Y.; Lord, R. C.; Rich, A. *J. Am. Chem. Soc.* **1967**, *89*, 496.

(39) Moad, G.; Rizzardo, E.; Thang, S. H. *Polymer* **2008**, *49*, 1079.

(40) Janoschka, T.; Teichler, A.; Krieg, A.; Hager, M. D.; Schubert, U. S. *J. Polym. Sci., Part A: Polym. Chem.* **2012**, *50*, 1394.

(41) Spijker, H. J.; Dirks, A. J.; van Hest, J. C. M. *J. Polym. Sci., Part A: Polym. Chem.* **2006**, *44*, 4242.

(42) Lu, A.; Smart, T. P.; Epps, T. H.; Longbottom, D. A.; O'Reilly, R. K. *Macromolecules* **2011**, *44*, 7233.

(43) Manders, B. G.; Smulders, W.; Aerdts, A. M.; van Herk, A. M. *Macromolecules* **1997**, *30*, 322.

(44) Van Der Meer, R.; Linssen, H. N.; German, A. L. *J. Polym. Sci., Polym. Chem. Ed.* **1978**, *16*, 2915.

(45) Van Herk, A. M.; Dröge, T. *Macromol. Theory Simul.* **1997**, *6*, 1263.

(46) Habibi, A.; Vasheghani-Farahani, E.; Semsarzadeh, M. A.; Sadaghiani, K. *Polym. Int.* **2003**, *52*, 1434.

(47) Odian, G. *Principles of Polymerization, Fourth Edition*, John Wiley & Sons, Inc., Hoboken, New Jersey, **2004**.

(48) Fox, T. G. *Bull. Am. Phys. Soc* **1956**, *1*, 123.

(49) Kuo, S. W.; Xu, H. Y.; Huang, C. F.; Chang, F. C. *J. Polym. Sci. Pt. B-Polym. Phys.* **2002**, *40*, 2313.

(50) Báez, J.; Marcos-Fernández, Á.; Galindo-Iranzo, P. *J. Polym. Res.* **2011**, *18*, 1137.

(51) Kuo, S.-W.; Tsai, H.-T. *Macromolecules* **2009**, *42*, 4701.

(52) Painter, P. C.; Veytsman, B.; Kumar, S.; Shenoy, S.; Graf, J. F.; Xu, Y.; Coleman, M. M. *Macromolecules* **1997**, *30*, 932.

(53) Coleman, M. M.; Xu, Y.; Painter, P. C. *Macromolecules* **1994**, *27*, 127.

(54) Kyogoku, Y.; Lord, R. C.; Rich, A. *Proc. Natl. Acad. Sci. U. S. A.* **1967**, *57*, 250.

(55) Wu, Y.-C.; Kuo, S.-W. *J. Mater. Chem.* **2012**, *22*, 2982.

(56) Patterson, J. P.; Sanchez, A. M.; Petzetakis, N.; Smart, T. P.; Epps III, T. H.; Portman, I.; Wilson, N. R.; O'Reilly, R. K. *Soft Matter* **2012**, *8*, 3322.

Chapter 3. Exploiting nucleobase-containing materials – from monomers to complex morphologies using RAFT dispersion polymerization

3.1 Abstract

The synthesis of nucleobase-containing polymers was successfully performed by RAFT dispersion polymerization in both chloroform and 1,4-dioxane and self-assembly was induced during the polymerizations. A combination of scattering and microscopy techniques were used to characterize the morphologies. It was found that the morphologies of self-assembled nucleobase-containing polymers are solvent dependent. By varying the DP of the core-forming block, only spherical micelles with internal structures were obtained in chloroform when using only adenine-containing methacrylate or a mixture of adenine-containing methacrylate and thymine-containing methacrylate as monomers. However, higher order structures and morphology transitions were observed in 1,4-dioxane. A sphere-rod-lamella-twisted bilayer transition was observed in this study. Moreover, the kinetics of the dispersion polymerizations were studied in both solvents, suggesting a different formation mechanism in these two systems.

3.2 Introduction

The specific hydrogen bonding interactions between nucleobase pairs play a key role in nature for precise biosynthesis and stereospecific molecular assembly. Inspired by nature, nucleobases have been employed in synthetic polymer chemistry to control polymer tacticity,[1] to mediate polymer composition or sequence[2-4] and to template polymerizations.[5-7] Moreover, nucleobase interactions have also been applied to drive self-assembly[8-12] and to achieve a biomimetic segregation/templating approach to polymerizations.[13] This pioneering work has expanded the window for further investigation into nucleobase materials.[14] However, to our knowledge, although various morphologies, including large vesicles,[8] rods[9] and spheres,[13] have been obtained, there is still very little research into the systematic study of the self-assembly of nucleobase-containing polymers. This might result from the poor solubility of nucleobase-containing copolymers, some of which which are only fully soluble in polar organic solvents. Therefore, nucleobase-containing polymers with a relatively high degree of polymerization (DP) have to be synthesized in polar solvents (*e.g.*, DMSO, DMF) to avoid precipitation or to achieve good control; self-assembly is then achieved by post-polymerization processing. These multiple steps limit the synthesis, self-assembly, and other associated studies of nucleobase-containing polymers. Thus, a facile approach to make well-controlled nucleobase-containing polymers and to prepare their corresponding self-assemblies is worthy of investigation.

Heterogeneous polymerizations (including dispersion, emulsion, suspension and precipitation) are easily performed and widely used in industry.[15] In particular heterogeneous polymerizations using controlled/living radical polymerization (CRP) techniques are of great interest recently,[16-18] as they couple the advantages of

heterogeneous polymerizations with the living nature of CRP. This approach has been exploited for the synthesis of block copolymers by reversible addition-fragmentation chain-transfer (RAFT) polymerization,[16,19-21] various forms of atom-transfer radical polymerization (ATRP),[22,23] nitroxide-mediated polymerizations (NMP),[24,25] and other CRP techniques.[26-28] Moreover, some of these processes have been developed for the systematic design of 'nanoobjects' simply by varying the polymerization conditions.[29-40] For example, RAFT dispersion polymerization has been used to grow solvent-insoluble new blocks from solvent-soluble/miscible monomers in the presence of a solvent-soluble macromolecular chain transfer agent (macro-CTA) in both aqueous and organic media.[29,30,41] Block copolymers with narrow molecular weight distributions have been obtained. Moreover, self-assemblies with controlled size and morphology are formed during the polymerization process without further steps. Spherical micelles, wormlike micelles and vesicles were usually obtained sequentially by increasing the length of the insoluble block.[29,41] However, in some cases (*e.g.*, when a relatively long macro-CTA was used[30]) only spherical micelles with different sizes were observed. Furthermore, a few novel morphologies (*e.g.*, lumpy rod,[42] framboidal morphology,[43] or concentric vesicle[44]) or morphology transitions were observed on introduction of a special monomer or condition. In general, heterogeneous CRP has been demonstrated as a facile approach to make common polymers and their corresponding nanostructures. However, little work has been exploited for the synthesis of nucleobase-containing polymers and nanostructures by heterogeneous CRP, which is challenged by the interacting nature of nucleobases, leading to a complex and unpredictable system. Therefore, in this work, we have firstly taken advantage of heterogeneous CRP to

prepare nucleobase-containing polymers and produce their corresponding self-assemblies directly simultaneously.

The nucleobases used in this study, adenine and thymine, are known as complementary base pairs in DNA. In synthetic chemistry, it has been proven that hydrogen bonding interactions still exist between modified adenine and thymine as long as the interaction sites of purine and pyrimidine functionalities are not trapped.[13,14] Methacryloyl-type monomers containing adenine and thymine were previously synthesized and polymerized as discussed in Chapter 2.[4] Moreover, it has been found that both chloroform ($CHCl_3$) and 1,4-dioxane are good solvents to solubilize these monomers and more importantly support the nucleobase interactions (the measured association constants between monomers, K_{asso} = 20 M^{-1} in chloroform at 60 °C[4,45] and K_{asso} = 12 M^{-1} in 1,4-dioxane at 60 °C). According to our previous report in Chapter 2, driven by the appearance of monomer interactions, an alternating copolymer has a tendency to be formed in $CHCl_3$ when monomers containing adenine and thymine are copolymerized. A similar tendency is also expected in 1,4-dioxane.[2] However, the resulting copolymer is insoluble in both $CHCl_3$ and 1,4-dioxane due to the presence of the strong hydrogen bonding interactions among copolymers. Therefore, both $CHCl_3$ and 1,4-dioxane are ideal solvents for the RAFT dispersion polymerization of these nucleobase-containing monomers. Poly(methyl methacrylate) (PMMA) has been selected as the macro-CTA, as it is readily soluble in both $CHCl_3$ and 1,4-dioxane and can be synthesized with good control by RAFT polymerization using 2-cyano-2-propyl dodecyl trithiocarbonate (CPDT) as a chain transfer agent (CTA).[46] As far as we know, this robust method has yet to be applied to synthesize nucleobase-containing polymers or to provide their corresponding nanostructures. Herein, we demonstrate the synthesis

of well-controlled nucleobase-containing polymers and a range of their corresponding nanostructures by RAFT dispersion polymerization. Moreover, new and complex morphologies have been observed in this system.

3.3 Results and discussion

3.3.1 Nucleobase-containing monomers

Nucleobase-containing monomers, 2-(2-(adenine-9-yl)acetoxyl) ethyl methacrylate (AMA) and 2-(2-(thymine-1-yl)acetoxyl) ethyl methacrylate (TMA) shown in Figure 3.1, were synthesized and the homopolymerization and copolymerization of both monomers were demonstrated in Chapter 2.[4] The results showed that the hydrogen bonding interactions between AMA and TMA were solvent-dependent. Monomer interactions occurred in $CHCl_3$, but were suppressed in DMF. Moreover, the apparent reactivity ratios of copolymerizations of AMA and TMA were investigated. The results indicated that the presence and absence of monomer interactions could result in copolymers with different compositions (alternating copolymers tended to be formed in $CHCl_3$ and statistical copolymers were most likely to be synthesized in DMF).

In this Chapter, monomer interactions between AMA and TMA were also investigated *via* ^{1}H NMR spectroscopy in deuterated 1,4-dioxane (1,4-dioxane-d_8) using the same procedure as described in Chapter 2 (Figure 3.1). It was found that increasing the concentration of AMA resulted in a small downfield chemical shift of imide proton of TMA (labeled * in Figure 3.1) at both room temperature and 60 °C. This observation suggests the presence of weak nucleobase interactions in 1,4-dioxane, which is weaker than in $CHCl_3$ but stronger than in DMF due to their different hydrogen bonding acceptor ability.[47] The resulting Job plot (Figure 3.2) indicates the formation of a 1:1 complex between AMA and TMA in 1,4-dioxane. The measured association constant is 12 M^{-1} using Hildebrand – Benesi plot, where the calculation was as same as it in Chapter 2 (Figure 3.3). This further indicates that the monomer interactions in 1,4-dioxane are slightly weaker than those in $CHCl_3$

(K_a = 20 M^{-1}). Furthermore, it has been reported that both $CHCl_3$ and 1,4-dioxane are good solvents to support nucleobase interactions among polymers.[48,49] Moreover, both AMA and TMA are soluble in these two solvents. Therefore, similar observations on polymerization of the two monomers were expected in 1,4-dioxane to those in $CHCl_3$.

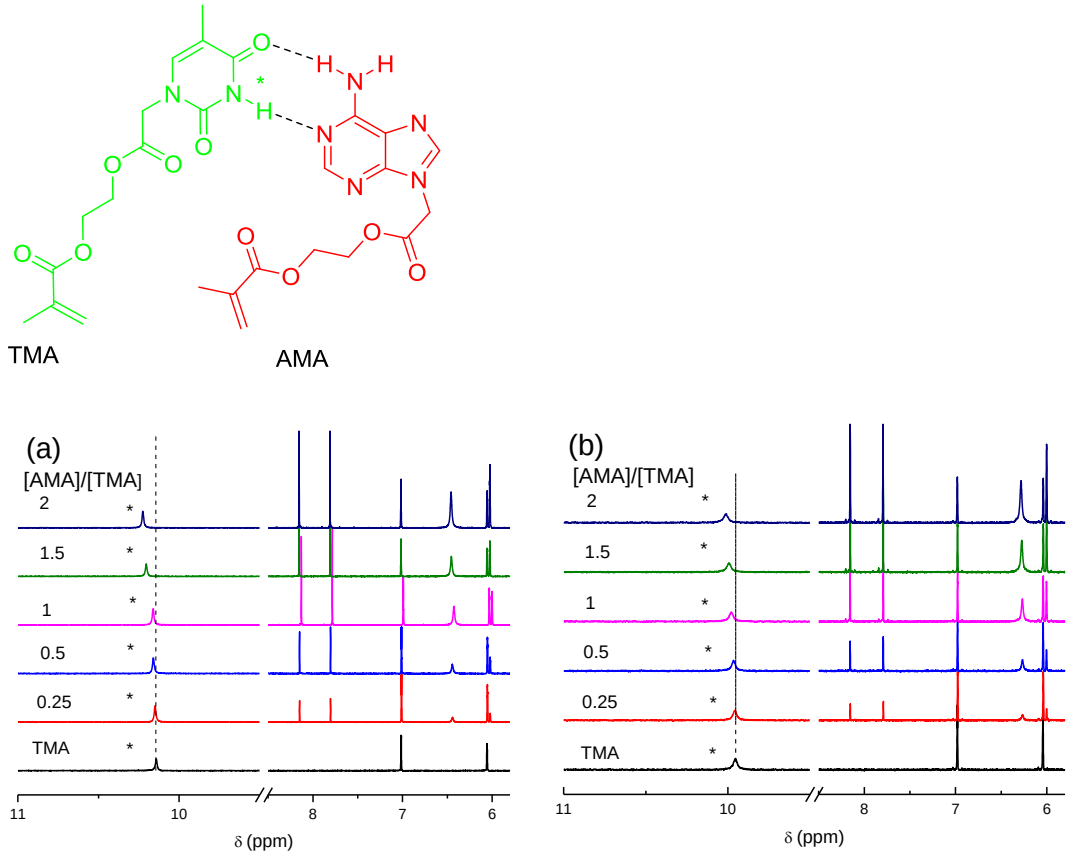

Figure 3.1 The expected hydrogen bonding interactions of the adenine-thymine pair is shown where the key imine signal used in the ^{1}H NMR spectroscopy study is indicated with a * (top); ^{1}H NMR spectra of the AMA and TMA mixtures with varying concentrations of AMA: [TMA] = 5 mM; [AMA] = 0, 1.25, 2.5, 5, 7.5, 10 mM. (a) 1,4-dioxane-d_8, at 25 °C; (b) 1,4-dioxane-d_8, at 60 °C.

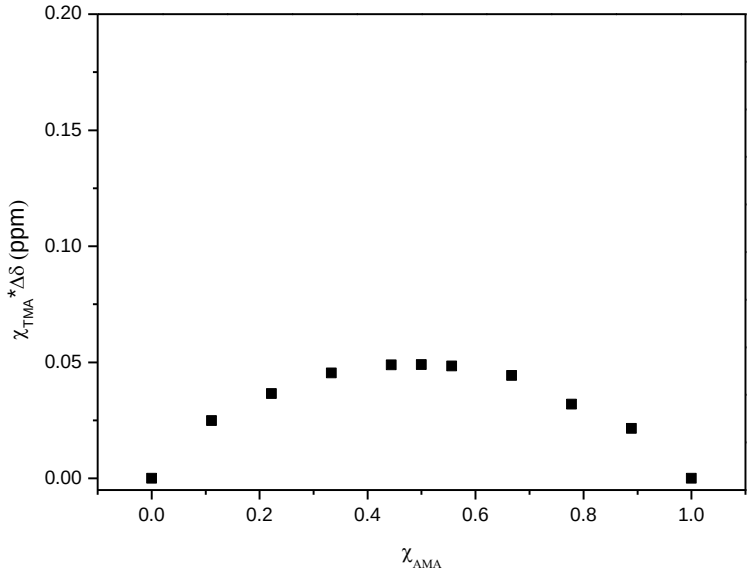

Figure 3.2 Job plot to determine the stoichiometry of the complex of AMA and TMA in 1,4-dioxane-d_8 ([AMA]+[TMA] = 40 mM) at 60 °C.

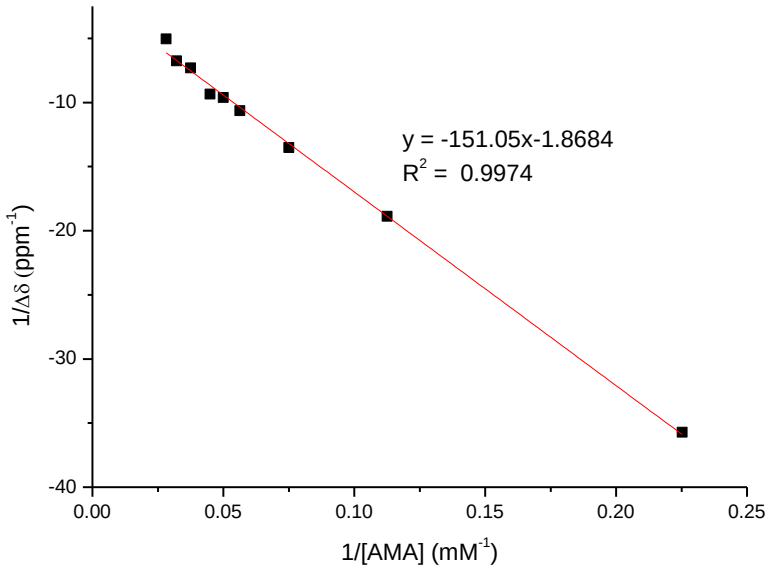

Figure 3.3 Hildebrand – Benesi plot based on 1:1 complex of AMA and TMA in 1,4-dioxane-d_8 at 60 ^{o}C.

$1/\Delta\delta = 1/(K_a\Delta\delta_{max}[AMA]) + 1/\Delta\delta_{max}$.

$1/\Delta\delta_{max} = -1.8684$, $1/K_a\Delta\delta_{max} = -151.05$, $K_a = 12\ M^{-1}$

3.3.2 Synthesis of the macro-CTA

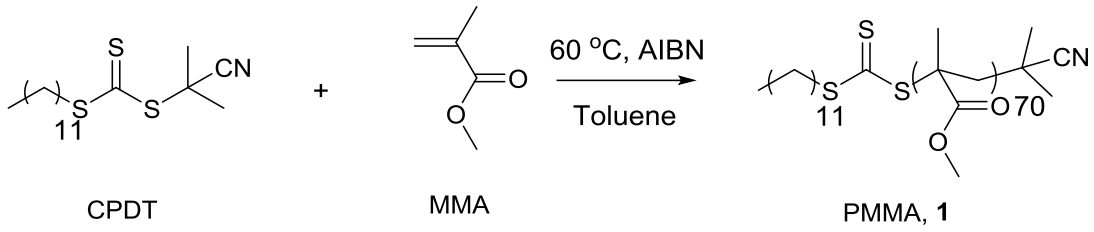

CPDT MMA PMMA, **1**

Scheme 3.1 Synthetic route for the macro-CTA (PMMA, **1**).

The synthetic route for macro-CTA poly(methyl methacrylate) (PMMA) is shown in Scheme 3.1. PMMA was synthesized using 2-cyano-2-propyl dodecyl trithiocarbonate (CPDT) as the CTA, AIBN as the initiator, and toluene as the solvent. The polymerization was stopped at a relatively low conversion (~ 36%) to ensure good end-group fidelity. The DP of the PMMA macro-CTA was determined by ^{1}H NMR spectroscopy by comparing the integration of the backbone signals with those of the end group from CPDT (Figure 3.4, left). The resulting DP of PMMA was *ca.* 70. Furthermore, SEC (DMF eluent, PMMA standards) was used to determine the molecular weight and the molecular weight distribution. The molecular weight from SEC was 7.4 kDa, which is also consistent with the molecular weight determined from ^{1}H NMR spectroscopy. The molecular weight distribution of the resultant polymer was narrow ($Đ_M$ = 1.24). Additionally, RI and UV (309 nm, from the trithiocarbonate end group) chromatograms overlap well, indicating good end group fidelity (Figure 3.4, right). The characterization data for the PMMA macro-CTA are shown in Table 3.1.

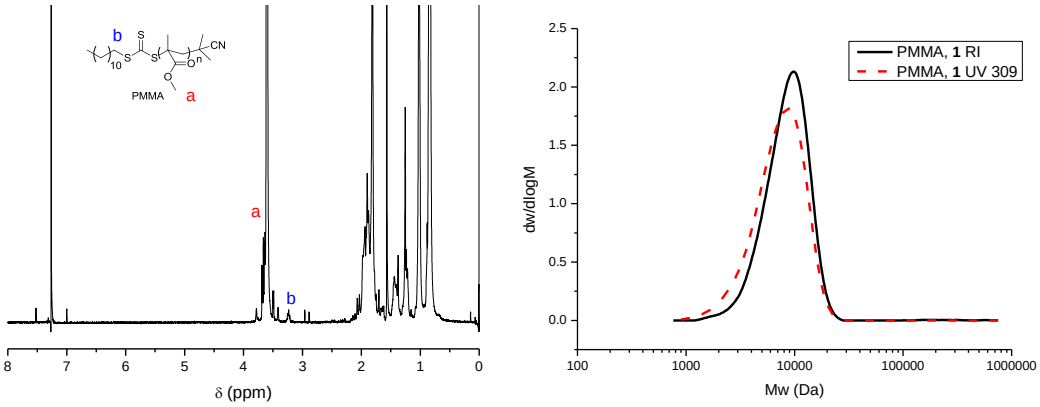

Figure 3.4 ^{1}H NMR spectrum in $CDCl_3$ and SEC trace (DMF eluent, PMMA standards) of PMMA, **1.**

3.3.3 Synthesis of diblock copolymers

To synthesize diblock copolymers, RAFT polymerizations were performed in both $CHCl_3$ and 1,4-dioxane, first using exclusively AMA and then using a 1:1 mixture of AMA and TMA as monomers (Scheme 3.2). Polymerizations were performed at 60 °C, using AIBN as the radical initiator and **1** as the PMMA macro-CTA. The DP of the nucleobase block was varied by adding different equivalences of the monomer to macro-CTA. It should be noted that AMA and TMA are both soluble in $CHCl_3$ and 1,4-dioxane, but form insoluble homopolymers or copolymers in these two solvents. This suggests that RAFT dispersion polymerization would proceed and self-assembly would be induced by the polymerizations.[30]

The characterization data of all polymers are shown in Table 3.1. High conversion ($\geq$ 90%) was attained for each chain extension polymerization as determined by ^{1}H NMR spectroscopy. Comparison of the SEC traces of macro-CTA and the synthesized diblock copolymers (Figure 3.5 and 3.6) indicate that well-defined diblock copolymers were obtained with relatively high blocking efficiencies and low macro-CTA contamination. In most cases well-defined polymers with narrow dispersity values were obtained ($Đ_M$ < 1.40), consistent with previously reported

systems,[29,30] although some polymers were found to possess slightly higher dispersities. However, the nature of nucleobases leads to potential interactions among monomers and polymers and hence results in a complex polymerization system which may account for the observed broadening of dispersity in some cases.

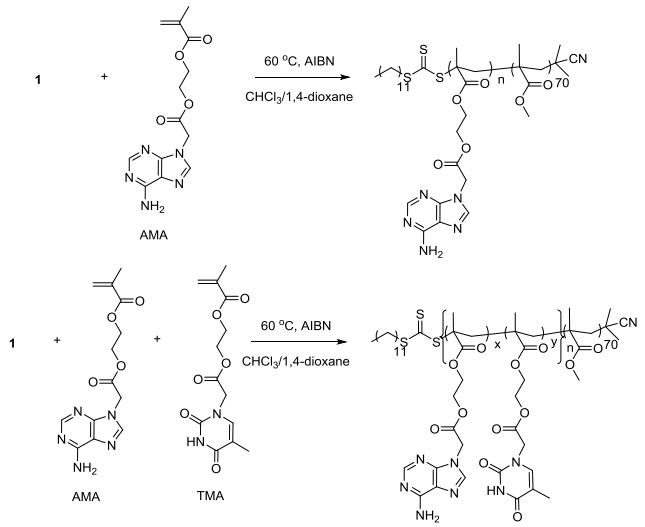

Scheme 3.2 Synthetic route for the nucleobase-containing diblock copolymers using RAFT polymerization.

Table 3.1 Characterization data of nucleobase-containing polymers

Solvent	Polymer/polymerization	Conv. (%)	$M_{n,th}$ (kDa)	$M_{n,\ NMR}$[a] (kDa)	$M_{n,\ SEC}$[b] (kDa)	$Đ_M$
toluene	$PMMA_{70}$ **1**	36	4.5	7.0	7.4	1.24
$CHCl_3$	$PMMA_{70}$-*b*-$PAMA_{50}$ **2**	92	20.5	21.4	24.7	1.46
$CHCl_3$	$PMMA_{70}$-*b*-($PAMA_{0.5}$-*co*-$PTMA_{0.5}$)$_{50}$ **3**	95	21.3	26.8	26.1	1.32
$CHCl_3$	$PMMA_{70}$-*b*-$PAMA_{100}$ **4**	95	37.0	40.3	41.1	1.20
$CHCl_3$	$PMMA_{70}$-*b*-($PAMA_{0.5}$-*co*-$PTMA_{0.5}$)$_{100}$ **5**	98	37.0	44.8	38.2	1.76
1,4-dioxane	$PMMA_{70}$-*b*-$PAMA_{50}$ **6**	92	20.5	21.4	25.2	1.39
1,4-dioxane	$PMMA_{70}$-*b*-($PAMA_{0.5}$-*co*-$PTMA_{0.5}$)$_{50}$ **7**	90	20.5	23.8	25.6	1.25
1,4-dioxane	$PMMA_{70}$-*b*-$PAMA_{100}$ **8**	98	37.0	40.3	32.0	1.21
1,4-dioxane	$PMMA_{70}$-*b*-($PAMA_{0.5}$-*co*-$PTMA_{0.5}$)$_{100}$ **9**	90	37.0	44.8	30.5	1.36
1,4-dioxane	$PMMA_{70}$-*b*-$PAMA_{150}$ **10**	99	52.0	55.6	38.6	1.09
1,4-dioxane	$PMMA_{70}$-*b*-($PAMA_{0.5}$-*co*-$PTMA_{0.5}$)$_{150}$ **11**	90	52.0	54.7	38.4	1.50

[a]determined by ^{1}H NMR spectroscopy; [b]determined by SEC analysis (DMF eluent, PMMA standards).

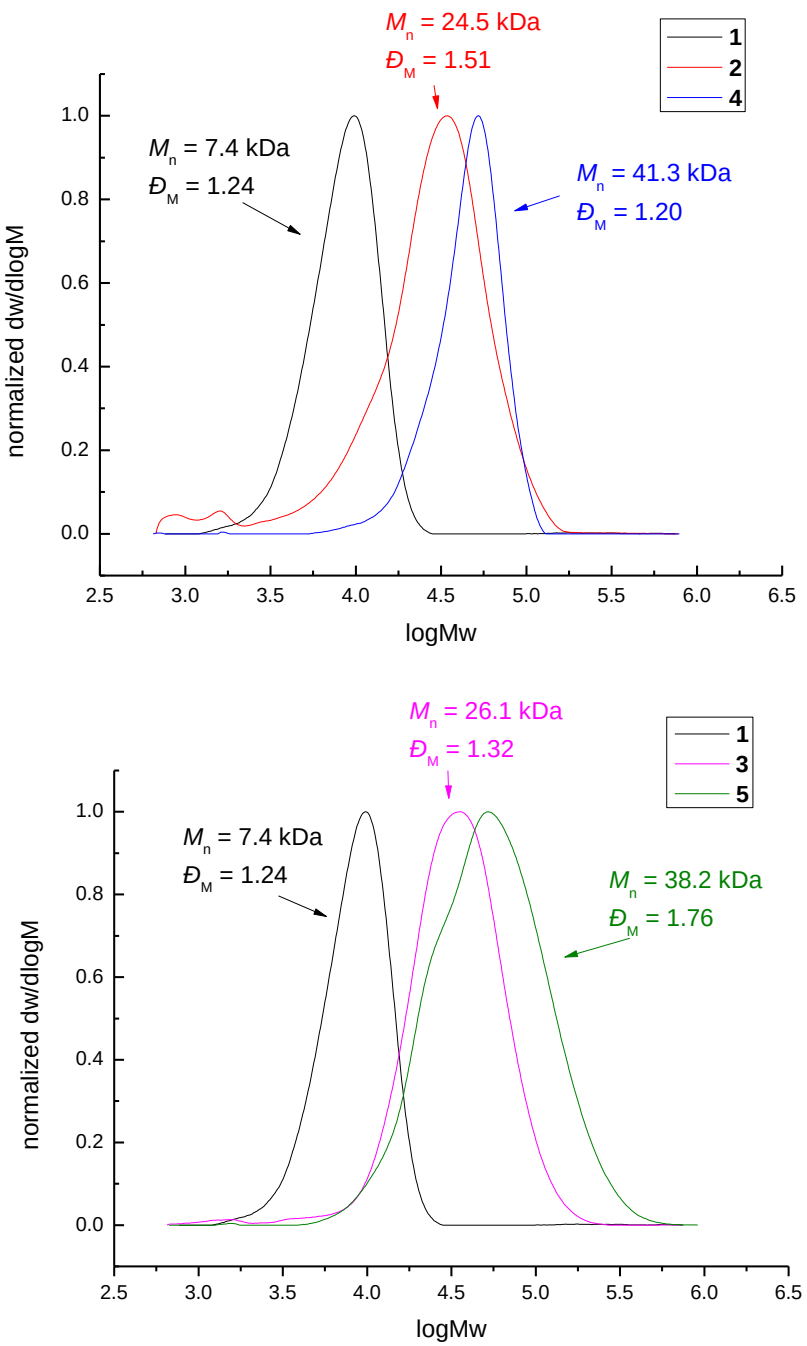

Figure 3.5 SEC traces of polymers **1** ($PMMA_{70}$), **2** ($PMMA_{70}$-*b*-$PAMA_{50}$), **4** ($PMMA_{70}$-*b*-$PAMA_{100}$) and **3** ($PMMA_{70}$-*b*-($PAMA_{0.5}$-*co*-$PTMA_{0.5}$)$_{50}$), **5** ($PMMA_{70}$-*b*-($PAMA_{0.5}$-*co*-$PTMA_{0.5}$)$_{100}$) prepared by RAFT dispersion polymerization in $CHCl_3$. (DMF eluent, PMMA standards).

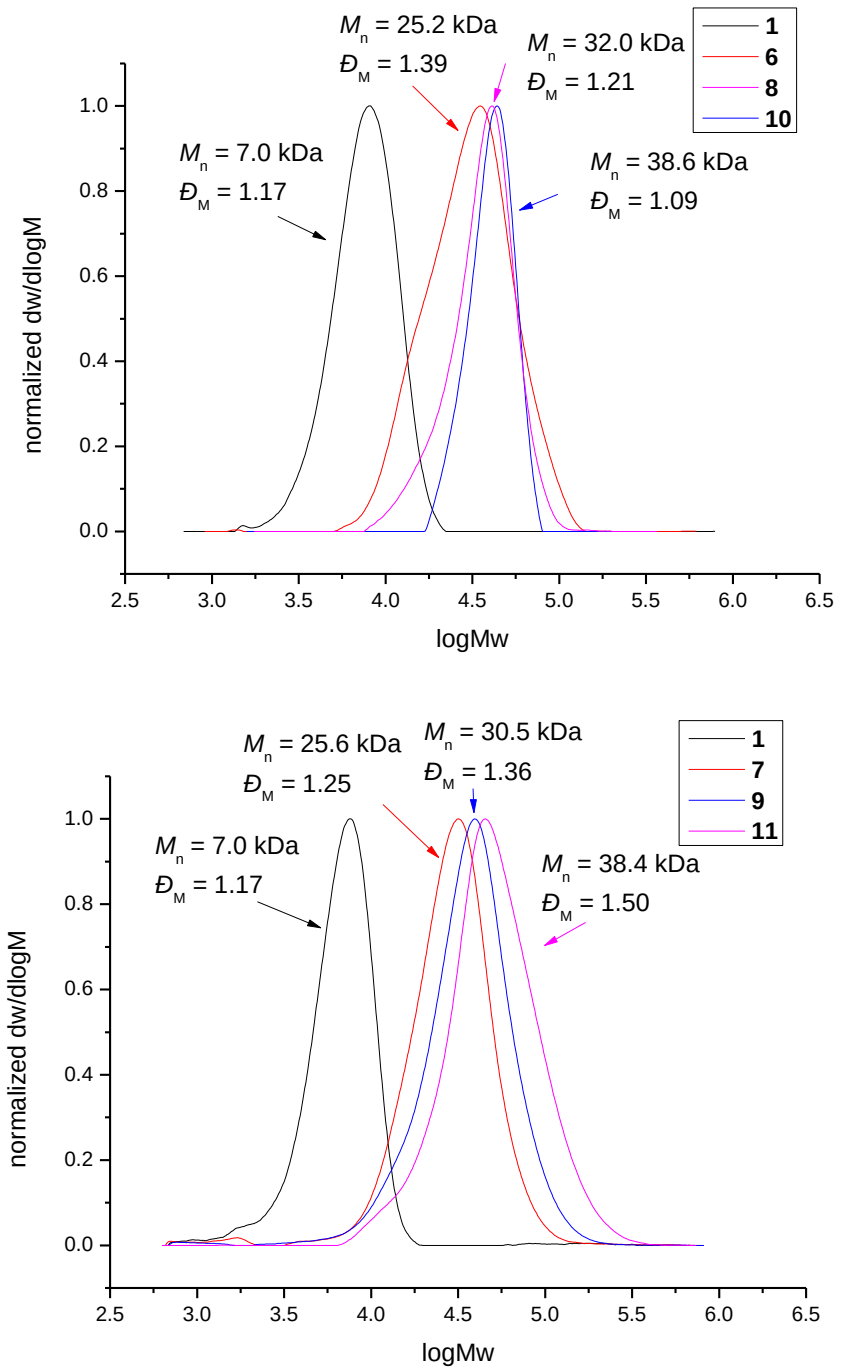

Figure 3.6 SEC traces of polymers **1** ($PMMA_{70}$), **6** ($PMMA_{70}$-*b*-$PAMA_{50}$), **8** ($PMMA_{70}$-*b*-$PAMA_{100}$), **10** ($PMMA_{70}$-*b*-$PAMA_{150}$) and **7** ($PMMA_{70}$-*b*-($PAMA_{0.5}$-*co*-$PTMA_{0.5}$)$_{50}$), **9** ($PMMA_{70}$-*b*-($PAMA_{0.5}$-*co*-$PTMA_{0.5}$)$_{100}$), **11 (**($PMMA_{70}$-*b*-($PAMA_{0.5}$-*co*-$PTMA_{0.5}$)$_{150}$)**,** prepared by RAFT dispersion polymerization in 1,4-dioxane. (DMF eluent, PMMA standards).

3.3.4 Kinetics of RAFT dispersion polymerization 3 in $CHCl_3$

The kinetics of the RAFT dispersion polymerization in $CHCl_3$ were studied by chain-extending the PMMA macro-CTA using a 1:1 mixture of AMA and TMA at 60 °C. Monomer conversion data obtained by ^{1}H NMR spectroscopy are shown in Figure 3.7 for a target diblock copolymer of $PMMA_{70}$-*b*-($PAMA_{0.5}$-*co*-$PTMA_{0.5}$)$_{50}$, **3**. It should be noted that conversions of each monomer were very similar during the whole polymerization. High conversion (≥ 85%) was obtained after 10 hours. The evolution of SEC traces with monomer conversion is shown in Figure 3.8. Interestingly, obvious bimodal peaks were observed at low conversions (3 hours and 5 hours). The SEC traces after 3 hours and 5 hours show that the high molecular weight polymer traces stay the same, but the peaks for the low molecular weight polymers change. As the polymerization proceeds, the low molecular weight polymer trace decreases in intensity when the peaks for the high molecular weight polymer are normalized. This observation indicates that the macro-CTA did not undergo chain extension at the same time or at the same rate. However, the resultant diblock copolymers with low dispersity values were obtained at high conversions ($Đ_M$ = 1.32). Three separate polymerizations with the same starting mixture were also performed and stopped at designated reaction times (4 hours, 10 hours and 16 hours). The monomer conversion data and SEC traces are shown in Figure 3.9. Similar results were observed, demonstrating that this phenomenon is reproducible and repeatable. This observation is different to the previously reported results in the literature, where the molecular weight increases linearly with conversion, indicating that an unusual RAFT dispersion polymerization is occurring in this system.

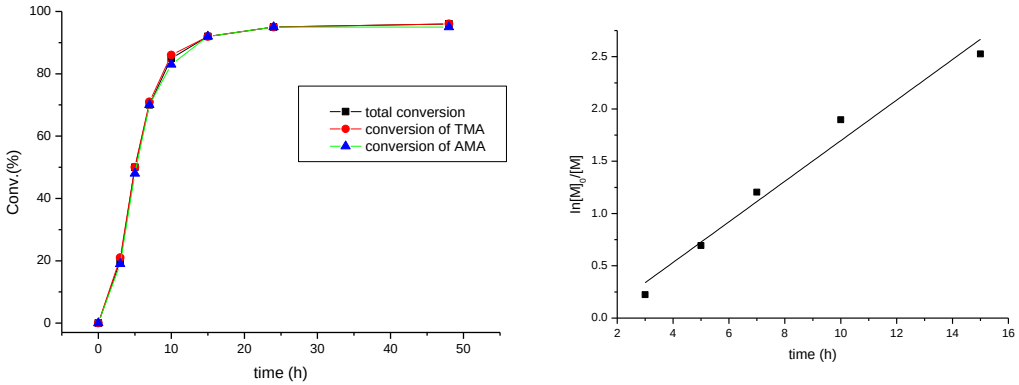

Figure 3.7 Conversion *vs.* time plot and corresponding semi-logarithmic plot obtained for the dispersion polymerization of a 1:1 mixture of AMA and TMA at 60 °C using a $PMMA_{70}$ macro-CTA in $CHCl_3$. The target diblock composition was $PMMA_{70}$-*b*-($PAMA_{0.5}$-*co*-$PTMA_{0.5}$)$_{50}$, **3**.

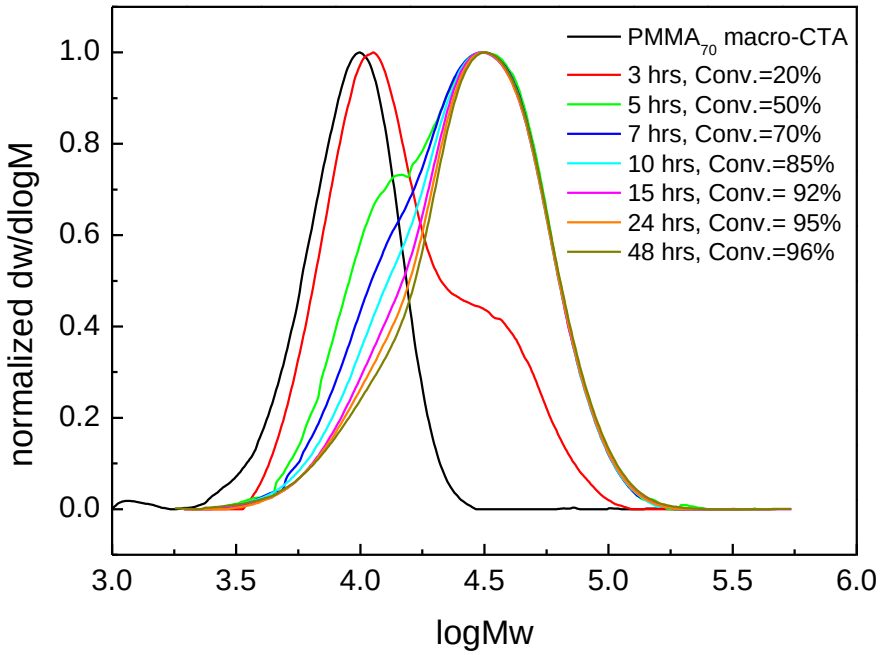

Figure 3.8 SEC traces (DMF as eluent, PMMA standard) with monomer conversion using a $PMMA_{70}$ macro-CTA for the RAFT dispersion polymerization of a 1:1 mixture of AMA and TMA in $CHCl_3$ at 60 °C. The target diblock composition was $PMMA_{70}$-*b*-($PAMA_{0.5}$-*co*-$PTMA_{0.5}$)$_{50}$, **3**.

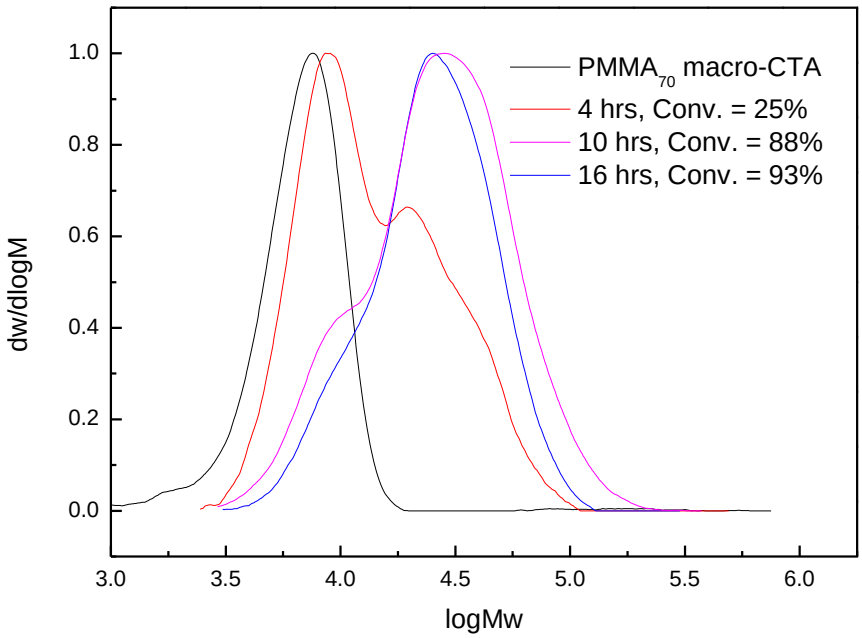

Figure 3.9 SEC traces and their corresponding monomer conversions obtained from separate RAFT dispersion polymerizations, which were stopped at different reaction times. Note that the condition of the RAFT dispersion polymerization is the same as was used for the kinetic study of **3**, $PMMA_{70}$-*b*-($PAMA_{0.5}$-*co*-$PTMA_{0.5}$)$_{50}$.

3.3.5 Kinetic study on morphologies induced by polymerization 3 in $CHCl_3$

To assess the evolution of morphology and size distribution with monomer conversion in this RAFT dispersion polymerization in $CHCl_3$, the polymerization solution **3** was also periodically sampled and analyzed by unstained dry-state TEM on graphene oxide (GO)[50] and DLS analysis,[51] the results of which are shown in Figure 3.10. During the polymerization the mixture became translucent after approximately 3 hours (20% conversion) and as the polymerization proceeded, the mixture became more opalescent, but no precipitation was observed. It should be noted that no additional change in transparency was observed by visual inspection after 10 hour, which is also consistent with the high monomer conversion obtained after 10 hours. These observations suggest that self-assembly was induced in this polymerization system. Moreover, small-angle neutron scattering (SANS)

experiment was conducted at the end of the polymerization, which allows access to all morphologies available in solution.

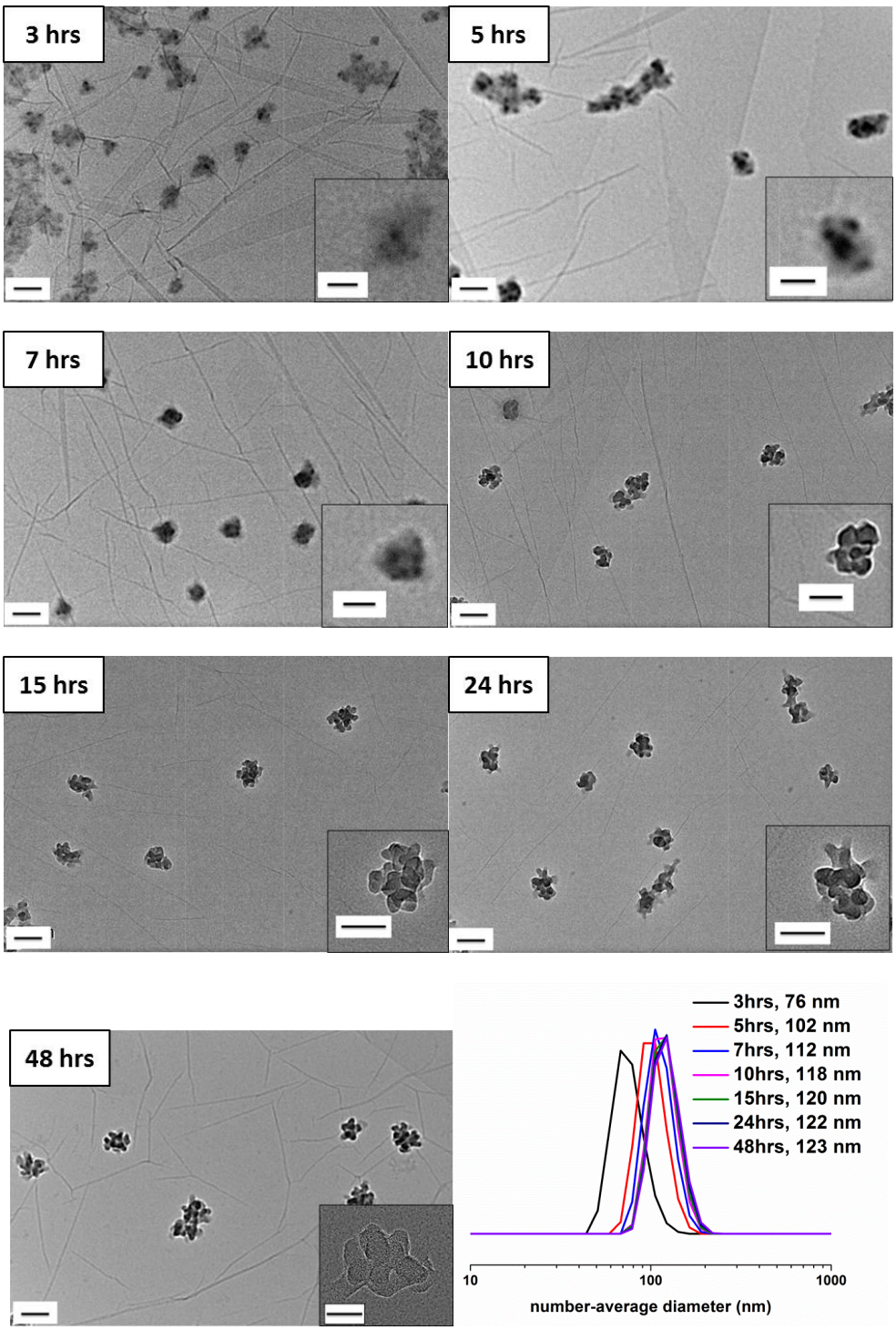

Figure 3.10 Evolution of the self-assembly by unstained TEM analysis and number-average diameter as determined by DLS with monomer conversion using a $PMMA_{70}$ macro-CTA for the RAFT dispersion polymerization of a 1:1 mixture of AMA and TMA in $CHCl_3$ at 60 °C. The target diblock composition was $PMMA_{70}$-*b*-($PAMA_{0.5}$-*co*-$PTMA_{0.5}$)$_{50}$, **3**. Scale bar: 100 nm (inset: 50 nm). The inset image of the 48 hour sample was taken by TEM at a higher magnification (150 k).

After 3 hours, when monomer conversion was about 20% and a bimodal SEC trace was obtained (Figure 3.8, SEC trace of 3 hours), close to spherical micelles with some evidence of internal structure (tiny dark dots inside assembly) were observed with a number-average diameter of 76 nm (Figure 3.10, TEM and DLS of 3 hours). Increasing the conversion to 50% (Figure 3.8, SEC trace of 5 hours) also resulted in the observation of spherical micelles with internal structure (Figure 3.10, TEM of 5 hours). It should be noted that at this conversion (50%) a bimodal SEC trace was still observed, but compared to the copolymers obtained at 3 hours, the relative ratio of the two populations was reversed (more polymers with high molecular weight were obtained at 5 hours). Larger spherical micelles were observed for the 7 hour sample and 70% monomer conversion was achieved (Figure 3.10, 7 hours). Moreover, as mentioned above, the low molecular weight trace reduced further (Figure 3.8, SEC trace of 7 hours). Once the conversion increased to 85%, when monodisperse diblocks were generally obtained (Figure 3.8, SEC trace of 10 hours), popcorn-like structures were observed by TEM (Figure 3.10, TEM of 10 hours). There was no obvious morphology change observed with further increasing monomer conversion (Figure 3.10-15 hours, 24 hours, and 48 hours). The sample from 48 hours was also characterized by TEM at a higher magnification (150 k), which is shown in the inset of Figure 3.10 (48 hrs). An internal structure is clearly observed and thus popcorn-like micelles were the final structure attained in this case. Moreover, the particles were treated with sonication for 1 hour to test their stability. No obvious size and morphology changes were observed, suggesting high stability of the particles (Figure 3.11). SANS was conducted on a concentrated liquid sample (20 mg/mL), which was directly obtained after polymerization without further dilution. Unfortunately, models including a Guinier-Porod, a ‘Raspberry’, a ‘Fuzzy sphere’ and a ‘Polycore

shell' were unsuccessfully fitted. A fractal model with some dispersity for the subunits was used to determine some dimensions of the assembly (Figure 3.12).[52] For a fractal object of fractal dimension *d (i.e.* its mass *M* scales with its size *R* according to $M \alpha R^d$), the scattering cross-section follows $I(q) \alpha q^{-d}$. Thus it is possible to determine the fractal dimension at low *q* with a power law when plotting log(*I*(*q*)) *versus* log (*q*).[53] A fractal dimension of 2.9 was found which correlates with a mass fractal and indicates a 3D-object was afforded.

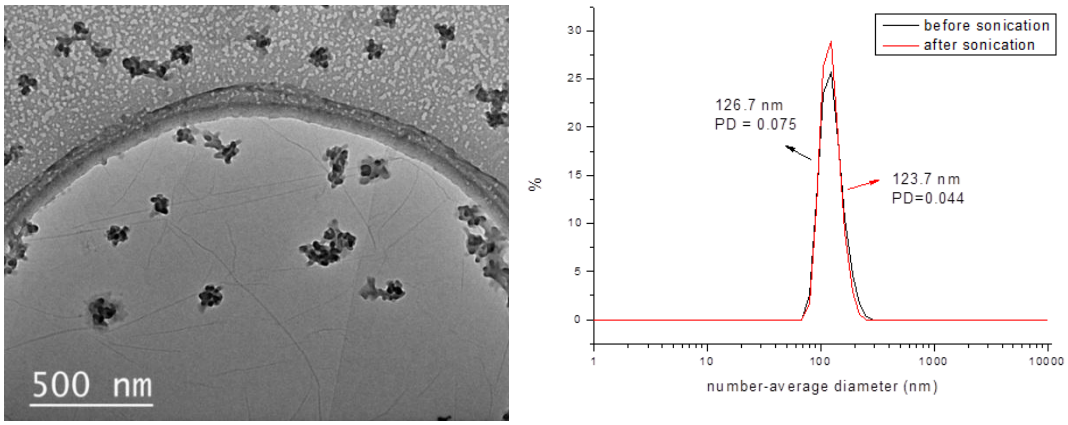

Figure 3.11 TEM and DLS of self-assembly prepared by **3** upon sonication for 1 hour.

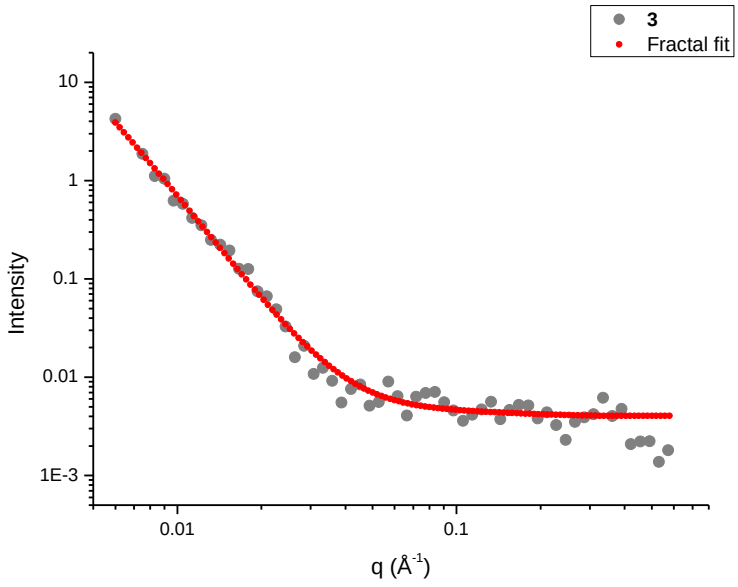

Figure 3.12 SANS experiment profile and fitting of the solution of **3**, $PMMA_{70}$-*b*-($PAMA_{0.5}$-*co*-$PTMA_{0.5}$)$_{50}$ with a fractal model.

3.3.6 Morphologies induced by polymerizations in $CHCl_3$

To further study the morphologies induced by polymerization in $CHCl_3$, a range of diblock copolymers $PMMA_{70}$-*b*-($PAMA_x$-*co*-$PTMA_y$)$_n$ (Table 3.1, polymers **2**, **3**, **4**, and **5**) were analyzed by TEM to assess their morphologies. Predominantly spherical structures were observed when using $CHCl_3$ as the polymerization solvent (Figure 3.13). When chain extended with exclusively AMA, irregular but almost spherical micelles were observed (Figure 3.13, **2** and **4**). TEM images reveal that the sizes of particles increase significantly by targeting higher DP values for the core-forming block (Figure 3.13 polymer **2**, DP is 50; Figure 3.13 polymer **4**, DP is 100). This observation was also confirmed by DLS studies, where the number-average diameters of particles increased from 68 nm to 169 nm when the targeted DP of the AMA polymer (PAMA) block went from 50 to 100 (Figure 3.13). No additional morphologies were obtained when further increasing the DP of the PAMA block to 150 (polymer **12**) and 200 (polymer **13**) (Table 3.2, Figure 3.14 and 3.15). However, the sizes of the spherical particles continued to increase and the periphery of the particles became smoother with increasing length of PAMA blocks. In addition, a thymine-containing containing mediator, 1-hexylthymine was synthesized according to a previous method.[1] The synthetic route was shown in Scheme 3.3 and the mediator was characterized by ^{1}H NMR and ^{13}C DEPT NMR spectroscopy, suggesting a successful synthesis (Figure 3.16). RAFT dispersion polymerizations **2** and **4** were further carried out in the presence of the thymine-containing mediator (ratio of monomer: mediator = 1:1), named as **2'** and **4'** respectively. High conversions were obtained for polymerizations **2'** and **4'** (83% for **2'** and 95% for **4'**). The resultant self-assemblies were characterized by TEM analysis, where

spherical particles were again observed, showing that little effect of thymine-mediator on the resultant morphologies (Figure 3. 17).

In the case of a mixture of AMA and TMA as monomers, spherical structures with rough surfaces were obtained (Figure 3.13, **3** and **5**). The particles grew bigger when a higher DP of the core-forming block was targeted. This size change was again witnessed by a combination of TEM and DLS. In particular, the morphology of particles prepared by polymerizations **4** and **5** by TEM analysis is very similar to the structure, staggered lamella, which has been observed previously by Liu and coworkers.[54] In Liu's work, the staggered lamella morphology was formed due to the strong π-π stacking interactions between side groups, which could be disassembled into small sheetlike nanostructures upon ultrasonication, suggesting that the small sheets might act as primary building blocks.[54] These staggered lamellae exhibited extended blood circulation duration and fastest cellular uptake compared to spheres, large compound vesicles, and smooth disks.[54] In our study, there are relative strong hydrogen bonding interactions and π-π stacking interactions between nucleobase side groups, which might contribute to the formation of similar structures based on TEM analysis. Moreover, it was noted that the sizes obtained from DLS are larger than those observed by TEM, which is due to the collapsed structure of the polymers in the dry-state.

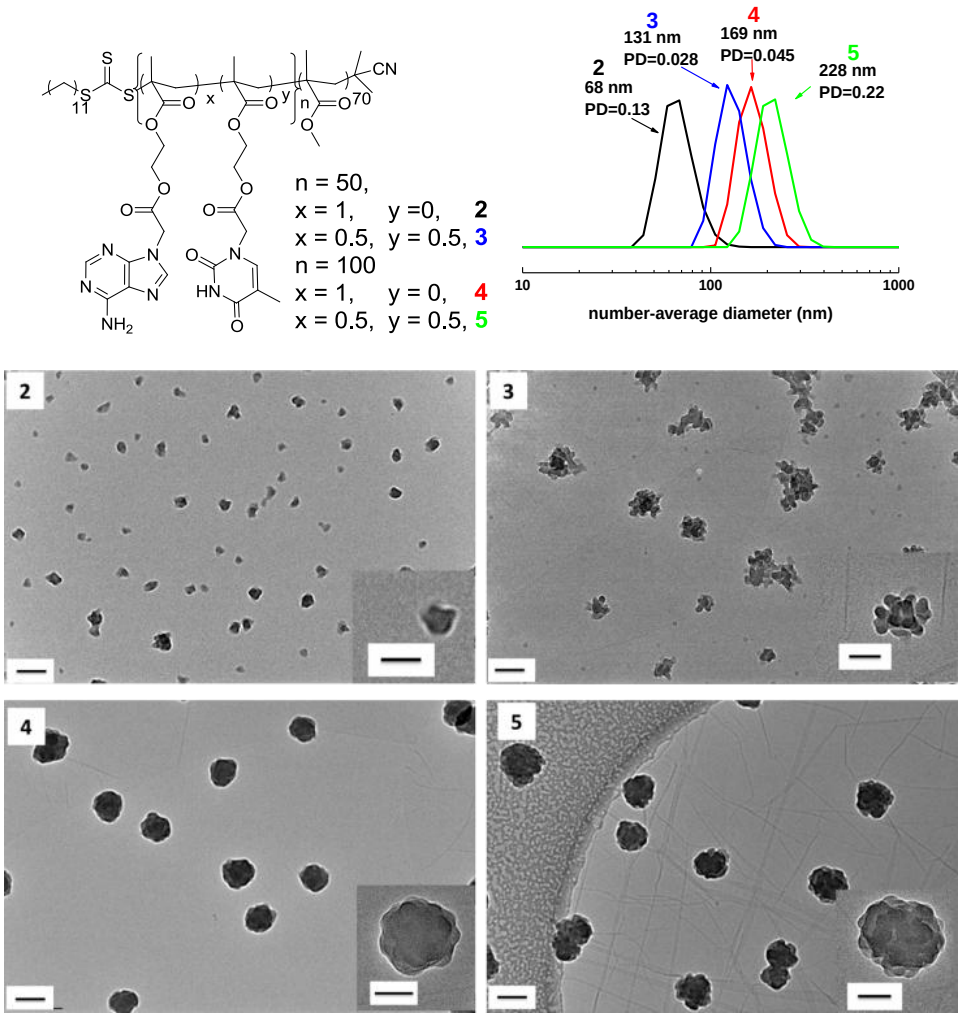

Figure 3.13 Representative TEM images of self-assemblies prepared by RAFT dispersion polymerization in $CHCl_3$, their corresponding polymer structures and DLS particle size distributions of **2** ($PMMA_{70}$-*b*-$PAMA_{50}$), **3** ($PMMA_{70}$-*b*-($PAMA_{0.5}$-*co*-$PTMA_{0.5}$)$_{50}$), **4** ($PMMA_{70}$-*b*-$PAMA_{100}$) and **5** ($PMMA_{70}$-*b*-($PAMA_{0.5}$-*co*-$PTMA_{0.5}$)$_{100}$). Scale bar 100 nm (inset 50 nm).

Table 3.2 Characterizaion data of $PMMA_{70}$-*b*-$PAMA_n$ with higher PAMA DPs

Solvent	Polymer/polymerization	Conv. (%)	$M_{n,th}$ (kDa)	$M_{n,NMR}$[a] (kDa)	$M_{n,SEC}$[b] (kDa)	$Đ_M$
$CHCl_3$	$PMMA_{70}$-*b*-$PAMA_{150}$, **12**	85	45.2	44.5	38.3	1.27
$CHCl_3$	$PMMA_{70}$-*b*-$PAMA_{200}$, **13**	85	58.0	54.0	38.6[c]	1.35[c]

[a]determined by ^{1}H NMR spectroscopy in DMSO-d_6; [b]determined by SEC analysis (DMF eluent, PMMA standards); [c]polymer is not fully soluble in DMF.

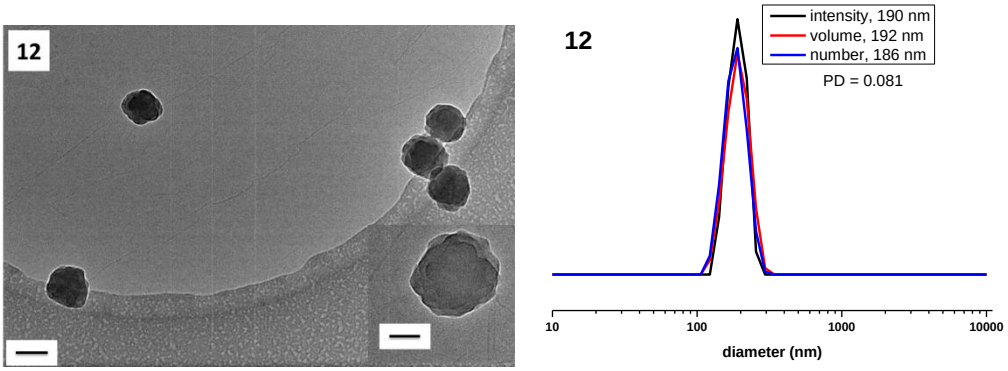

Figure 3.14 TEM and DLS analysis of target polymer **12**, $PMMA_{70}$-*b*-$PAMA_{150}$ prepared in $CHCl_3$. Scale bar 100 nm (inset: 50 nm).

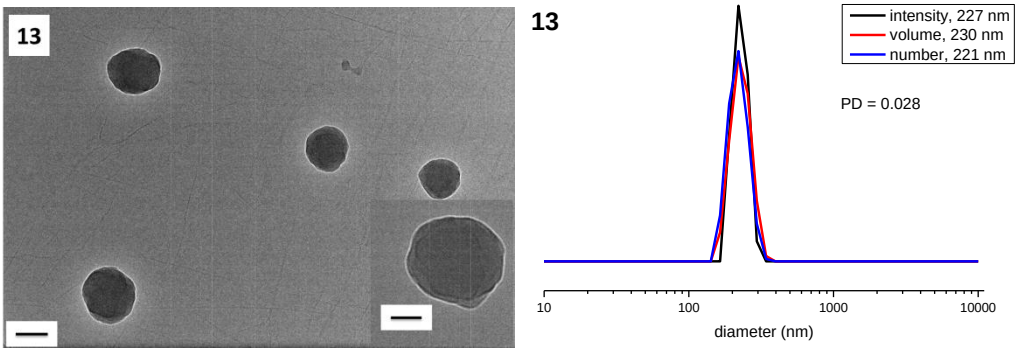

Figure 3.15 TEM and DLS analysis of target polymer **13**, $PMMA_{70}$-*b*-$PAMA_{200}$ prepared in $CHCl_3$. Scale bar 100 nm (inset: 50 nm).

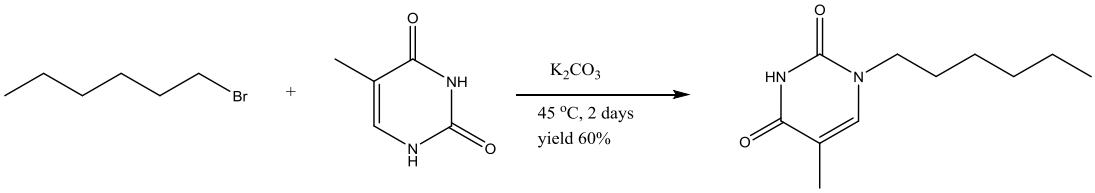

Scheme 3.3 Synthetic route for thymine-containing mediator, 1-hexyl thymine.

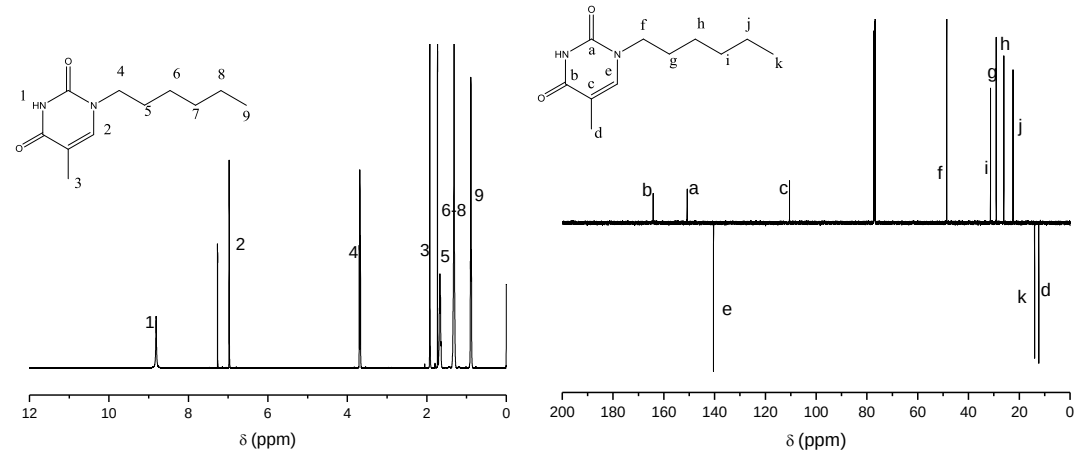

Figure 3.16 ^{1}H NMR and ^{13}C DEPT NMR spectra of thymine-containing mediator in $CDCl_3$.

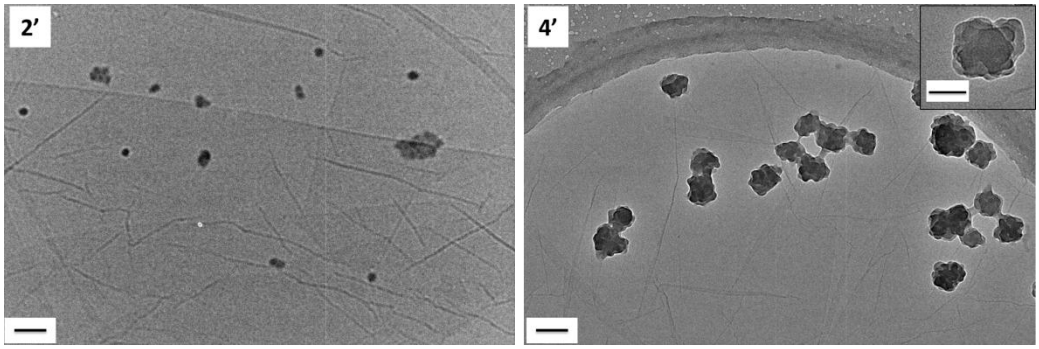

Figure 3.17 Representative unstained TEM images on GO-TEM grids of self-assemblies **2'** and **4'** prepared by RAFT dispersion polymerization in $CHCl_3$ with thymine-containing mediator for target copolymers **2** ($PMMA_{70}$-*b*-$PAMA_{50}$) and **4** ($PMMA_{70}$-*b*-$PAMA_{100}$). Scale bar 100 nm (inset: 50 nm).

As observed above, in terms of a mixture of AMA and TMA as monomers, the micelles, prepared by polymerization **3,** appeared to be 'popcorn-like' structures. To further study these structures, AFM was carried out on the same GO-grid as was used in TEM microscopy. From AFM images, 'popcorn-like' structures along with a few small spheres are clearly observed (Figure 3.18). Moreover, the heights of the large particles were measured as around 80 nm (Figure 3.18), which fit well with the results shown from TEM and is close to the value from DLS analysis. To eliminate the possibility that the popcorn-like structures were formed simply by aggregation or fusion of smaller micelles, which may result from the cooling process or a drying-effect, variable-temperature SLS and DLS were utilized to obtain more details about the popcorn structures. As these techniques are conducted on a sample in solution, the structure can retain in their solvated state and thus artifacts caused by drying, which could happen during TEM sample preparation, should not occur.

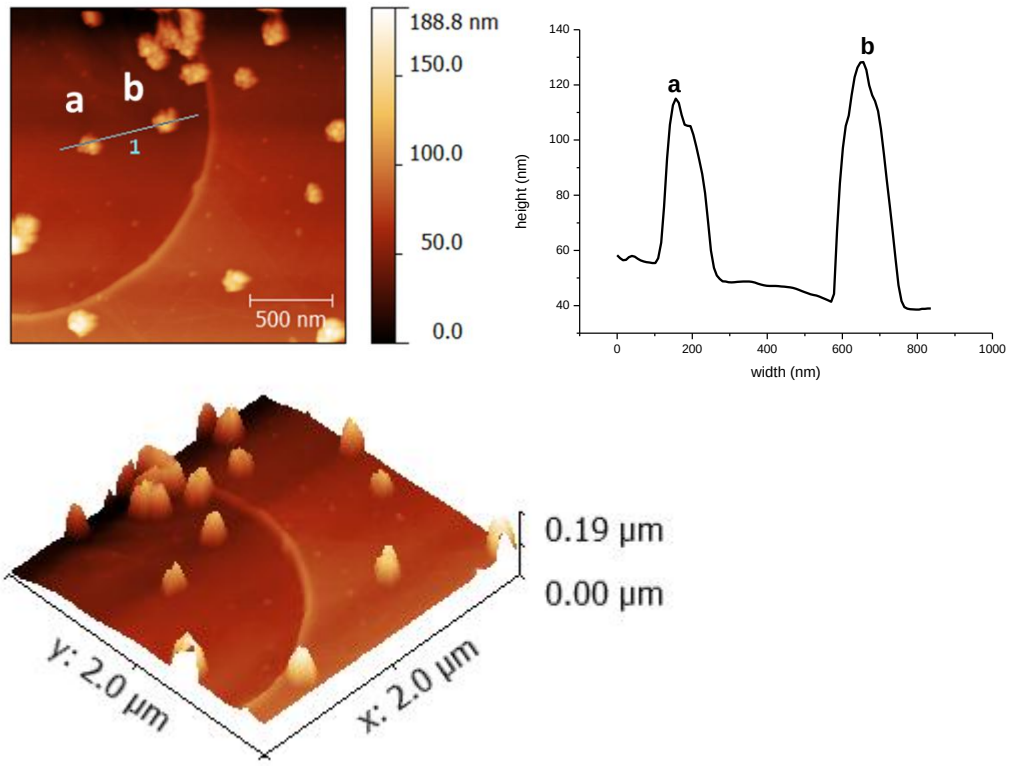

Figure 3.18 AFM height image (top left) and three-dimensional AFM image (bottom) of self-assembly prepared by polymerization **3**, $PMMA_{70}$-*b*-($PAMA_{0.5}$-*co*-$PTMA_{0.5}$)$_{50}$ and the corresponding height profile (top right).

There was no size change observed by variable-temperature DLS (Figure 3.19). The number-average diameters of 'popcorn-like' particles were measured at different concentrations (0.032 mg/mL to 1 mg/mL) and at variable temperatures (20 °C to 60 °C). It was found that at one temperature (20 °C to 60 °C) there was no obvious size change upon dilution. Meanwhile, no change in size was observed by DLS analysis when a sample was heated from 20 °C to 60 °C and then cooled down from 60 °C to 20 °C. Furthermore, the aggregation numbers were carefully measured by SLS at both 20 °C and 50 °C, which are close to the temperatures used for microscopy sample preparation and polymerization respectively. The Zimm equation (Equation 1.10, in Chapter 1) is often used to determine weight average molecular weight of the particles and radius of gyration (R_g) by extrapolation of the data to zero angle and zero concentration

(more details in Chapter 1, Section 1.5.2.2). The concentrations of the sample ranged from 0.25 mg/mL to 0.031 mg/mL. It was determined that there was no significant change in aggregation number observed from the results of SLS (Figure 3.20 and 3.21, N_{agg} = 29,000 at 20 °C and N_{agg}= 33,000 at 50 °C). P-ratio (R_g/R_H, ratio between radius of gyration and hydrodynamic radius) at both temperatures were calculated to be smaller than 1 (R_g/R_H = 0.81 at 20 °C and R_g/R_H = 0.79 at 50 °C), indicating that the particles were solid spheres at both temperatures. However, it should be noted that the calculated large aggregation numbers indicate the formation of complex spheres rather than simple core-shell structures. These results prove that the particles were stable when heating from room temperature to 50 °C and thus suggests that the 'popcorn-like' structure observed by TEM was formed during the polymerization and was not induced by cooling down or a drying effect upon TEM analysis.

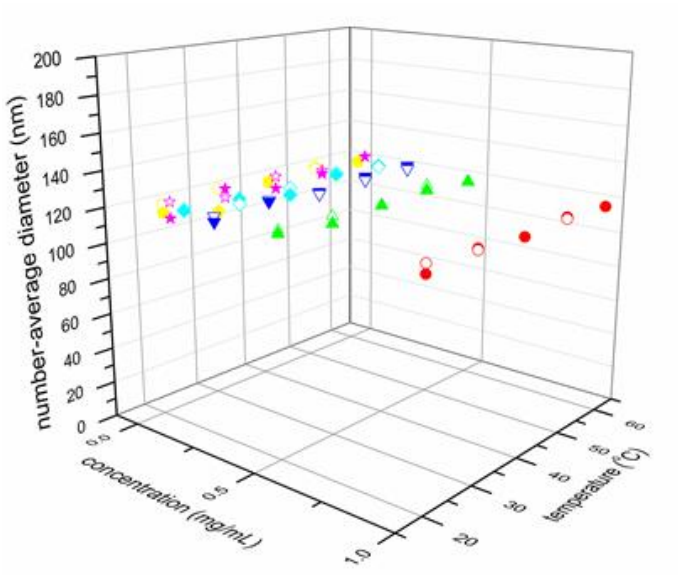

Figure 3.19 Number-average diameters of self-assembly with different concentrations of polymerization **3**, $PMMA_{70}$-*b*-($PAMA_{0.5}$-*co*-$PTMA_{0.5}$)$_{50}$ at different temperatures measured by variable temperature DLS (hollow symbol is for heating cycle; solid symbol is for cooling cycle).

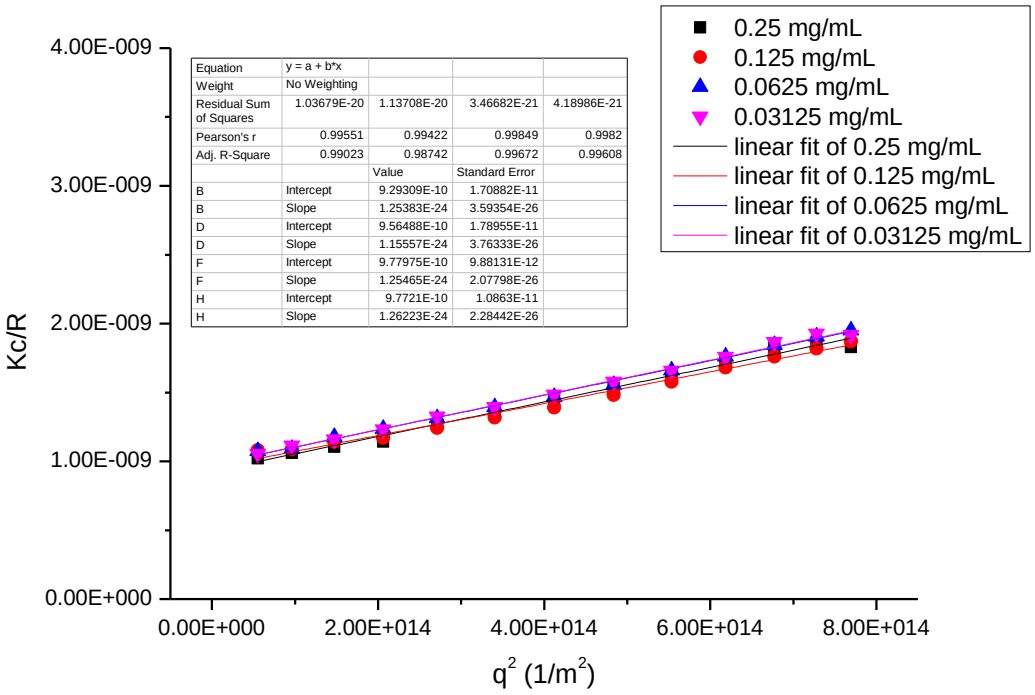

Figure 3.20 Zimm plots for self-assembly prepared by polymerization **3**, $PMMA_{70}$-*b*-$(PAMA_{0.5}$-*co*-$PTMA_{0.5})_{50}$ in $CHCl_3$ measured by SLS at 20 °C.

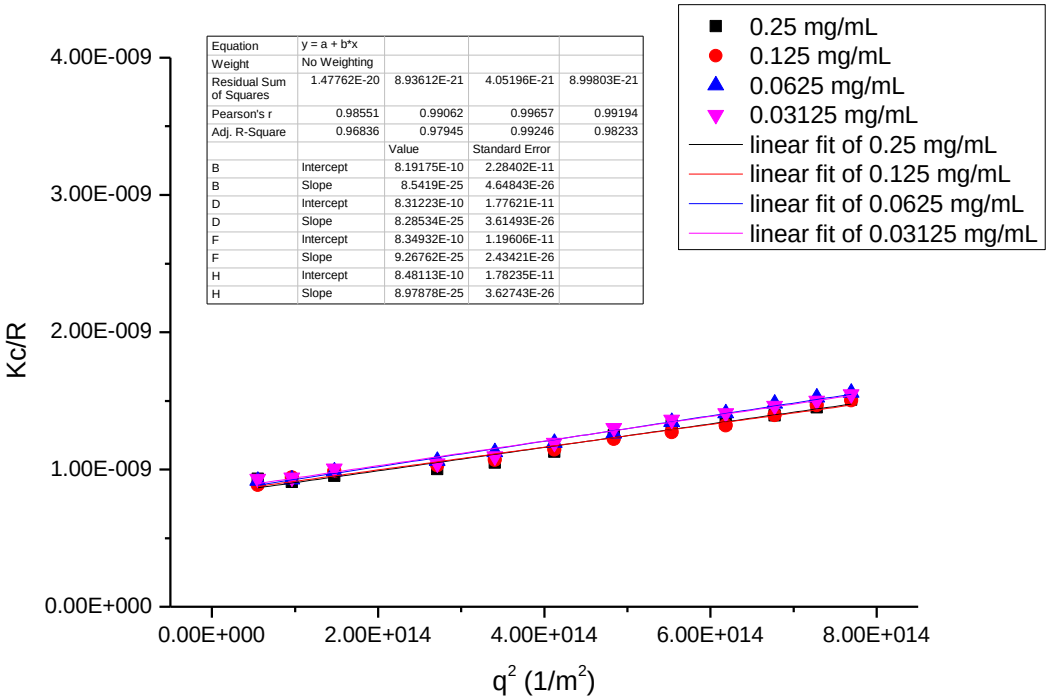

Figure 3.21 Zimm plots for self-assembly prepared by polymerization **3**, $PMMA_{70}$-*b*-$(PAMA_{0.5}$-*co*-$PTMA_{0.5})_{50}$ in $CHCl_3$ measured by SLS at 50 °C.

To further investigate the stabilities of the irregular particles, the size of the self-assemblies prepared by polymerization **2** and **5** were also measured at different temperatures by DLS (Figure 3.22). No size change was detected by DLS analysis. This suggests that the particles formed in $CHCl_3$ were very stable upon heating, although they appear to be irregular in shape as determined by TEM analysis. The stability of staggered lamellae **5** was also studied by sonication. No obvious size and morphology changes were observed upon sonication for 1 hour (Figure 3.23), showing that the staggered lamellae were highly stable due to the strong hydrogen bonding interactions. A few small sheet-like nanostructures were observed when the staggered lamellae were treated with sonication for 8 hours (Figure 3.24), which was consistent with the observation in the literature by Liu and coworkers.[54]

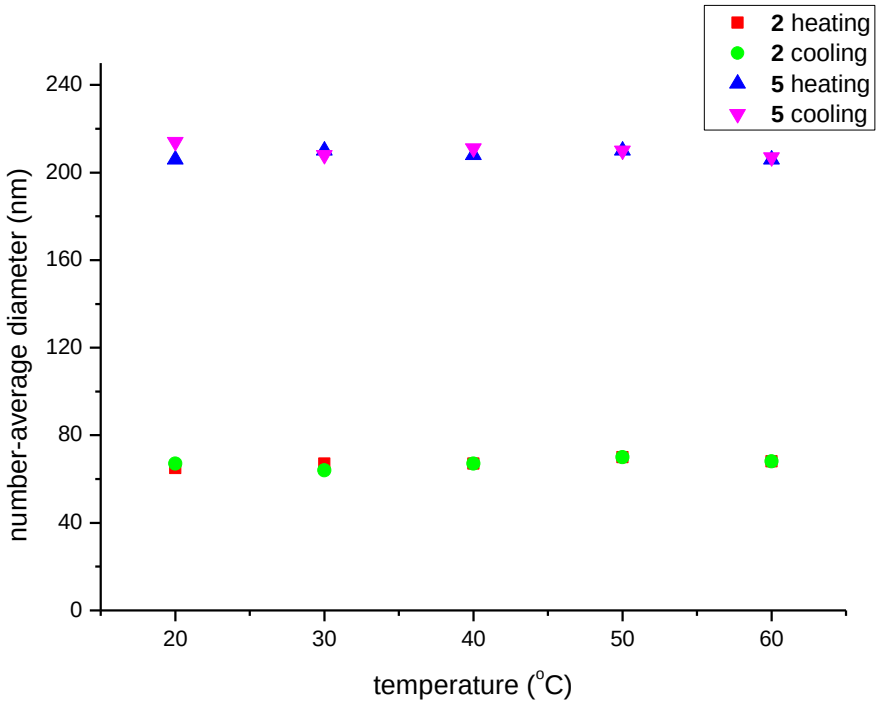

Figure 3.22 Number-average diameters of self-assemblies prepared by polymerization **2**, $PMMA_{70}$-*b*-$PAMA_{50}$ and **5**, $PMMA_{70}$-*b*-$PAMA_{100}$ at different temperatures measured by variable temperature DLS.

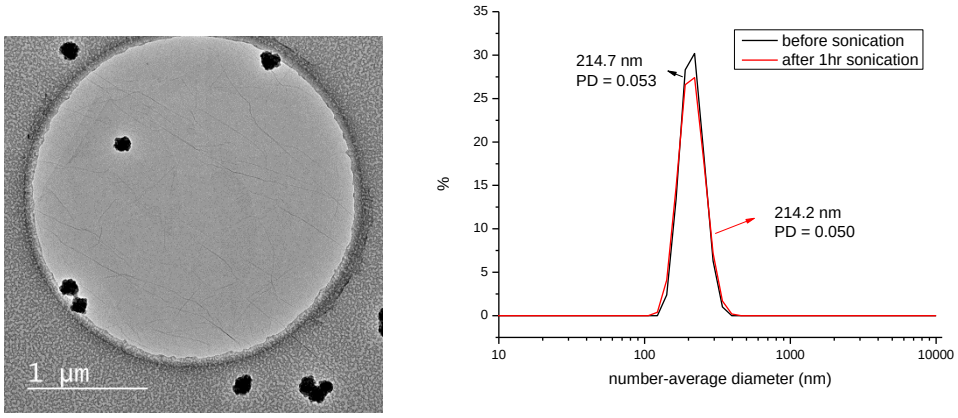

Figure 3.23 TEM and DLS of self-assembly prepared by polymerization **5**, $PMMA_{70}$-*b*-$PAMA_{100}$ after sonication for 1 hour.

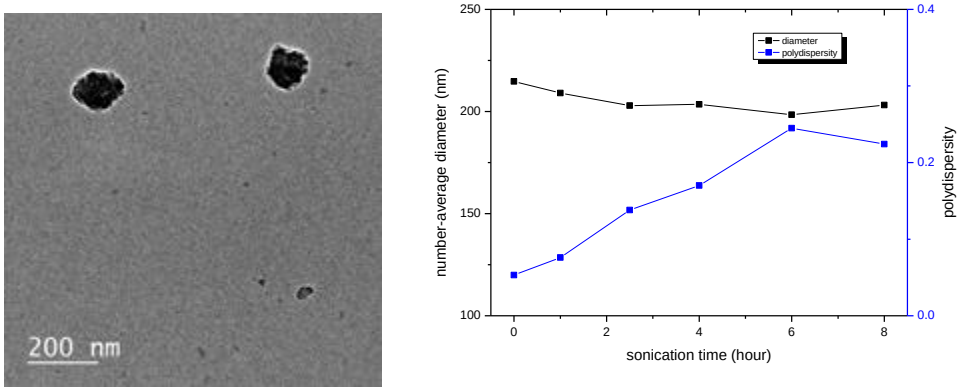

Figure 3.24 TEM and DLS of self-assembly prepared by polymerization **5**, $PMMA_{70}$-*b*-$PAMA_{100}$ after sonication for 8 hours.

3.3.7 Effect of anisole on the morphologies induced by polymerizations in $CHCl_3$

To further study the formation of staggered lamella morphology as observed in Figure 3.13, polymerizations were also performed for target polymers $PMMA_{70}$-*b*-$(PAMA_x$-*co*-$PTMA_y)_{100}$ in the presence of the aromatic solvent, anisole. Anisole is not a good solvent for the monomer AMA, therefore, mixtures of anisole and chloroform were selected as the solvents in this study. In the case of only AMA as the monomer, AMA became barely soluble in the presence of anisole. The optimized conditions were determined to be a chloroform/anisole ratio of 5:1, with the monomer concentration kept the same as polymerization **4** (Table 3.3 and Figure

3.25 **4a**). By TEM analysis, it was found that staggered lamellae were still observed to be the predominant morphology; however, a few small micelles were also observed. This observation indicates that the formation of staggered lamellae was interrupted by the addition of the aromatic solvent. This is expected as the aromatic solvent can competitively interact with adenine and thus affect the π-π stacking interactions between nucleobases (anisole can have an effect on interchain π-π stacking between conjugated polymers[55]).

Table 3.3 Characterization of polymers synthesized in the presence of anisole

Polymerization /polymer	Solvent ($CHCl_3$: anisole)	Monomers	Conv. (%)	$M_{n,th}$ (kDa)	$M_{n,NMR}$[a] (kDa)	$M_{n,SEC}$[b] (kDa)	$Đ_M$
$PMMA_{70}$-*b*-$PAMA_{100}$, **4a**	5:1	AMA	85	32.5	33.0	32.8	1.27
$PMMA_{70}$-*b*-($PAMA_{0.5}$-*co*-$PTMA_{0.5}$)$_{100}$, **5a**	1:1	AMA and TMA (1:1)	Precipitation occurred				
$PMMA_{70}$-*b*-($PAMA_{0.5}$-*co*-$PTMA_{0.5}$)$_{100}$, **5b**	2:1	AMA and TMA (1:1)	90	34.0	35.0	37.6	1.48
$PMMA_{70}$-*b*-($PAMA_{0.5}$-*co*-$PTMA_{0.5}$)$_{100}$, **5c**	5:1	AMA and TMA (1:1)	98	36.4	37.0	38.2	1.58

[a]determined by ^{1}H NMR spectroscopy in DMSO-d_6; [b]determined by SEC analysis (DMF eluent, PMMA standards).

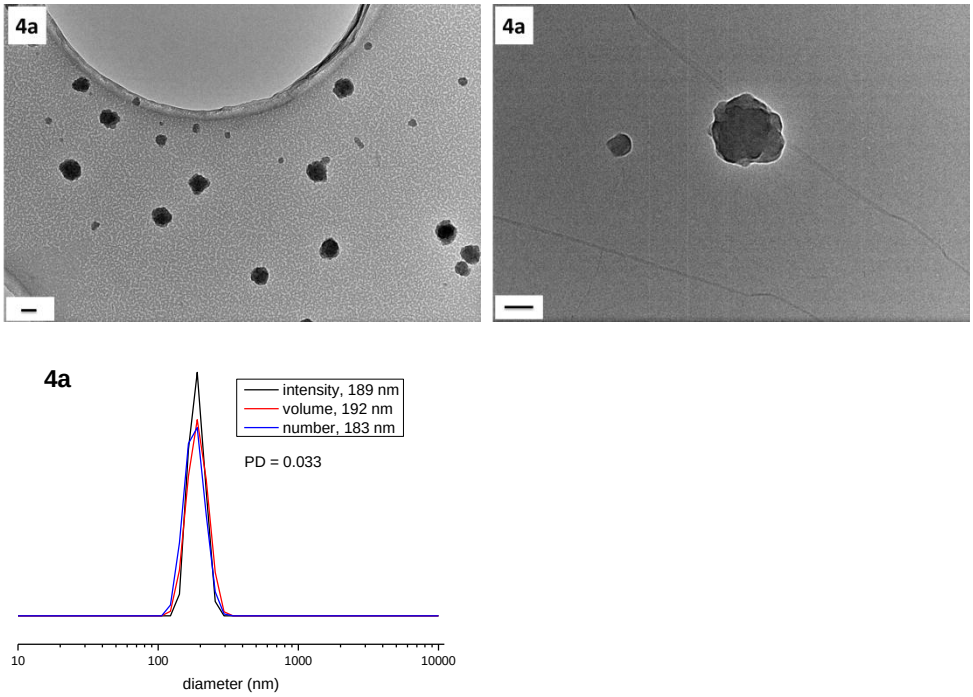

Figure 3.25 TEM and DLS analysis of target polymer **4a**, $PMMA_{70}$-*b*-$PAMA_{100}$ in a mixture of chloroform and anisole (5:1). Scale bar left: 100 nm; right: 50nm.

In the system with a mixture of AMA and TMA as the monomers, mixtures of chloroform and anisole at different ratios were investigated (Table 3.3, **5a – 5c**). Precipitation instead of self-assembly was observed when the ratio of chloroform to anisole was 1:1 (**5a**). When the ratio of chloroform to anisole was changed to 2:1, a mixture of aggregations of staggered lamellae and small sheet-like micelles was observed (Figure 3.26 **5b**). The aggregations might be formed due to the poorer solubility of polymers in the presence of anisole. Furthermore, the formation of small sheet-like micelles might result from the interruption of π-π stacking caused by anisole. Further varying the ratio of chloroform to anisole to 5:1 also led to the aggregations of staggered lamellae with some small micelles (Figure 3.27 **5c**). It was also noticed that there were less small micelles at a higher chloroform/anisole ratio. These results indicate that the formation of staggered lamellae can be affected by the addition of an aromatic solvent. This further suggests that π-π stacking interactions between nucleobases could be one of the driving forces for the formation of

staggered lamellae in this study. However, the exact reason for this behavior needs further investigation.

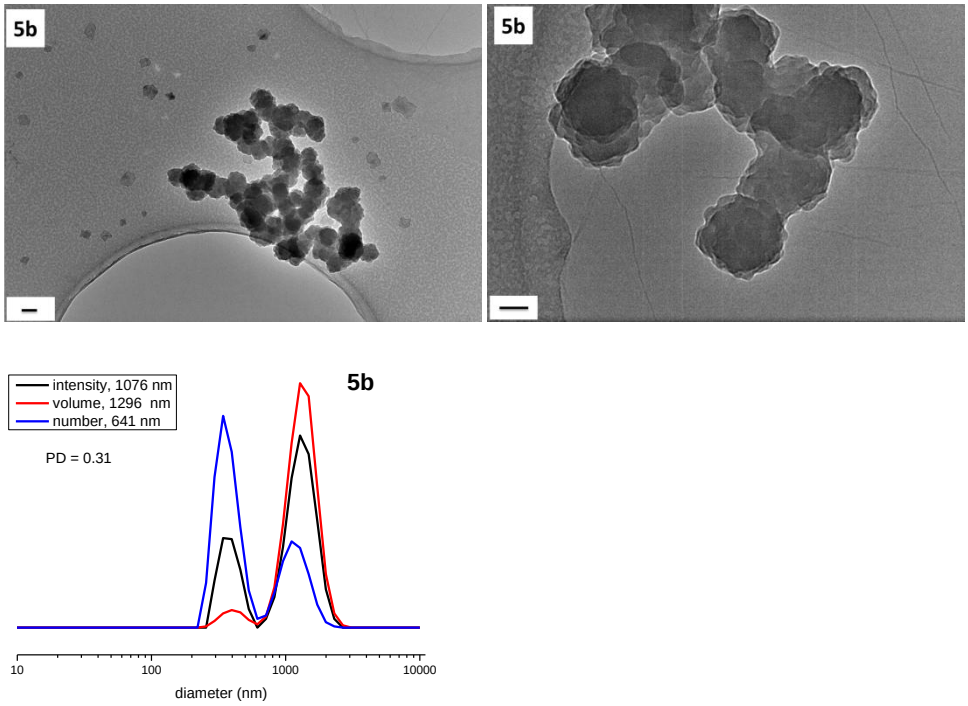

Figure 3.26 TEM and DLS analysis of target polymer **5b**, $PMMA_{70}$-*b*-($PAMA_{0.5}$-*co*-$PTMA_{0.5}$)$_{100}$, in a mixture of chloroform and anisole (2:1). Scale bar left: 100 nm; right: 50 nm.

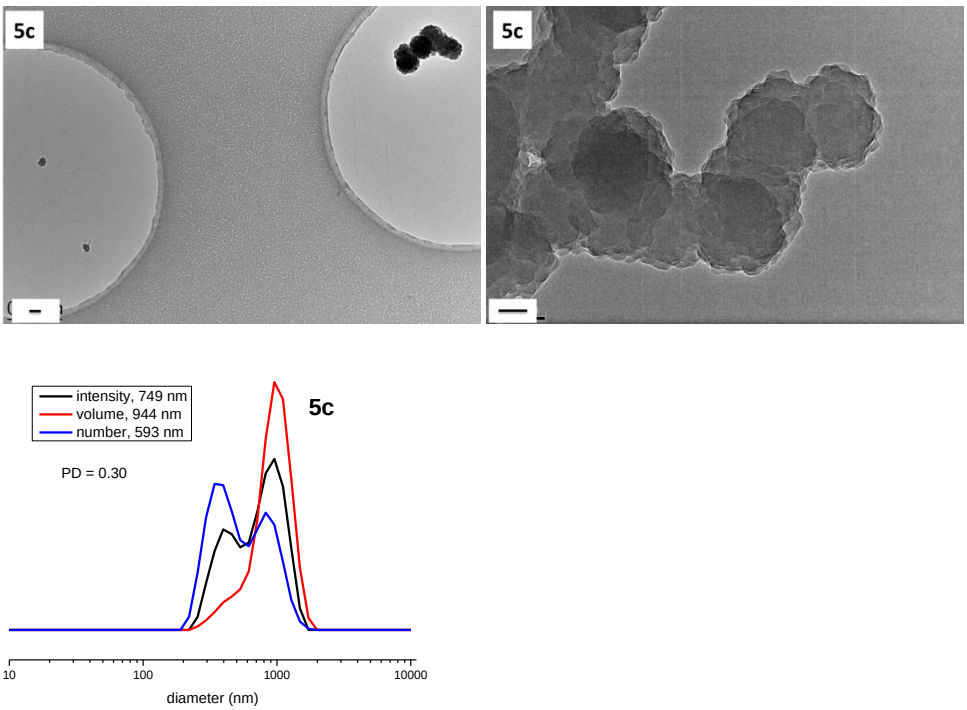

Figure 3.27 TEM and DLS analysis of target polymer **5c**, $PMMA_{70}$-*b*-($PAMA_{0.5}$-*co*-$PTMA_{0.5}$)$_{100}$, in a mixture of chloroform and anisole (5:1). Scale bar left: 100 nm; right: 50 nm.

3.3.8 Kinetics of RAFT dispersion polymerization 7 in 1,4-dioxane

The kinetics of RAFT dispersion polymerizations were also investigated in 1,4-dioxane. Monomer conversion data obtained by ^{1}H NMR spectroscopy is shown in Figure 3.28 for the target diblock copolymer **7**, $PMMA_{70}$-*b*-($PAMA_{0.5}$-*co*-$PTMA_{0.5}$)$_{50}$. Both monomers were incorporated at the same rate. It should be noted that polymerization conditions used for polymerization **7** were identical to polymerization **3** except for the choice of solvent. 80% monomer conversion was obtained after 15 hours and conversion reached 90% after 24 hours. Compared to the rate of polymerization in $CHCl_3$, polymerization in 1,4-dioxane is slightly slower (85% of monomer conversion after 10 hours in $CHCl_3$). The evolution of SEC traces with monomer conversion is shown in Figure 3.29. In general, the molecular weight of the polymer was found to increase linearly with conversion and dispersities remained narrow. Compared to polymerizations performed in $CHCl_3$, monomodal diblock copolymers were attained at each conversion, which is consistent with previously reported systems in the literature.[30] These results indicate that the RAFT dispersion polymerization of a mixture of AMA and TMA in 1,4-dioxane differs significantly to that in $CHCl_3$.

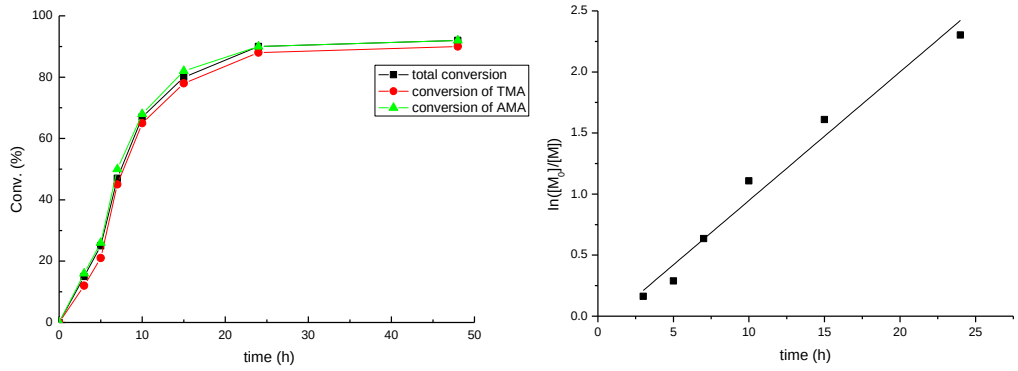

Figure 3.28 Conversion *vs.* time plot and corresponding semi-logarithmic plot obtained for the dispersion polymerization of a 1:1 mixture of AMA and TMA at 60 °C using a PMMA macro-CTA in 1,4-dioxane. The target diblock composition was polymer **7**, $PMMA_{70}$-*b*-($PAMA_{0.5}$-*co*-$PTMA_{0.5}$)$_{50}$.

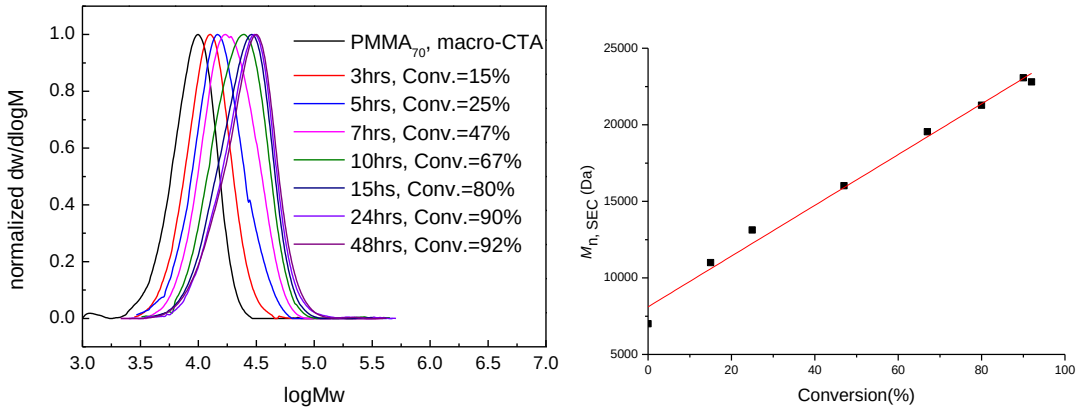

Figure 3.29 Evolution of SEC traces (DMF as eluent, PMMA standard) with monomer conversion (left) and molecular weight *vs* converions plot (right) using a $PMMA_{70}$ macro-CTA for the RAFT dispersion polymerization of a 1:1 mixture of AMA and TMA in 1,4-dioxane at 60 °C. The target diblock composition was polymer **7**, $PMMA_{70}$-*b*-($PAMA_{0.5}$-*co*-$PTMA_{0.5}$)$_{50}$.

3.3.9 Kinetic study on morpholgies induced by polymerization 7 in 1,4-dioxane

The polymerization mixture of **7** appeared clear until 7 hours (47% conversion), but became more opalescent as the polymerization proceeded further. There was no obvious difference in transparency after 15 hours which was also consistent with monomer conversion (high conversion attained after 15 hours). To monitor the evolution of particle morphology as the polymerization progressed, samples were also prepared for TEM analysis. The representative TEM images and their corresponding size distributions are shown in Figure 3.30. At low monomer conversion when the polymerization solution looked clear (3 hours, 5 hours, and 7 hours), exclusively spherical micelles were observed (Figure 3.30). The hydrodynamic diameter of these micelles was less than 40 nm by DLS. Further increasing the monomer conversion (10 hours, 67% conversion) led to a mixture of spherical micelles and short wormlike micelles (Figure 3.30, 10 hours). When high conversion was reached (80%, 15 hours), a mixture of some remaining spherical micelles and longer wormlike micelles were observed (Figure 3.30, 15 hours). There

was no significant morphology change after 15 hours and a phase comprising of spherical and wormlike micelles was obtained as the final structure for polymerization **7** (Figure 3.30, 24 hours and 48 hours).

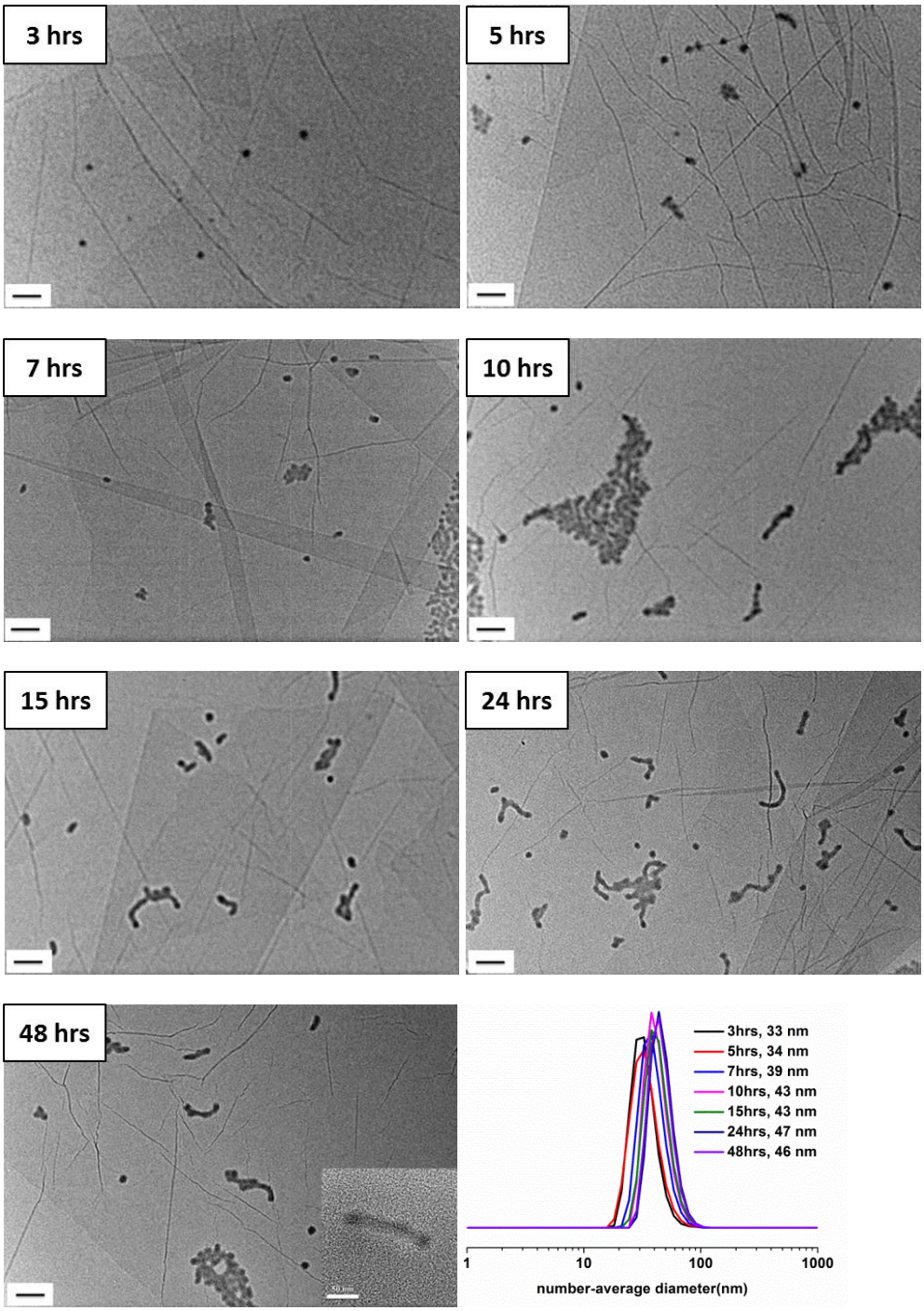

Figure 3.30 Evolution of the self-assembly by unstained TEM analysis and number-average diameter as determined by DLS with monomer conversion using a $PMMA_{70}$ macro-CTA for the RAFT dispersion polymerization of a 1:1 mixture of AMA and TMA in 1,4-dioxane at 60 °C. The target diblock composition was polymer **7**, $PMMA_{70}$-*b*-$(PAMA_{0.5}$-*co*-$PTMA_{0.5})_{50}$. Scale bar: 100 nm. The inset image of 48 hours was taken by TEM at a higher magnification (60 k).

Small-angle X-ray scattering (SAXS) was performed on this sample (48 hours) to provide a global view of the resultant morphologies. The Guinier-Porod model was used to provide information on the shape of the scattering objects (R_g and anisotropy).[56,57] The high-q range was not taken into account for this model as it does not reproduce oscillations characteristic of form factors for monodisperse scattering objects. A dimension parameter of 0.42 was obtained, which suggests the presence of slightly elongated objects, or a mixture of spherical and elongated particles (Table 3.4 and Figure 3.31). From TEM analysis, the second option is more plausible. More complex structural models based on shape form factors of scattering objects were also applied for SAXS analysis: a model for spherical objects with some dispersity (Polycore model[58]) and a model for cylindrical particles (Cylinder model[57]). The particles were assumed to have a uniform density for both models. Neither the cylinder nor the sphere models provided high quality fits, thus a linear combination of these two models (named the Sum model) was created to take into account the two morphologies present in solution as seen by TEM (Figure 3.31). These results thus confirm the hypothesis made based on the results of the Guinier-Porod fit: both spherical and cylindrical micelles coexist in solution. Furthermore, the spheres were found to possess a similar radius to the cylinders (Table 3.5). Owing to the fact that the SAXS data were normalized, the scale parameter given by the models is equal to the volume fraction, and thus it is possible to estimate the number ratio between cylinders and spheres (Table 3.5). It was determined that the volume fraction of cylindrical micelles is bigger than that of the spherical objects, however by number there are more spheres than cylinders in solution. The evolution of morphology also indicates that the wormlike micelles observed were formed by the fusion of the spherical micelles, which is consistent with the reported mechanism

of sphere-to-worm transitions.[29] A possible reason for this transition is that the relatively high polymer curvature results in a lower stabilizer chain density and thus less effective steric stabilization at the cylinder-ends, which further induces fusion. Furthermore, compared to polymerization **3** which was performed in $CHCl_3$, the self-assembled structures formed in 1,4-dioxane were indeed different (popcorn-like structures were formed in $CHCl_3$). This further suggests that the RAFT dispersion polymerization of a mixture of AMA and TMA in 1,4-dioxane is significantly different to the same polymerization in $CHCl_3$. In other words, solvent choice plays an important role on morphologies formed by the RAFT dispersion polymerization of nucleobase-containing monomers.

Table 3.4 Guinier-Porod model fitting data for polymer **7** in 1,4-dioxane

Polymer	R_g (nm)	s[a]
$PMMA_{70}$-*b*-($PAMA_{0.5}$-*co*-$PTMA_{0.5}$)$_{50}$, **7**	11.8 ± 0.1	0.422 ± 0.001

[a] 's' stands for dimension parameter. s = 0 for a sphere. s = 1 for a cylinder. s = 2 for a plate

Table 3.5 Sum model fitting data for polymer **7** in 1,4-dioxane

Polymer	Length of cylinder (nm)	Radius of cylinder (nm)	Radius of sphere (nm)	Volume fraction (cylinder : sphere)	Number fraction (cylinder : sphere)
7	104 ± 1	12 ± 1	14 ± 1	0.31:0.19	1:2.51

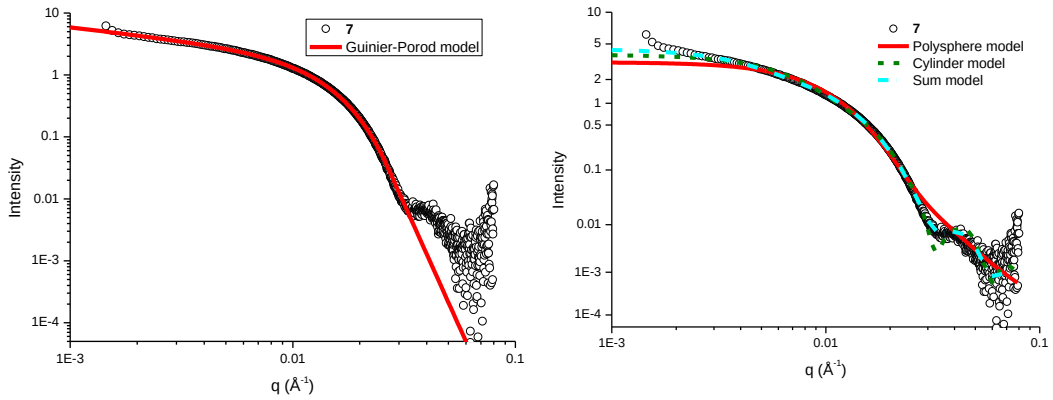

Figure 3.31 SAXS analysis of polymer **7,** $PMMA_{70}$-*b*-($PAMA_{0.5}$-*co*-$PTMA_{0.5}$)$_{50}$ prepared in 1,4-dioxane. Experimental profile and Guinier-Porod fit (left); experimental profile and fits with sphere, cylinder and sum models (right).

3.3.10 Morphologies induced by polymerization in 1,4-dioxane

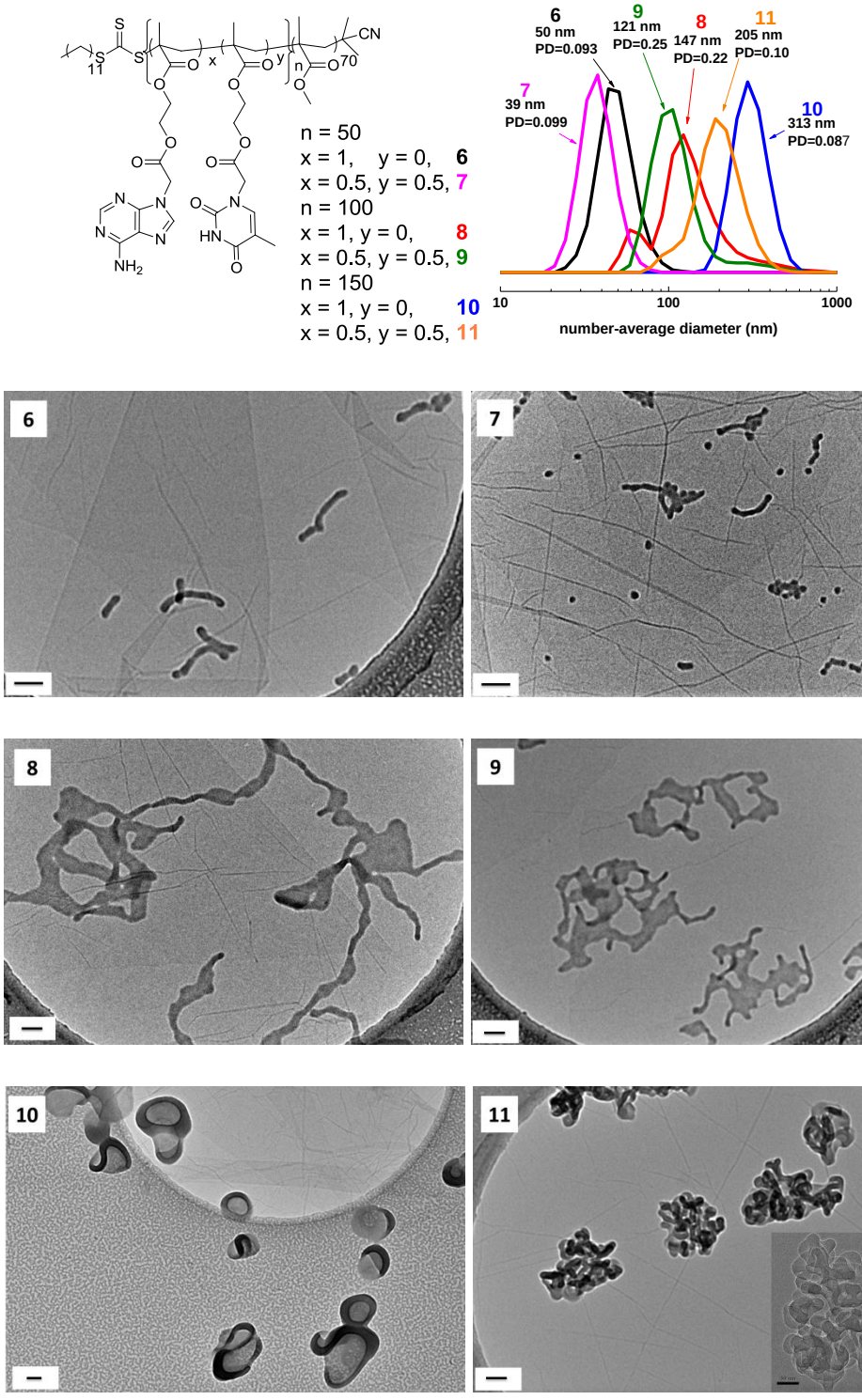

Figure 3.32 Representative TEM images of self-assemblies prepared by RAFT dispersion polymerization in 1,4-dioxane, their corresponding polymer structures and DLS particle size distributions of **6** ($PMMA_{70}$-*b*-$PAMA_{50}$), **7** ($PMMA_{70}$-*b*-($PAMA_{0.5}$-*co*-$PTMA_{0.5}$)$_{50}$), **8** ($PMMA_{70}$-*b*-$PAMA_{100}$), **9** ($PMMA_{70}$-*b*-($PAMA_{0.5}$-*co*-$PTMA_{0.5}$)$_{100}$), **10** ($PMMA_{70}$-*b*-$PAMA_{150}$)and **11** ($PMMA_{70}$-*b*-($PAMA_{0.5}$-*co*-$PTMA_{0.5}$)$_{150}$). Scale bar: 100 nm (inset 50 nm). The inset of **11** was taken by TEM with a higher magnification of 50 k.

To further study the morphologies induced by polymerization in 1,4-dioxane, a range of diblock copolymers $PMMA_{70}$-*b*-$(PAMA_x$-*co*-$PTMA_y)_n$ (Table 3.1 and Figure 3.32, polymer **6** -**11**) prepared in 1,4-dioxane were analyzed by TEM to assess their morphologies. Representative TEM images are shown in Figure 3.30. Higher order morphologies were observed in this system in comparison to when $CHCl_3$ was used as the polymerization solvent. AFM was also utilized to further assess the morphology of these high order structures and provide accurate height information. SAXS experiments were also performed on some samples to provide more details on the resultant morphologies in solution. DLS was also used to analyze the morphologies and the results of number-average diameters are summarized (Figure 3.32). It was observed that by increasing the DP of the core-forming block, the size of the self-assemblies increased significantly. It should be noted that due to the high order morphologies obtained in these systems, the sizes obtained from DLS are relative values (for DLS, the assumption that the particles are spherical is made).[59] However, as CONTIN analysis is able to detect multiple populations in solution and obtain polydispersity information, the results from DLS are still valuable even if the structures are not spherical.

3.3.10.1 AMA polymerizations

When only AMA was used as the monomer, cylinders along with some remaining spherical micelles were observed by TEM for a PAMA target DP of 50 (Figure 3.32, **6**). The lengths of the cylinders are about 150 nm as estimated from TEM images. Moreover, the widths of cylinders are very close to the diameter of the spheres (*ca.*30 nm). On close inspection of these TEM images, the cylinder growth in these polymerizations appears to result from the fusion

of spherical micelles. This mechanism of cylinder formation has been reported previously as mentioned above.[29,30] These morphologies could also be clearly observed by AFM. The heights of cylinders are about 15 nm for polymerization **6**, which is also very consistent with the heights of the spheres formed in this system (Figure 3.33). SAXS was also performed on this sample and the analysis was conducted in the same way as for polymer **7**, which further confirmed the results obtained by TEM and AFM: a mixed phase of cylinders (length of 158 nm, radius of 15 nm) and spheres (radius of 18 nm) with a larger volume fraction of cylinders compared to spheres (Table 3.6 and 3.7, Figure 3.34). This observation further suggests that the cylinders were formed by the fusion of spherical micelles.

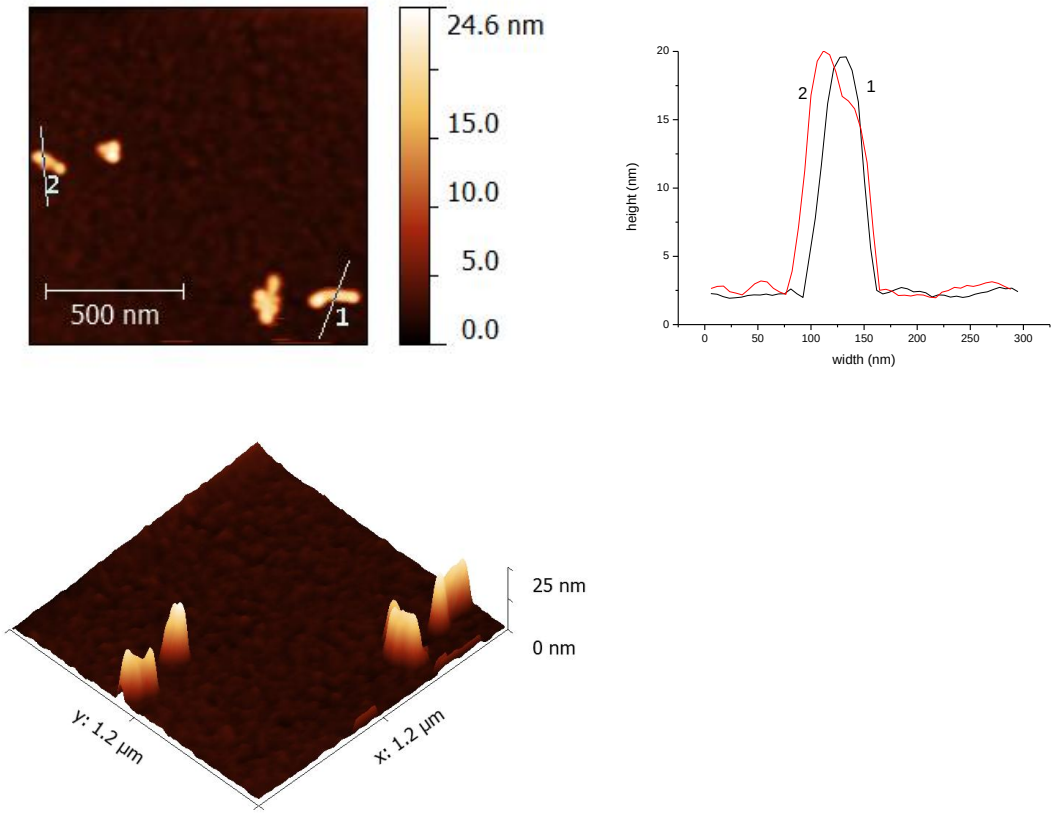

Figure 3.33 AFM height image (top left) and three-dimensional AFM image (bottom) of self-assembly prepared by polymerization **6** and the corresponding height profile (top right).

Table 3.6 Guinier-Porod model fitting data for polymer **6** in 1,4-dioxane

Polymer	R_g (nm)	s[a]
$PMMA_{70}$-*b*-$PAMA_{50,}$ **6**	14.7 ± 0.1	0.520 ± 0.001

[a] 's' stands for dimension parameter. s = 0 for sphere. s = 1 for cylinder. s = 2 for plate

Table 3.7 Sum model fitting data for polymer **6** in 1,4-dioxane

Polymer	Length of cylinder (nm)	Radius of cylinder (nm)	Radius of sphere (nm)	Volume fraction (cylinder : sphere)	Number fraction (cylinder : sphere)
6	158 ± 1	15 ± 1	18 ± 1	0.43:0.23	1:2.45

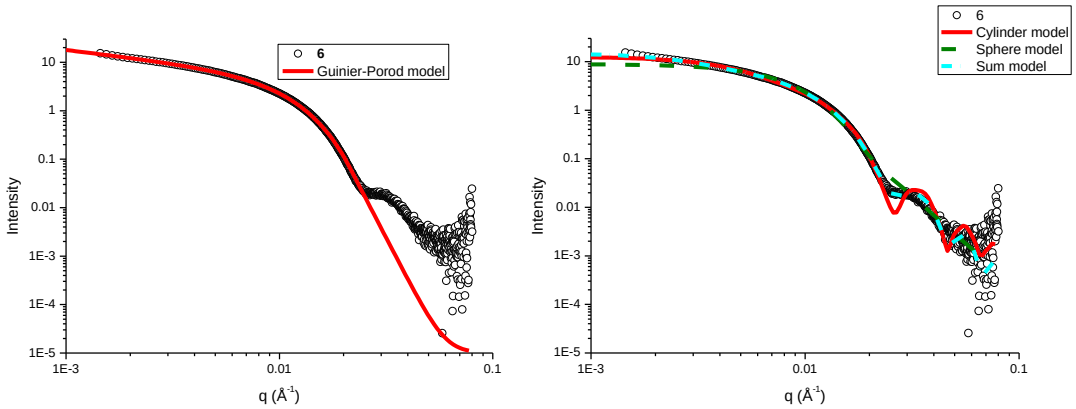

Figure 3.34 SAXS analysis of polymer **6.** Experimental profile and Guinier-Porod fit (left); experimental profile and fits with sphere, cylinder and sum models (right).

Targeting a DP of 100 led to the formation of lamellae with 'tentacles'. This morphology has been previously reported and has been termed as octopus-like morphology.[29] The 'main-body' of the octopus (lamellae) looks relatively flat when observed by TEM (Figure 3.32, **8**). AFM was also conducted to allow access to more details about this structure. The heights of the structures were measured to give a value of 15 nm (Figure 3.35). Furthermore, the 'main-bodies' of the octopus appear to be a similar height, which further proves the formation of flat lamellae. This octopus-like morphology is considered as an intrinsic intermediate morphology between worms and bilayers during the process of polymerization.[29] Therefore, 'jellyfish' morphology or vesicles

would be expected to form as a result of further increasing the length of the nucleobase-containing block.

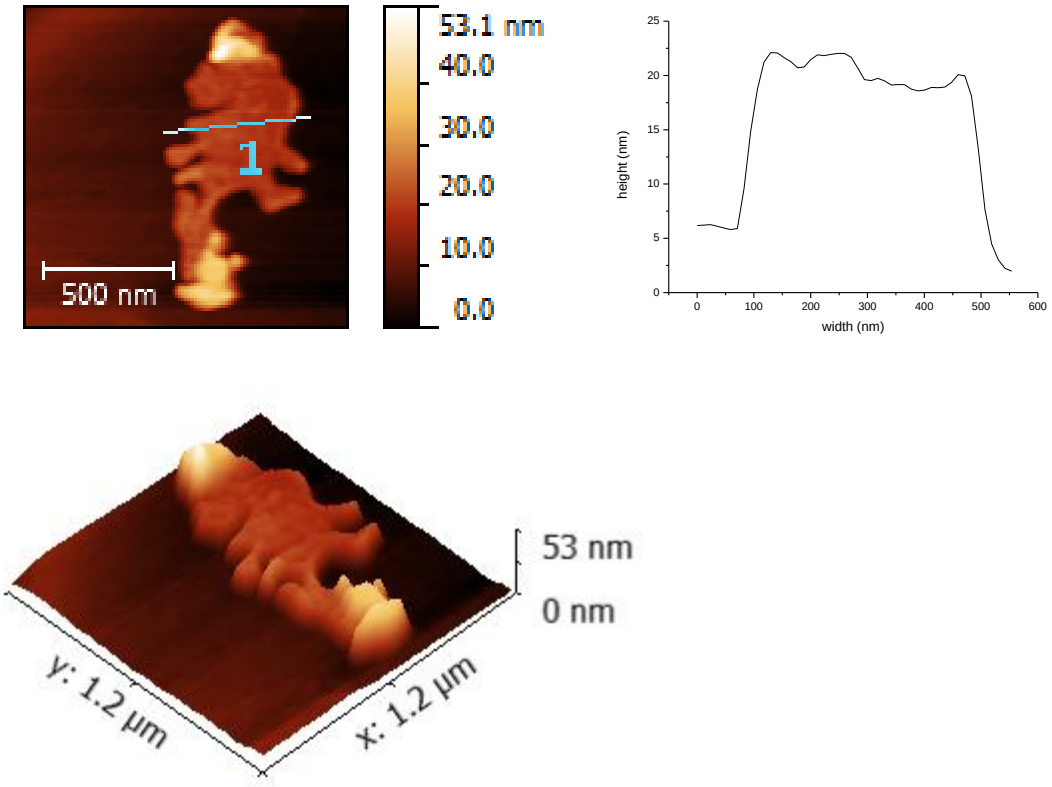

Figure 3.35 AFM height image (top left) and three-dimensional AFM image (bottom) of self-assembly prepared by polymerization **8**, $PMMA_{70}$-*b*-$PAMA_{100}$ and the corresponding height profile (top right).

However, different morphologies were unexpectedly observed by TEM when the target DP of the core-forming block was increased to 150. The octopus 'tentacles' underwent fusion and completely disappeared and lamellae which were either partially wrapped-up or slightly twisted were observed (Figure 3.32, **10**). It seems that a vesicle phase started to form but was disrupted. AFM was also performed to characterize the new morphologies. For polymerization **10**, the height was estimated to be about 100 nm to 250 nm (Figure 3.36), much higher than the flat lamellae which were observed above (Figure 3.35, height *ca.* 15 nm). The height analysis of the aggregations suggests that the lamellae are no longer flat. SLS was conducted on this sample to further study

the morphology in solution. As the scatterers are very large ($q \times R_g > 1$ over the whole q-range investigated), the Zimm formulation is not applicable. Therefore, the shape of scatters is determined by the plot of q-dependency of R/Kc.[60] The particle fractal dimension determined from the log-log plot of R/Kc as a function of q is 2.5 (Figure 3.37), which is not a reported value (2 is for thin disks and 3 is for 3D-objects with smooth surfaces), indicating the formation of a novel structure. It further suggests that these structures might be partially enclosed.

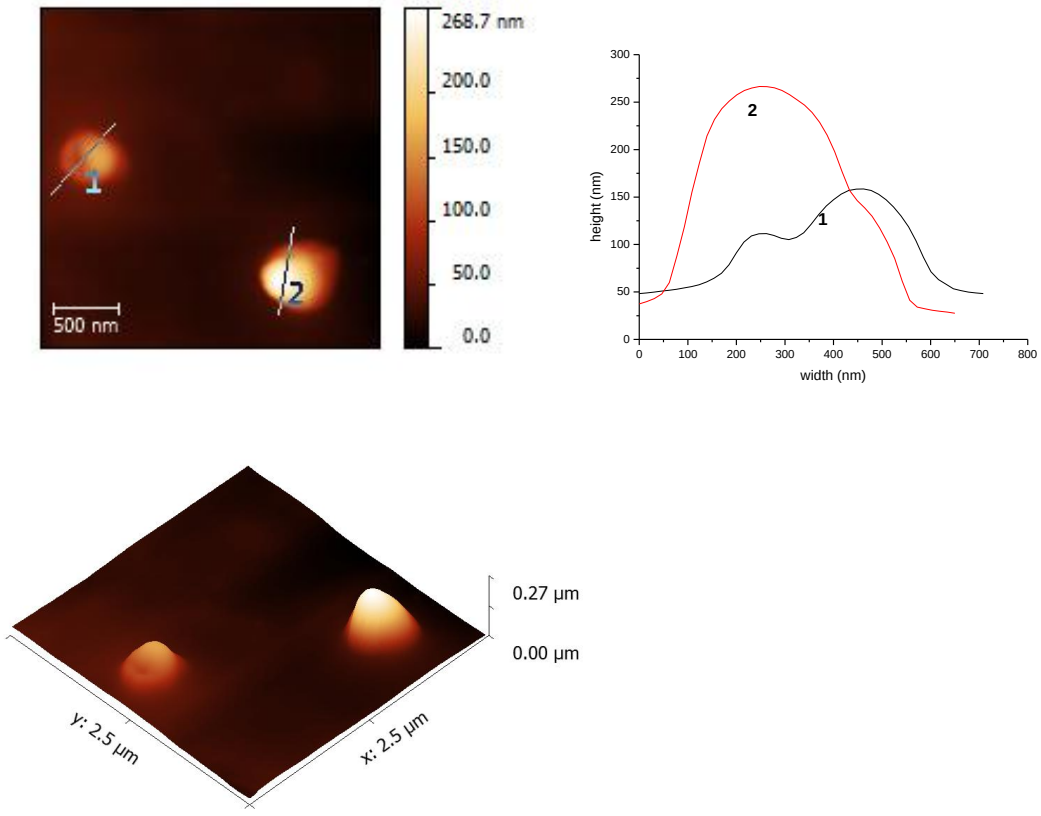

Figure 3.36 AFM height image (top left) and three-dimensional AFM image (bottom) of self-assembly prepared by polymerization **10**, $PMMA_{70}$-*b*-$PAMA_{150}$ in 1,4-dioxane and the corresponding height profile (top right).

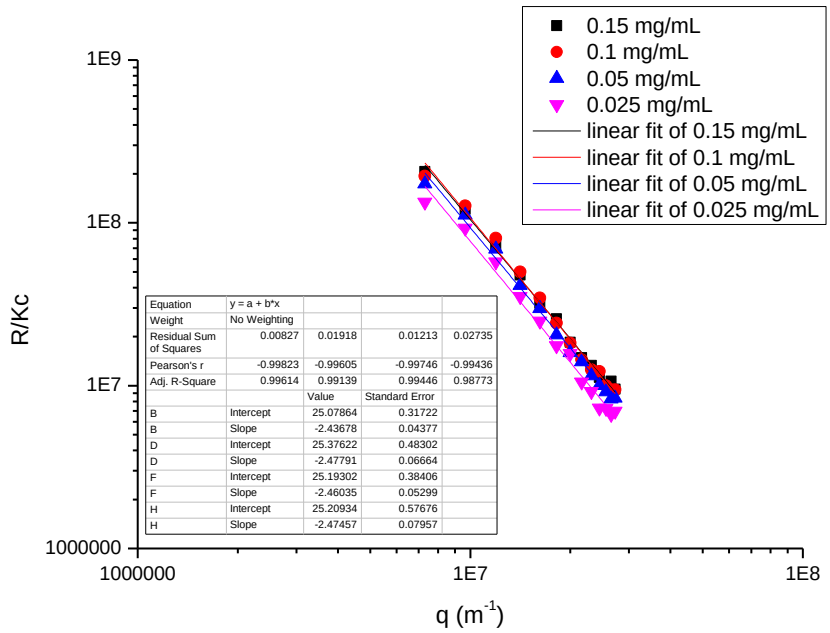

Figure 3.37 *R/Kc* of self-assembly **10**, $PMMA_{70}$-*b*-$PAMA_{150}$ in 1,4-dioxane as a function of the scattering wave vector *q* for different concentrations.

3.3.10.2 AMA and TMA copolymerizations

When a 1:1 mixture of AMA and TMA were used as monomers, the sample exhibited a mixed sphere and cylinder phase when the target DP was 50 (Figure 3.32, **7**), the morphology of which was also observed in the kinetic study of **7** (Figure 3.30). The lengths of the cylinder are about 100 nm and the diameters of spheres are around 20 nm by TEM analysis. Estimated by AFM, the cylinders' heights are around 15 nm (Figure 3.38), which is also consistent with the size of the spheres and further proves the fusion mechanism of the sphere-to-worm transition.

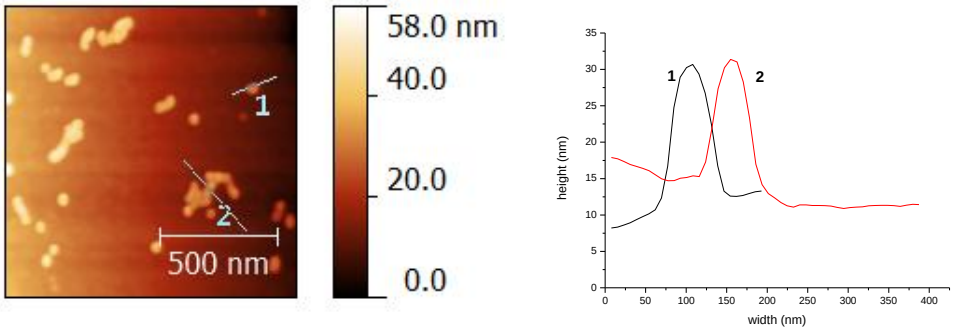

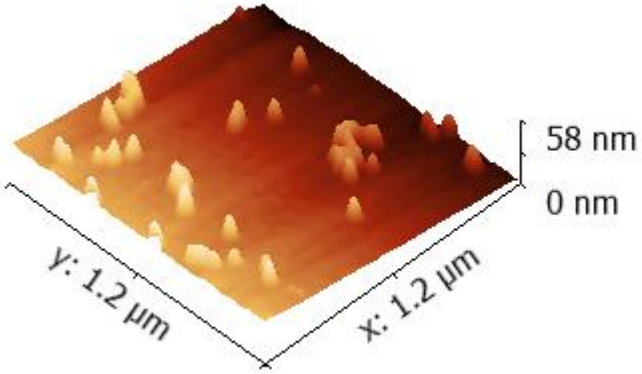

Figure 3.38 AFM height image (top left) and three-dimensional AFM image (bottom) of self-assembly prepared by polymerization **7** and the corresponding height profile (top right).

Similar to the case when exclusively AMA was used, targeting a DP of 100 generated lamellae along with 'tentacles' (Figure 3.32, **9**). AFM was also conducted to allow access to more details about this structure. The heights of the structures were measured to give a value of 15 nm (Figure 3.39). Furthermore, the 'main-bodies' of the octopuses were also confirmed to be flat by analyzing the AFM height image. SAXS analysis further confirmed the formation of lamellae with "tentacles": A Guinier-Porod fit gave a dimension variable value of 1.59, which indicates either the presence of morphologies between rods and plates or the presence of a mixture of these two morphologies (Table 3.8, Figure 3.40 top). Detailed modeling was then carried out to obtain more information by using a linear sum of a dilute lamellar form factor model[61,62] with various cylinder models: no dispersity, dispersity on the length or dispersity on the radius[57] (Figure 3.40 and Table 3.9 for the three sum models). Better data fit was obtained with the model having some dispersity on the radius, as previously observed for cylindrical structures.[63,64] The sum model resulted in a mixture of lamellae with a thickness of 20 nm (slightly larger than by TEM and AFM, which is often the case as SAXS is performed in solution and TEM and AFM in a dried state) and cylinders with a length of 80 nm and radius of 12 nm.

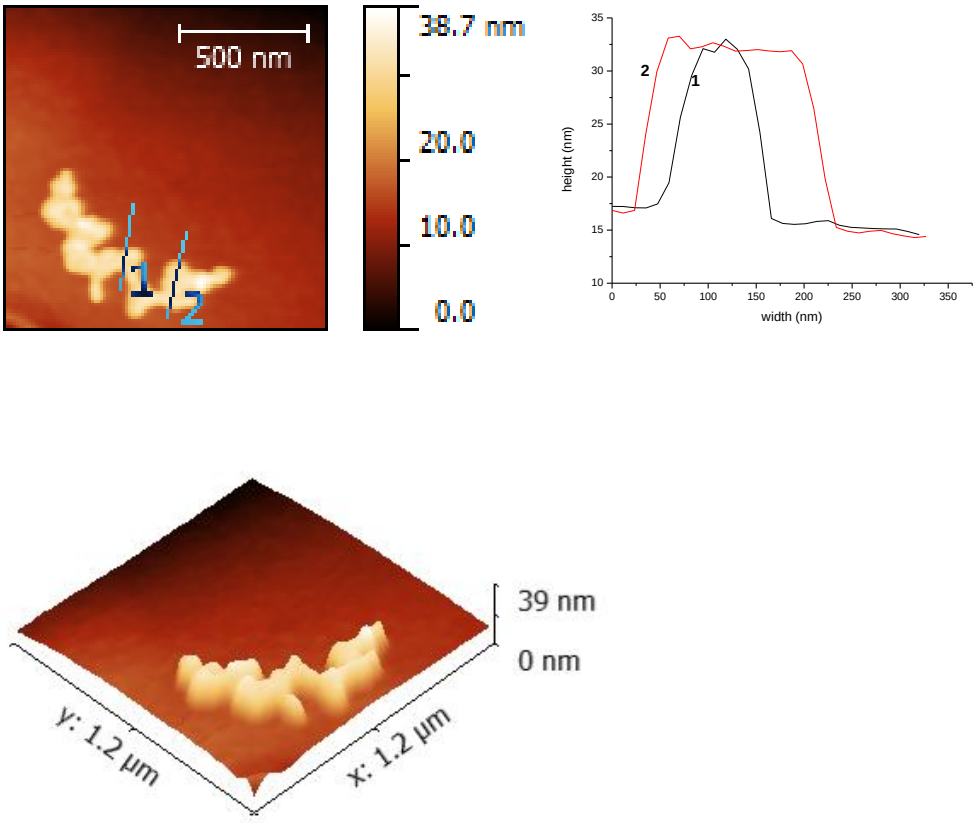

Figure 3.39 AFM height image (top left) and three-dimensional AFM image (bottom) of self-assembly prepared by polymerization **9**, $PMMA_{70}$-*b*-($PAMA_{0.5}$-*co*-$PTMA_{0.5}$)$_{100}$ and the corresponding height profile (top right).

Table 3.8 Guinier-Porod model fitting data for polymer **9** in 1,4-dioxane.

Polymer	R_g (nm)	s[a]
$PMMA_{70}$-*b*-($PAMA_{0.5}$-*co*-$PTMA_{0.5}$)$_{100}$ **9**	8.2 ± 0.1	1.593 ± 0.001

a 's' stands for dimension parameter. s = 0 for sphere. s = 1 for cylinder. s = 2 for plate

Table 3.9 Size and morphology of the fitted nanostructures for **9**.[a]

Model[b]	Bilayer thickness (nm)	Dispersity of thickness	Radius of cylinder (nm)	Length of cylinder (nm)	Dispersity of cylinder
cyl	17.4 ± 0.1	0.10 ± 0	16.7 ± 0.1	79.1 ± 0.3	-
cypl	17.5 ± 0.1	0.05 ± 0.02	16.8 ± 0.1	78.1 ± 0.6	0.10 ± 0.01
cypr	20.1 ± 0.2	0.05 ± 0.01	12.0 ± 0.2	80.1 ± 0.3	0.35 ± 0.01

[a]SLD solvent and morphologies were locked at 9.559 and 7.546 10^{-6} Å^{-2};
[b]cyl stands for lamellar model with cylinder model; cypl stands for lamellar model with polylength cylinder model; cypr stands for lamellar model with polyradius cylinder model.

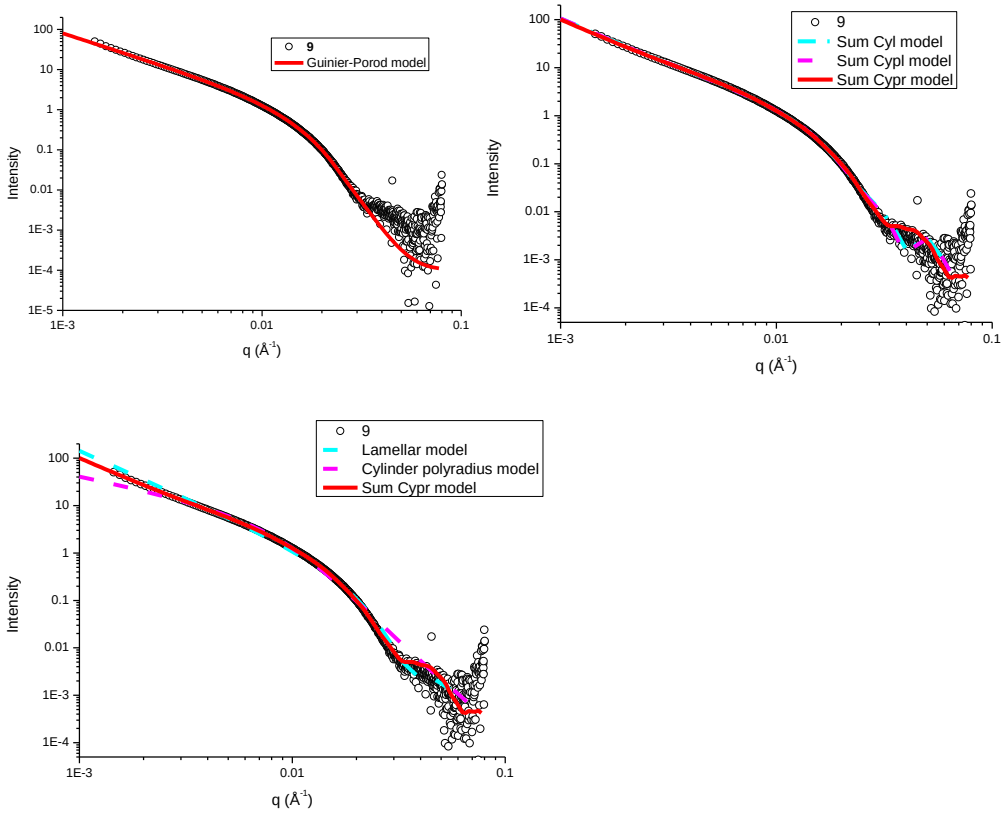

Figure 3.40 SAXS analysis of polymer **9** $PMMA_{70}$-*b*-$(PAMA_{0.5}$-*co*-$PTMA_{0.5})_{100}$. Experimental profile and Guinier-Porod fit (top left); experimental profile and fits with different sum models: lamellar model with cylinder model (Sum Cyl model), with polylength cylinder model (Sum Cypl model), and with polyradius cylinder model (Sum Cypr model) (top right); experimental profile and fits with lamellar, cylinder polyradius and sum models (bottom).

Further increasing the target DP to 150 led to the observation of a new structure. High resolution TEM was used to obtained a clear image of this structure (Figure 3.32, inset of **11**). In comparison to the equivalent polymerization in 1,4-dioxane using only AMA as the monomer, a 'jellyfish' morphology or pure vesicle phase was also not produced in this system and deeply twisted lamellas/cylinders were obtained. AFM was also performed to characterize the new morphologies. The heights of aggregations prepared by polymerization **11** were analyzed and the average height is about 150 nm, which is higher than that of the mono-lamella. Knot-like structures were also observed (Figure 3.41). SAXS analysis performed on this

sample did not allow a proper Guinier-Porod fit which could indicate the presence of too many different morphologies or morphologies which are not recognized by the Guinier-Porod model. A fractal model with disperse cylinders as building blocks was used to fit the experimental data (Figure 3.42). A fractal dimension of 3.3 was found, indicating that a 3D-object was formed. Unfortunately, this model does not reflect the twisted cylinders. Generally speaking, this observation suggests that more complex and higher order structures were generated in these systems.

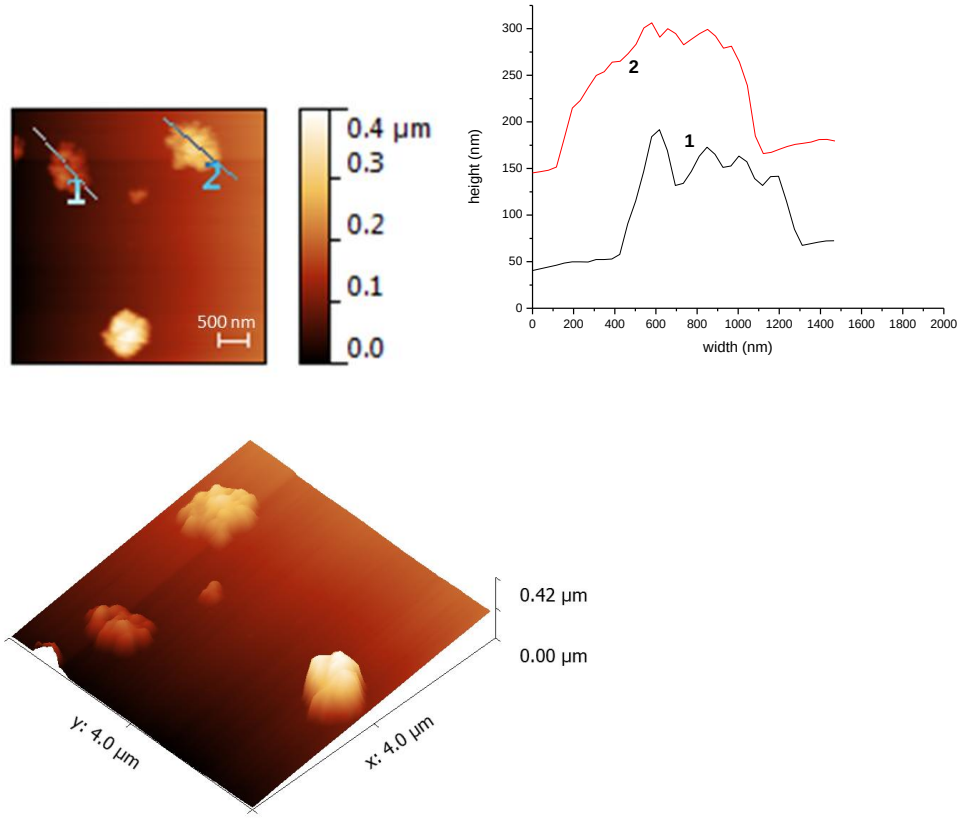

Figure 3.41 AFM height image (top left) and AFM phase image (bottom, scale bar 500 nm) of self-assembly prepared by polymerization **11,** $PMMA_{70}$-*b*-$(PAMA_{0.5}$-*co*-$PTMA_{0.5})_{150}$ and the corresponding height profile (top right) performed on mica.

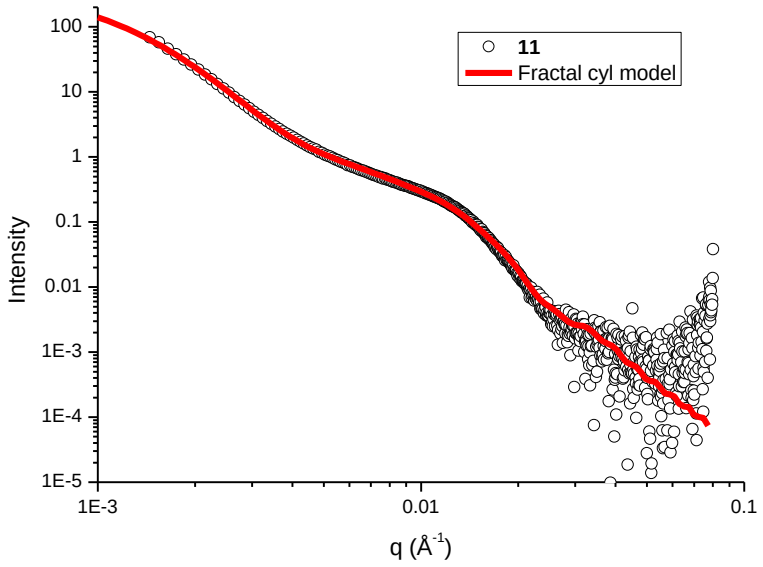

Figure 3.42 SAXS analysis of polymer **11**, $PMMA_{70}$-*b*-$(PAMA_{0.5}$-*co*-$PTMA_{0.5})_{150}$. Experimental profile and fractal fit.

3.3.11 Discussion

As mentioned in the monomer study section above, both $CHCl_3$ and 1,4-dioxane are low polarity solvents and support nucleobase interactions among polymers.[48,49] However, different polymerization and self-assembly behavior were observed in these two media when using nucleobase-containing monomers in RAFT dispersion polymerization. Moreover, a diversity of morphologies was observed in this nucleobase-containing system. We hypothesize that a combination of complementary nucleobase interactions and solubility (determined by a balance of intermolecular forces between solvent and solute) leads to this novel behavior.

Although hydrogen bonding interactions between adenine and thymine exist in both solvents as reported,[48,49] the difference in solubility of the nucleobases also needs to be taken into account. In other words, there is a competition of nucleobase-nucleobase interactions and intermolecular forces between nucleobases and solvent (nucleobase solubility). Moreover, we observe that the solubility of nucleobases in 1,4-dioxane is relatively higher than in $CHCl_3$, indicating a stronger intermolecular

force between the nucleobase and 1,4-dioxane than $CHCl_3$. This is supported by the observation that the monomers (particularly AMA) have better solubility in 1,4-dioxane than in $CHCl_3$, which is assessed by the visual inspection that at room temperature AMA is fully soluble in 1,4-dioxane at 20 mg/mL, but not in $CHCl_3$. It was also observed that the homopolymer of TMA with a low DP (*ca.* 20) is soluble in 1,4-dioxane but not in $CHCl_3$. Therefore, the nucleobase interactions are much stronger in $CHCl_3$ and the intermolecular force between nucleobases and solvent (solubility of nucleosbase) can be ignored. However, in 1,4-dioxane, the effect of intermolecular forces between nucleobases and solvent (solubility of the nucleobase) cannot be ignored, and even overtake the importance of nucleobase interactions for monomers or polymer with a low DP due to the relatively low local concentration of nucleobase compared to the amount of solvent. However, with the formation of higher DP polymers or increasing local concentration of nucleobases, the nucleobase interactions become more and more important.

Based on the observations and discussion above, we hypothesize that compared to 1,4-dioxane, the solubility of nucleobase-containing polymers in $CHCl_3$ is poorer and thus leads to a lower critical micelle degree of polymerization (CMDP), which is a key parameter in the process of dispersion polymerization and can be influenced greatly by many factors, including the solvent used.[31,65-67] Moreover, as nucleobase interactions are the main interactions among monomers and polymers in $CHCl_3$, frozen core-forming nucleobase-containing blocks are induced above the CMDP. This in turn can affect the chain propagation, which results in different polymerization rates as observed in the kinetic study in $CHCl_3$. Furthermore, as a result of the frozen core formed in $CHCl_3$, morphology transitions cannot occur

during the process of dispersion polymerization and hence only spheres were observed.

In contrast, a higher critical micelle degree of polymerization (CMDP) and relatively mobile growing polymer chains are expected in 1,4-dioxane due to the better solubility of the core-forming polymers, including both homopolymers of AMA and copolymers of AMA and TMA. This could lead to a controlled chain extension as observed in the kinetic study of the polymerization in 1,4-dioxane and also allow access to ergodic aggregates during dispersion polymerization. However, with increasing length of the nucleobase-containing blocks or local concentration of the nucleobases, the nucleobase interactions appear to be the main interactions and the growing polymer chains are no longer mobile. As a result, the morphology transitions are hindered and hence twisted structures are generated instead of vesicles (Figure 3.32, **10** and **11**). Complementary nucleobase interactions between adenine and thymine are stronger than adenine-adenine interactions.[68,69] Therefore, a slightly folded structure was observed for the polymerization of **10**, while a deeply twisted structure was afforded in the polymerization of **11**.

3.4 Conclusion

In conclusion, copolymers containing nucleobases were synthesized by RAFT dispersion polymerization and the obtained polymers were well-controlled in terms of molecular weight and molecular weight distributions. Moreover, self-assembly was induced during the RAFT dispersion polymerizations in $CHCl_3$ and 1,4-dioxane, using monomers containing adenine and thymine. Different morphological evolutions were observed in these two media. Only spheres were observed for polymerizations in $CHCl_3$ with increasing size upon increasing the length of the core-forming blocks. In contrast, morphology transitions from spheres through cylinders to lamellae were observed in 1,4-dioxane due to better chain mobility. However, the transitions were disrupted by the presence of strong nucleobase interactions with increasing length of the nucleobase-containing polymers. This study provides insights into understanding the properties of nucleobase-containing polymers and also offers a simple method to prepare self-assemblies containing nucleobases. By simply varying the corona-forming block into a biologically compatible polymer, this route is expected to have potential applications in drug delivery and other biological aspects.

3.5 Experimental section

3.5.1 Materials

Methyl methacrylate (MMA) was bought from Aldrich and passed through a column of neutral alumina to remove inhibitor. 2,2-Azo-bis(isobutyronitrile) (AIBN) was purchased from Molekula and recrystallized from methanol. 2-cyano-2-propyl dodecyl trithiocarbonate (CPDT) was synthesized according to the published method.[46] The synthesis of monomers 2-(2-(adenine-9-yl)acetoxyl) ethyl methacrylate (AMA) and 2-(2-(thymine-1-yl)acetoxyl) ethyl methacrylate (TMA) is based on our previous work in chapter 2.[4] Thymine-containing mediator, 1-hexyl thymine, was synthesized according to a previous method.[1] 1,4-Dioxane, $CHCl_3$, and other solvents were used as received from Fisher Scientific. Deuterated solvents were purchased from Apollo Scientific.

3.5.2 Instrumentation

^{1}H NMR spectra were recorded on a Bruker DPX-300 or DPX-400 spectrometer with DMSO-d_6, 1,4-dioxane-d_8 or deuterated chloroform ($CDCl_3$) as the solvent. The chemical shifts of protons were reported relative to tetramethylsilane at $\delta = 0$ ppm when using $CHCl_3$ or solvent residues (DMSO ^{1}H: 2.50 ppm; 1,4-dioxane: 3.53 ppm).

SEC was obtained in HPLC-grade DMF containing 5 mM NH_4BF_4 at 50 °C, with a flow rate of 1.0 mL per minute, on a set of two PLgel 5 μm Mixed-D columns, plus one guard column. SEC data was analyzed with Cirrus SEC software calibrated using polymethyl methacrylate (PMMA) standards. The SEC was equipped with both refractive index (RI) and UV detectors.

TEM observations were performed on a JEOL 2000FX electron microscope at an acceleration voltage of 200 kV. High magnification TEM images were obtained from a JEOL 2100FX electron microscope at an acceleration voltage of 200 kV. All TEM samples were prepared on graphene oxide (GO)-coated carbon grids (Quantifoil R2/2), which allows high contrast TEM images to be acquired without staining.[50] Generally, a drop of sample (20 μL) was deposited on a grid, blotted immediately and left to air dry.

Hydrodynamic diameters (D_h) and size distributions of the self-assemblies were determined by DLS. The DLS instrumentation consisted of a Malvern Zetasizer NanoS instrument operating at 25 °C with a 4 mW He-Ne 633-nm laser module. Measurements were made at a detection angle of 173 ° (back scattering), and Malvern Zetasizer 7.03 software was used to analyze the data. Static light scattering (SLS) measurements were conducted with an ALV CGS3 (λ =632 nm) at both 20 °C and 50 °C. The data were collected from 30 ° up to 150 ° with an interval of 10 °, calibrated with filtered toluene and filtered $CHCl_3$ or 1,4-dioxane as backgrounds. The refractive index increment of polymer **3** in $CHCl_3$ was measured to be 0.053 mL/g and polymer **10** in 1,4-dioxane was measured to be 0.033 mL/g.

Atomic force microscopy (AFM) images were taken in tapping mode on a Multimode AFM with Nanoscope IIIA Controller with Quadrex. Silicon AFM tips were used with a nominal spring constant and resonance frequency of 3.5 Nm^{-1} and 75 kHz (MikroMasch NSC18). Samples were imaged either on the same quantifoil Cu/GO grids used in TEM analysis or onto freshly cleaved mica discs (Agar Scientific, G250-2). Data were analyzed using Gwyddion software.

Sonication experiments were carried out with a Sonopuls (Bandelin) ultrasonic homogenizer HD 2200 equipped with a MS72 microtip at a frequency of 2 kHz.

Small-angle neutron scattering (SANS) experiments were recorded on the ISIS neutron beam facility, sans2d instrument at the Rutherford Appleton Laboratory, Oxford. Sample **3** was measured at 20 mg/mL in $CDCl_3$, which provides a high contrast in scattering length to the polymer. Small-angle X-ray scattering (SAXS) were carried out on the SAXS-WAXS beamline at the Australian Synchrotron facility at a photon energy of 15 keV. The samples were prepared in 1,4-dioxane and were run using 1.5 mm diameter quartz capillaries. The measurements were collected at 25 °C with a sample to detector distance of 7.160 m to give a q range of 0.0015 to 0.08 $Å^{-1}$, where q is the scattering vector and is related to the scattering angle (2θ) and the photon wavelength (λ) by the following equation:

$$q = \frac{4\pi \sin(\theta)}{\lambda} \qquad (1)$$

All patterns were normalized to fixed transmitted flux using a quantitative beam stop detector. The scattering from a blank (1,4-dioxane) was measured in the same location as sample collection and was subtracted for each measurement. The two-dimensional SAXS images were converted into one-dimensional SAXS profiles (I(q) *versus* q) by circular averaging, where I(q) is the scattering intensity. ScatterBrain and NCNR Data Analysis IGOR PRO software were used to plot and analyze SAXS and SANS data.[70] The scattering length density of the solvents and monomers were calculated using the "Scattering Length Density Calculator" provided by NIST Center for Neutron Research.

3.5.3 Polymerization of methyl methacrylate (MMA)

The typical procedure of RAFT homopolymerization of MMA was as follows: MMA (x), CPDT (1 eq), and AIBN (0.1 eq) were dissolved in toluene. The mixture was thoroughly degassed *via* 4 freeze-pump-thaw cycles, filled with oxygen-free nitrogen and then immersed in an oil bath at 60 °C for 5 hours. The reaction was quenched by putting into a liquid nitrogen bath and exposing to air. The mixture was precipitated in MeOH and filtered. The solid was dissolved in THF and precipitated again. The precipitation procedure was repeated 3 times in total. The light yellow polymers were dried in a vacuum oven overnight and characterized by ^{1}H NMR spectroscopy and DMF size-exclusion chromatography (SEC) (PMMA standards). The DP of the block was varied by adding different amounts of the monomer.

^{1}H NMR (400 MHz, $CDCl_3$, ppm): δ = 3.60 (s, $3H_{backbone\text{-}PMMA}$, OCH_3), δ = 3.25 – 3.22 (t, $2H_{end\text{-}group}$, $CH_2SC{=}S$), δ = 1.96 – 1.81 (m, $2H_{backbone\text{-}PMMA}$, CH_2CCH_3), δ = 1.51 – 1.33 (m, $18H_{end\text{-}group}$, $SCH_2CH_2(CH_2)_9CH_3$), δ = 1.30 – 0.75 (m, $3H_{backbone\text{-}PMMA}$, CH_2CCH_3).

3.5.4 Synthesis of block polymers using PMMA as macro-CTA

The typical procedure was as follows: PMMA (1 eq), AMA (x), TMA (y), and AIBN (0.1 eq) were dissolved in 1,4-dioxane or $CHCl_3$. The mixture was thoroughly degassed *via* 4 freeze-pump-thaw cycles, filled with oxygen-free nitrogen and then immersed in an oil bath at 60 °C for 24 hours. The reaction was quenched by exposing to air and cooling down. The mixture was precipitated in MeOH and washed with MeOH several times. The light yellow polymers were dried in a vacuum oven overnight and characterized by ^{1}H NMR spectroscopy and DMF SEC (PMMA standards). The DP of the block was varied by adding different amounts of the monomer.

^{1}H NMR (400 MHz, DMSO-d_6, ppm):δ = 11.73 – 11.58 (br, 1H$_{backbone\text{-}PTMA}$, N*H*CO), δ = 8.23 – 8.05 (d, 2H$_{backbone\text{-}PAMA}$, two NC*H*N of adenine), δ = 7.64 – 7.28 (d, 3H$_{backbone\text{-}PAMA+PTMA}$, N$H_2$ of adenine and NC*H*=CCH$_3$ of thymine), δ = 5.27 – 4.85 (br, 2H$_{backbone\text{-}PAMA}$, NC*H*2COO), δ = 4.80 – 3.80 (m, 10H$_{backbone\text{-}PAMA+PTMA}$, OC$H_2CH_2$O of PAMA and OC$H_2CH_2$OCOC$H_2$ of PTMA), δ = 3.70 – 3.40 (s, 3H$_{backbone\text{-}PMMA}$, OCH_3), δ = 2.12 – 1.50 (m, 3H$_{backbone\text{-}PTMA}$, 2H$_{backbone}$, CH=C(CH_3) of thymine and CH_2CCH$_3$ of backbone), δ = 1.30 – 0.50 (m, 3H$_{backbone}$, CH$_2$CCH_3)

3.5.5 Kinetics of the dispersion polymerization for a target diblock copolymer PMMA$_{70}$-*b*-(PAMA$_{0.5}$-*co*-PTMA$_{0.5}$)$_{50}$

PMMA$_{70}$ macro-CTA (35 mg, 0.005 mmol), AMA (38 mg, 0.125 mmol), TMA (37mg, 0.125 mmol), and AIBN (0.1 mg, 0.0005 mmol) were dissolved in 6 mL of $CHCl_3$ or 1,4-dioxane. The mixture was thoroughly degassed *via* 4 freeze-pump-thaw cycles, filled with oxygen-free nitrogen and then immersed in an oil bath at 60 °C. An aliquot of the polymerization solution was taken at designated times for ^{1}H NMR spectroscopy, SEC, DLS and TEM characterization.

3.6 References

(1) Tao, Y.; Satoh, K.; Kamigaito, M. *Macromol. Rapid Commun.* **2011**, *32*, 226.

(2) Takemoto, K.; Akashi, M.; Inaki, Y. *J. Polym. Sci., Polym. Chem. Ed.* **1974**, *12*, 1861.

(3) Akashi, M.; Kita, Y.; Inaki, Y.; Takemoto, K. *J. Polym. Sci., Polym. Chem. Ed.* **1979**, *17*, 301.

(4) Kang, Y.; Lu, A.; Ellington, A.; Jewett, M. C.; O'Reilly, R. K. *ACS Macro Lett.* **2013**, *2*, 581.

(5) Khan, A.; Haddleton, D. M.; Hannon, M. J.; Kukulj, D.; Marsh, A. *Macromolecules* **1999**, *32*, 6560.

(6) South, C. R.; Weck, M. *Macromolecules* **2007**, *40*, 1386.

(7) Lo, P. K.; Sleiman, H. F. *J. Am. Chem. Soc.* **2009**, *131*, 4182.

(8) Ilhan, F.; Galow, T. H.; Gray, M.; Clavier, G.; Rotello, V. M. *J. Am. Chem. Soc.* **2000**, *122*, 5895.

(9) Bazzi, H. S.; Sleiman, H. F. *Macromolecules* **2002**, *35*, 9617.

(10) Thibault, R. J.; Hotchkiss, P. J.; Gray, M.; Rotello, V. M. *J. Am. Chem. Soc.* **2003**, *125*, 11249.

(11) Spijker, H. J.; Dirks, A. J.; van Hest, J. C. M. *J. Polym. Sci., Part A: Polym. Chem.* **2006**, *44*, 4242.

(12) Sijbesma, R. P.; Beijer, F. H.; Brunsveld, L.; Folmer, B. J. B.; Hirschberg, J. H. K. K.; Lange, R. F. M.; Lowe, J. K. L.; Meijer, E. W. *Science* **1997**, *278*, 1601.

(13) McHale, R.; Patterson, J. P.; Zetterlund, P. B.; O'Reilly, R. K. *Nature Chem.* **2012**, *4*, 491.

(14) McHale, R.; O'Reilly, R. K. *Macromolecules* **2012**, *45*, 7665.

(15) Oh, J. K. *J. Polym. Sci., Part A: Polym. Chem.* **2008**, *46*, 6983.

(16) Jennings, J.; Beija, M.; Kennon, J. T.; Willcock, H.; O'Reilly, R. K.; Rimmer, S.; Howdle, S. M. *Macromolecules* **2013**, *46*, 6843.

(17) Cunningham, M. F. *Prog. Polym. Sci.* **2008**, *33*, 365.

(18) Zetterlund, P. B.; Aldabbagh, F.; Okubo, M. *J. Polym. Sci., Part A: Polym. Chem.* **2009**, *47*, 3711.

(19) Ladmiral, V.; Semsarilar, M.; Canton, I.; Armes, S. P. *J. Am. Chem. Soc.* **2013**, *135*, 13574.

(20) Zhang, X. W.; Boisson, F.; Colombani, O.; Chassenieux, C.; Charleux, B. *Macromolecules* **2014**, *47*, 51.

(21) Luo, Y.; Wang, X.; Zhu, Y.; Li, B.-G.; Zhu, S. *Macromolecules* **2010**, *43*, 7472.

(22) Kagawa, Y.; Minami, H.; Okubo, M.; Zhou, J. *Polymer* **2005**, *46*, 1045.

(23) Kitayama, Y.; Kagawa, Y.; Minami, H.; Okubo, M. *Langmuir* **2010**, *26*, 7029.

(24) Nicolas, J.; Ruzette, A.-V.; Farcet, C.; Gérard, P.; Magnet, S.; Charleux, B. *Polymer* **2007**, *48*, 7029.

(25) Farcet, C.; Charleux, B.; Pirri, R. *Macromolecules* **2001**, *34*, 3823.

(26) Kitayama, Y.; Kishida, K.; Minami, H.; Okubo, M. *J. Polym. Sci., Part A: Polym. Chem.* **2012**, *50*, 1991.

(27) Kitayama, Y.; Yorizane, M.; Minami, H.; Okubo, M. *Polym. Chem.* **2012**, *3*, 1394.

(28) Tonnar, J.; Lacroix-Desmazes, P.; Boutevin, B. *Macromolecules* **2007**, *40*, 6076.

(29) Blanazs, A.; Madsen, J.; Battaglia, G.; Ryan, A. J.; Armes, S. P. *J. Am. Chem. Soc.* **2011**, *133*, 16581.

(30) Fielding, L. A.; Derry, M. J.; Ladmiral, V.; Rosselgong, J.; Rodrigues, A. M.; Ratcliffe, L. P. D.; Sugihara, S.; Armes, S. P. *Chem. Sci.* **2013**, *4*, 2081.

(31) Sun, J.-T.; Hong, C.-Y.; Pan, C.-Y. *Soft Matter* **2012**, *8*, 7753.

(32) Huang, C.-Q.; Pan, C.-Y. *Polymer* **2010**, *51*, 5115.

(33) Zhang, X.; Boissé, S. p.; Zhang, W.; Beaunier, P.; D'Agosto, F.; Rieger, J.; Charleux, B. *Macromolecules* **2011**, *44*, 4149.

(34) Zhang, W.; D'Agosto, F.; Dugas, P.-Y.; Rieger, J.; Charleux, B. *Polymer* **2013**, *54*, 2011.

(35) Jia, Z.; Bobrin, V. A.; Truong, N. P.; Gillard, M.; Monteiro, M. J. *J. Am. Chem. Soc.* **2014**, *136*, 5824.

(36) Zayas, H. A.; Truong, N. P.; Valade, D.; Jia, Z.; Monteiro, M. J. *Polym. Chem.* **2013**, *4*, 592.

(37) Karagoz, B.; Esser, L.; Duong, H. T.; Basuki, J. S.; Boyer, C.; Davis, T. P. *Polym. Chem.* **2014**, *5*, 350.

(38) Karagoz, B.; Boyer, C.; Davis, T. P. *Macromol. Rapid Commun.* **2014**, *35*, 417.

(39) Su, Y.; Xiao, X.; Li, S.; Dan, M.; Wang, X.; Zhang, W. *Polym. Chem.* **2014**, *5*, 578.

(40) Pei, Y.; Lowe, A. B. *Polym. Chem.* **2014**, *5*, 2342.

(41) Cai, W.; Wan, W.; Hong, C.; Huang, C.; Pan, C. *Soft Matter* **2010**, *6*, 5554.

(42) Sugihara, S.; Armes, S. P.; Blanazs, A.; Lewis, A. L. *Soft Matter* **2011**, *7*, 10787.

(43) Chambon, P.; Blanazs, A.; Battaglia, G.; Armes, S. P. *Macromolecules* **2012**, *45*, 5081.

(44) Zhang, W.-J.; Hong, C.-Y.; Pan, C.-Y. *Macromolecules* **2014**, *47*, 1664.

(45) Kyogoku, Y.; Lord, R. C.; Rich, A. *J. Am. Chem. Soc.* **1967**, *89*, 496.

(46) Chong, Y. K.; Moad, G.; Rizzardo, E.; Thang, S. H. *Macromolecules* **2007**, *40*, 4446.

(47) Reichardt, C. *Solvents and Solvent Effects in Organic Chemistry*, Wiley, **2003**.

(48) Lutz, J.-F.; Thünemann, A. F.; Rurack, K. *Macromolecules* **2005**, *38*, 8124.

(49) Lutz, J.-F.; Thünemann, A. F.; Nehring, R. *J. Polym. Sci., Part A: Polym. Chem.* **2005**, *43*, 4805.

(50) Patterson, J. P.; Sanchez, A. M.; Petzetakis, N.; Smart, T. P.; Epps III, T. H.; Portman, I.; Wilson, N. R.; O'Reilly, R. K. *Soft Matter* **2012**, *8*, 3322.

(51) Patterson, J. P.; Robin, M. P.; Chassenieux, C.; Colombani, O.; O'Reilly, R. K. *Chem. Soc. Rev.* **2014**, *43*, 2412.

(52) Teixeira, J. *J. Appl. Crystallogr.* **1988**, *21*, 781.

(53) Beaucage, G. *J. Appl. Crystallogr.* **1995**, *28*, 717.

(54) Hu, X.; Hu, J.; Tian, J.; Ge, Z.; Zhang, G.; Luo, K.; Liu, S. *J. Am. Chem. Soc.* **2013**, *135*, 17617.

(55) He, M.; Zhao, L.; Wang, J.; Han, W.; Yang, Y.; Qiu, F.; Lin, Z. *ACS Nano* **2010**, *4*, 3241.

(56) Hammouda, B. *J. Appl. Crystallogr.* **2010**, *43*, 716.

(57) Guinier, A.; Fournet, G. *Small-angle scattering of X-rays*, Wiley, **1955**.

(58) Bartlett, P.; Ottewill, R. H. *J. Chem. Phys.* **1992**, *96*, 3306.

(59) Petzetakis, N.; Walker, D.; Dove, A. P.; O'Reilly, R. K. *Soft Matter* **2012**, *8*, 7408.

(60) Catrouillet, S.; Fonteneau, C.; Bouteiller, L.; Delorme, N.; Nicol, E.; Nicolai, T.; Pensec, S.; Colombani, O. *Macromolecules* **2013**, *46*, 7911.

(61) Nallet, F.; Laversanne, R.; Roux, D. *J. Phys. II France* **1993**, *3*, 487.

(62) Berghausen, J.; Zipfel, J.; Lindner, P.; Richtering, W. *J. Phys. Chem. B* **2001**, *105*, 11081.

(63) Sun, L.; Petzetakis, N.; Pitto-Barry, A.; Schiller, T. L.; Kirby, N.; Keddie, D. J.; Boyd, B. J.; O'Reilly, R. K.; Dove, A. P. *Macromolecules* **2013**, *46*, 9074.

(64) Pitto-Barry, A.; Kirby, N.; Dove, A. P.; O'Reilly, R. K. *Polym. Chem.* **2014**, *5*, 1427.

(65) Zheng, G.; Pan, C. *Macromolecules* **2005**, *39*, 95.

(66) Zheng, G.; Zheng, Q.; Pan, C. *Macromol. Chem. Phys.* **2006**, *207*, 216.

(67) Ji, W.; Yan, J.; Chen, E.; Li, Z.; Liang, D. *Macromolecules* **2008**, *41*, 4914.

(68) Mather, B. D.; Baker, M. B.; Beyer, F. L.; Berg, M. A. G.; Green, M. D.; Long, T. E. *Macromolecules* **2007**, *40*, 6834.

(69) Kyogoku, Y.; Lord, R. C.; Rich, A. *Proc. Natl. Acad. Sci. U. S. A.* **1967**, *57*, 250.

(70) Kline, S. *J. Appl. Crystallogr.* **2006**, *39*, 895.

Chapter 4. RAFT dispersion polymerization: A method to tune the morphologies of thymine-containing self-assembly

4.1 Abstract

The synthesis and self-assembly of thymine-containing polymers were performed using RAFT dispersion polymerization. A combination of microscopy and scattering techniques was used to analyze the morphologies. There were two general observations from this study: (1) the obtained aggregations induced by the polymerizations were well-defined; (2) the copolymers produced possessed broad dispersities. Moreover, a variety of polymerization parameters, including polymerization solvent, the amount of monomers, the length of macro-CTA and the presence of an adenine-containing mediator, were investigated and exhibited significant effects on the final aggregation's size and morphology and copolymer properties.

4.2 Introduction

Heterogeneous polymerizations, including dispersion, emulsion, suspension and precipitation polymerizations, are easily performed and widely used in industry.[1] Recently the combination of heterogeneous polymerization with controlled/living radical polymerization (CRP) is of great interest, given that this approach can compile the advantages of heterogeneous polymerization with the controlled nature of CRP.[2,3] CRP techniques including reversible addition-fragmentation chain-transfer polymerization (RAFT),[2,4,5] various forms of atom-transfer radical polymerization (ATRP),[6,7] nitroxide-mediated polymerizations (NMP),[8,9] and other CRP methods[10-12] have been readily applied in this area. Some of these processes have enormous advantages for the design of well-defined nanoobjects and the synthesis of their corresponding block copolymers.[13-18] For example, RAFT dispersion polymerization has been widely developed to grow a solvent-insoluble polymer block from a solvent-soluble monomer in the presence of a solvent-soluble macromolecular chain transfer agent (macro-CTA). In most cases, by simply varying the polymerization conditions, a range of common morphologies (spheres, cylinders, vesicles) and a few novel structures (lumpy rod,[19] framboidal morphology,[20] concentric vesicle,[21] and knot-like structure[22]) can be obtained. In addition, the resultant block copolymers are generally obtained with good blocking efficiencies and relatively low dispersities.

In Chapter 3 we have demonstrated the synthesis of nucleobase-containing materials by using RAFT dispersion polymerization.[22] In our study, poly(methyl methacrylate) (PMMA) was used as the macro-CTA and only adenine-containing monomer or a mixture of adenine-containing monomer and thymine-containing monomer were used as the monomers. RAFT dispersion polymerizations were investigated in both chloroform and 1,4-dioxane. It was found that in these

conditions polymers obtained were generally well-controlled in terms of molecular weight and molecular weight distribution. Moreover, it was also observed that the choice of polymerization solvent played a key role on the final morphologies achieved.

Thymine is one of the natural nucleobases in DNA and binds to adenine *via* complementary hydrogen bonding interactions to stabilize the DNA. Moreover, it is also well-known that thymine could form triple hydrogen bonds with diaminopurine or its derivatives. Based on these properties, thymine is commonly used for controlling polymer tacticity,[23] templating polymerizations,[24-26] facilitating molecular self-assembly and aggregations,[27-30] and protecting active moieties.[31] However, there are still few reports on the systematic study of the self-assembly of thymine-containing polymers of various chain length. Considering the advantages of RAFT dispersion polymerizations, we have applied this approach to readily prepare a variety of thymine-containing nanostructures. However, compared to our previous work on RAFT dispersion polymerization to prepare nucleobase-containing nanostructures,[22] contrasting results in terms of morphology and molecular weight distributions of the resultant polymers have been observed: (1) the morphologies produced are more various and well-defined; (2) the resultant polymers are bimodal in most cases. The narrow dispersity of block copolymers is considered as one of the prerequisites for the formation of well-defined self-assemblies.[32] However, this study shows in an unprecedented manner that well-defined nanoobjects can still be attained although the formed block copolymers possess broad dispersities. To our knowledge, there is little research into the study of the solution behaviour of polydisperse block amphiphiles.[33-36] Block copolymers with broad dispersities affect the interfacial curvatures, allowing structures with nonconstant interfacial mean curvatures but

thermodynamic stabilized to form (*e.g.* prolate-spheroid micells,[33] stabilized vesicles[36] and more complex structures[35,37]). In order to further extend this concept and study these observed differences, we have performed RAFT dispersion polymerizations of a thymine-containing monomer and also investigated the effects of polymerization factors on the resultant morphologies and polymers.

4.3 Results and discussion

4.3.1 Synthesis of macro-CTA

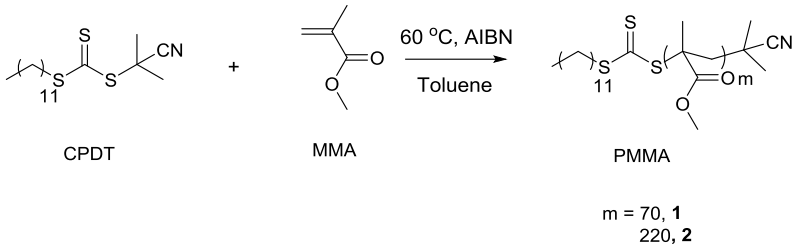

Scheme 4.1 Synthetic route for the macro-CTA (PMMA, **1** and **2**).

The synthetic route for the PMMA macro-chain transfer agent (macro-CTA) is shown in Scheme 4.1. CPDT was used as the CTA as it is suitable for the polymerization of methacrylate and nucleobase-containing monomers.[38,39] The polymerizations were stopped at relatively low conversion to ensure good end group fidelity. The DP of the PMMA macro-CTA was determined by ^{1}H NMR spectroscopy by comparing the integration of PMMA backbone signals with those of the end group from CPDT. The resulting DPs of PMMA were *ca*. 70 and 220 (polymer **1** and **2**). SEC analysis (DMF as eluent, PMMA standards) was used to further determine the molecular weight and the molecular weight distribution (Figure 4.1). In addition to the observed narrow molecular weight distributions, the molecular weights from SEC are consistent with the results from ^{1}H NMR spectroscopy. Furthermore, the RI SEC trace and UV SEC trace (λ = 309 nm from trithiocarbonate end group) overlap well, suggesting good end group fidelity.

Table 4.1 Characterization data of macro-CTA, PMMA

Polymers/target polymers	Solvent/mediator	Conv. (%)	$M_{n,\,th}$ (kDa)	$M_{n,\,NMR}$ (kDa)[a]	$M_{n,\,SEC}$ (kDa)[b]	$Đ_M$
$PMMA_{70}$, **1**	toluene	36	4.5	6.8	7.0	1.17
$PMMA_{220}$, **2**	toluene	57	22.6	22.0	21.5	1.19

[a]determined by ^{1}H NMR spectroscopy; [b]determined by SEC analysis (DMF eluent, PMMA standards).

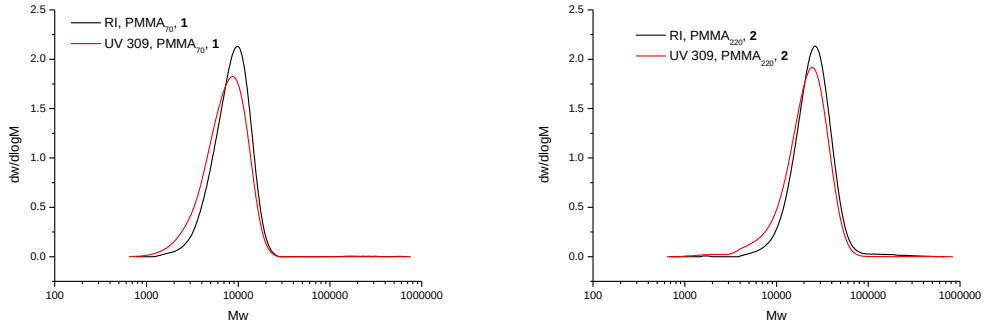

Figure 4.1 SEC analysis of macro-CTA, PMMA (polymer **1** and polymer **2**) (DMF eluent, PMMA as stardards).

4.3.2 Homopolymerization of TMA

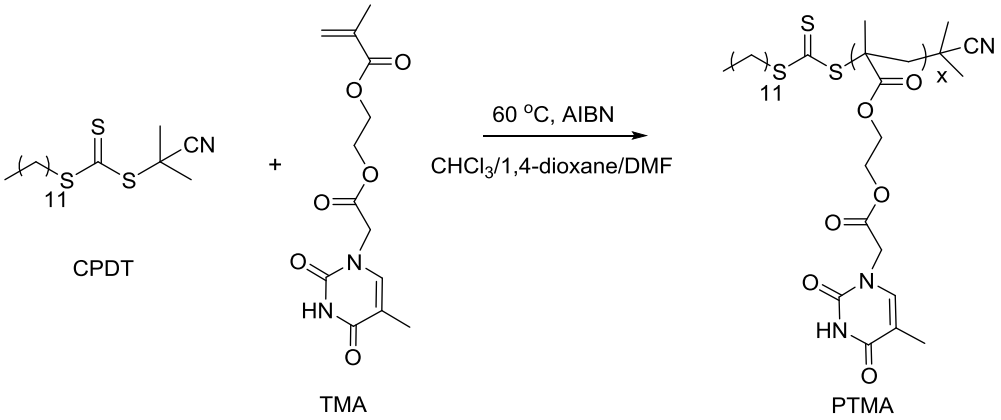

Scheme 4.2 Synthetic route for the TMA homopolymer.

Homopolymerizations of TMA in chloroform and DMF were studied in Chapter 2 using CPDT as a CTA.[38] Although TMA could be polymerized in chloroform, due to the heterogeneous system, the polymerization was not well-controlled.[38] However, polymer (PTMA) obtained using DMF as the polymerization solvent was well-defined in terms of molecular weight and molecular weight distribution.[38] In this Chapter, the homopolymerization of TMA in 1,4-dioxane was also performed to further investigate the feasibility of the polymerization of TMA.

The solubility of PTMA in 1,4-dioxane was slightly higher than in chloroform, and precipitation of the polymer still occurred as the polymerization proceeded, however, the molecular weight distribution of the resultant polymer was slightly narrower and

the resultant molecular weight was relatively controlled compared to polymerization in chloroform (Figure 4.2 and Table 4.2). These observations suggest that it is possible to perform RAFT dispersion polymerizations of TMA using 1,4-dioxane as the solvent.

Table 4.2 Characterization data of PTMA homopolymer

Polymers/target polymers	Solvent/mediator	Conv. (%)	$M_{n,\,th}$ (kDa)	$M_{n,\,NMR}$ (kDa)[a]	$M_{n,\,SEC}$ (kDa)[b]	$Đ_M$
$PTMA_{40}$, **3**	1,4-dioxane	61	7.5	11.7	12.3	1.14

[a]determined by ^{1}H NMR spectroscopy in DMF-d_7; [b]determined by SEC analysis (DMF eluent, PMMA standards).

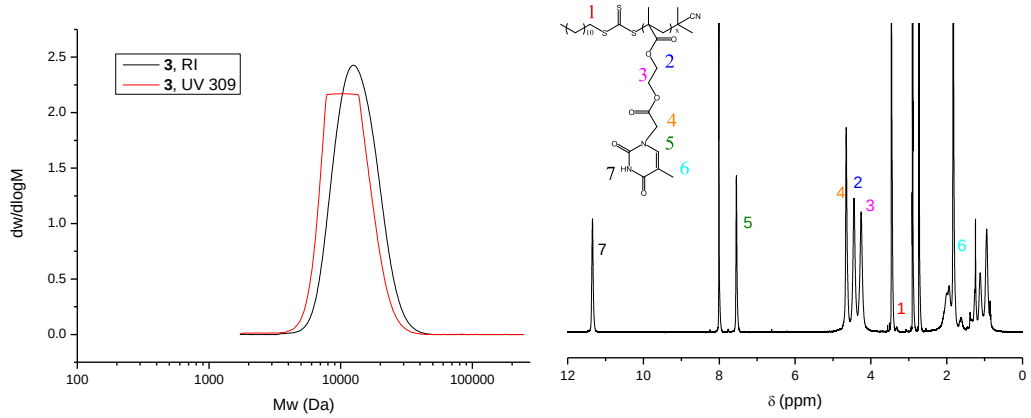

Figure 4.2 SEC (DMF eluent, PMMA as stardards) and ^{1}H NMR (DMF-d_7) analysis of homopolymer PTMA, **3** polymerized in 1,4-dioxane.

4.3.3 RAFT dispersion polymerizations of TMA

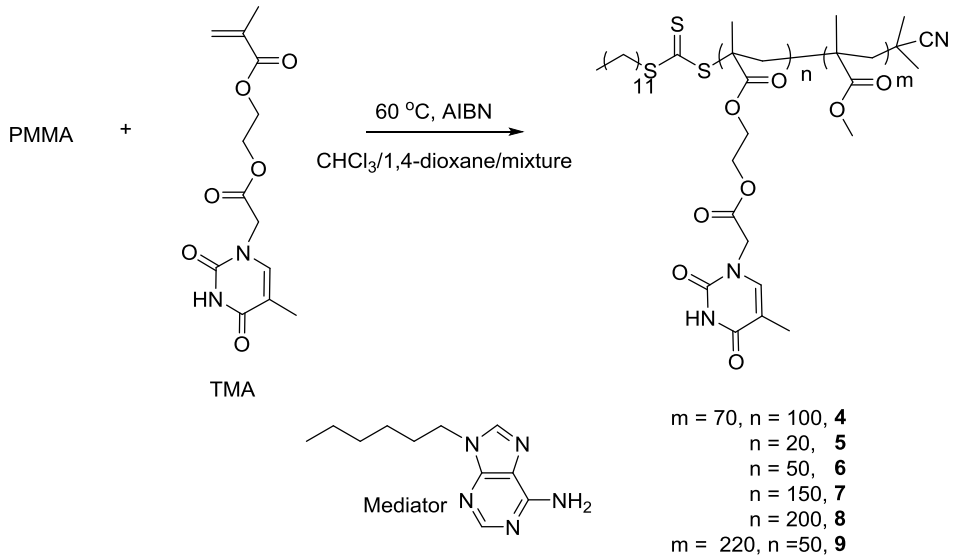

Scheme 4.3 Synthetic route for thymine-containing diblock copolymers by RAFT dispersion polymerization using PMMA as the macro-CTA.

RAFT dispersion polymerizations of TMA were performed at 60 °C using PMMA as the macro-CTA and AIBN as the initiator (Scheme 4.3). The conversions of the polymerizations were determined by ^{1}H NMR spectroscopy and the molecular weight and molecular weight distributions were analyzed by SEC (DMF as eluent, PMMA as standards). The morphologies induced by the polymerizations were characterized by both light scattering and microscopy analysis. In addition, the effects of a range of polymerization parameters (including polymerization solvent, the amount of monomers, the length of macro-CTA and the presence of an adenine-containing mediator) on polymerizations were studied.

4.3.3.1 Effect of solvent

Table 4.3 Characterization data for polymer **4**, $PMMA_{70}$-*b*-$PTMA_{100}$, prepared in different solvents

Polymers/target polymers	Solvent	Conv. (%)	$M_{n,\,th}$ (kDa)	$M_{n,\,NMR}$ (kDa)[a]	$M_{n,\,SEC}$ (kDa)[b]	$Đ_M$
$PMMA_{70}$-*b*-$PTMA_{100}$, **4-100**	chloroform	97	36.1	45.1	42.8	2.88
$PMMA_{70}$-*b*-$PTMA_{100}$,**4-75**	chloroform:1,4-dioxane = 75:25	94	35.2	--	38.0	1.96
$PMMA_{70}$-*b*-$PTMA_{100}$, **4-50**	chloroform: 1,4-dioxane = 50:50	92	34.6	--	37.9	2.72
$PMMA_{70}$-*b*-$PTMA_{100}$, **4-33**	chloroform: 1,4-dioxane = 33:67	93	34.9	--	35.0	2.84
$PMMA_{70}$-*b*-$PTMA_{100}$, **4-25**	chloroform: 1,4-dioxane = 25:75	91	34.3	--	35.5	2.29
$PMMA_{70}$-*b*-$PTMA_{100}$, **4-12.5**	chloroform: 1,4-dioxane = 12.5:87.5	90	34.0	--	34.0	1.96
$PMMA_{70}$-*b*-$PTMA_{100}$, **4-0**	1,4-dioxane	87	33.1	--	30.0	1.44

[a]determined by ^{1}H NMR spectroscopy in DMSO-d_6 and without polymer purification, some values are not attainable; [b]determined by SEC analysis (DMF eluent, PMMA standards).

As observed in our previous study, solvent plays a key role in RAFT dispersion polymerizations of nucleobase-containing monomers,[22] where different morphologies can be achieved by using different solvent. In this study, pure chloroform, 1,4-dioxane, and mixtures of the two at various ratios

were selected as the polymerization solvents to study the effect of solvent on the RAFT dispersion polymerization of TMA (Table 4.3). The initial ratio of macro-CTA:TMA:AIBN was 1:100:0.1 and PMMA with a DP of 70 was used as the macro-CTA (the polymers/polymerizations were named as **4-X**; **X** was the composition of chloroform in a mixture of chloroform and 1,4-dioxane). It was observed that by varying the ratio of polymerization solvents, a range of morphologies were obtained for the target block copolymer $PMMA_{70}$-*b*-$PTMA_{100}$.

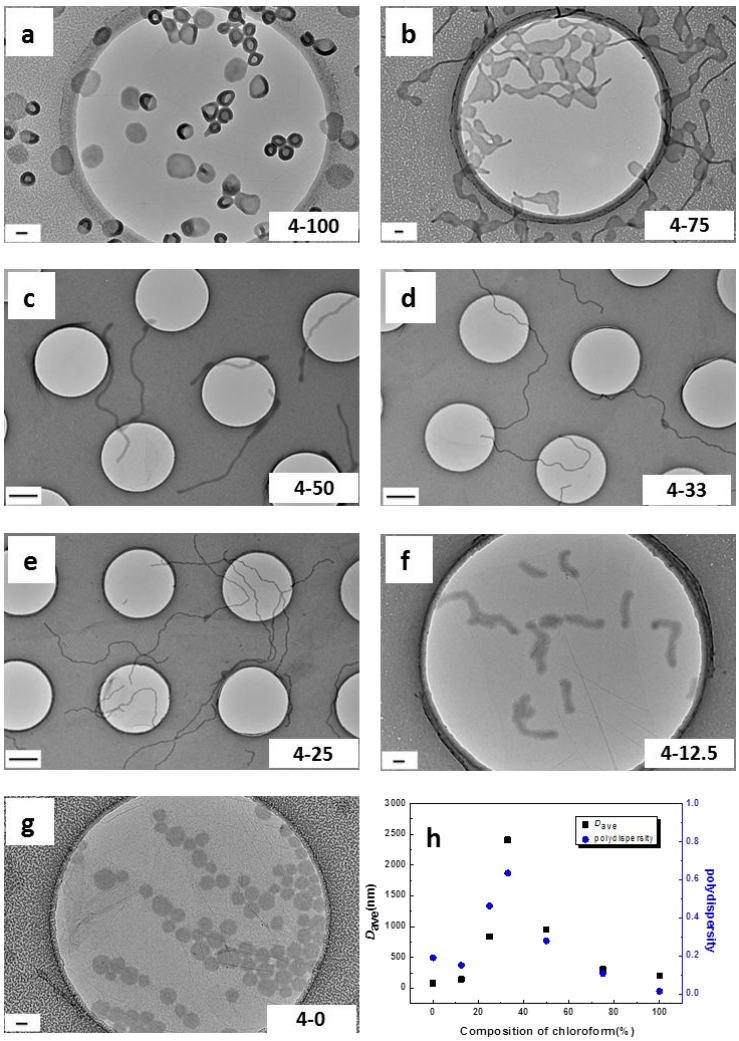

Figure 4.3 Representative TEM images of self-assemblies prepared by RAFT dispersion polymerizations for a target polymer $PMMA_{70}$-*b*-$PTMA_{100}$, **4-X** in different solvents (from **a** to **g**: volume compositions of $CHCl_3$ in the mixtures of $CHCl_3$ and 1,4-dioxane were 100%, 75%, 50%, 33%, 25%, 12.5% and 0%) and their corresponding size and size distributions (h). Scale bar: 100 nm (1000 nm for c, d, and e).

When pure chloroform was used as the polymerization solvent, vesicles were clearly observed by TEM analysis (Figure 4.3a, **4-100**). From DLS analysis, the number-average hydrodynamic diameter of the vesicles was 195 nm (Figure 4.4 top). In addition, to eliminate the possibility of artefact effects caused by dry-state TEM, SLS was also conducted on the sample to further determine the morphology (Figure 4.4 bottom). The concentrations of the sample ranged from 0.3 mg/mL to 0.1 mg/mL. P-ratio (R_g/R_H, ratio between radius of gyration and hydrodynamic radius) were calculated close to 1 (R_g/R_H = 1.17), indicating the formation of hollow structures.[40] SANS was also conducted on a highly concentrated sample (20 mg/mL), which was obtained directly from the polymerization solution without dilution (Figure 4.5). The Guinier-Porod fit was firstly applied to give information on the shape of the assemblies,[41] Spherical morphologies were confirmed from this fit (Figure 4.5 top left and Table 4.4). The thickness of the membrane was firstly determined by using a plot of $q^2I(q)$ *versus* q (Figure 4.5 top right).[42] The first minimum of a plot of $q^2I(q)$ *versus* q (highlighted with a line in Figure 4.5 top right) corresponds to the first zero of the membrane factor given by:

$$d=2\pi/q$$

where d is the membrane thickness. Such a plot gave a membrane thickness of 41 nm. To investigate the assembly structure in more detail, the polycoreshell ratio model (from the NIST package) was also used (Figure 4.5 bottom).[43] In this model, both core and shell are polydisperse and the core is considered as the solvent filled lumen of the vesicles. From the fit, the thickness of the shell (the membrane in our study) is determined to be 38.3 nm and the radius of the core (the lumen in this study) is 70.0 nm with a dispersity of both the core and

the shell of 0.18. The thickness of the membrane correlates well with the value determined using the $q^2I(q)$ *versus* q plot. The total radius (108.3 nm) is also highly consistent with the results from DLS and TEM analysis (Table 4.5). Moreover, the scattering length density (SLD) of the shell is coherent with experimental or theoretical values of both PMMA and PTMA. These results further prove the formation of vesicles when pure chloroform was used as the polymerization solvent.

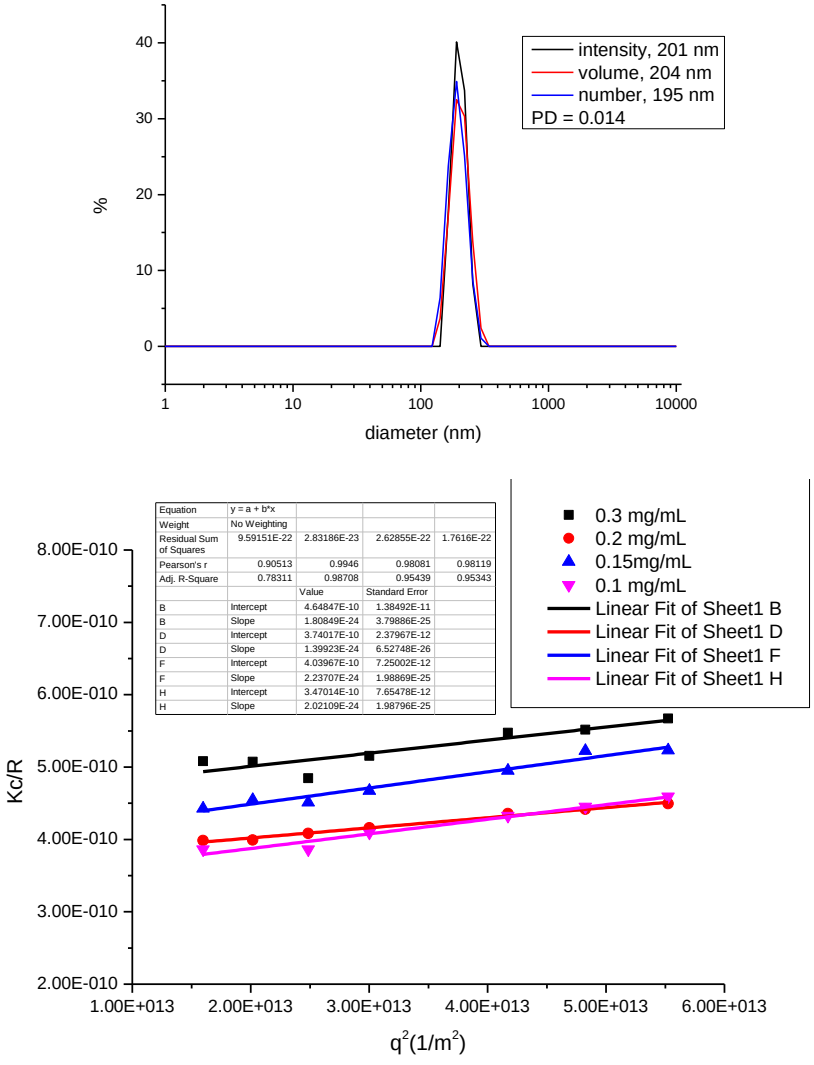

Equation	y = a + b*x			
Weight	No Weighting			
Residual Sum of Squares	9.59151E-22	2.83186E-23	2.62855E-22	1.7616E-22
Pearson's r	0.90513	0.9946	0.98081	0.98119
Adj. R-Square	0.78311	0.98708	0.95439	0.95343
		Value	Standard Error	
B	Intercept	4.64847E-10	1.38492E-11	
B	Slope	1.80849E-24	3.79886E-25	
D	Intercept	3.74017E-10	2.37967E-12	
D	Slope	1.39923E-24	6.52748E-26	
F	Intercept	4.03967E-10	7.25002E-12	
F	Slope	2.23707E-24	1.98869E-25	
H	Intercept	3.47014E-10	7.65478E-12	
H	Slope	2.02109E-24	1.98796E-25	

Figure 4.4 DLS distribution and Zimm plots for self-assembly prepared by polymerization **4-100**, $PMMA_{70}$-*b*-$PTMA_{100}$ in chloroform.

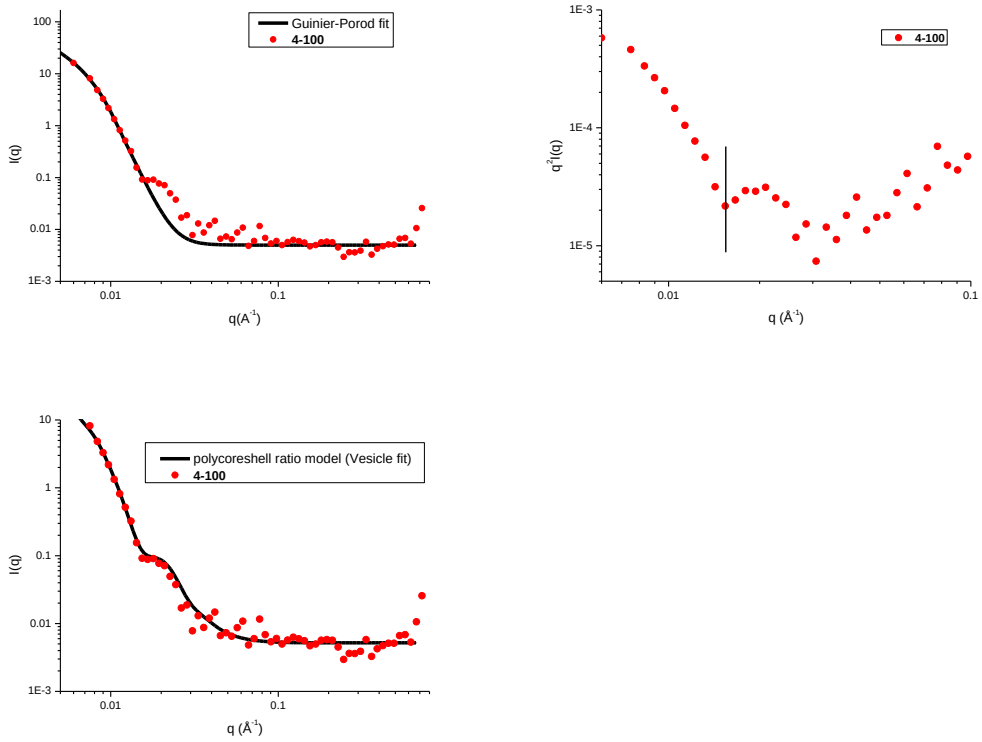

Figure 4.5 SANS analysis of polymer **4-100**, $PMMA_{70}$-*b*-$PTMA_{100}$ in chloroform: experimental profile and Guinier-Porod fit (top left); plot to determine the thickness of the membrane (top right); experimental profile and polycoreshell ratio fit (bottom).

Table 4.4 Data from Guinier-Porod fit

Sample	R_g (nm)	s[a]
$PMMA_{70}$-*b*-$PTMA_{100,}$ **4-100**	25.6	0.70

[a]s = 0: spheres; s = 1: rods; s = 2: platelets

Table 4.5 Data from polycoreshell ratio model for **4-100**[a]

Core radius (nm)	Shell thickness (nm)	Total radius (nm)
70.0	38.3	108.3

[a]The SLDs of the solvent and the core were fixed while the other parameters were left to float. Fittings with various manually inputted starting parameters were used to assess the validity of the fit.

When a mixture of chloroform and 1,4-dioxane (volume composition of chloroform: 75%) was used as the solvent, a morphology of lamellae with tentacles was observed, which had a hydrodynamic diameter of 312 nm by DLS (Figure 4.3b, **4-75**). AFM was conducted on this sample, which showed the heights of lamellae were *ca.* 25 nm (Figure 4.6). Further decreasing the volume composition of chloroform to 50% led to the formation of long

cylinders. From TEM analysis, the cylinders were around 5 μm long (Figure 4.3c, **4-50**). Even longer and thinner cylinders were observed when the compositions of chloroform were 33% and 25%, respectively (Figure 4.3d, **4-33** and 4.3e, **4-25**). These cylinders were more than 10 μm in length and around 55 nm in width by TEM analysis. However, when the amount of chloroform was dropped to 12.5%, much shorter worm-like structures were obtained (Figure 4.3f, **4-12.5**) and the width of cylinders slightly increased to 75 nm.

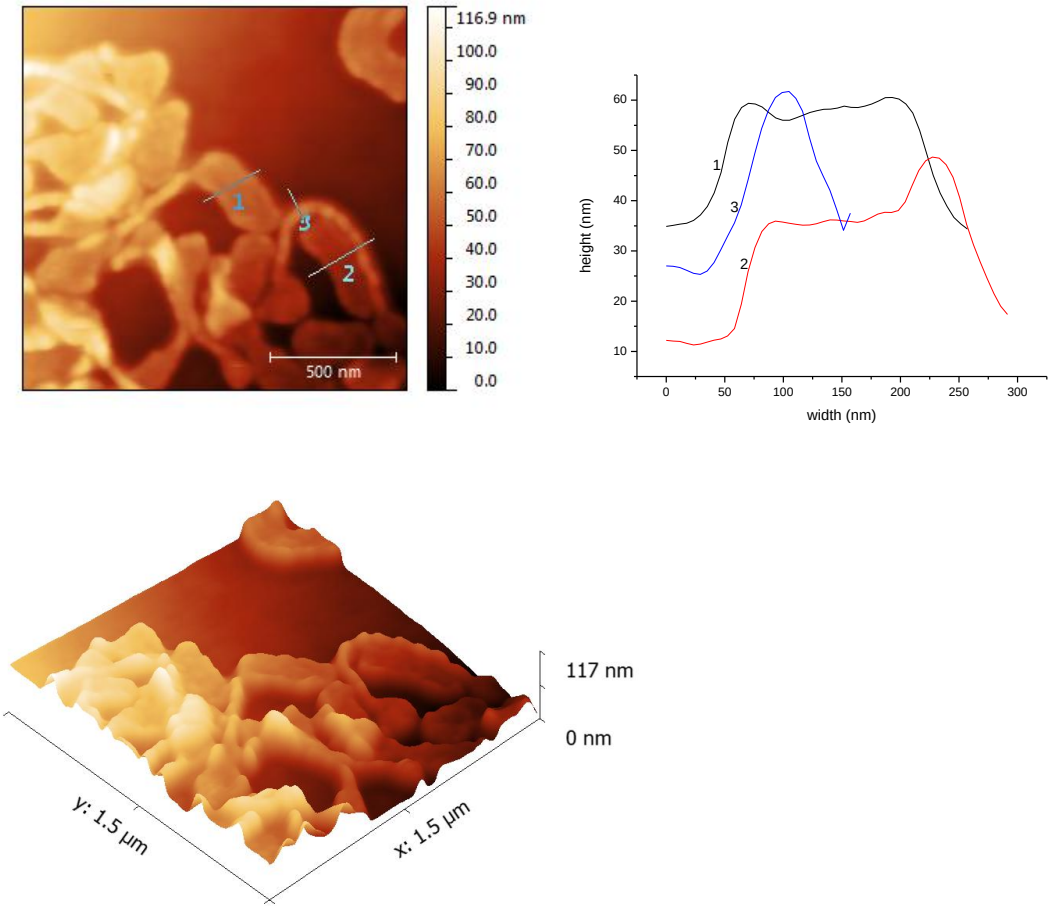

Figure 4.6 AFM height image (top left) and three-dimensional AFM image (bottom) of self-assembly prepared by polymerization **4-75**, $PMMA_{70}$-*b*-$PTMA_{100}$ in a mixture of chloroform and 1,4-dioxane (3:1, v/v) and corresponding height profile (top right)

In the case of pure 1,4-dioxane as the solvent, low contrast disk-like structures with a diameter of 100 nm were observed by TEM analysis (Figure 4.3g, **4-0**).

SAXS was used to further analyze the morphology in solution (Figure 4.7). Kratky plots for spheres and cylinders were drawn from the raw data to emphasize deviation from the high-q behavior of the scattering intensity (Figure 4.7 left). The sphere plot ($q^2I(q)$ *versus* q) showed a horizontal asymptote at high q values which suggests the presence of spheres. In the meantime the cylinder plot ($qI(q)$ *versus* q) also tended to a horizontal asymptote at high-q values thus confirming the presence of cylinders in solution. Such plots can suggest the morphologies have both spherical and cylindrical features. Slopes of -1 and -2 were observed on the log($I(q)$) *versus* log(q) plot, which suggests the presence of rods with a really short length (disk-like structures). The two tangents intersect at an approximate q value of 0.007 $Å^{-1}$ which gives a rough estimation of the diameter of the structures to be 90 nm. This value correlates well with the one obtained by TEM. Finally different models were applied on this structure. Attempts to analyze this profile with disperse spherical uniform model,[43] uniform convex lens,[44,45] or uniform cylindrical models (with short length to account for disks)[41] yielded poor quality data fits, which suggests that the morphologies were not convex lenses, simple spheres or disks (Figure 4.7 right, Table 4.6). A core-shell cylindrical model with dispersity on the radius of the core provided better results (Figure 4.7 right) although the fits still not very good (Table 4.6, quality of fit, X^2 is expected to below 8 K).[41] Structures were obtained with a radius of the core of about 9 nm, a thickness of the corona of 8 nm and a core length or depth of 3 nm. These above results were consistent with previous observations in the literature, where prolate-spheroid micelles were observed.[33] In the reference, the formation of prolate-spheroid micelles was driven by broad dispersity of block copolymers. As the

polymer obtained in this study was also with a broad dispersity, we suggest a similar structure to prolate-spheroid micelle was obtained in this study. However, the tremendous difference of dimensions obtained between the structure models and the linear fits by SAXS (closer to TEM data) suggests that the former does not reflect the entire sample, which might be due to the solvation effect. Based on these observations, we suggest the structures observed in this study were prolate-spheroid micelles/planar oblate spheroids rather than normal cylinders or disks. AFM was also conducted on this sample. The heights of the structures were *ca.* 3 – 5 nm (Figure 4.8), which explained the reason for the low contrast observed in TEM analysis.

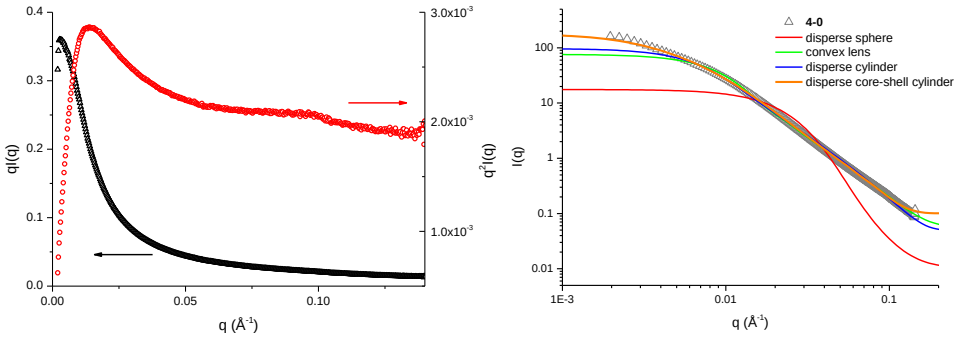

Figure 4.7 SAXS analysis of polymer **4-0**, $PMMA_{70}$-*b*-$PTMA_{100}$ in 1,4-dioxane. Kratky plots for spheres and cylinders (left); experimental profile and fits with different models: disperse spheres (PCR), convex lens (CL), disperse cylinder (CYPR), and core-shell cylinder (CSCYPR) (right).

Table 4.6 Data from fitting model for polymer **4-0,** $PMMA_{70}$-*b*-$PTMA_{100}$ in 1,4-dioxane

Model	disperse spheres	convex lens	disperse cylinder	core-shell cylinders
Radius core (nm)	4.9	29.3	21.6	8.8
Dispersity	0.4	-	0.3	0.7
Radius shell (nm)	-	-	-	8.4
Length (nm)	-	-	2.8	3.4
End cap radius	-	273	-	-
X^2 (quality of the fit)	3285k	837k	530k	59k

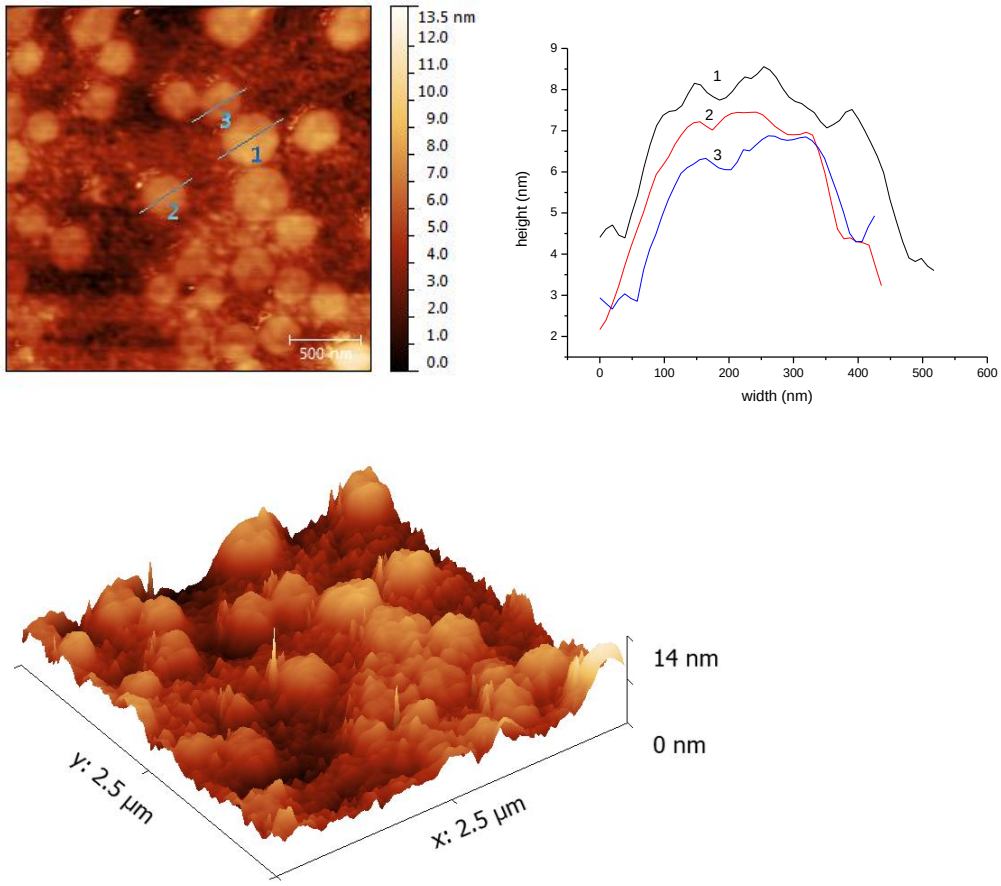

Figure 4.8 AFM height image (top left) and three-dimensional AFM image (bottom) of self-assembly prepared by polymerization **4-0**, $PMMA_{70}$-*b*-$PTMA_{100}$ in 1,4-dioxane and corresponding height profile (top right)

These results show that various morphologies can be accessed by varying the composition of solvent during the RAFT dispersion polymerization of TMA. However, the polymers obtained in each condition were not monodisperse (Figure 4.9). Indeed bimodal chromatograms were observed by SEC analysis in each case. Additionally, the RI and UV (λ = 309 nm) traces of polymers **4** were overlapped, which generally showed the similar trend regardless of bimodal shapes (Figure 4.10), suggesting that the occurrences of chain extension of macro-CTA, rather than conventional free radical polymerizations of TMA monomer. Indeed a discrepancy between RI and UV (λ = 309) trace was observed (the RI and UV (λ = 309) traces were not perfectly overlapped), which was mainly caused by the differences between

RI and UV detector (there is a deviation in retention time between two detectors as a result of two separate detectors; the intensity of response collected from the two detector correspond to polymer's weight and number of end group, respectively) (Figure 4.10 bottom right).

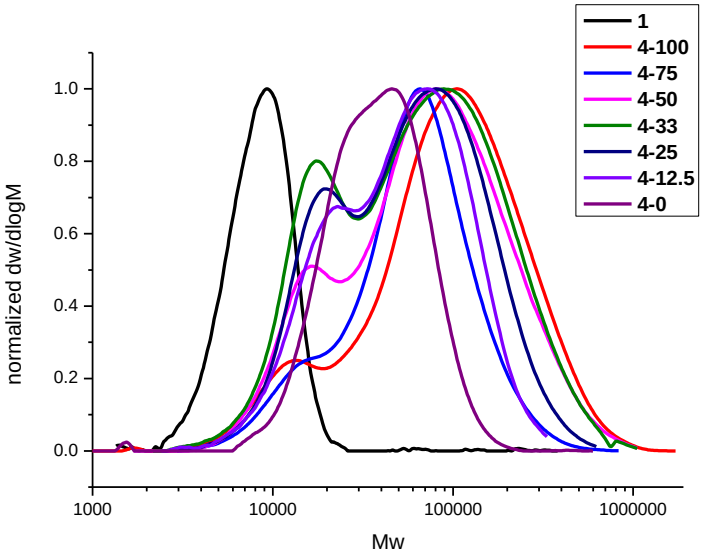

Figure 4.9 Normalized SEC traces of polymer **1** and **4** (DMF eluent, PMMA as standards).

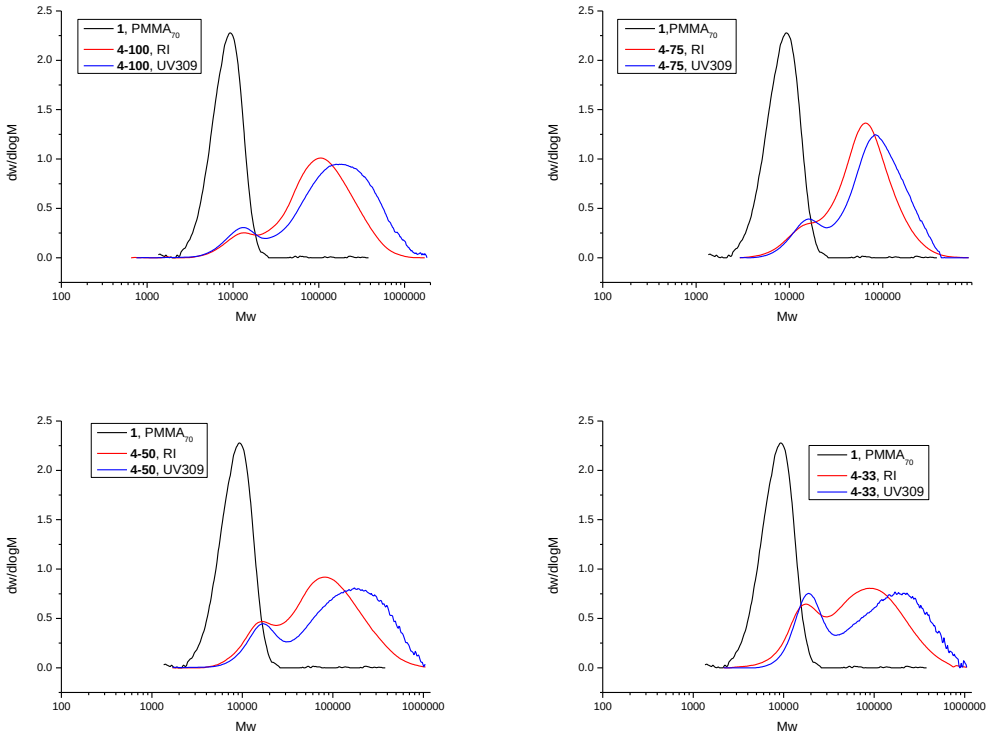

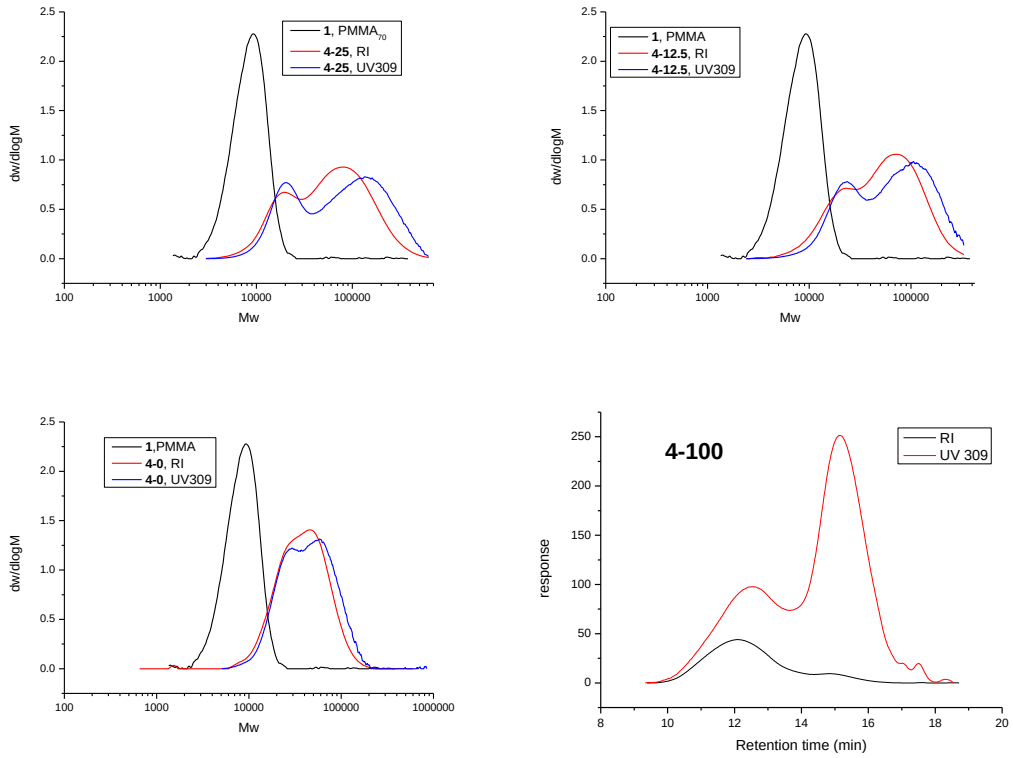

Figure 4.10 SEC analysis of polymer **1** and polymers **4** (DMF eluent, PMMA as stardards) prepared by **4**, $PMMA_{70}$-*b*-$PTMA_{100}$ in different solvents.

To eliminate the possibility that TMA monomer had undergone side-reactions during the polymerization, mixtures of TMA and CTA were stirred at 60 °C in chloroform under N_2 atmosphere for 24 hours. Monitoring by ^{1}H NMR spectroscopy analysis, there was no obvious change of signal and peak integration observed before and after heating, which indicated that both TMA and the CTA were stable under the polymerization conditions (Figure 4.11). In addition, Kamigaito and coworkers polymerized an acrylamide monomer *N*-(6-acetamidopyridin-2-yl)acrylamide, which possessed amide protons in the structure, at 60 °C in $CHCl_3$ using trithiocarbonate as a CTA and was able to further chain extend this polymer.[23] Bernard and coworkers synthesized a range of CTA containing thymine group that were successfully used in RAFT polymerizations.[46] These observations further indicated the stability of thymine-containing species with trithiobarbonate. Therefore, it was concluded that the observed bimodal distributions of the polymers were induced by the RAFT

dispersion polymerization process rather than the side reactions caused by TMA with CTA.

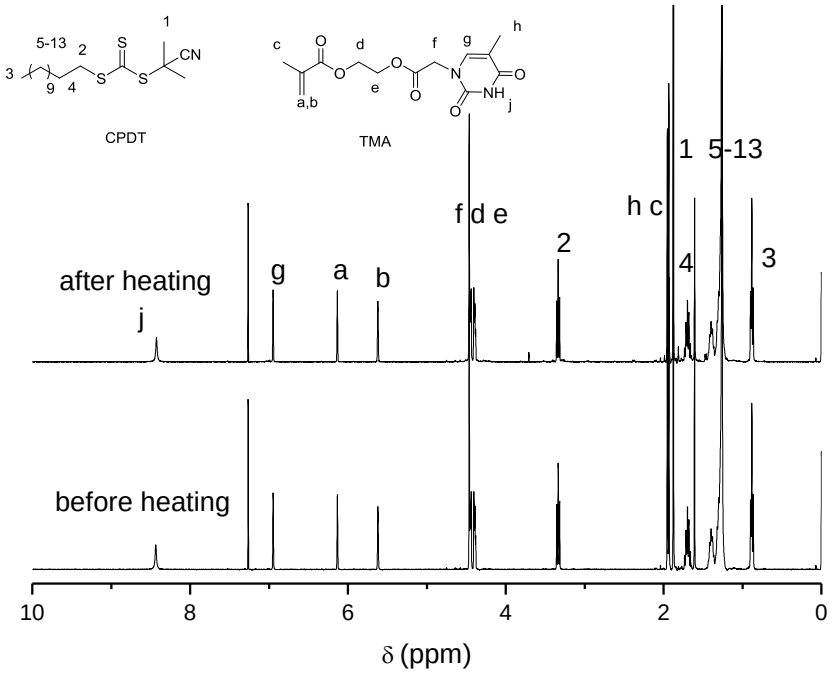

Figure 4.11 ^{1}H NMR spectra of a mixture of TMA and CTA (CPDT) in chloroform before and after heating for 24 hours.

DLS was also used to analyze the morphologies. However, due to the highly elongated structures obtained in these systems, the sizes obtained from DLS are relative values and not equal to their radius or length (as the hydrodynamic radius reported by DLS is the theoretical radius of a hard sphere).[47] Moreover, the analysis of large structures by DLS is not accurate as the length scale is limited.

4.3.3.2 Effect of amount of TMA

In addition to the effect of the solvent used for the polymerizations, the effect of varying the amount of TMA monomer was also investigated in the presence of DP 70 PMMA macro-CTA. Both chloroform and 1,4-dioxane were studied as the polymerization solvents.

Table 4.7 Characterization data for polymers $PMMA_{70}$-*b*-$PTMA_x$ prepared in $CHCl_3$

Polymers/target polymers	Solvent/mediator	Conv. (%)	$M_{n,\,th}$ (kDa)	$M_{n,\,NMR}$ (kDa)[a]	$M_{n,\,SEC}$ (kDa)[b]	$Đ_M$
$PMMA_{70}$-*b*-$PTMA_{100}$, **4-100**	chloroform	97	36.1	45.1	42.8	2.88
$PMMA_{70}$-*b*-$PTMA_{20}$, **5**	chloroform	95	12.7	12.0	12.2	1.67
$PMMA_{70}$-*b*-$PTMA_{50}$, **6a**	chloroform	92	20.8	26.2	34.7	2.01

[a]determined by ^{1}H NMR spectroscopy in DMSO-d_6; [b]determined by SEC analysis (DMF eluent, PMMA standards).

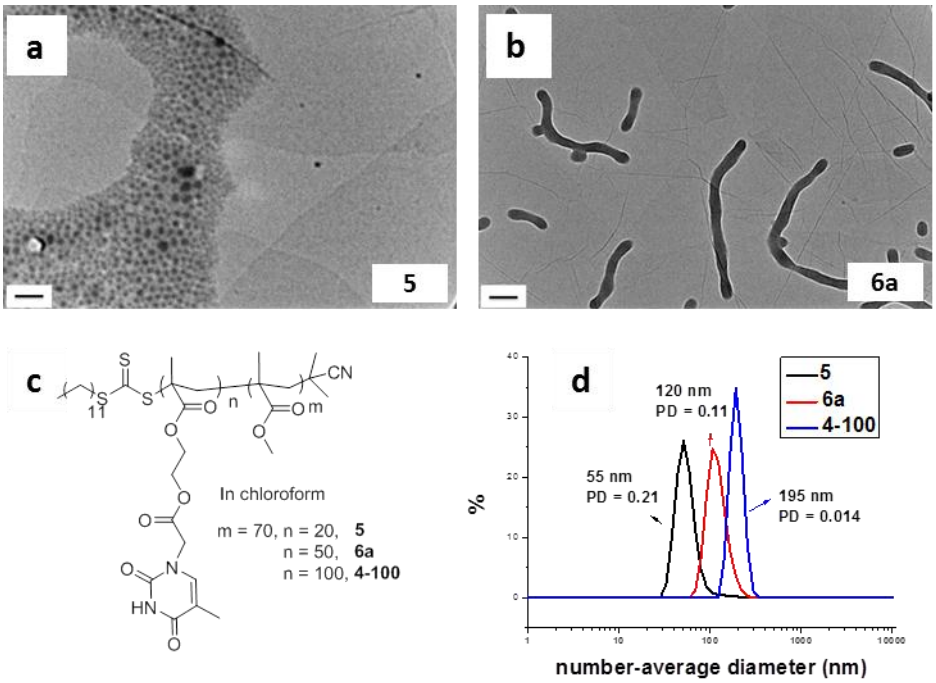

Figure 4.12 Representative TEM images of self-assemblies prepared by RAFT dispersion polymerization in chloroform for a target copolymer $PMMA_{70}$-*b*-$PTMA_x$, their corresponding structures (c) and DLS particle size distributions (d) with increasing TMA block length. Scale bar: 100 nm

In chloroform the target DPs of the thymine-containing block were 20, 50, and 100 and different morphologies were obtained with increasing the amount of TMA monomer (Table 4.7, polymers **5**, **6a**, and **4-100**). When the DP of the thymine-containing block was 20, spherical micelles were observed by TEM analysis (Figure 4.12a, **5**). The morphology was also studied using SLS (Figure 4.13). The P-ratio

(R_g/R_H = 0.79) was calculated to be smaller than 1, indicating the formation of solid spheres under these polymerization conditions.

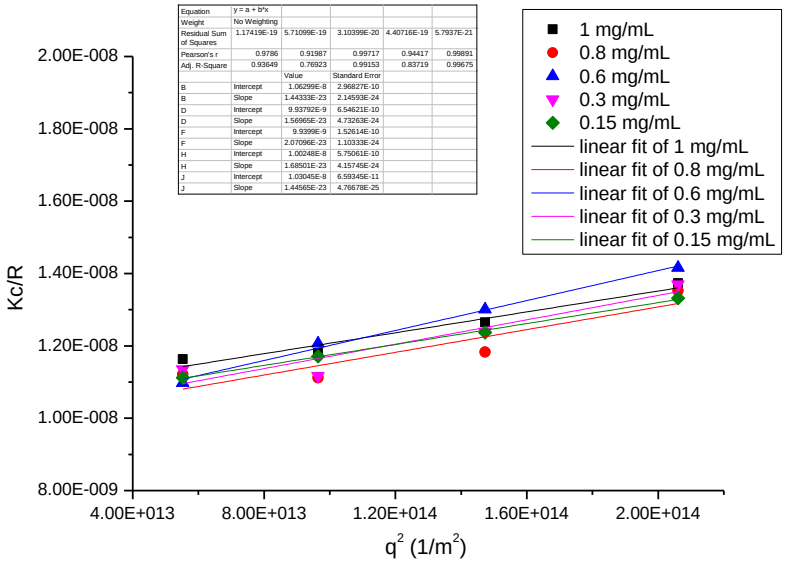

Figure 4.13 Zimm plot for self-assembly prepared by **5**, $PMMA_{70}$-*b*-$PTMA_{20}$ in chloroform.

Further increasing the DP of the thymine-containing block to 50 resulted in the formation of cylinders (Figure 4.12b, **6a**). The length of cylinders is more than 500 nm by TEM analysis, however, some remaining spherical micelles were observed. To further determine the morphologies in solution, SANS was also conducted on the sample with a TMA block length of 50, **6a**. The Guinier-Porod model was used firstly to provide information on the shape of the scattering objects (R_g and anisotropy). A dimension parameter of 1.32 was obtained, indicating the formation of elongated objects (Table 4.8). However, as the minimum q value is 0.004 $Å^{-1}$ and the structures are relatively big (R_g > 100 nm), it is difficult to have full confidence in this fit (Figure 4.14, left and Table 4.8). As a mixture of spheres and cylinders were observed by TEM analysis, a linear combination (sum model fit) of a model for spheres with some dispersity (sphere fit)[48] and a model for cylinders with some dispersity (cylinder fit) was created to analyse the structures in solution (Figure 4.14, right). These results confirm the observation by TEM analysis that both cylinders

and spheres coexist in solution. However, the information on the length of the cylinders and the volume ratio between the spherical and cylindrical micelles given by the fitting (Table 4.9) was not accurate as the camera length was too small for the dimensions of the assemblies.

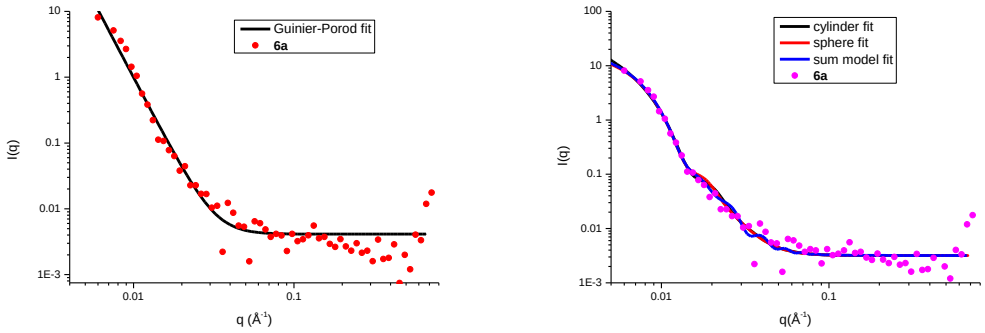

Figure 4.14 SANS analysis of polymer **6a**, $PMMA_{70}$-*b*-$PTMA_{50}$ in chloroform. Experimental profile and Guinier-Porod fit (left); experimental profile and fits with sphere, cylinder and sum models (right).

Table 4.8 Data obtained from Guinier-Porod fit for polymer **6a,** $PMMA_{70}$-*b*-$PTMA_{50}$

Sample	R_g (nm)	s		Guinier fit (R_g, nm)
6a	62.2	1.32	High errors	29.5 (not enough *q* values so minimise the value)

s = 0: spheres; s = 1: rods; s = 2: platelets

Table 4.9 Data from sum of sphere model and cylinder model for polymer **6a**, $PMMA_{70}$-*b*-$PTMA_{50}$

Cyl radius (nm)	Cyl length (nm)	Sphere radius (nm)
21.2	2484	32.3

When the DP of the thymine-containing block increased to 100, a pure phase of vesicles was observed by TEM analysis, which has been discussed in detail above (Figure 4.3a, **4-100**).

Thus, with increasing the amount of TMA, a morphology transition, sphere-cylinder-vesicle was observed in chloroform. This observation is consistent with the previous observation in the literature for RAFT dispersion polymerizations.[13] However, it should be noted that all the polymers are again obtained with a broad distribution (Figure 4.15).

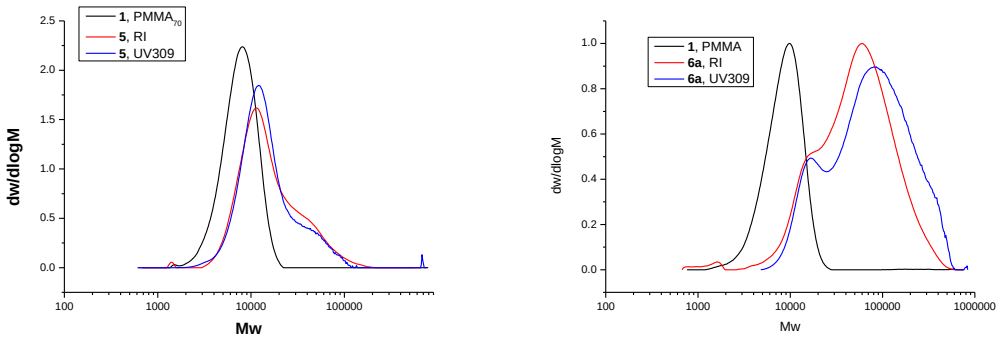

Figure 4.15 SEC analysis of polymers prepared by **5**, $PMMA_{70}$-*b*-$PTMA_{20}$ and **6a**, $PMMA_{70}$-*b*-$PTMA_{50}$ in chloroform (DMF eluent, PMMA as standards).

In comparison, when 1,4-dioxane was used as the solvent, a sphere-cylinder-vesicle transition was not observed with increasing the block length of PTMA (Table 4.10 and Figure 4.16). The possible reason for this observation is that the polymers have better solubilities and weaker interactions in 1,4-dioxane than chloroform, thus the driving force was not enough for the formation of a range of high order structures. In addition, prolate-spheroid micelles/planar oblate spheroids were suggested to be obtained as the structures appeared low contrast by TEM analysis and moreover the sizes of micelle increased with increasing the amounts of TMA, observed by a combination of TEM and DLS analysis (Figure 4.16). In the previous literature the prolate-spheroid micelles were formed due to the broad dispersity of block copolymers ($Đ_M$ = 1.74).[33] In our study, the polymers obtained in 1,4-dioxane also had the broad dispersities ($Đ_M$ = 1.24 – 2.21), which could drive the formation of prolate-spheroid micelles/ planar oblate spheroids and also was consistent with the observations in the literature.[33] AFM was then conducted on these samples. It was found that the heights of polymerization **7**, $PMMA_{70}$-*b*-$PTMA_{150}$, were *ca.* 10 – 15 nm (Figure 4.17), while the heights of polymerization **8**, $PMMA_{70}$-*b*-$PTMA_{200}$, were *ca.* 30 nm (Figure 4.18). These results showed that with increasing the amounts of

TMA, larger and thicker prolate-spheroid micelles/ planar oblate spheroids were formed.

Table 4.10 Characterization data for $PMMA_{70}$-*b*-$PTMA_x$ prepared in 1,4-dioxane

Polymers/target polymers	Solvent/mediator	Conv. (%)	$M_{n,\,th}$ (kDa)	$M_{n,\,NMR}$ (kDa)[a]	$M_{n,\,SEC}$ (kDa)[b]	$Đ_M$
$PMMA_{70}$-*b*-$PTMA_{100}$, **4-0**	1,4-dioxane	87	33.1	--	30.0	1.44
$PMMA_{70}$-*b*-$PTMA_{50}$, **6b**	1,4-dioxane	80	18.5	19.0	16.4	1.24
$PMMA_{70}$-*b*-$PTMA_{150}$, **7**	1,4-dioxane	95	49.8	--	40.1	1.84
$PMMA_{70}$-*b*-$PTMA_{200}$, **8**	1,4-dioxane	90	61.0	--	49.5	2.21

[a]determined by ^{1}H NMR spectroscopy in DMSO-d_6; [b]determined by SEC analysis (DMF eluent, PMMA standards).

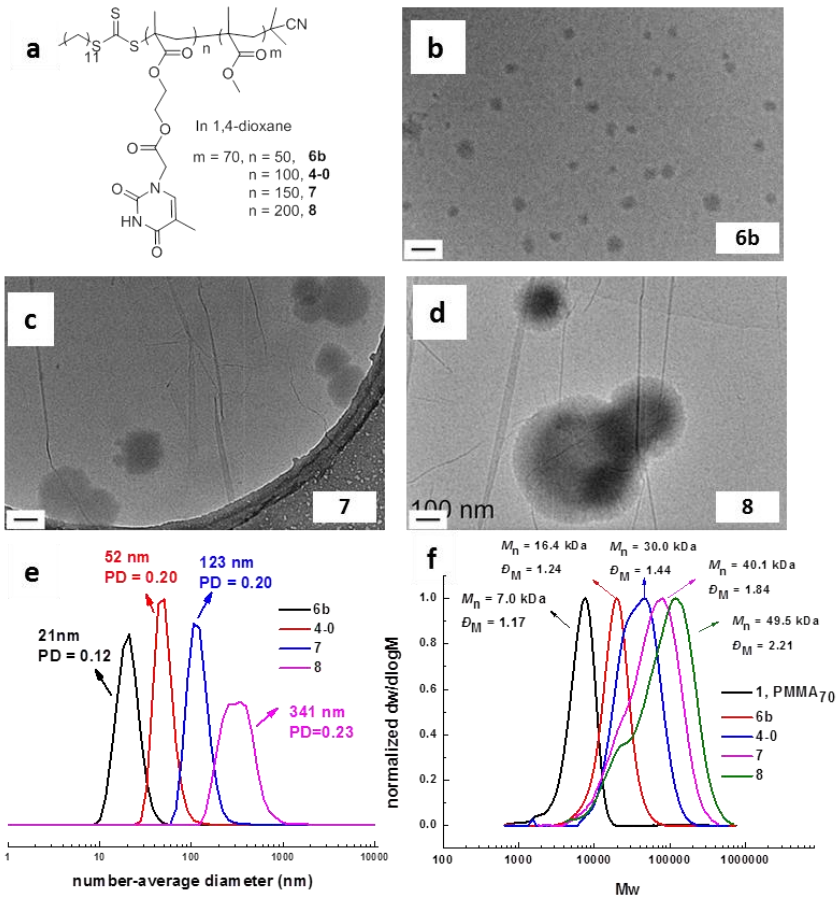

Figure 4.16 Representative TEM images of self-assemblies prepared by RAFT dispersion polymerization in 1,4-dioxane for a target copolymer $PMMA_{70}$-*b*-$PTMA_X$, (**6a**, **4-0**, **7**, **8**), their corresponding structures (a), DLS particle size distributions (e) and SEC traces (f) with increasing TMA block length (DMF as eluent, PMMA standards). Scale bar: 100 nm.

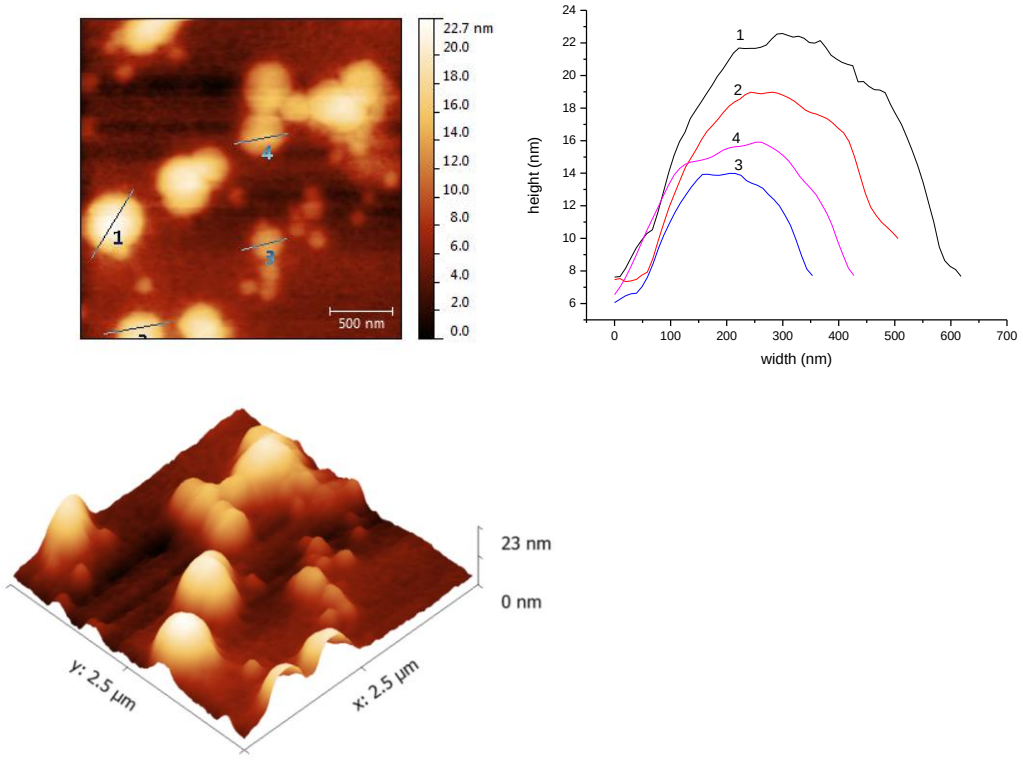

Figure 4.17 AFM height image (top left) and three-dimensional AFM image (bottom) of self-assembly prepared by polymerization **7**, $PMMA_{70}$-*b*-$PTMA_{150}$ in 1,4-dioxane and corresponding height profile (top right).

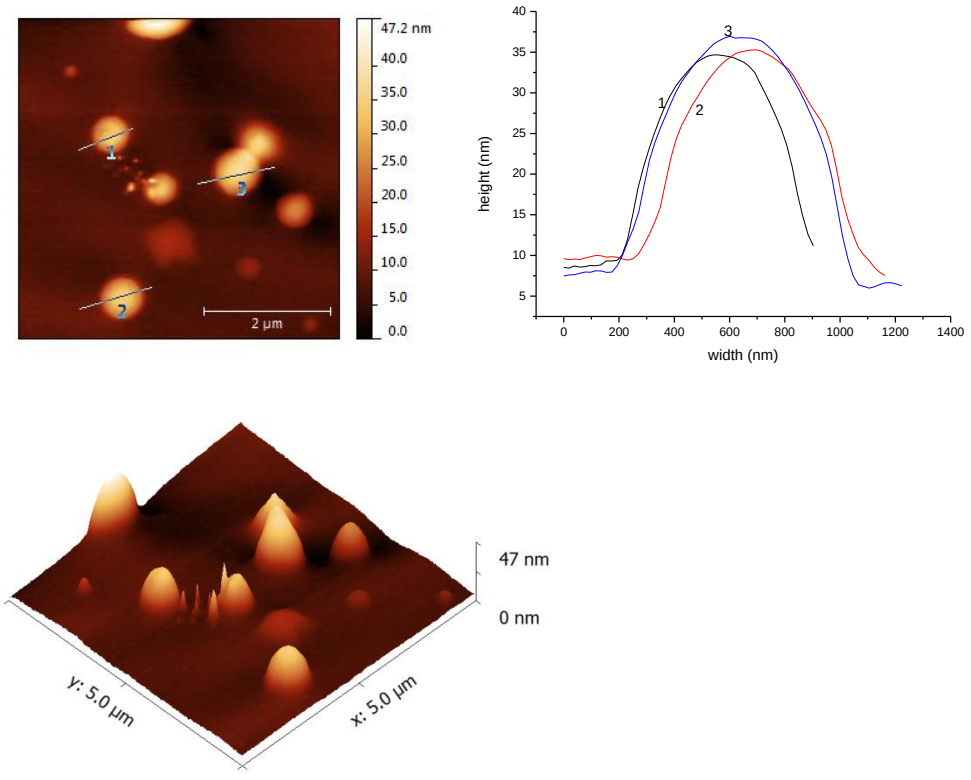

Figure 4.18 AFM height image (top left) and three-dimensional AFM image (bottom) of self-assembly prepared by polymerization **8**, $PMMA_{70}$-*b*-$PTMA_{200}$ in 1,4-dioxane and corresponding height profile (top right).

4.3.3.3 Effect of adenine-containing mediator

A mediator has been used in nucleobase-containing chemistry to avoid the precipitation of polymer, protect the activity of a catalyst[49] or control polymer tacticity.[23] Inspired by the previous study,[49] an adenine-containing mediator was used in our work to investigate its effect on the resultant morphologies of self-assembly and as well as the resultant copolymers. The adenine-containing mediator, 9-hexyladenine was synthesized according to previous literature (Scheme 4.4) with reasonable yield.[50] The mediator was firstly characterized by ^{1}H NMR and ^{13}C DEPT NMR (Figure 4.19). All the peaks could be assigned successfully and the integration of each peak corresponds to the molecule structure. In addition, elemental analysis and high resolution mass spectroscopy were used to characterize the product, showing the successful synthesis.

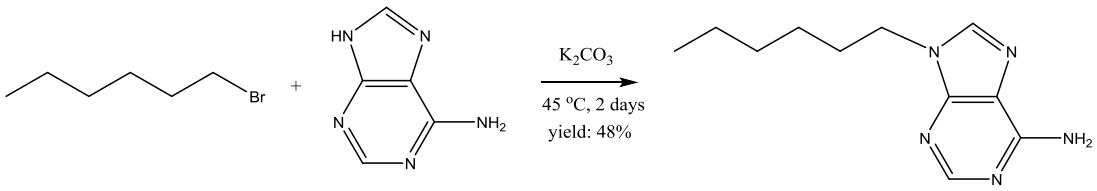

Scheme 4.4 Synthetic route for adenine-containing mediator.

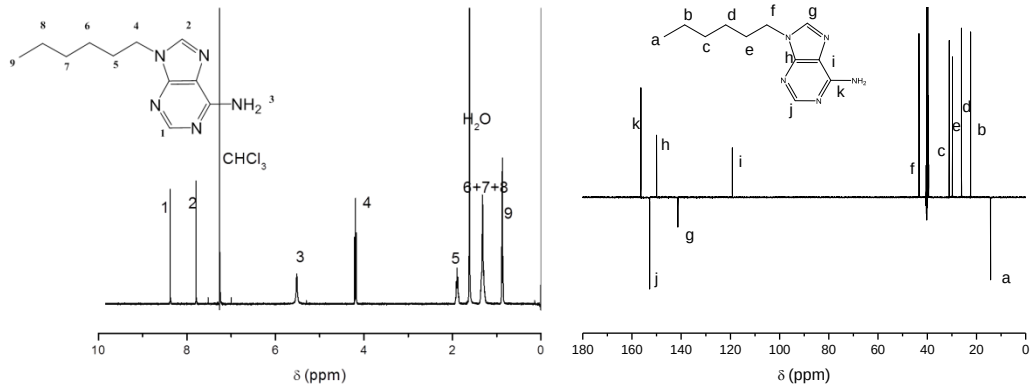

Figure 4.19 ^{1}H NMR (in $CDCl_3$) and ^{13}C DEPT NMR (in DMSO-d_6) spectra of adenine-containing mediator.

In this study, RAFT dispersion polymerization was carried out in the presence of the adenine-containing mediator (amount of TMA: mediator = 1:1) using $PMMA_{70}$ as the macro-CTA and chloroform as the solvent. The targeted DPs of the thymine-containing block were 20, 50 and 100 (Table 4.11, **5'**, **6a'**, and **4-100'**).

Table 4.11 Characterization data for polymers **5'**, **6a'**, and **4-100'** prepared in the presence of adenine-mediator

Polymers/target polymers	Solvent/mediator	Conv. (%)	$M_{n,\,th}$ (kDa)	$M_{n,\,NMR}$ (kDa)[a]	$M_{n,\,SEC}$ (kDa)[b]	$Đ_M$
$PMMA_{70}$-*b*-$PTMA_{20}$, **5'**	chloroform + Adenine -mediator	66	9.6	--	10.2	1.27
$PMMA_{70}$-*b*-$PTMA_{50}$, **6a'**	chloroform + Adenine-mediator	87	20.1	--	22.2	2.19
$PMMA_{70}$-*b*-$PTMA_{100}$, **4-100'**	chloroform + Adenine-mediator	95	35.5	--	33.5	3.10

[a]determined by ^{1}H NMR spectroscopy in DMSO-d_6; [b]determined by SEC analysis (DMF eluent, PMMA standards).

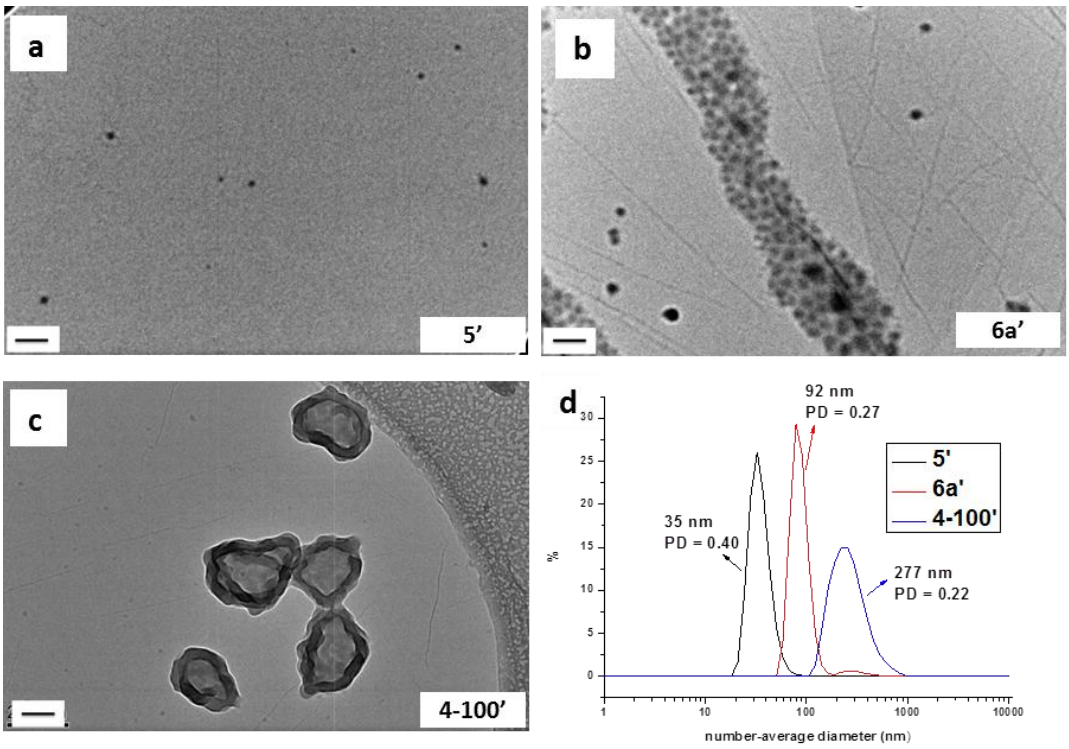

Figure 4.20 Representative unstained TEM images on GO-TEM grids of self-assemblies prepared by RAFT dispersion polymerization in chloroform with adenine-containing mediator for a target copolymer $PMMA_{70}$-*b*-$PTMA_x$, **5'**, **6a'** and **4-100'** and DLS distributions (d). Scale bar: 100 nm.

When the DP of the thymine-containing block was 20, small spherical micelles were obtained (Figure 4.20a, **5'**). The morphology obtained in the presence of the mediator was very close to the morphology obtained in the absence of the mediator (Figure 4.12a, **5**). According to DLS analysis, the diameter of spheres prepared from **5'** was *ca.* 35 nm, while for spheres prepared from **5** the diameter was *ca.* 55 nm. Moreover, the dispersity of the resultant copolymer obtained in the presence of the mediator was much narrower compared to the copolymer obtained in the absence of mediator (Figure 4.21, left). However, the monomer conversion was relatively low (66%) compared to other dispersion polymerizations. A possible reason for the low conversion is that the solubility of TMA is improved in the presence of mediator, which weakens the force of driving TMA from solution into the core of the self-assembly and thus leads to incomplete monomer conversion.

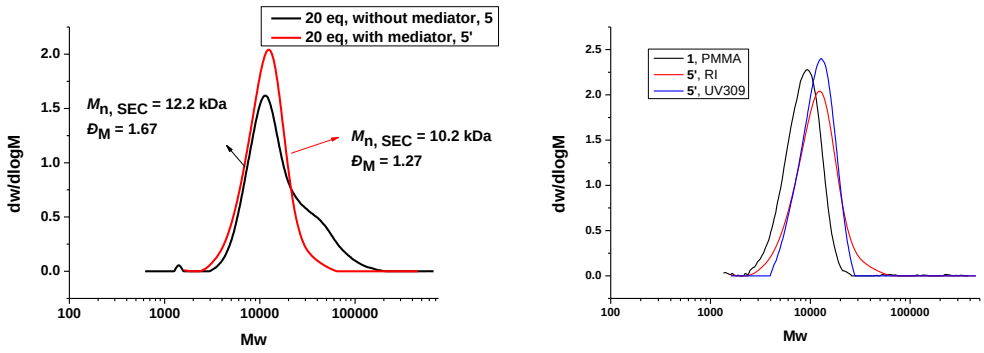

Figure 4.21 SEC traces of resultant copolymers obtained with (**5'**) or without mediator (**5**) for target copolymer $PMMA_{70}$-*b*-$PTMA_{20}$ (DMF as eluent, PMMA as standards).

In the case of the DP 50 TMA block, spherical micelles were observed in the presence of the mediator (Figure 4.20b, **6a'**), which is obviously different from the result without mediator (Figure 4.12b, **6a**, where cylinders were formed). In the presence of the adenine-containing mediator, the solubility of PTMA in chloroform increases, which should decrease the apparent packing parameter of the assembly[51]

therefore spherical micelles were formed instead of cylinders. However, unfortunately the polymer obtained was still bimodal as observed using SEC analysis (Table 4.11, $Đ_M = 2.19$).

Further increasing the DP to 100 resulted in a morphology of vesicles (Figure 4.20c, **4-100'**). Compared to the resultant well-defined vesicle morphology prepared in the absence of mediator (Figure 4.3a, **4-100**), the ill-defined vesicles possessed wrinkled membranes, which are thought to be due to the disturbance caused by the complementary interactions between thymine functionality and adenine-containing mediator. Although the presence of mediator could improve the polymers' solubility, the effect becomes weaker with increasing the length of the thymine-containing block. Therefore, the packing parameter remains similar in both the presence and absence of mediator and thus the general morphology stays the same.

When adenine-containing mediator is added to the system, a limited change of morphology is observed. Moreover, the obvious improvement of the resultant copolymer is only observed for the short thymine-containing block (DP 20). The longer the thymine-containing block, the less effect the adenine mediator has on both the morphologies and molecular weight distribution of the resultant polymers.

4.3.3.4 Effect of macro-CTA

When PMMA with a DP of 70 was used as the macro-CTA above, all the polymers obtained were poorly defined and bimodal distributions were observed by SEC analysis in most of the conditions ($Đ_M \approx 2$). In order to improve the control of polymerization, a macro-CTA with a higher DP was studied as it should be better able to stabilize the solvent-insoluble thymine blocks. The target DP of the thymine-

containing block was kept constant at 50, while PMMA with a DP of 220 ($PMMA_{220}$, **2**) was used as the macro-CTA for comparison with $PMMA_{70}$, **1**.

Table 4.12 Characterization data for polymers **9a** and **9b**

Polymers/target polymers	Solvent/mediator	Conv. (%)	$M_{n,\,th}$ (kDa)	$M_{n,\,NMR}$ (kDa)[a]	$M_{n,\,SEC}$ (kDa)[b]	$Đ_M$
$PMMA_{220}$-*b*-$PTMA_{50}$, **9a**	chloroform	91	35.5	34.4	34.3	1.72
$PMMA_{220}$-*b*-$PTMA_{50}$, **9b**	1,4-dioxane	61 (24 hours); 85 (96 hours)	34.1	35.7	30.1	1.17

[a]determined by ^{1}H NMR spectroscopy in DMSO-d_6; [b]determined by SEC analysis (DMF eluent, PMMA standards).

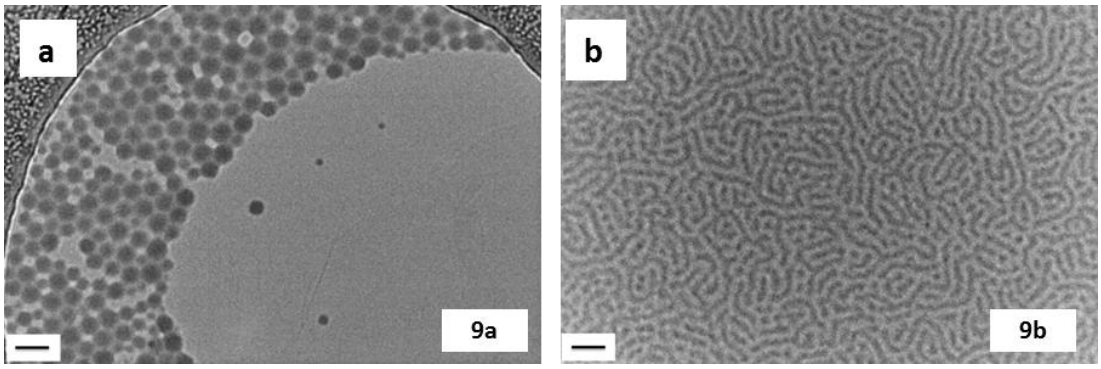

Figure 4.22 Representative TEM images of self-assemblies prepared by RAFT dispersion polymerization for a target copolymer $PMMA_{220}$-*b*-$PTMA_{50}$ in (a) chloroform, **9a**; (b) 1,4-dioxane, **9b**. Scale bar: 100 nm

In chloroform, spherical micelles were observed by TEM analysis when $PMMA_{220}$ was used (Figure 4.22a, **9a)**, which was different from the morphology in the case of $PMMA_{70}$ as expected (Figure 4.12b, **6a**, where cylinders were observed). This is because the longer PMMA block changes the packing parameter and interfacial curvature of the assembly.[32] Moreover, compared to the polymer prepared using $PMMA_{70}$ as the CTA, the resultant copolymer was slightly better controlled although a bimodal peak was also observed by SEC analysis (Figure 4.23, $Đ_M$ = 1.72; for **6a**, $Đ_M$ = 2.01).

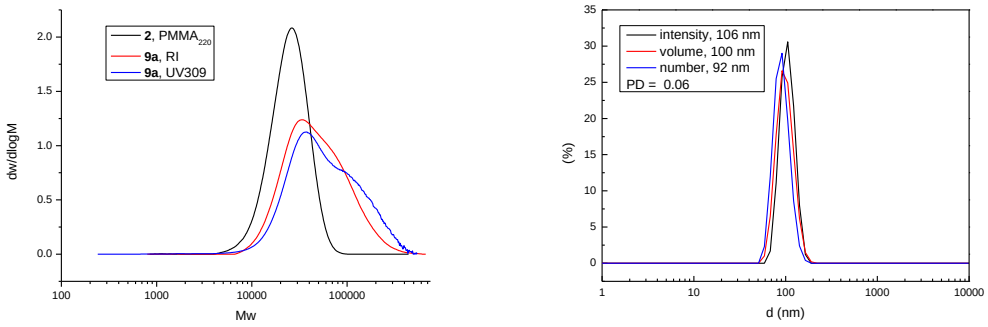

Figure 4.23 SEC analysis of polymer **9a** (DMF eluent, PMMA as standards) and DLS distribution of self-assembly prepared by **9a**, $PMMA_{220}$-*b*-$PTMA_{50}$ in chloroform.

In contrast, when 1,4-dioxane was used as the solvent, the resultant self-assembly was not well-defined as determined by both TEM and DLS analysis (Figure 4.22b and Figure 4.24). From TEM analysis, a phase-separated pattern was observed. Moreover, the broad distribution of self-assembly determined using DLS analysis suggested that the resultant structure was not stable in solution. The proposed reason for this observation is that the polymer is more soluble and thus there is less driving force to assemble (smaller solvophobic effect). However, due to the presence of the longer macro-CTA and improvement of the apparent solubility of the polymer, it was found that the polymer obtained was well-controlled in terms of molecular weight and dispersity (Figure 4.24, $Đ_M$ = 1.17).

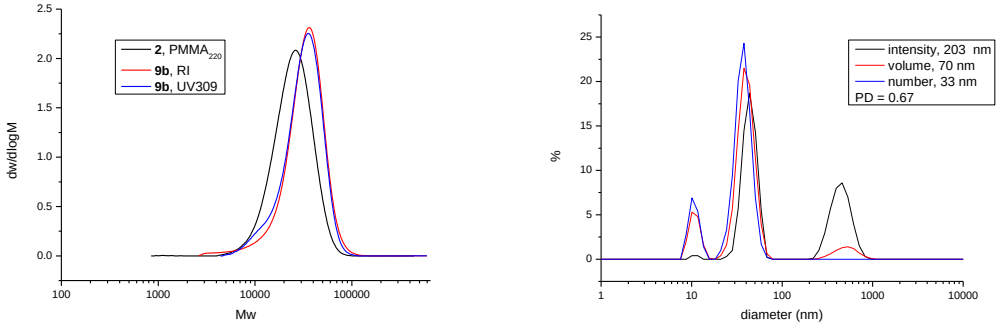

Figure 4.24 SEC analysis of polymer **9b** (DMF eluent, PMMA as standards) and DLS distribution of self-assembly prepared by **9b**, $PMMA_{220}$-*b*-$PTMA_{50}$ in 1,4-dioxane.

When the length of thymine-containing block is kept constant, changing the length of PMMA block can lead to different morphologies in both chloroform and 1,4-dioxane. Moreover, it is also found that longer PMMA block can allow access to slightly better copolymers in terms of molecular weight and molecular weight distribution although the improvement is limited.

4.3.3.5 Discussion

In this study, nearly all the block copolymers obtained appeared bimodal by SEC analysis. However, the resultant morphologies of the thymine-containing self-assemblies were surprisingly well-organized, leading to a range of well-defined and unexpected morphologies. We assume that these observations resulted from a combination of the nature of thymine-containing materials and the mechanism of RAFT dispersion polymerization. According to previous studies in the literature, although the polydisperse block copolymers exhibit different preferential curvature, they still enable formation of well-defined morphologies in some cases.[33,34] Similar results are also observed in this study although the structures are induced by the RAFT dispersion polymerization rather than post-polymerization self-assembly approaches. We assume that the resultant polydisperse block copolymers result from both thermodynamic and kinetic controls of the polymerization to minimize the total free energy, but the exact reason is still unclear.

Compared to adenine-containing or adenine/thymine coexisting materials, thymine-containing materials with a similar structure have better solubility in most solvents. Therefore, the mobility of the thymine-containing block is higher than both adenine-containing and adenine/thymine coexisting blocks; thus the thymine containing self-assemblies provide greater access to a wide

variety of morphologies and morphology transitions in comparison to our previous work.[22] In addition, for dispersion polymerizations, polymerization proceeds in the polymer particles as they absorb monomers from the continuous phase.[52] However, as thymine-thymine interactions are relatively weak and TMA has good solubility in both chloroform and 1,4-dioxane, we hypothesize that the force driving monomer into the core of the particles is modest and thus the aggregates can readily establish a thermodynamic equilibrium, which further leads to the formation of well-defined structures.

4.4 Conclusion

In conclusion, RAFT dispersion polymerizations were applied to thymine-containing materials using PMMA as the macro-CTA. Effects of various factors including polymerization solvent, the amount of monomer, the length of macro-CTA and the presence of an adenine-containing mediator were investigated. In general, there were two observations: (1) the resultant aggregates induced by the polymerizations are well established, a large variety of morphologies, some of which were unusual and unexpected were formed and the morphology can be tuned by variation of the above factors; (2) the resultant copolymers are polydisperse. Although the exact reasons for these observations need to be further investigated, this study demonstrates a facile approach to prepare a variety of thymine-containing nanoobjects as well as providing insights into understanding the effect of polydisperse block copolymers on self-assembly.

4.5 Experimental section

4.5.1 Materials

Methyl methacrylate (MMA) was bought from Aldrich and passed through a column of neutral alumina to remove inhibitor. 2,2-Azo-bis(isobutyronitrile) (AIBN) was purchased from Molekula and recrystallized twice from methanol. The synthesis of 2-cyano-2-propyl dodecyl trithiocarbonate (CPDT) was based on a previous reference.[53] Thymine-functionalized monomer, 2-(2-(thymine-1-yl)acetoxyl) ethyl methacrylate (TMA), was synthesized according to our published method.[38] Adenine-containing mediator, 9-hexyladenine, was synthesized according to a previous report.[50] 1,4-Dioxane, chloroform ($CHCl_3$), and other solvents were used as received from Fisher Scientific. Deuterated solvents were bought from Apollo Scientific.

4.5.2 Instrumentation

^{1}H NMR spectra were recorded on a Bruker DPX-300 or DPX-400 spectrometer with DMSO-d_6 or deuterated chloroform ($CDCl_3$) as the solvent. The chemical shifts of protons were reported relative to tetramethylsilane at δ = 0 ppm or solvent residues ($CHCl_3$ ^{1}H: 7.26 ppm; DMSO ^{1}H: 2.50 ppm).

Size exclusion chromatography (SEC) was performed in HPLC grade DMF containing 5 mM NH_4BF_4 at 50 °C, with a flow rate of 1.0 mL per minute, on a set of two PLgel 5 μm Mixed-D columns, plus one guard column. SEC data was analyzed with Cirrus SEC software calibrated using polymethyl methacrylate (PMMA) standards. The SEC was equipped with both refractive index (RI) and UV detectors.

Transmission electron microscopy (TEM) observations were performed on a JEOL 2000FX electron microscope at an acceleration voltage of 200 kV. All TEM samples were prepared on graphene oxide (GO)-coated carbon grids (Quantifoil R2/2) which allows high contrast TEM images to be acquired without staining.[54] Generally, a drop of sample (20 μL) was deposited on a grid which was placed on a piece of filter paper and then left to air dry.

Hydrodynamic diameters (D_h) and size distributions of the self-assemblies were determined by dynamic light scattering (DLS). The DLS instrumentation consisted of a Malvern Zetasizer NanoS instrument operating at 25 °C with a 4 mW He-Ne 633-nm laser module. Measurements were made at a detection angle of 173 ° (back scattering), and Malvern Zetasizer 7.03 software was used to analyze the data. The viscosity of the mixtures of $CHCl_3$ and 1,4-dioxane is estimated by a simplified equation[55]:

$$\mathrm{In}\eta = X_1 * \mathrm{In}\eta_1 + X_2 * \mathrm{In}\eta_2$$

Where η is the viscosity of the solution, and X_1, X_2, η_1, η_2 are the mole fractions and viscosities of the two components in a binary mixture.

Static light scattering (SLS) measurements were performed with an ALV CGS3 (λ = 632 nm) at 20 °C. The data was collected from 12 ° up to 30 ° with an interval of 2 ° or 30 ° up to 150 ° with an interval of 10 °, calibrated with filtered toluene and filtered $CHCl_3$ as backgrounds. The refractive index increment of the polymer in $CHCl_3$ was measured to be 0.053 mL/g.

Atomic force microscopy (AFM) images were taken in tapping mode on a Multimode AFM with Nanoscope IIIA Controller with Quadrex. Silicon AFM tips were used with a nominal spring constant and resonance frequency of 3.5 Nm^{-1} and 75 kHz (MikroMasch NSC18). Samples were imaged either on the same quantifoil

Cu/GO grids used in TEM analysis or onto freshly cleaved mica discs (Agar Scientific, G250-2). Data were analyzed using Gwyddion software.

Small-angle neutron scattering (SANS) experiments were recorded on the ISIS neutron beam facility, sans2d instrument at the Rutherford Appleton Laboratory, Oxford. Samples were measured at 20 mg/mL in $CDCl_3$, which provides a high contrast in scattering length to the polymer. Small-angle X-ray scattering (SAXS) experiments were carried out on the SAXS-WAXS beamline at the Australian Synchrotron facility at a photon energy of 15 keV. The samples were prepared in 1,4-dioxane and were run using 1.5 mm diameter quartz capillaries. The measurements were collected at 25 °C with a sample to detector distance of 7.160 m to give a q range of 0.0015 to 0.08 $Å^{-1}$, where q is the scattering vector and is related to the scattering angle (2θ) and the photon wavelength (λ) by the following equation:

$$q = \frac{4\pi \sin(\theta)}{\lambda}$$

All patterns were normalized to fixed transmitted flux using a quantitative beam stop detector. The scattering from the solvent was measured in the same location as sample collection and was subtracted for each measurement. The two-dimensional SAS images were converted into one-dimensional SAS profiles (I(q) *versus* q) by circular averaging, where I(q) is the scattering intensity. ScatterBrain and NCNR Data Analysis IGOR Pro software were used to plot and analyze SAXS and SANS data.[56] The scattering length density of the solvents and monomers were calculated using the "Scattering Length Density Calculator" provided by NIST Center for Neutron Research.[57]

4.5.3 Homopolymerization of TMA

The typical procedure of RAFT polymerizations of TMA was as follows: TMA, CPDT (1 eq) and AIBN (0.1 eq) were dissolved in 1,4-dioxane. The mixture was degassed *via* 4 freeze-pump-thaw cycles, filled with nitrogen and then immersed into an oil bath at 60 °C. The polymerization was quenched by putting into a liquid nitrogen bath and exposing to air. The mixture was concentrated and precipitated into cold methanol. The polymer was washed with methanol several times and dried in a vacuum oven. The polymer was characterized by ^{1}H NMR spectroscopy and SEC (DMF eluent, PMMA standards).

^{1}H NMR (400 MHz, DMF-d_7, ppm) of PTMA: δ = 11.34 (br, 1H$_{\text{backbone-PTMA}}$, N*H*CO of pyrimidine), δ = 7.55 (br s, 1H$_{\text{backbone-PTMA}}$, NC*H*=CCH$_3$ of pyrimidine), δ = 4.65–4.26 (t, 6H$_{\text{backbone-PTMA}}$, OC*H*$_2$C*H*$_2$OCOC*H*$_2$), δ = 3.34 – 3.30 (t, 2H$_{\text{end-group}}$, C*H*$_2$SC=S), δ = 2.30 – 1.27 (m, 5H$_{\text{backbone-PTMA}}$, C*H*$_2$CCH$_3$ and NCH=CC*H*$_3$ of pyrimidine; 20H$_{\text{end-group}}$, SCH$_2$(C*H*$_2$)$_{10}$CH$_3$), δ = 1.30 – 0.75 (m, 3H$_{\text{backbone-PTMA}}$, CH$_2$CC*H*$_3$).

4.5.4 Polymerization of methyl methacrylate (MMA)

The typical procedure of RAFT polymerizations of MMA was as follows: MMA, CPDT (1 eq) and AIBN (0.1 eq) were dissolved in toluene. The mixture was degassed *via* 4 freeze-pump-thaw cycles, filled with nitrogen and then immersed into an oil bath at 60 °C. The polymerization was quenched by putting into a liquid nitrogen bath and exposing to air. The mixture was precipitated into cold methanol and filtered. The polymer was dissolved in THF and precipitated again. This precipitation procedure was repeated 3 times in total to remove unreacted monomer. The light yellow polymers were dried in a vacuum oven and characterized by ^{1}H NMR spectroscopy and SEC (DMF eluent, PMMA standards).

^{1}H NMR (400 MHz, $CDCl_3$, ppm): δ = 3.60 (s, $3H_{backbone\text{-}PMMA}$, OCH_3), δ = 3.25 – 3.22 (t, $2H_{end\text{-}group}$, $CH_2SC{=}S$), δ = 1.96 – 1.81 (m, $2H_{backbone\text{-}PMMA}$, CH_2CCH_3), δ = 1.51 – 1.33 (m, $18H_{end\text{-}group}$, $SCH_2CH_2(CH_2)_9CH_3$), δ = 1.30 – 0.75 (m, $3H_{backbone\text{-}PMMA}$, CH_2CCH_3).

4.5.5 Synthesis of block polymers using PMMA as macro-CTA

The typical procedure was as follows: PMMA (1 eq), TMA (X), adenine mediator (X) and AIBN (0.1 eq) were dissolved in chloroform, 1,4-dioxane or mixtures of the two solvents. The mixtures were thoroughly degassed *via* 4 freeze-pump-thaw cycles, filled with nitrogen and then immersed into an oil bath at 60 °C. The polymerizations were quenched by exposing to air and cooling down. The mixture was precipitated in methanol and washed with methanol several times. The polymers were dried in a vacuum oven and characterized by ^{1}H NMR spectroscopy and SEC (DMF eluent, PMMA standard). The DP of the block was varied by adding different amounts of TMA.

^{1}H NMR (400 MHz, DMSO-d_6, ppm):δ = 11.42 – 11.29 (br, $1H_{backbone\text{-}PTMA}$, $NHCO$), δ = 7.50 – 7.33 (s, $1H_{backbone\text{-}PTMA}$, $NCH{=}CCH_3$ of pyrimidine), δ = 4.70 – 3.90 (m, $6H_{backbone\text{-}PTMA}$, $OCH_2CH_2OCOCH_2$ of PTMA), δ = 3.64 – 3.50 (s, $3H_{backbone\text{-}PMMA}$, OCH_3), δ = 2.12 – 1.50 (m, $3H_{backbone\text{-}PTMA}$, $CH{=}C(CH_3)$ of pyrimidine; $2H_{backbone}$, CH_2CCH_3 of backbone; $20H_{end\text{-}group}$, $SCH_2(CH_2)_{10}CH_3$), δ = 1.30 – 0.50 (m, $3H_{backbone}$, CH_2CCH_3).

4.5.6 Synthesis of 9-hexyladenine

The synthesis of 9-hexyladenien was according to the previous method:[50] to a suspension of adenine (2 g, 15 mmol) in DMF (40 mL), anhydrous potassium carbonate (2.4 g, 17.4 mmol) was added. The mixture was stirred for 30 minutes. 1-

bromohexane (3 mL, 17.4 mmol) was added to the solution at an ice bath and then the mixture was further stirred for 2 days at 45 °C. The mixture was poured into water (100 mL) and then extracted with ethyl acetate (3 × 100 mL). The organic layer was combined, washed with brine and dried by anhydrous $MgSO_4$. The mixture was concentrated and the residue was purified by column chromatography (5% MeOH/DCM) to give a white solid.

^{1}H NMR (400 MHz, $CDCl_3$, ppm): δ = 8.38 (s, 1H, purine *H*-2), δ = 7.79 (s, 1H, purine *H*-8), δ = 5.58 (s, 2H, NH_2), δ = 4.21 – 4.18 (t, 2H, $CH_3(CH_2)_4CH_2$-purine, $^3J_{H-H}$ = 7.2 Hz,), δ = 1.97 – 1.84 (quintet, 2H, $CH_3(CH_2)_3CH_2CH_2$-purine, $^3J_{H-H}$ = 7.1 Hz), δ = 1.40 – 1.24 (m, 6H, $CH_3(CH_2)_3CH_2CH_2$-purine), δ = 0.90 – 0.85 (t, 3H, $CH_3(CH_2)_3CH_2CH_2$-purine, $^3J_{H-H}$ = 7.0 Hz).

^{13}C NMR (125 MHz, DMSO-d_6, ppm): δ = 156.4 (purine *C*-6), δ = 152.8 (purine *C*-2), δ = 150.0 (purine *C*-4), δ = 141.3 (purine *C*-8), δ = 119.2 (purine *C*-5), δ = 43.3 ($CH_3(CH_2)_4CH_2$-purine), δ = 31.1 ($CH_3CH_2CH_2(CH_2)_2CH_2$-purine), δ = 29.8 ($CH_3(CH_2)_3CH_2CH_2$-purine), δ = 26.1 ($CH_3(CH_2)_2CH_2CH_2CH_2$-purine), δ = 22.4 ($CH_3CH_2(CH_2)_4$-purine), δ = 14.3 ($CH_3CH_2(CH_2)_4$-purine).

HR-MS (MaXis): m/z $[M+H]^+$ found 220.1558, expected 220.1557.

Elemental analysis found: C 60.26, H 7.77, N 31.92; expected ($C_{11}H_{17}N_5$): C 60.25, H 7.81, N 31.94.

4.6 References

(1) Oh, J. K. *J. Polym. Sci., Part A: Polym. Chem.* **2008**, *46*, 6983.

(2) Jennings, J.; Beija, M.; Kennon, J. T.; Willcock, H.; O'Reilly, R. K.; Rimmer, S.; Howdle, S. M. *Macromolecules* **2013**, *46*, 6843.

(3) Cunningham, M. F. *Prog. Polym. Sci.* **2008**, *33*, 365.

(4) Ladmiral, V.; Semsarilar, M.; Canton, I.; Armes, S. P. *J. Am. Chem. Soc.* **2013**, *135*, 13574.

(5) Zhang, X. W.; Boisson, F.; Colombani, O.; Chassenieux, C.; Charleux, B. *Macromolecules* **2014**, *47*, 51.

(6) Kitayama, Y.; Kagawa, Y.; Minami, H.; Okubo, M. *Langmuir* **2010**, *26*, 7029.

(7) Kagawa, Y.; Minami, H.; Okubo, M.; Zhou, J. *Polymer* **2005**, *46*, 1045.

(8) Nicolas, J.; Ruzette, A.-V.; Farcet, C.; Gérard, P.; Magnet, S.; Charleux, B. *Polymer* **2007**, *48*, 7029.

(9) Farcet, C.; Charleux, B.; Pirri, R. *Macromolecules* **2001**, *34*, 3823.

(10) Kitayama, Y.; Kishida, K.; Minami, H.; Okubo, M. *J. Polym. Sci., Part A: Polym. Chem.* **2012**, *50*, 1991.

(11) Kitayama, Y.; Yorizane, M.; Minami, H.; Okubo, M. *Polym. Chem.* **2012**, *3*, 1394.

(12) Tonnar, J.; Lacroix-Desmazes, P.; Boutevin, B. *Macromolecules* **2007**, *40*, 6076.

(13) Fielding, L. A.; Derry, M. J.; Ladmiral, V.; Rosselgong, J.; Rodrigues, A. M.; Ratcliffe, L. P. D.; Sugihara, S.; Armes, S. P. *Chem. Sci.* **2013**, *4*, 2081.

(14) Blanazs, A.; Madsen, J.; Battaglia, G.; Ryan, A. J.; Armes, S. P. *J. Am. Chem. Soc.* **2011**, *133*, 16581.

(15) Sun, J.-T.; Hong, C.-Y.; Pan, C.-Y. *Soft Matter* **2012**, *8*, 7753.

(16) Zhang, X.; Boissé, S. p.; Zhang, W.; Beaunier, P.; D'Agosto, F.; Rieger, J.; Charleux, B. *Macromolecules* **2011**, *44*, 4149.

(17) Jia, Z.; Bobrin, V. A.; Truong, N. P.; Gillard, M.; Monteiro, M. J. *J. Am. Chem. Soc.* **2014**, *136*, 5824.

(18) Karagoz, B.; Esser, L.; Duong, H. T.; Basuki, J. S.; Boyer, C.; Davis, T. P. *Polym. Chem.* **2014**, *5*, 350.

(19) Sugihara, S.; Armes, S. P.; Blanazs, A.; Lewis, A. L. *Soft Matter* **2011**, *7*, 10787.

(20) Chambon, P.; Blanazs, A.; Battaglia, G.; Armes, S. P. *Macromolecules* **2012**, *45*, 5081.

(21) Zhang, W.-J.; Hong, C.-Y.; Pan, C.-Y. *Macromolecules* **2014**, *47*, 1664.

(22) Kang, Y.; Pitto-Barry, A.; Willcock, H.; Quan, W.-D.; Kirby, N.; Sanchez, A. M.; O'Reilly, R. K. *Polym. Chem.* **2015**, *6*, 106.

(23) Tao, Y.; Satoh, K.; Kamigaito, M. *Macromol. Rapid Commun.* **2011**, *32*, 226.

(24) South, C. R.; Weck, M. *Macromolecules* **2007**, *40*, 1386.

(25) McHale, R.; Patterson, J. P.; Zetterlund, P. B.; O'Reilly, R. K. *Nature Chem.* **2012**, *4*, 491.

(26) Lo, P. K.; Sleiman, H. F. *J. Am. Chem. Soc.* **2009**, *131*, 4182.

(27) Tao, Y.; Yang, Y.; Shi, D.; Chen, M.; Yang, C.; Liu, X. *Polymer* **2012**, *53*, 1551.

(28) Thibault, R. J.; Hotchkiss, P. J.; Gray, M.; Rotello, V. M. *J. Am. Chem. Soc.* **2003**, *125*, 11249.

(29) Ilhan, F.; Galow, T. H.; Gray, M.; Clavier, G.; Rotello, V. M. *J. Am. Chem. Soc.* **2000**, *122*, 5895.

(30) Boal, A. K.; Ilhan, F.; DeRouchey, J. E.; Thurn-Albrecht, T.; Russell, T. P.;

Rotello, V. M. *Nature* **2000**, *404*, 746.

(31) Stubbs, L. P.; Weck, M. *Chem. Eur. J.* **2003**, *9*, 992.

(32) Blanazs, A.; Armes, S. P.; Ryan, A. J. *Macromol. Rapid Commun.* **2009**, *30*, 267.

(33) Schmitt, A. L.; Repollet-Pedrosa, M. H.; Mahanthappa, M. K. *ACS Macro Lett.* **2012**, *1*, 300.

(34) Lim Soo, P.; Eisenberg, A. *J. Polym. Sci., Part B: Polym. Phys.* **2004**, *42*, 923.

(35) Wang, X.; Davis, J. L.; Hinestrosa, J. P.; Mays, J. W.; Kilbey, S. M. *Macromolecules* **2014**, *47*, 7138.

(36) Terreau, O.; Luo, L.; Eisenberg, A. *Langmuir* **2003**, *19*, 5601.

(37) Jain, S.; Bates, F. S. *Macromolecules* **2004**, *37*, 1511.

(38) Kang, Y.; Lu, A.; Ellington, A.; Jewett, M. C.; O'Reilly, R. K. *ACS Macro Lett.* **2013**, *2*, 581.

(39) Zhang, K.; Fahs, G. B.; Aiba, M.; Moore, R. B.; Long, T. E. *Chem. Commun.* **2014**, *50*, 9145.

(40) Peng, H.; Chen, D.; Jiang, M. *J. Phys. Chem. B* **2003**, *107*, 12461.

(41) Guinier, A.; Fournet, G. *Small-angle scattering of X-rays*, Wiley, **1955**.

(42) Hocine, S.; Brulet, A.; Jia, L.; Yang, J.; Di Cicco, A.; Bouteiller, L.; Li, M.-H. *Soft Matter* **2011**, *7*, 2613.

(43) Hayter, J. B. *Physics of amphiphiles--micelles, vesicles, and microemulsions*, Varenna on Lake Como, Villa Monastero, **1983**.

(44) Kaya, H. *J. Appl. Crystallogr.* **2004**, *37*, 223.

(45) Kaya, H.; De Souza, N.-R. *J. Appl. Crystallogr.* **2004**, *37*, 508.

(46) Chen, S.; Bertrand, A.; Chang, X.; Alcouffe, P.; Ladavière, C.; Gérard, J.-F.

O.; Lortie, F. D. R.; Bernard, J. *Macromolecules* **2010**, *43*, 5981.

(47) Patterson, J. P.; Robin, M. P.; Chassenieux, C.; Colombani, O.; O'Reilly, R. K. *Chem. Soc. Rev.* **2014**, *43*, 2412.

(48) Bartlett, P.; Ottewill, R. H. *J. Chem. Phys.* **1992**, *96*, 3306.

(49) Romulus, J.; Weck, M. *Macromol. Rapid Commun.* **2013**, *34*, 1518.

(50) Wang, Z.; Yu, Y.; Zhang, D.; Zhu, D. *Chin. Sci. Bull.* **2006**, *51*, 1947.

(51) Rodríguez-Hernández, J.; Chécot, F.; Gnanou, Y.; Lecommandoux, S. *Prog. Polym. Sci.* **2005**, *30*, 691.

(52) Odian, G. *Principles of Polymerization, Fourth Edition*, John Wiley & Sons, Inc., Hoboken, New Jersey, **2004**.

(53) Chong, Y. K.; Moad, G.; Rizzardo, E.; Thang, S. H. *Macromolecules* **2007**, *40*, 4446.

(54) Patterson, J. P.; Sanchez, A. M.; Petzetakis, N.; Smart, T. P.; Epps III, T. H.; Portman, I.; Wilson, N. R.; O'Reilly, R. K. *Soft Matter* **2012**, *8*, 3322.

(55) Reed, T. M.; Taylor, T. E. *J. Phys. Chem.* **1959**, *63*, 58.

(56) Kline, S. *J. Appl. Crystallogr.* **2006**, *39*, 895.

(57) Calculator, N. S. L. D. http://www.ncnr.nist.gov/resources/sldcalc.html.

Chapter 5. Self-assembly of nucleobase-containing block copolymers in aqueous solution

5.1 Abstract

Amphiphilic nucleobase-containing block copolymers with poly(oligo(ethylene glycol) methyl ether methacrylate) as the hydrophilic blocks and nucleobase-containing blocks as the hydrophobic segments were successfully synthesized using RAFT polymerization. Two types of nucleobase-containing methacrylate monomers were synthesized and polymerized, one of which contained two ester groups in the structure and the other which only possessed one ester group in the backbone. It was found that the nucleobase-containing polymers with two ester groups in the backbone could be hydrolyzed in the presence of water (18.2 MΩ·cm), while the other nucleobase polymers containing one ester group in their structure were relatively stable in an aqueous environment. The self-assembly behavior of both classes of block copolymer were investigated using both direct dissolution and solvent switch methods with better results obtained using the solvent switch method. In addition, effects of the common solvent on the resultant morphologies were investigated, which showed that depending on the identity of common solvent (DMF or DMSO), spherical micelles and bicontinuous micelles could be obtained respectively. Moreover, the effects of annealing the self-assemblies were explored. It was found that annealing could lead to better-defined spherical micelles and induce a morphology transition from bicontinuous micelles to onion-like vesicles, which was considered to occur due to a structural rearrangement induced by complementary nucleobase interactions resulting from the annealing process.

5.2 Introduction

The incorporation of nucleobase functionalities in synthetic polymer chemistry is of interest, as these polymers can be applied in various fields such as template polymerizations[1-4] and supramolecular self-assemblies.[5-10] For example, Rotello and coworkers demonstrated the formation of giant vesicles,[5] Au-containing particles,[11] and thermally reversible microspheres,[8] which were formed through the self-assembly of nucleobase-containing polymers. Sleiman and coworkers prepared nucleobase-containing norbornene block copolymers *via* ROMP, which could self-assemble into rods unexpectedly given the large corona:core ratio (DP of corona: DP of core = 50:5).[7] In previous Chapters, the preparation of a range of nucleobase-containing morphologies by RAFT dispersion polymerization was demonstrated, however, these self-assemblies were mostly prepared in organic solvents such as chloroform, THF, and 1,4-dioxane. To our knowledge, there is relatively little research into the study of self-assembly of nucleobase-containing synthetic polymers in aqueous solutions.[6,12-15] One significant report by the van Hest group synthesized poly(ethylene glycol)(PEG)-*b*-poly(nucleobase) block copolymers *via* ATRP and investigated the self-assembly behavior of the amphiphilic block copolymers in aqueous solutions. This work indicated that the nucleobase interactions between adenine and thymine moieties played a crucial role in the block copolymer assembly.[6] Based on this pioneering work, our goal is to further study the aqueous self-assembly behavior of nucleobase-containing polymers and exploit the effects of self-assembly preparation methods and annealing on the resultant morphologies.

In solution, amphiphilic block copolymers can assemble into a variety of morphologies, of which the most common morphologies are spherical micelles, cylindrical micelles and vesicles.[16,17] More complex structures have also been

reported such as disk-like,[18,19] toroidal,[20-22] helix[23,24] and bicontinuous micelles.[25-29] For example, Holder and Sommerdijk *et al.* reported the formation and detailed characterization of bicontinuous micelles.[29,30] In these reports block copolymers containing peptide,[28] semicrystalline[26,29] and amorphous[27] segments were all ultilized to prepare bicontinuous micelles, which were analyzed and visualized in detail by cryo electron tomography (cryoET). In addition, the factors affecting the formation of bicontinuous micelles were also investigated, including the selection of common solvent,[27] the sequence of peptide,[28] molecular weight distribution,[28] temperature,[26] and polymer composition.[27,29] More recently, they reported that both the outer diameters and internal pore sizes of bicontinuous nanoparticles could be tuned simply by changing the initial polymer conditions and tuning the hydrophobic-hydrophilic fractions, respectively, which is a very exciting demonstration as it allows for the use of bicontinuous nanospheres in many fields such as controlled release[31] and templates for inorganic or hybrid materials.[29] However, bicontinuous micelles prepared by nucleobase-containing polymers have not been reported. In this work, bicontinuous micelles and onion-like structures were observed through the self-assembly of nucleobase-containing polymers in aqueous solutions.

Polymers prepared from oligo(ethylene glycol) monomers are of interest in the biochemistry field.[32] These polymers possess graft structures comprised of a carbon-carbon backbone and multiple oligo(ethylene glycol) side chains. Although they are not standard linear poly(ethylene glycol)s (PEG), as the oligo(ethylene glycol) chains take up a large weight fraction in the polymer structure, such polymers are still water-soluble and biocompatible in most cases.[32] In addition, these polymers may exhibit stimuli-responsive properties, such as temperature-responsive behavior, which are not attainable with linear PEG.[32-34] Moreover, these polymers are easy to

polymerize to prepare either homopolymers or copolymers using well-established controlled radical polymerization techniques.[32,35,36] Based on the above factors, poly(oligo(ethylene glycol) methyl ether methacrylate (POEGMA) was selected as the hydrophilic block in this study, which was prepared using RAFT polymerization. Block copolymers were then prepared by RAFT polymerization using either adenine-containing methacrylate, thymine-containing methacrylate or a 1:1 mixture of these two methacrylate monomers. Self-assemblies of these nucleobase-containing block copolymers were subsequently prepared and investigated in aqueous solutions. In addition, factors affecting the resultant morphologies including sample preparation methods, common solvents, and annealing were also studied in this Chapter.

5.3 Results and discussion

5.3.1 Synthesis of POEGMA

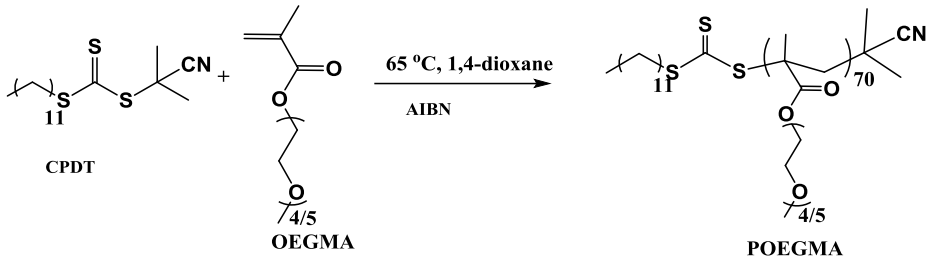

Scheme 5.1 Synthetic route for $POEGMA_{70}$.

POEGMA was synthesized by RAFT polymerization, using 2-cyano-2-propyldodecyl trithiocarbonate (CPDT) as the CTA, AIBN as the initiator (CTA:AIBN = 1:0.1), and 1,4-dioxane as the solvent (Scheme 5.1). The monomer conversion for the polymerization was 57%, obtained from ^{1}H NMR spectroscopy. The DP of the purified POEGMA was *ca.* 70, determined by ^{1}H NMR spectroscopy by comparing the integration of the signal 'a' from CPDT with those 'b, c, d' from the backbone of the polymer (Figure 5.1). Furthermore, SEC was used to characterize the molecular weight and molecular weight distribution of $POEGMA_{70}$ and revealed a narrow molecular weight distribution ($Đ_M$ = 1.18) (Figure 5.1 and Table 5.1). In addition, RI and UV (309 nm, from the trithiocarbonate end group) traces overlap well, indicating good end group fidelity.

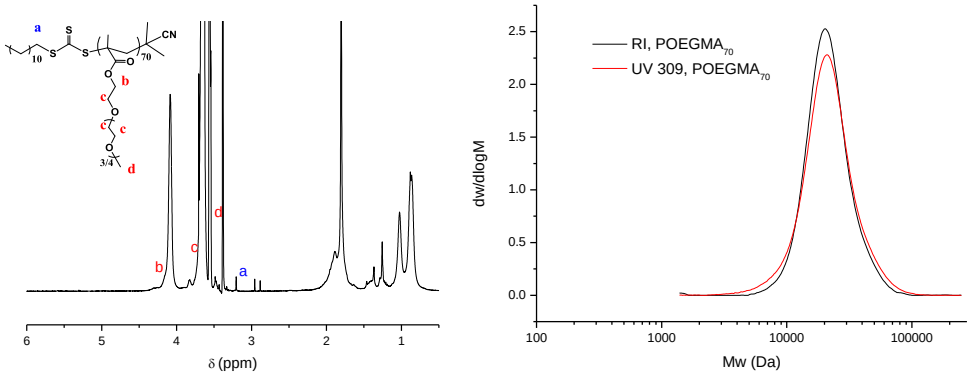

Figure 5.1 ^{1}H NMR spectrum of $POEGMA_{70}$ in $CDCl_3$ and SEC traces (DMF as eluent, PMMA as standards).

Table 5.1 Characterization data of POEGMA

Polymer	$M_{n,th}$ (kDa)	$M_{n,NMR}$ (kDa)[a]	$M_{n,SEC}$ (kDa)[b]	$Đ_M$	T_{cp} (°C)[c]
$POEGMA_{70}$	20.5	21.0	19.5	1.18	65

[a]determined by ^{1}H NMR spectroscopy; [b]determined by SEC analysis (DMF as eluent, PMMA as standards); [c] T_{cp} represents cloud point of the polymer solution (10 mg/mL in water).

POEGMA should exhibit temperature-responsive behavior and generally display a lower critical solution temperature (LCST), which has been widely reported in previous reports.[32] Herein, the cloud point of POEGMA with a DP of 70 prepared in this study was estimated by turbidity using variable-temperature UV-vis spectrometer. A POEGMA solution in 18.2 MΩ·cm water with a polymer concentration of 10 mg/mL was heated from 25 – 85 °C at a rate of 0.5 °C/min and then cooled down at the same rate. The heating/cooling cycles were repeated 3 times in total. The temperature of the cloud point was found to be *ca.* 65 °C, determined as the midpoint of inflection of the transmittance curves, which is consistent with the values reported in the literature.[32]

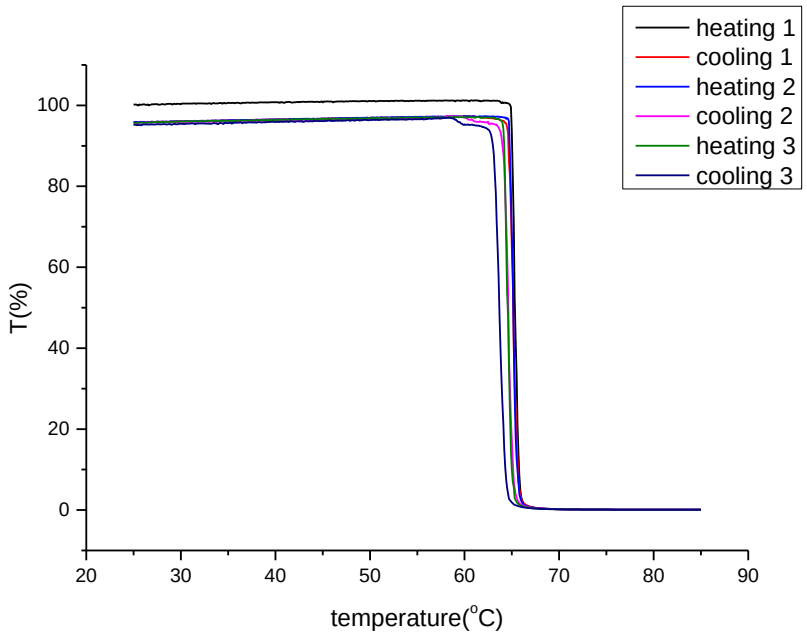

Figure 5.2 Plots of transmittance as a function of temperature (λ = 500 nm, heating/cooling rate 0.5 °C/min) measured for an aqueous solution of $POEGMA_{70}$ (10 mg/mL).

5.3.2 Synthesis of block copolymers using AMA and TMA monomers, polymers 1 – 3

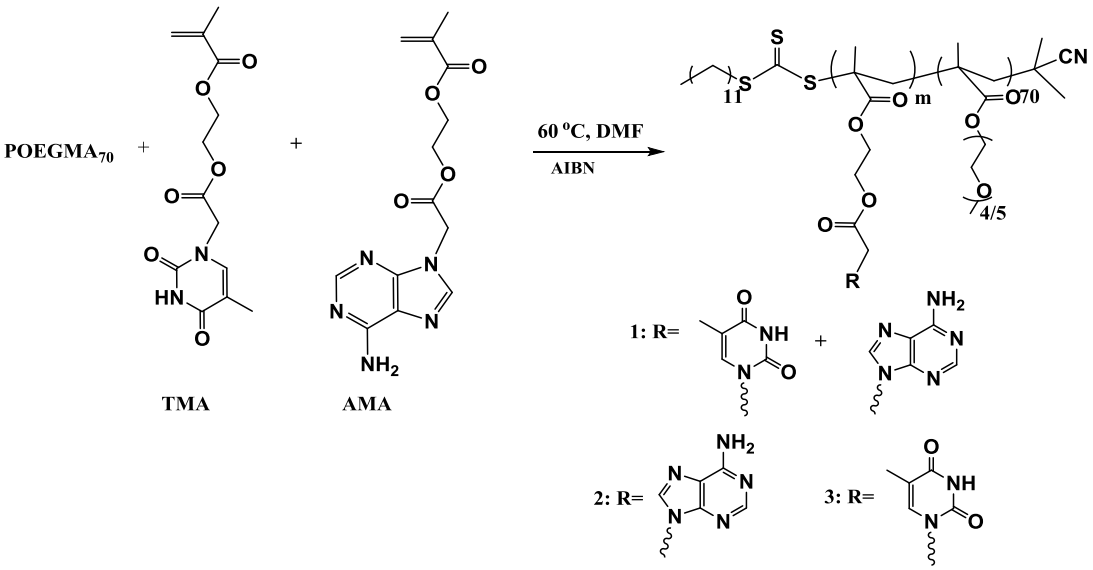

Scheme 5.2 Synthetic route for block copolymers using AMA and TMA monomers.

Table 5.2 Characterization data of block copolymers using AMA and TMA monomers

Polymer	$M_{n,th}$ (kDa)	$M_{n,NMR}$ (kDa)[a]	$M_{n,SEC}$ (kDa)[b]	$Đ_M$	DP of nucleobase[c]	f [d]
$POEGMA_{70}$-*b*-($PAMA_{0.5}$-*co*-$PTMA_{0.5}$)$_m$, **1**	51.1	57.3	42.3	1.36	121	0.37
$POEGMA_{70}$-*b*-$PAMA_m$, **2**	51.5	57.6	33.2	1.51	120	0.36
$POEGMA_{70}$-*b*-$PTMA_m$, **3**	50.6	55.9	41.4	1.56	118	0.38

[a]determined by ^{1}H NMR spectroscopy; [b]determined by SEC analysis (DMF as eluent, PMMA as standards); [c]DP calculated from $M_{n,NMR}$; [d]POEGMA weight fraction in the block copolymer calculated from $M_{n,NMR}$.

To synthesize nucleobase-containing block copolymers, RAFT polymerizations were performed in DMF, using exclusively AMA (polymer **2**), exclusively TMA (polymer **3**) and a 1:1 mixture of AMA and TMA (polymer **1**) as monomers. $POEGMA_{70}$ was used as the macro-CTA and AIBN was used as the initiator. The mole ratio of $POEGMA_{70}$:monomer:AIBN was kept to be 1:100:0.1 in each polymerization. High conversion (≥ 99%) was attained for each polymerization. The characterization data for all the block copolymers are shown in Table 5.2. It should be noted that the degree of polymerization (DP) of resultant nucleobase block was *ca.* 120 for each

polymer, which was determined by ^{1}H NMR spectroscopy by comparing integration of signals from nucleobase block with those from POEGMA block. In addition, POEGMA weight fraction in the copolymer (*f*) was calculated using molecular weight determined by ^{1}H NMR ($M_{n,\,NMR}$). Moreover, SEC traces of macro-CTA and the synthesized block copolymers were overlaid (Figure 5.3), where a clear shift in molecular weight distribution suggested the successful chain extension. However, it should be noted that the polymers were obtained with slightly broad molecular weight distributions, which may be due to the polymer solubility in DMF or an interaction with the SEC columns from the hydrogen-bonding sites all along the polymer chain.

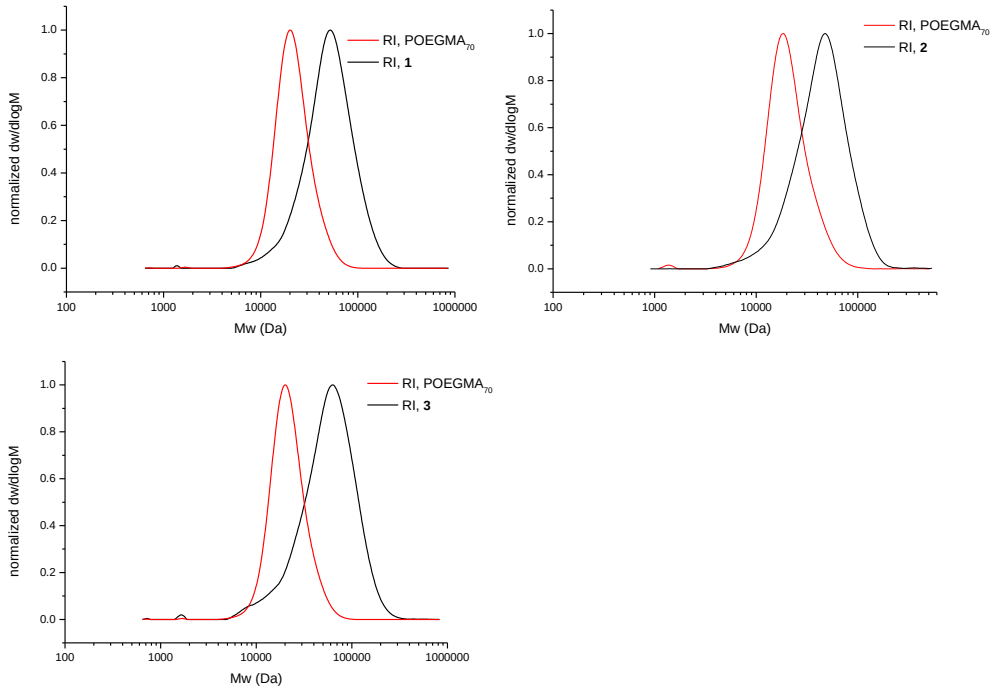

Figure 5.3 SEC traces of $POEGMA_{70}$ and polymers **1 - 3** prepared by RAFT polymerizations in DMF using $POEGMA_{70}$ as the macro-CTA (DMF as eluent, PMMA as standards).

5.3.3 Self-assembly of 1 by direct dissolution

Direct dissolution is considered the most facile method to prepare self-assemblies of polymers and therefore this method was applied first. Polymer **1** ($POEGMA_{70}$-*b*-

($PAMA_{0.5}$-*co*-$PTMA_{0.5}$)$_{121}$) was directly dissolved in 18.2 MΩ·cm water at a concentration of 1 mg/mL and then stirred at room temperature for 2 days to obtain an opalescent mixture (named as **1-DD-a**, for **polymer 1-direct dissolution-sample a**). The polymer mixture was diluted to 0.05 mg/mL for TEM and DLS analysis. Poorly defined aggregations including spheres, elongated micelles, and lamellae were observed by TEM analysis (Figure 5.4). In addition, DLS analysis shows the aggregation possessed a very broad size distribution (PD = 0.60) which also indicates the formation of multiple aggregating populations. Polymer **1** possesses a longer hydrophobic block than hydrophilic block (so-called 'crew-cut' structure)[37,38] and therefore the direct dissolution method may not be suitable according to previous studies.[17,39,40] In addition, polymer **1** possesses glassy nucleobase-containing hydrophobic blocks ($T_g \geq 115$ °C in bulk for AMA/TMA copolymer, Chapter 2), which suggests the polymer chains are frozen at room temperature. These factors account for the polydisperse aggregations which were formed when the direct dissolution method was used.

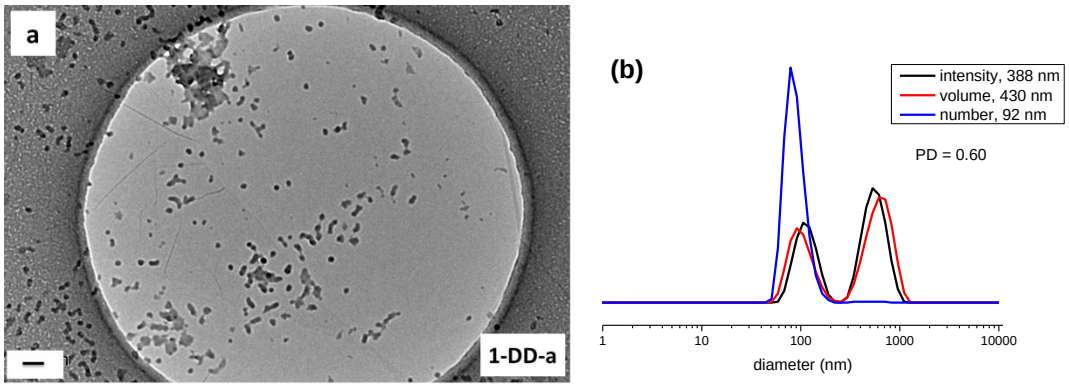

Figure 5.4 Representative TEM and DLS analysis of self-assembly prepared from **1** ($POEGMA_{70}$-*b*-($PAMA_{0.5}$-*co*-$PTMA_{0.5}$)$_{121}$) at room temperature using direct dissolution method, **1-DD-a**. Scale bar: 100 nm.

Heating is often used as a method to increase the mobility, flexibility or solubility of polymer chains.[41,42] It was therefore investigated whether heating could increase the mobility of the nucleobase-containing blocks leading to well-defined structures.

To this end, polymer **1** was added to 18.2 MΩ·cm water which had been heated to 90 °C to give a final concentration of 1 mg/mL and the mixture was subsequently allowed to equilibrated at 90 °C for 30 mins (**1-DD-b)**. The mixture (which contained visible solids as both POEGMA and nucleobase-containing blocks are insoluble in water at 90 °C) was then cooled down slowly to room temperature (20 – 28 °C) over *ca.* 60 min in an oil bath to give an opalescent solution. It should be noted that there were no solids observed by visual inspection in the final opalescent solution. The mixture was diluted to 0.05 mg/mL before being characterized by TEM and DLS analysis. Mixtures of high order structures, lamellae and vesicles, were observed from TEM images (Figure 5.5a), which indicated that the flexibility of the hydrophobic blocks were improved by heating. However, the aggregations were still ill-defined with multiple populations, which resulted in a broad size distribution as observed by DLS analysis (Figure 5.5b). Nevertheless, these observations were still very promising as they indicated that heating could be a key parameter to control the formation of aggregations in this study.

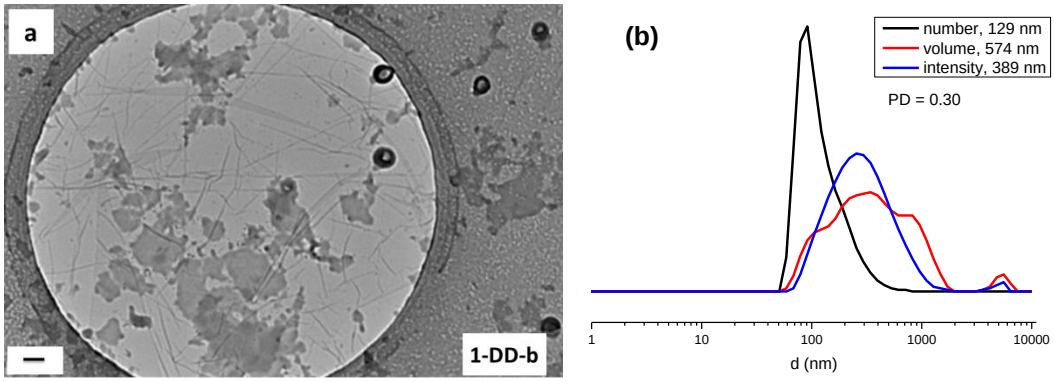

Figure 5.5 Representative TEM and DLS analysis of self-assembly prepared from **1** ($POEGMA_{70}$-*b*-($PAMA_{0.5}$-*co*-$PTMA_{0.5}$)$_{121}$) at 90 °C using direct dissolution method, **1-DD-b**. Scale bar: 100 nm.

Annealing is a common method for the formation of well-defined microphase separated block copolymers[43-45] and the self-assembly of DNA.[46-48] Annealing involves a heat treatment and a cooling process, where heating can make polymer

chains more mobile and cooling can refine structures. Herein, we take advantage of the annealing method and apply it to solution self-assemblies. Solutions of **1-DD-a** and **1-DD-b** with a concentration of 0.1 mg/mL were annealed (heated up from 15 °C – 85 °C and then cooled down from 85 °C – 15 °C with a rate of 1 °C/min) for 3 cycles (named as **1-DD-a'** and **1-DD-b'** respectively). The annealing experiments were performed on a variable-temperature UV-vis spectrometer (λ = 500 nm), which was also used for the LCST measurement described in section 5.3.1. It should be noted that the samples don't have absorptions in the range of wavelengths of visible light (390 nm – 700 nm), determined by both UV spectroscopy and visual inspection and therefore the 500 nm light should not affect the samples.

These annealed solutions were analyzed by TEM and DLS analysis (Figure 5.6). High-order and slightly better defined structures (spheres and vesicles) were observed for the annealed samples by TEM analysis (Figure 5.6 left). Moreover, compared to their corresponding mother-solutions, the size distributions become narrower as determined by DLS analysis (Figure 5.6 right). These results suggest that annealing is a promising approach to increase polymer flexibility during self-assembly and further induce well-controlled self-assembly structures. However, these self-assemblies were still not ideal because multiple populations were still present. Therefore, although promising results were obtained using the direct dissolution method, further studies would focus on alternative self-assembly methods.

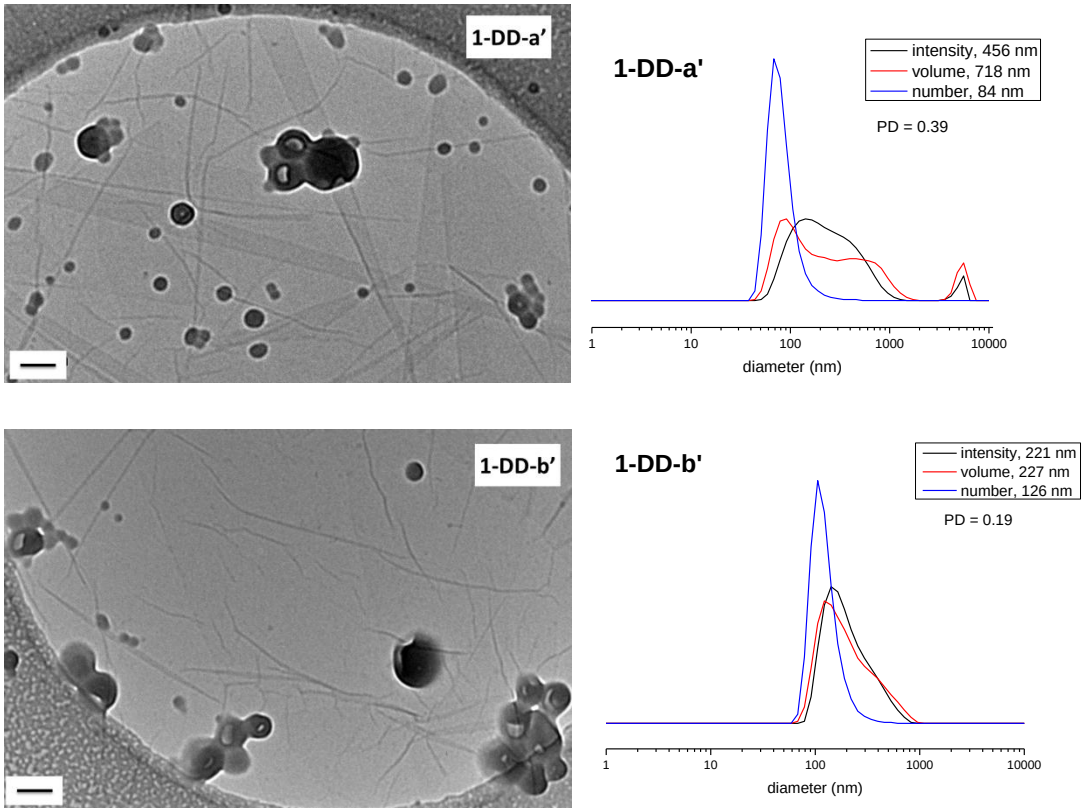

Figure 5.6 Representative TEM and DLS analysis of self-assemblies, **1-DD-a'** and **1-DD-b'** prepared by annealing 0.1 mg/mL of **1-DD-a** and **1-DD-b** respectively (annealing conditions: 15 °C – 85°C and then 85 °C – 15 °C with a rate of 1 °C/min for 3 cycles). Scale bar: 100 nm.

5.3.4 Self-assembly of polymers 1 – 3 by solvent switch using DMF as a common solvent

The solvent-switch method is considered a suitable approach to prepare crew-cut self-assemblies. Typically, the copolymers are firstly dissolved in a common solvent that is favorable for all blocks. Then a selective solvent which is a nonsolvent for one block is slowly added to the solution until a predetermined point, followed by addition of a large excess of non-solvent to freeze the morphologies. Finally the common solvent is removed by dialysis against the selective solvent to give the final self-assemblies.[41] Herein, the solvent-switch method is applied to prepare nucleobase-containing self-assemblies in water.

DMF was selected as the common solvent as both POEGMA and nucleobase-containing blocks are soluble in this solvent. Water was utilized as the selective

solvent which is only a good solvent for the POEGMA block. The initial polymer concentration in the common solvent was fixed as 8 mg/mL. Water was added to the solution at a rate of 1 mL/h until the final volume ratio between water and DMF was 8:1. The solution was then dialyzed against water, incorporating 6 water changes (6 × 1L). The final concentration was estimated by measuring the final volume and was *ca.* 1 mg/mL. The solutions were diluted to 0.2 mg/mL before being characterized by TEM and DLS analysis.

Self-assemblies prepared from polymers **1**, **2**, **3** and a 1:1 mixture of **2** and **3** are shown in Figure 5.7 (**X-DMF**, **X** is the polymer name: **1**, **2**, **3**, and **2+3**). Only spherical micelles were observed by TEM analysis. It should be noted that the unstained TEM images were prepared on graphene-oxide (GO) coated TEM grids and folds were usually observed on the backgrounds. The micelles were well-defined with narrow size distributions (< 0.18), which were determined by DLS analysis (Figure 5.8). Moreover, it was found that self-assemblies prepared from polymer **2**, $POEGMA_{70}$-*b*-$PAMA_{120}$ (**2-DMF**, PD = 0.096) were the more well-defined than those prepared from polymer **1**, $POEGMA_{70}$-*b*-$(PAMA_{0.5}$-*co*-$PTMA_{0.5})_{121}$ (**1-DMF,** PD = 0.13) and polymer **3**, $POEGMA_{70}$-*b*-$PTMA_{118}$ (**3-DMF**, PD = 0.18) as observed by both TEM and DLS analysis. The slight difference of polymer solubility in DMF may lead to this observation as thymine-containing polymers are more soluble in DMF (in an order of decreasing solubility in DMF: **3 > 1 > 2**).

As observed above, annealing is a good way to make better defined self-assemblies and it was therefore applied to 1 mg/mL solutions of **1-DMF**, **3-DMF**, and **2+3-DMF** to further investigate the effects of annealing (resultant solutions named as **1-DMF'**, **3-DMF'** and **2+3-DMF'** respectively). It was found that after annealing the micelles became more well-defined and possessed narrower size distributions (PD <

0.1) compared to the assemblies before annealing as observed by both TEM spectroscopy and DLS analysis (Figure 5.9). These results suggest that the polymer chains became more flexible by heating and then self-organized to form more stable and well-defined structures by slowly cooling.

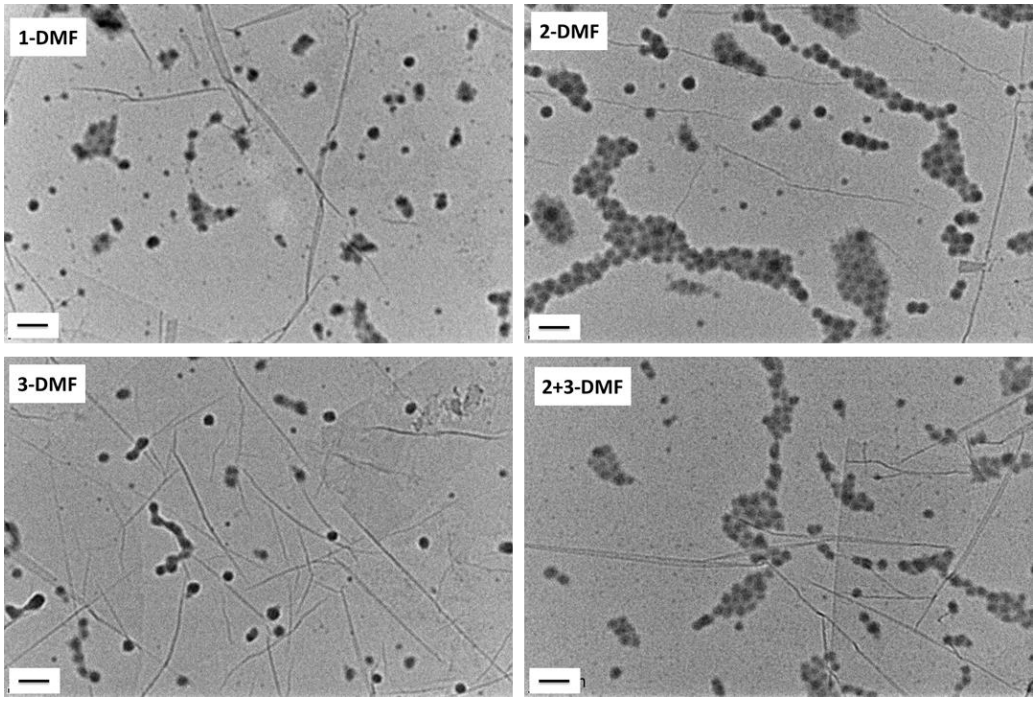

Figure 5.7 Representative unstained TEM images (on GO TEM grids) of self-assemblies prepared from polymers **1**, **2**, **3**, a 1:1 mixture of **2** and **3** by a solvent-switch method using DMF as the common solvent: **1-DMF**, **2-DMF**, **3-DMF**, and **2+3-DMF**. Scale bar: 100 nm.

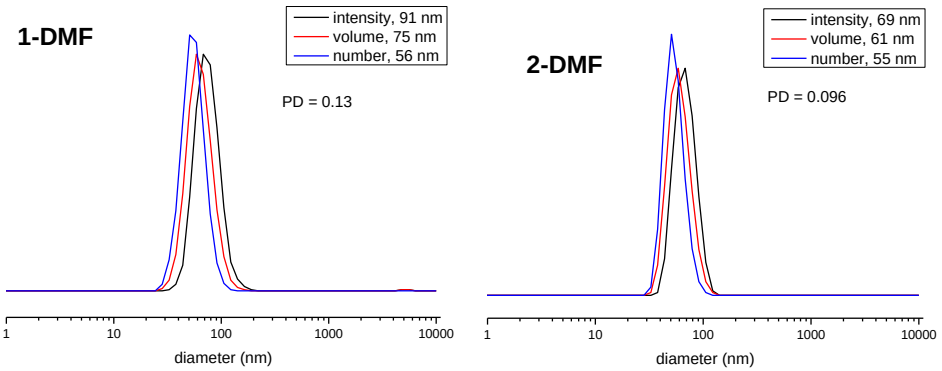

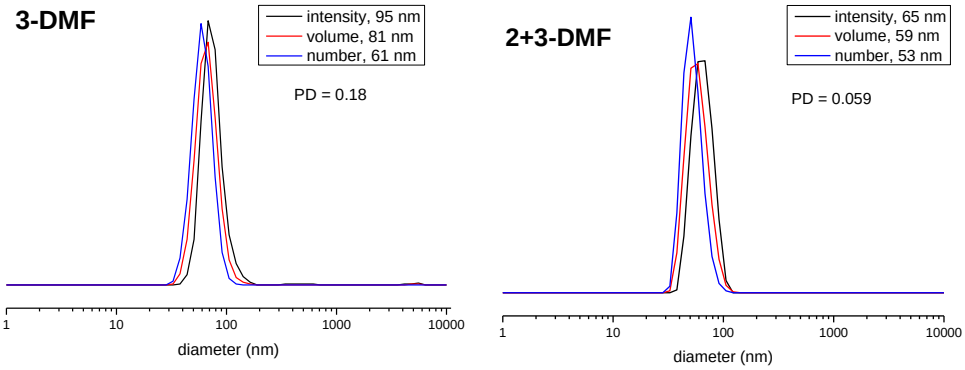

Figure 5.8 DLS analysis of self-assemblies prepared from polymers **1**, **2**, **3**, and a 1:1 mixture of **2** and **3** by a solvent-switch method using DMF as the common solvent: **1-DMF**, **2-DMF**, **3-DMF**, and **2+3-DMF**.

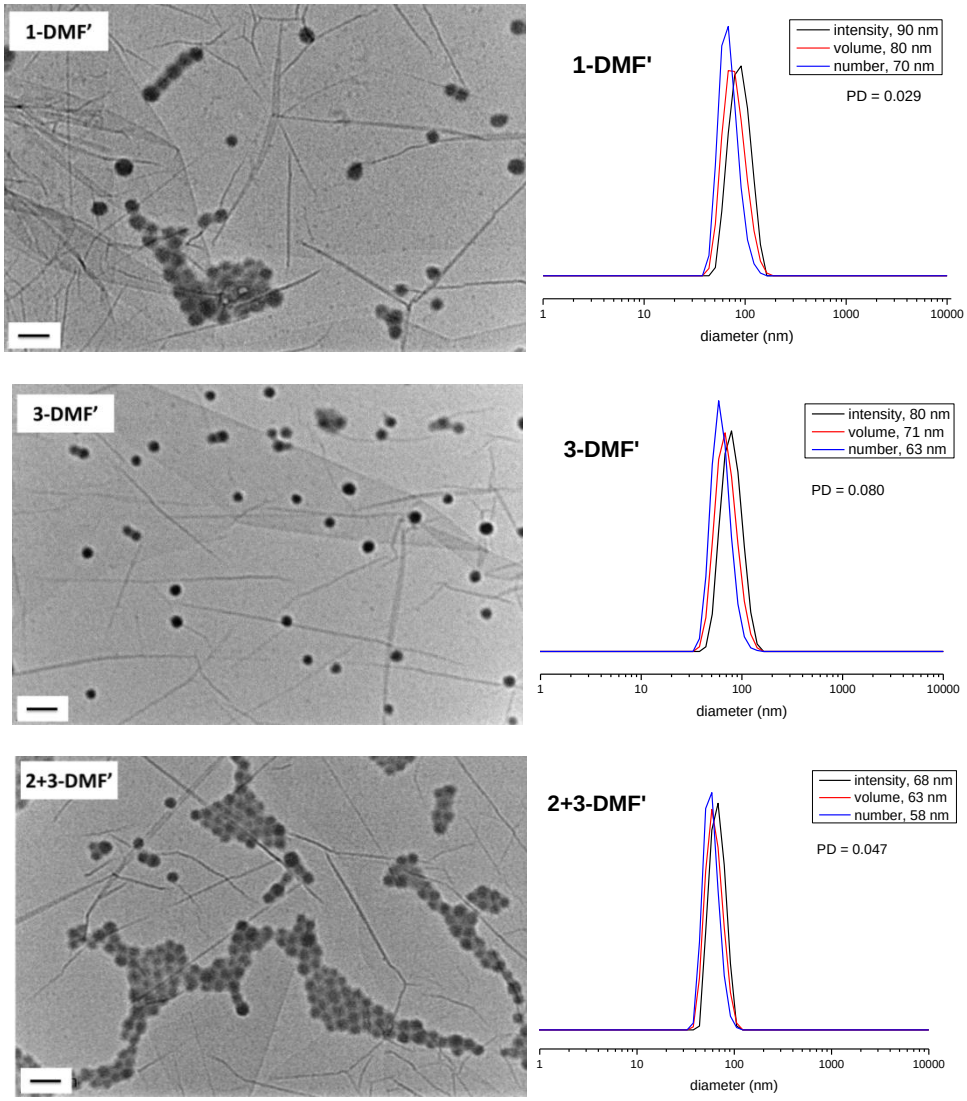

Figure 5.9 Representative TEM images and DLS analysis of self-assemblies **1-DMF'**, **3-DMF'**, and **2+3-DMF'** prepared by annealing solutions of **1-DMF**, **3-DMF**, and **2+3-DMF** (annealing conditions: 15 °C – 85°C and then 85 °C – 15 °C with a rate of 1 °C/min for 3 cycles). Scale bar: 100 nm.

5.3.5 Self-assembly of 1 – 3 by solvent switch using DMSO as a common solvent

According to previous studies, the selection of the common solvent influences the morphology of the aggregates as different common solvents can change the relative coil dimensions of the core and corona chains.[17,27,41] DMSO is observed to be a better solvent for nucleobase-containing polymers than DMF, as it is an extremely good hydrogen-bonding acceptor and with high electron donor capacity.[49] Therefore, DMSO could increase the solubility and stretching of the polymer chains, which may in turn affect the resultant morphologies.

5.3.5.1 Self-assembly of 1 – 3 using DMSO as a common solvent

Self-assemblies were prepared by a similar procedure to that used with DMF as the good solvent. The initial polymer concentration in the common solvent was fixed to be 8 mg/mL. Water was added to the solution at a rate of 1 mL/h until the final volume ratio between water and DMSO was 8:1. The solution was then dialyzed against water, incorporating 6 water changes (6 × 1L). The final concentration was estimated by measuring the final volume and was *ca.* 1 mg/mL. The solutions were diluted to 0.05 mg/mL before being characterized by TEM and DLS analysis.

Self-assemblies prepared from polymers **1**, **2**, **3** and a 1:1 mixture of **2** and **3** using DMSO as the common solvent are shown in Figure 5.10. When polymer **1**, $POEGMA_{70}$-*b*-$(PAMA_{0.5}$-*co*-$PTMA_{0.5})_{121}$ was used (Figure 5.10, **1-DMSO**), spherical micelles with internal structures, bicontinuous micelles, were observed with a diameter of *ca.* 160 nm by TEM observations, the size of which is consistent with the result from DLS analysis (180 nm, Figure 5.11). Moreover, it should be noted that the particles were in a narrow size distribution (PD = 0.045). In the case of polymer **2**, $POEGMA_{70}$-*b*-$PAMA_{120}$, precipitations occurred during the addition

of water into the solution (Figure 5.10, **2-DMSO**). The resultant solution was characterized by TEM analysis showing the formation of small micelles with a diameter of 20 nm. The size and size distribution from DLS analysis were very messy due to the presence of precipitate. Self-assembly of polymer **3**, $POEGMA_{70}$-*b*-$PTMA_{118}$ led to the formation of spherical micelles with a diameter of 50 nm by TEM observations (Figure 5.10, **3-DMSO**). Compared to the particles prepared from polymer **1**, these micelles were smaller in size and had less internal structure which might be due to the weaker nucleobase interactions among thymine functionalities than those between thymine and adenine pairs. Moreover, particles appeared to have a very narrow size distribution (PD = 0.029) and with a hydrodynamic diameter of 106 nm by DLS analysis. When a 1:1 mixture of polymer **2** and **3** was investigated (Figure 5.10, **2+3-DMSO**), spherical micelles with internal structures, bicontinuous micelles, were again observed, which was different from the morphology using DMF as the common solvent. The size of the particles was around 212 nm with a narrow size distribution (PD = 0.056) by DLS analysis.

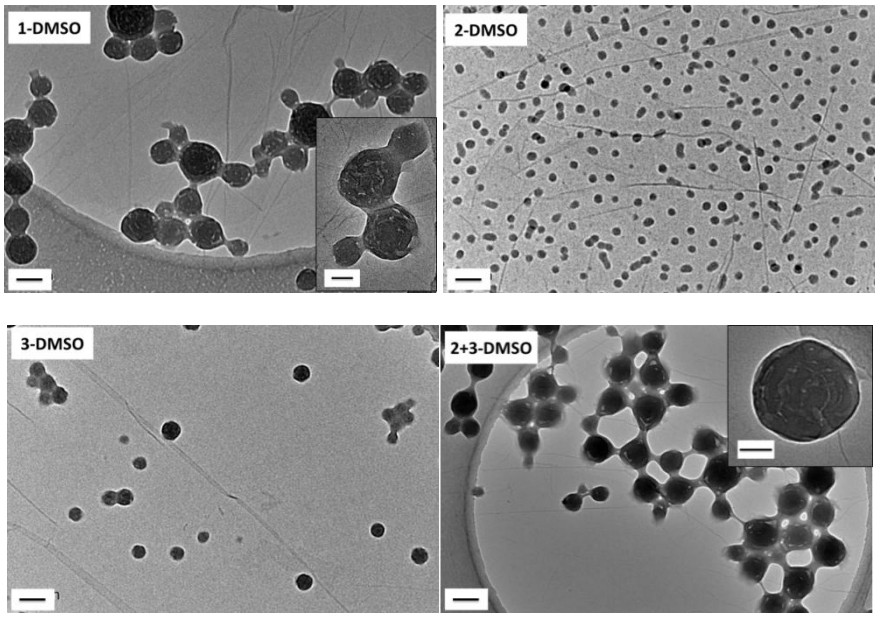

Figure 5.10 Representative TEM images of self-assemblies prepared from polymers **1**, **2**, **3**, a 1:1 mixture of **2** and **3** by a solvent-switch method using DMSO as the common solvent: **1-DMSO**, **2-DMSO**, **3-DMSO**, and **2+3-DMSO**. Scale bar: 100 nm (inset 50 nm).

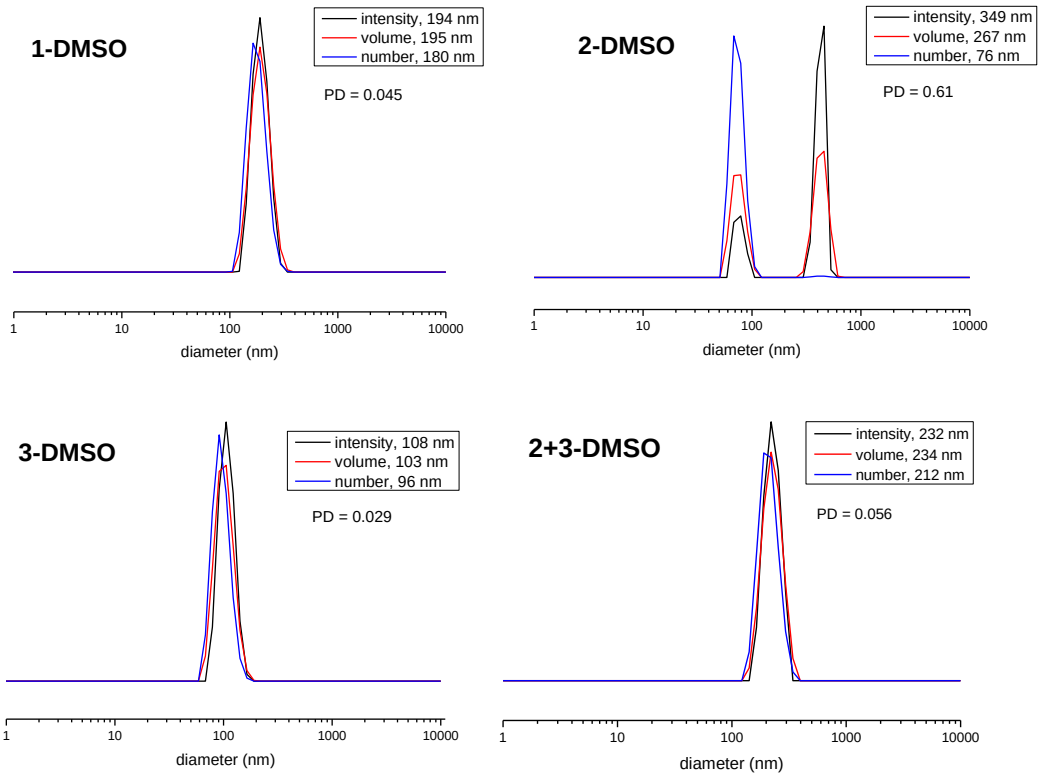

Figure 5.11 DLS analysis of self-assemblies prepared from polymers **1**, **2**, **3**, a 1:1 mixture of **2** and **3** by a solvent-switch method using DMSO as the common solvent: **1-DMSO**, **2-DMSO**, **3-DMSO**, and **2+3-DMSO**.

Different morphologies were observed when using different common solvents: DMF and DMSO. It should be noted that the weight fraction of POEGMA block in the polymers 1 – 3 (*f*) was *ca.* 0.37 (see Table 5.2). According to the rule of hydrophilic weight fraction ($f_{\text{hydrophilic}}$) for predicting resultant morphologies reported by Discher and Eisenberg (*i.e.*, vesicles ($f_{\text{hydrophilic}} \approx 35\% \pm 10\%$); cylindrically shapes ($f_{\text{hydrophilic}} < 50\%$); micelles ($f_{\text{hydrophilic}} > 45\%$); inverted structures ($f_{\text{hydrophilic}} < 25\%$)),[50,51] vesicle or cylinder structures were expected to form from polymers **1** – **3**. However, in this study, for self-assemblies prepared from polymers **1** – **3**, spheres were observed when using DMF as common solvent, while various structures were formed in the case of DMSO as the good solvent. It should be mentioned that these rules of weight fraction are sensitive to chain chemistry, molecular weight and chain structure.[51] To this end, deviation from these rules is still conceivable given the

nature of nucleobase materials (*i.e.*, presence of nulceobase interactions). In addition, there are three possible hypotheses to explain the differences observed:

(1) Nucleobase-containing polymers are more soluble in DMSO than DMF, leading to a higher degree of stretching of the core-forming blocks, thus affecting the dimensions between hydrophobic domains and hydrophilic corona chains.[17,27,41] In other word, in this study, polymer curvatures in DMF were expected to be smaller than those in DMSO due to the different polymer-solvent interactions. This observation was consistent with previous literature by Eisenberg and coworkers, where for self-assembly of polystyrene$_{200}$-*b*-poly(acrylic acid)$_{18}$, spheres and large compound micelles were observed when DMF and THF was used as the common solvent, respectively, due to the different solvent affinity for the polymer (*i.e.*, solubility parameter).[52]

(2) The viscosity of DMSO (η = 2.0 Ns/m^2, 25 °C) is higher than DMF (η = 0.80 Ns/m^2, 25 °C) and therefore leads to a slower water-organic phase mixing and a lower precipitation rate, which would be favorable to the formation of larger nanoparticles.[53] To this end, the formation of DMSO-polymer droplet in an aqueous environment was conceivable, which would favor the formation of bicontinuous, consistent with Holder and coworkers' proposals on the formation of bicontinuous micelles (*i.e.*, bicontinuous micelles originate from polymer-rich good solvent droplets and exchange of good-solvent with water lead to microphase separation and eventually the final morphology).[28,29]

(3) Nucleobase interactions affect the resultant structures. Although polymers **1** – **3** possessed similar weight fraction of POEGMA block, different aggregation behavior was observed. When DMSO was used as the common solvent, different morphologies were observed as shown in Figure 5.10. When adenine and thymine

were both present (Figure 5.10, **1-DMSO** and **2+3-DMSO**), micelles with internal structures were observed, which we assume is due to the presence of complementary nucloebase interactions. In comparison, for thymine-containing polymer **3**, particles with less internal structures were observed due to the relatively weak thymine-thymine interaction. For adenine-containing polymer **2**, precipitation was observed upon the addition of water into the solution, which may result from the poor solubility of PAMA blocks. Holder and coworkers previously reported the formation of complex morphologies from tripeptide-containing amphiphilic diblock copolymers and attributed that specific amino acid sequence of peptide resulted in the different aggregation behavior.[28] In our study, the different of nucleobase interactions rather than weight fraction played a key role in the resultant morphology, which is consistent with their observations.

5.3.5.2 Effect of annealing on self-assemblies using DMSO as a common solvent

The effect of annealing on the resultant morphologies prepared by the solvent-switch method using DMSO as the common solvent was also investigated. Annealing was applied to 0.1 mg/mL solutions of **1-DMSO**, **2-DMSO**, **3-DMSO** and **2+3-DMSO** using the same annealing procedures as above (named as **X-DMSO'**, **X** is the sample number). For polymer **1**, vesicles were observed with a narrow size distribution after annealing (Figure 5.12, **1-DMSO'**), which was different from the morphologies obtained before annealing (Figure 5.10, **1-DMSO**), therefore a solid-hollow transition was observed with annealing. For polymer **2**, only spherical micelles were observed after annealing (**2-DMSO'**). However, as mentioned above, precipitations were formed upon addition of water and thus the observed morphologies were only those structures which stayed in solution. When self-assemblies of **3-DMSO** were annealed, a mixture of spherical micelles and small vesicles was observed by TEM

analysis (Figure 5.12, **3-DMSO'**). DLS analysis shows that the particles with a hydrodynamic diameter of 101 nm were in a narrow size distribution. For the 1:1 mixture of polymer **2** and **3**, vesicles with a hydrodynamic diameter of 221 nm were observed after annealing (Figure 5.12, **2+3-DMSO'**).

In conclusion, a solid-hollow transition was observed for self-assemblies using DMSO as a common solvent which was induced by annealing. In order to confirm the observed transition, a combination of microscopy and light scattering was further used to characterize the morphologies before and after annealing. For samples **2+3-DMSO** and **2+3-DMSO'**, which were prepared before and after annealing with a solid and hollow structure respectively, were further investigated.

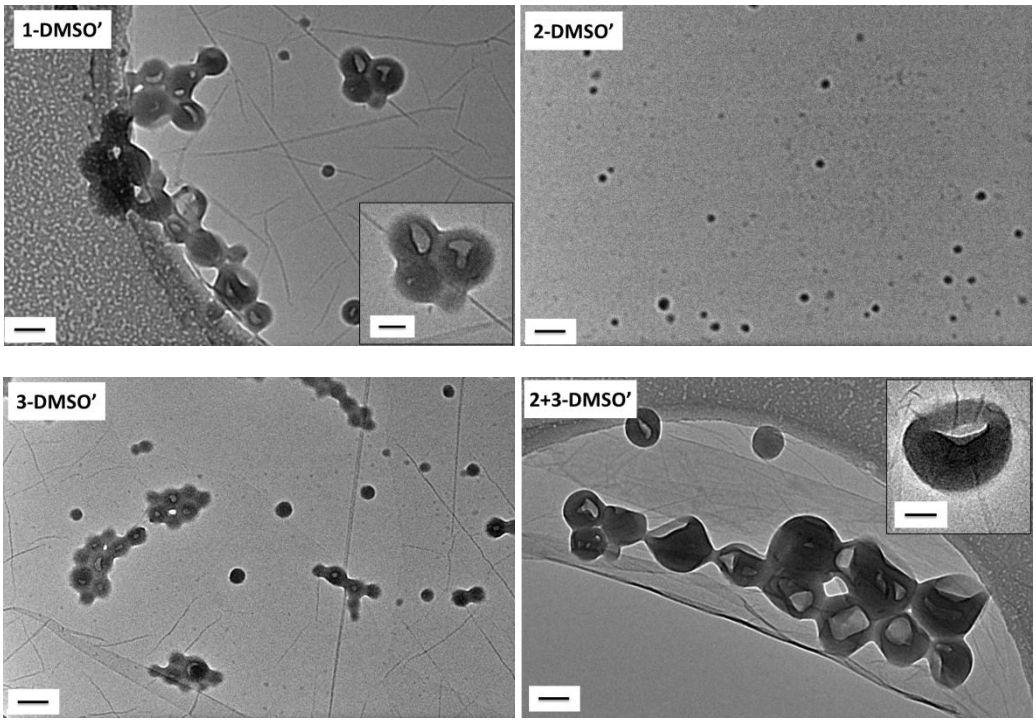

Figure 5.12 Representative TEM images of self-assemblies **1-DMSO'**, **2-DMSO'**, **3-DMSO'**, and **2+3-DMSO'** prepared by annealing 0.1 mg/mL solutions of **1-DMSO**, **2-DMSO**, **3-DMSO**, and **2+3-DMSO** (annealing conditions: 15 °C – 85°C and then 85 °C – 15 °C with a rate of 1 °C/min for 3 cycles). Scale bar: 100 nm (inset 50 nm).

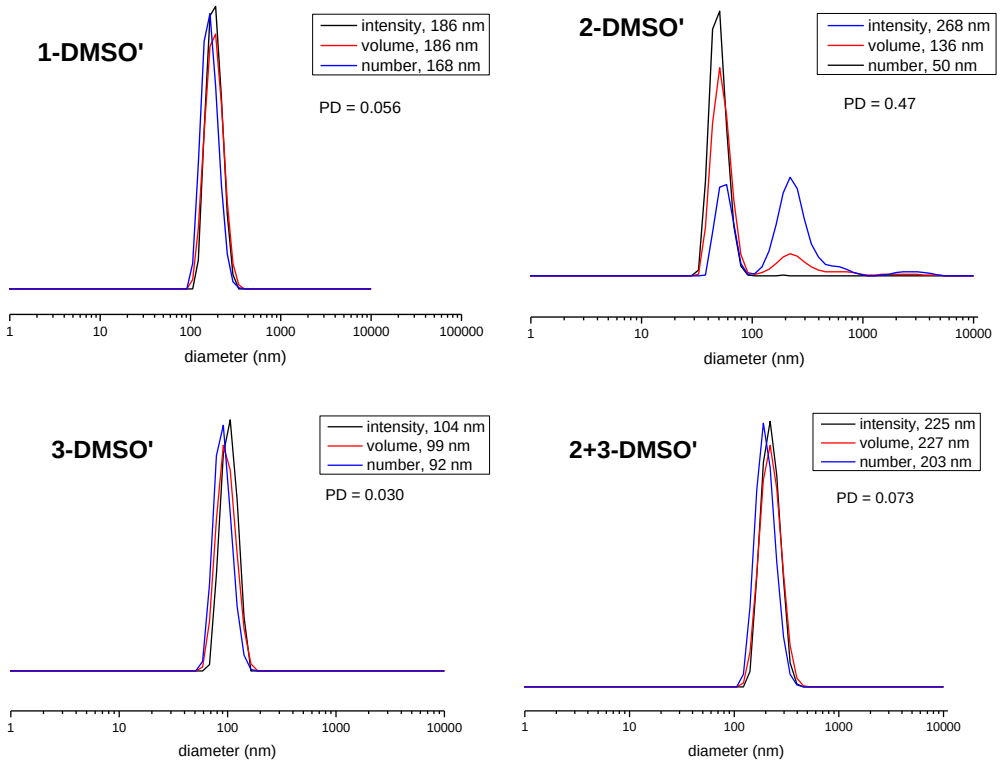

Figure 5.13 DLS analysis of self-assemblies **1-DMSO'**, **2-DMSO'**, **3-DMSO'**, and **2+3-DMSO'** prepared by annealing 0.1 mg/mL solutions of **1-DMSO**, **2-DMSO**, **3-DMSO**, and **2+3-DMSO** (annealing conditions: 15 – 85°C and then 85 – 15 °C with a rate of 1 °C/min for 3 cycles).

Dry-state TEM was used. However, instead of air-drying the sample naturally, a different approach, freeze-drying the sample, was used to prepare the TEM grids in order to minimize the artefacts caused by drying-effect. Herein, a drop of solution was deposited on a TEM grid and then immediately frozen in a liquid nitrogen bath to trap the shape of nanostructures in their solvated state, followed by freeze-drying the TEM grid. As the nanostructure was trapped in ice during freeze-drying, it can minimize the artefacts caused by dehydration. Self-assemblies of **2+3-DMSO** and **2+3-DMSO'** were prepared using this freeze-drying method and then characterized by TEM microscopy (Figure 5.14, a and b). Bicontinuous micelles with solid cores were clearly observed for **2+3-DMSO**, while hollow structures were observed for **2+3-DMSO'**. Morphologies of self-assemblies of **1-DMSO** and its corresponding annealed solution **1-DMSO'** were also confirmed using the freeze-dry method

(Figure 5.14, c and d), which was also consistent with the results obtained from the conventional dry-state TEM. However, this method is still limited as it requires removing water from the structure and keeping the sample at room temperature after drying, which would cause artefacts. In addition, cryo-TEM was also performed on self-assemblies of **2+3-DMSO** (Figure 5.15). Self-assemblies appeared to have same morphology with the observations from the dry-state TEM images although more details can be observed from cryo-TEM images.

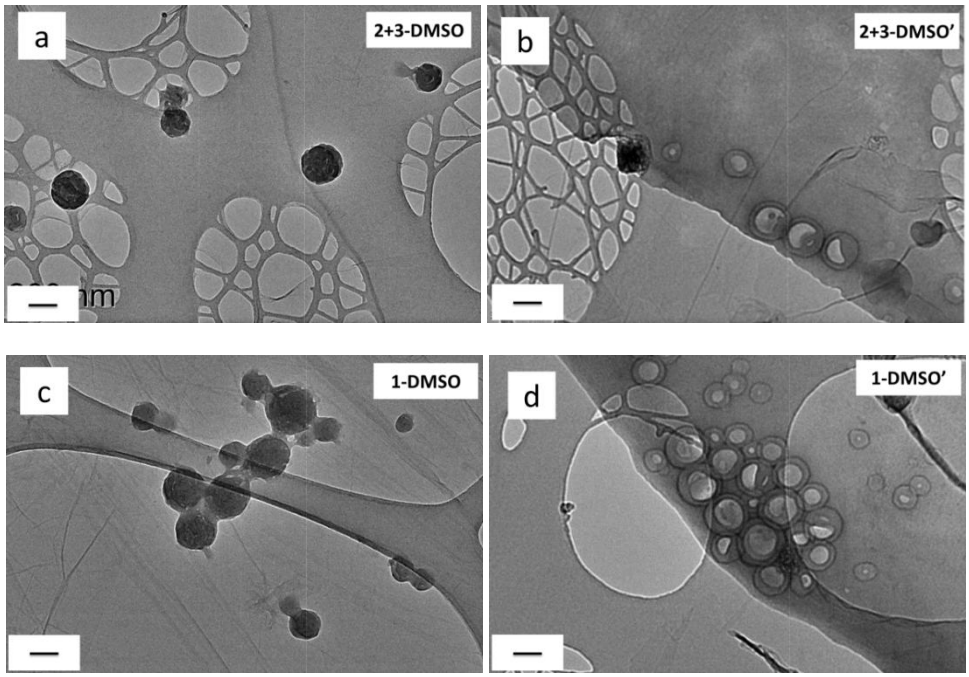

Figure 5.14 Representative TEM images of self-assemblies **2+3-DMSO** (a), **2+3-DMSO'** (b), **1-DMSO** (c), **and 1-DMSO'**(d) prepared by the freeze - dry method. Scale bar: 100 nm.

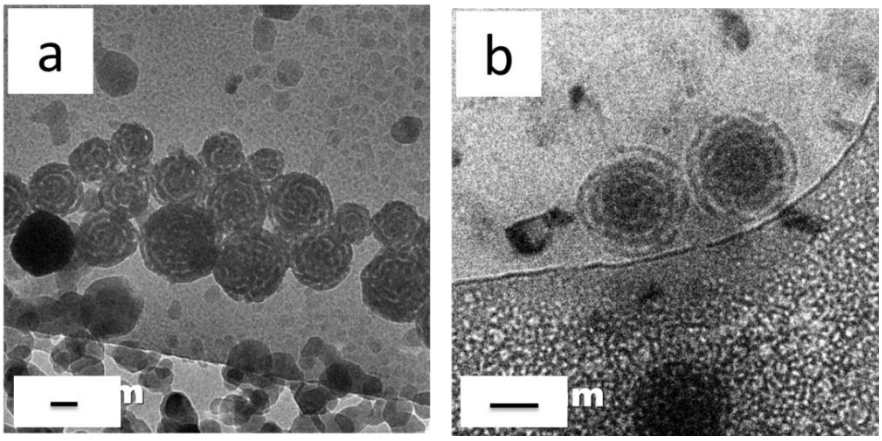

Figure 5.15 Cryo-TEM images of self-assemblies **2+3-DMSO** at a concentration of 0.1 mg/mL. Scale bar: 100 nm.

In addition to microscopy, SLS was also conducted on **2+3-DMSO** and its annealed solution **2+3-DMSO'**. The concentration of the samples ranged from 0.05 mg/mL to 0.01 mg/mL. In order to use the Zimm equation to determine weight-average molecular weights of the aggregates and radii of gyration of the particles, $q \times R_g < 1$ should be valid and thus the data collected from small scattering vectors (q) (12°-30°) was investigated (Figure 5.16).The ρ-ratio (R_g/R_H, ratio between radius of gyration and hydrodynamic radius) of **2+3-DMSO** was calculated to be 0.78，indicating the formation of solid spheres. In comparison, the ρ-ratio of **2+3-DMSO'** was determined to 1.02, indicating that the particles were hollow after annealing.[54] Moreover, the aggregation numbers of both solutions were determined from the results of SLS (N_{agg} = 16600 for **2+3-DMSO**, N_{agg} = 20100 for **2+3-DMSO'**). It should be noted that the calculated large aggregation number for **2+3-DMSO** suggests the formation of complex spheres rather than simple core-shell structures, while it is reasonable for vesicles, **2+3-DMSO'** to possess a large aggregation number.[54] This observation that there was a difference in aggregation number for self-assemblies before and after annealing, inspired us to investigate the kinetics of the morphology transition during annealing.

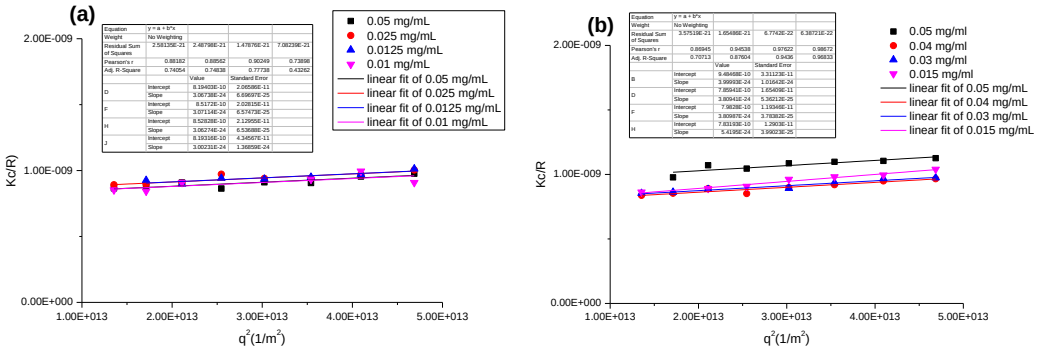

Figure 5.16 Zimm plots for self-assemblies (a) **2+3-DMSO**; (b) **2+3-DMSO'** by SLS.

The annealing procedure was always performed firstly by heating from 15 °C up to 85 °C and then cooling from 85 °C down to 15 °C. This heating-cooling cycle was

repeated 3 times in total. Herein, to investigate the morphology transition kinetically with annealing, the solution was sampled for TEM and DLS analysis after each cycle (Figure 5.17). It was found that after the first annealing cycle the bicontinuous micelles disassembled to form structures with tentacles. These tentacles further fused into lamellae in the second annealing cycle. After the third annealing cycle, the lamellae further self-organized to form vesicles as observed in **2+3-DMSO'**. These observations further support the hypothesis that annealing could make polymers rearrange to form structures that are more thermodynamically favorable.

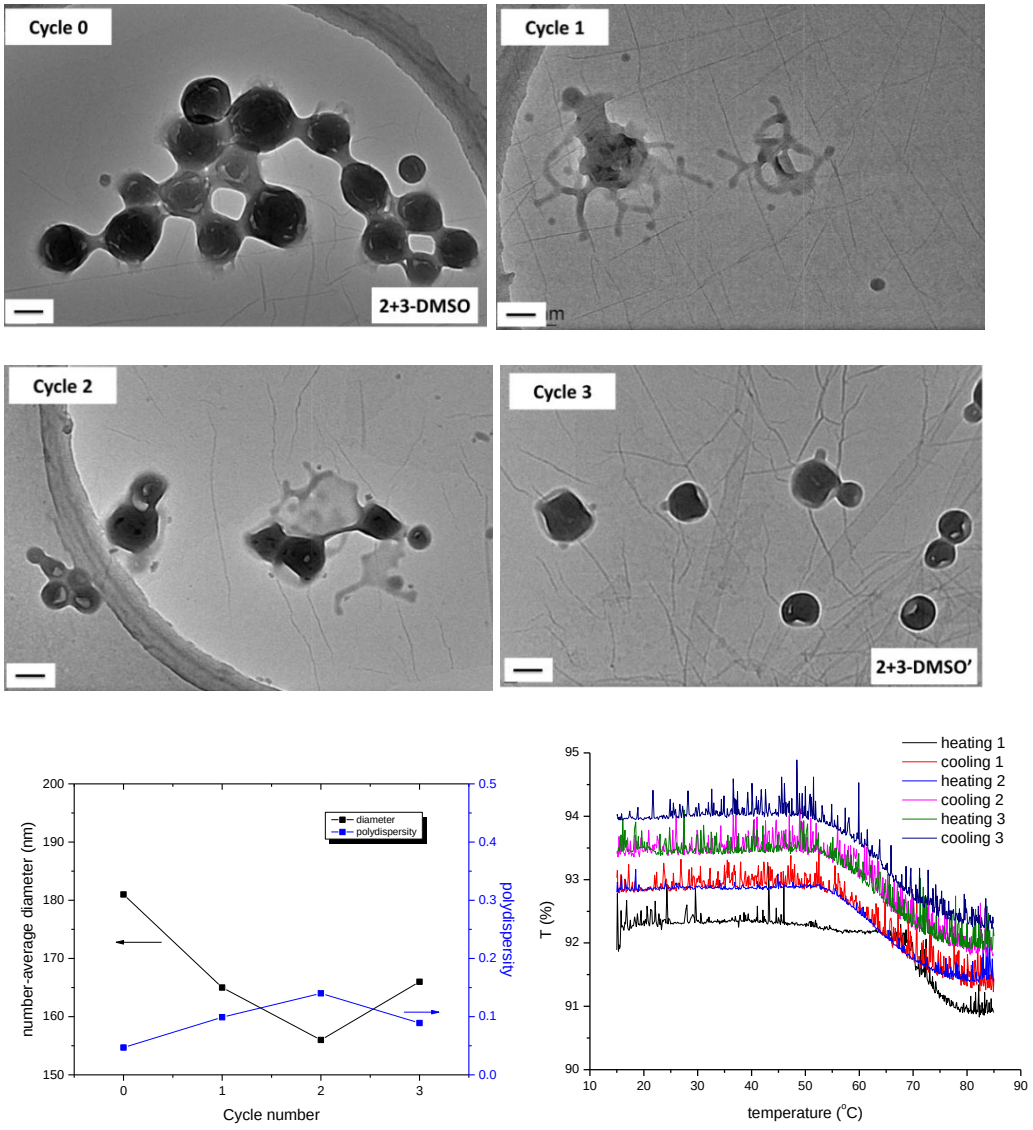

Figure 5.17 Evolution of self-assembly from **2+3-DMSO** to **2+3-DMSO'** by unstained TEM analysis, number-average diameter determined by DLS analysis, and plots of transmittance as a function of temperature (λ = 500 nm, 1 °C/min) with annealing cycles.

In conclusion, a solid-hollow transition, which was induced by annealing, was observed for self-assemblies using DMSO as a common solvent. According to the POEGMA weight fraction ($f \approx 0.37$), the formation of vesicles was reasonable. We assume there are two reasons for these observations: (1) during the annealing procedure, nucleobase-containing polymer chains became flexible upon heating and then, induced by nucleobase interactions, the polymers self-organized upon slowly cooling to form steady structures that are thermodynamically favorable; (2) the temperature-responsive corona blocks POEGMA became insoluble in water at high temperature (> 65 °C) although there is no precipitation observed and tended to aggregate to prevent a larger enthalpy penalty resulting from energetically unfavorable hydrophobe-water interactions. In summary, the rearrangement of polymer chains occurs to lower the total free energy of the system.

5.3.6 Study on stability of polymers 1 – 3 in aqueous environments

Ester groups are at risk of hydrolysis in aqueous environments.[55,56] To check the polymers' stability against water, polymer **1** and **2** were dissolved in both DMSO-d_6 and a mixture of H_2O and DMSO-d_6 (volume ratio between H_2O and DMSO-d_6 = 1:4) at a concentration of *ca.* 16 mg/mL. The solutions were left at both room temperature and 60 °C for one month and characterized periodically by ^{1}H NMR spectroscopy. No obvious changes were observed for polymer **1** in DMSO-d_6 at both room temperature and 60 °C (Figure 5.18 (1) and (3)), showing that polymer **1** was very stable in DMSO. In comparison, in the presence of water (volume fraction: 20%) extra peaks for both PTMA and PAMA were observed at both room temperature and 60 °C (Figure 5.18 (2) and (4)). The sharp peaks corresponded to small molecule nucleobases, which suggested that the polymers were hydrolyzed in the presence of water. Moreover, it was also observed that hydrolysis was much faster at 60 °C than

at room temperature as expected (Figure 5.18 (2) and (4)). However, due to the overlap of peaks, it was difficult to quantify the amount of polymer units that were hydrolyzed. Similar phenomenon was also observed for polymer **2** (Figure 5.19). These results showed that polymers were unfortunately unstable in the presence of a significant amount of water. Therefore, polymers that were obtained after self-assembly should be checked to determine whether hydrolysis occurred during self-assembly before carrying out further investigations.

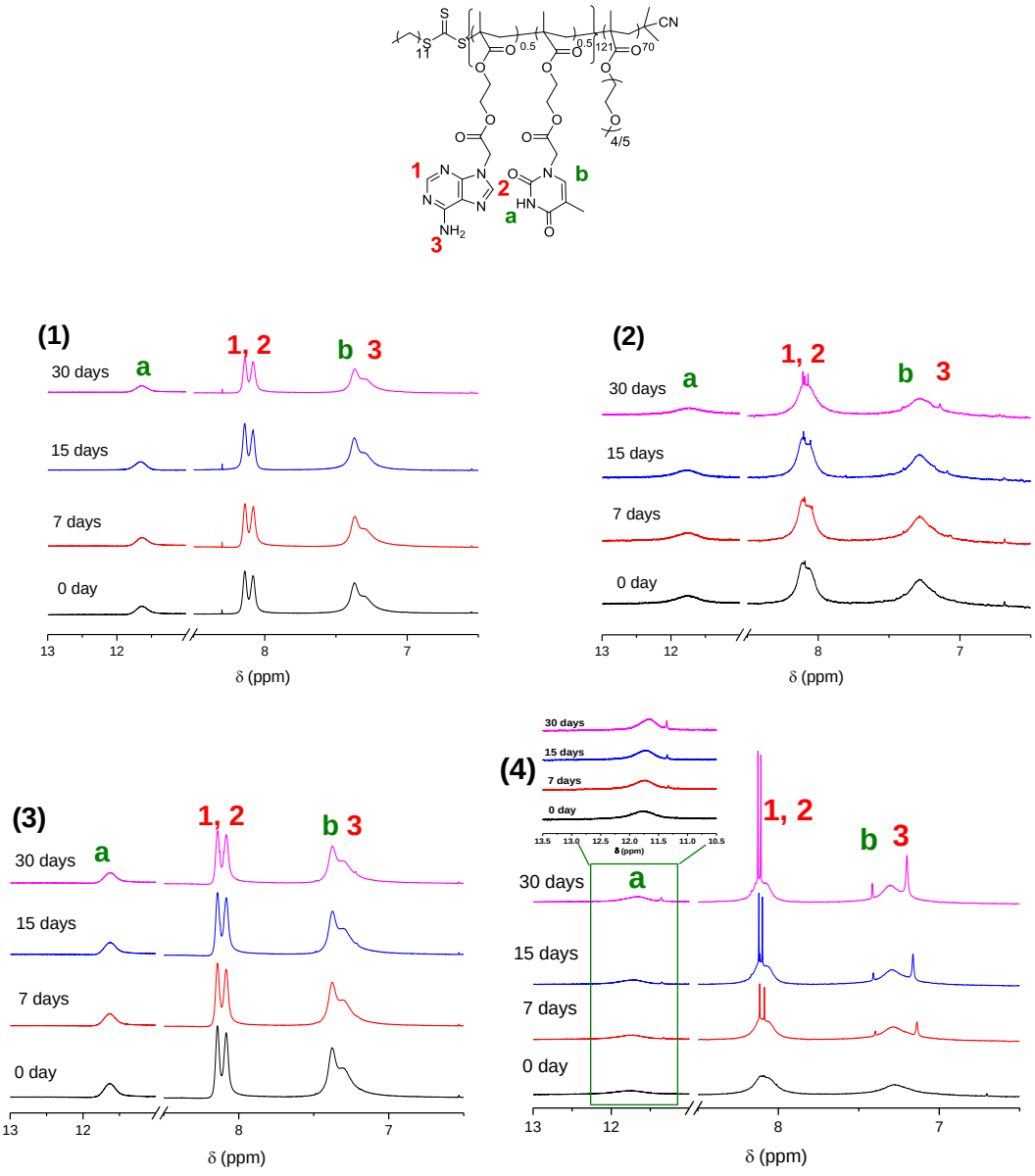

Figure 5.18 Structure of polymer **1** and ^{1}H NMR spectra of polymer **1** treated at different conditions with time: (1) in DMSO-d_6, at 25 °C; (2) in a mixture of H_2O and DMSO-d_6, at 25 °C; (3) in DMSO-d_6, at 60 °C; (4) in a mixture of H_2O and DMSO-d_6, at 60 °C.

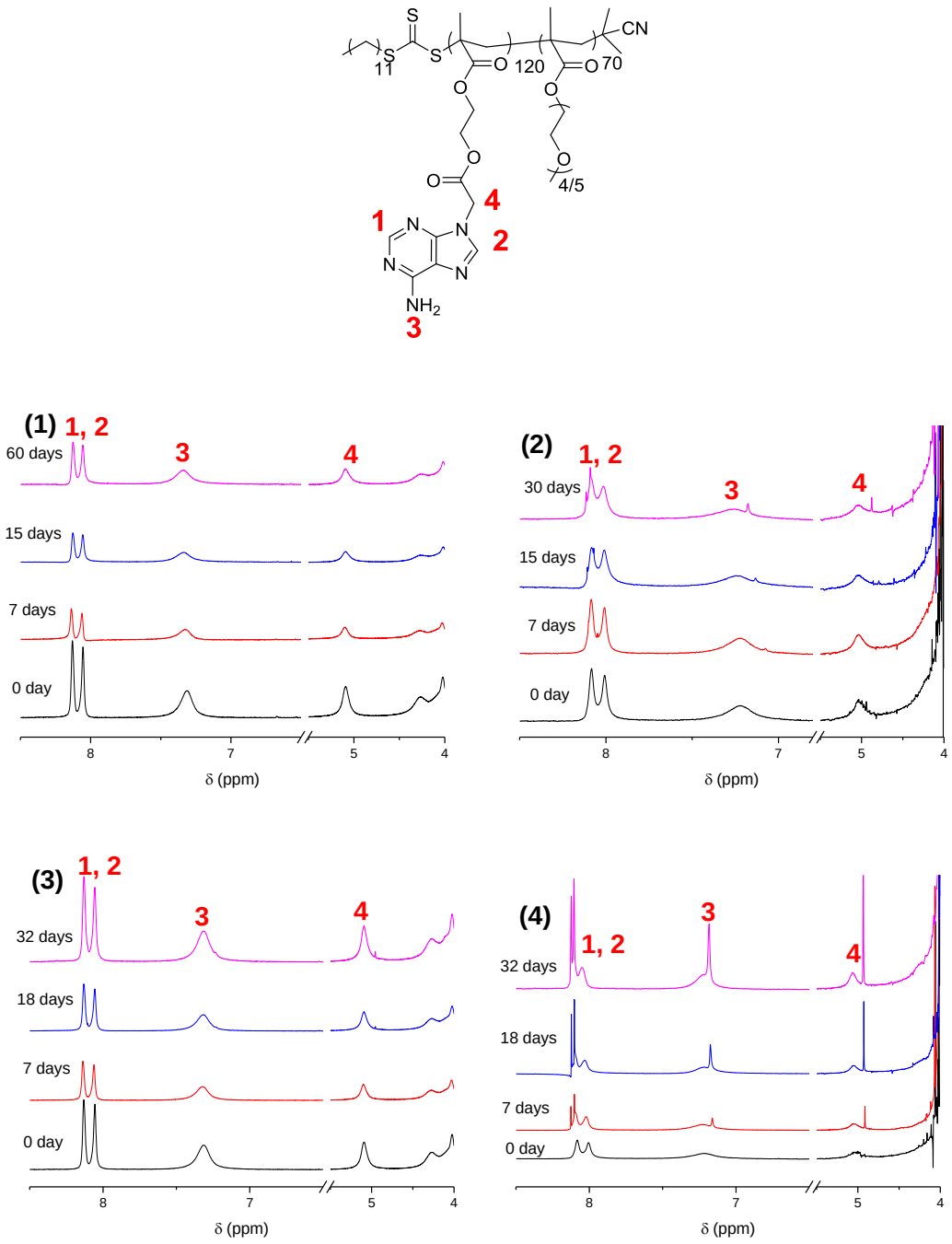

Figure 5.19 Structure of polymer **2** and ^{1}H NMR spectra of polymer **2** treated at different conditions with time: (1) in DMSO-d_6, at 25 °C; (2) in a mixture of H_2O and DMSO-d_6, at 25 °C; (3) in DMSO-d_6, at 60 °C; (4) in a mixture of H_2O and DMSO-d_6, at 60 °C.

A solution of **1-DMSO** and its annealed solution **1-DMSO'**, which were both prepared from polymer **1,** were freeze-dried and the resultant polymers were characterized by ^{1}H NMR spectroscopy. Unfortunately, extra peaks were observed in ^{1}H NMR spectra of the polymers after self-assembly compared to before self-assembly. These results suggested that a number of polymer units were hydrolyzed

during the self-assembly procedure although the nucleobase-containing blocks should be insoluble in water. As mentioned above, due to the overlap of peaks, it was very difficult to accurately quantify the amount of polymer units that were hydrolyzed during the self-assembly procedures. However, by comparing integrations of peaks 1, 2 and a, the fractions of hydrolyzed polymer units were estimated. For polymer **1** before annealing, the hydrolyzed fractions of PAMA and PTMA were approximately 28% and 10% respectively; for polymer **1** after annealing, the hydrolyzed fractions of PAMA and PTMA were about 31% and 18% respectively.

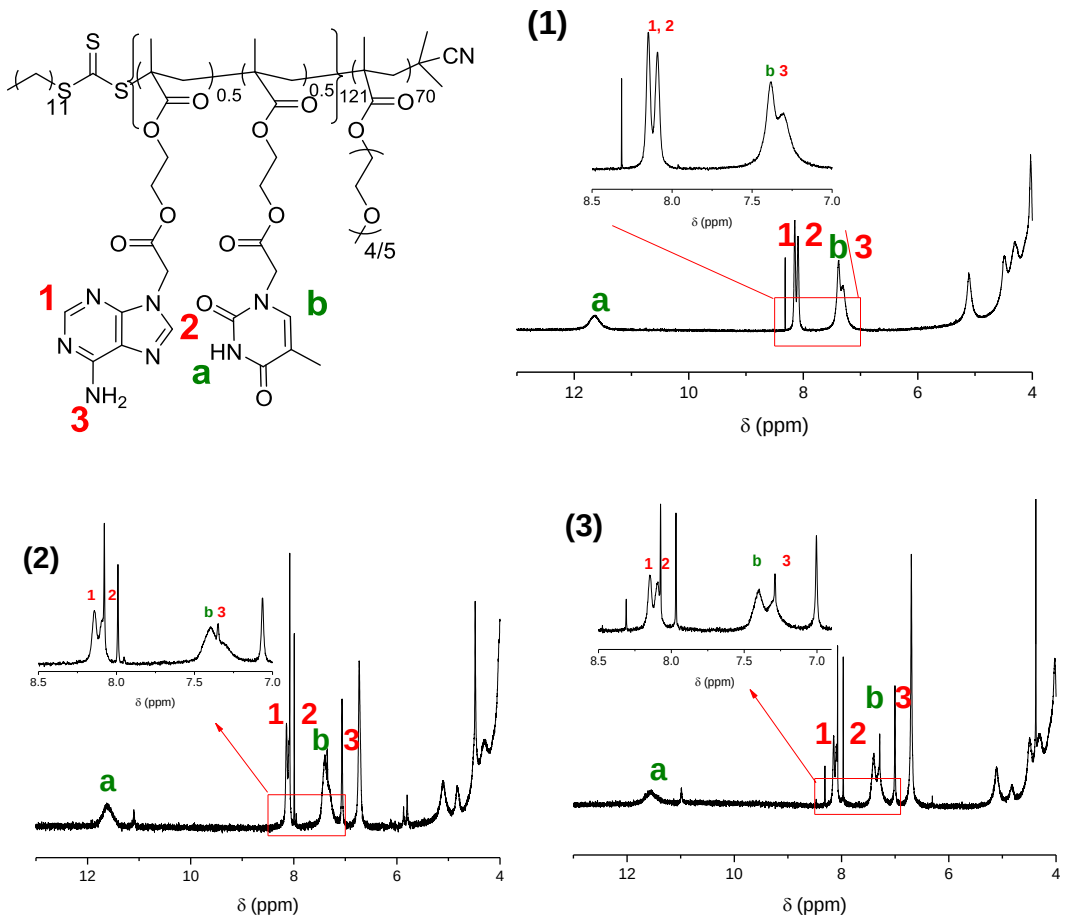

Figure 5.20 Structure and ^{1}H NMR spectra of polymer **1**: (1) before self-assembly; (2) after self-assembly before annealing; (3) after self-assembly and annealing. Self-assembly conditions: using DMSO as the common solvent and then adding H_2O into the solution; annealing conditions: 15 °C – 85°C and then 85 °C – 15 °C with a rate of 1 °C/min for 3 cycles.

Due to the occurrence of polymer hydrolysis in the presence of water, this feature may make the self-assembly system less stable. Moreover, it is also possible that the morphology transition observed above was induced by the hydrolysis, as the hydrolyzed polymers containing hydroxyethyl methacrylate (HEMA) units were considered less hydrophobic and more mobile. Therefore, to further study these observations, a series of new monomers and polymers with better stabilities were synthesized and used for further studies.

5.3.7 Synthesis of new monomers AMA2 and TMA2

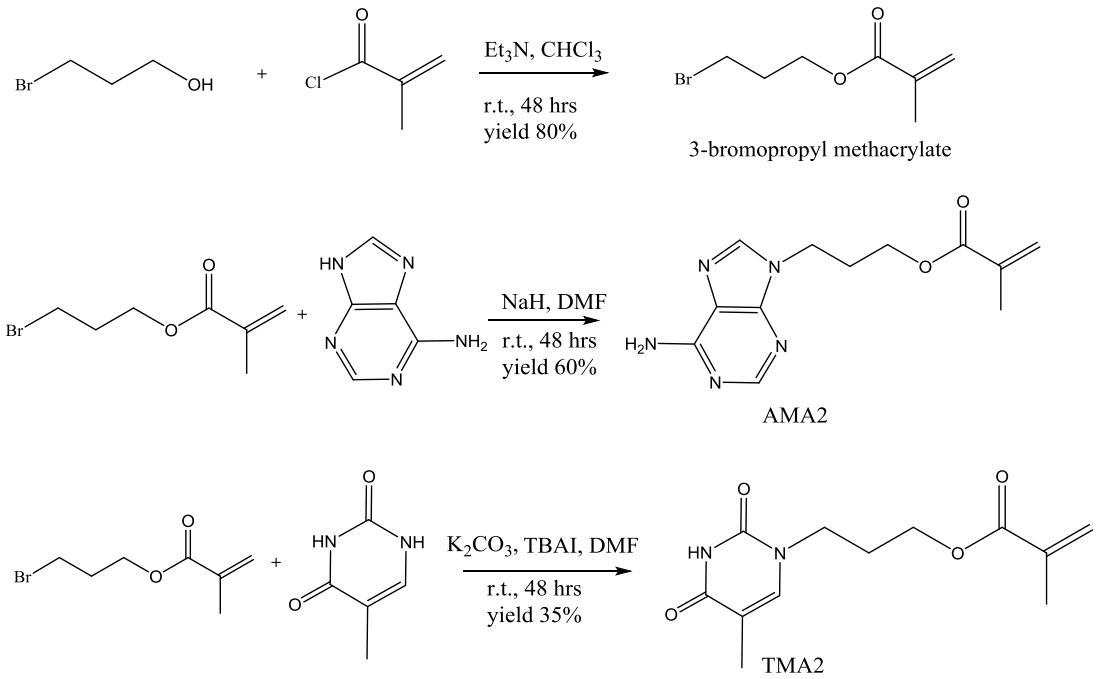

Scheme 5.3 Synthetic route for new monomers, AMA2 and TMA2.

AMA2 and TMA2 monomers without the sensitive ester group were synthesized according to previous reference.[57] The synthesis of the monomers was firstly confirmed by ^{1}H NMR and ^{13}C DEPT NMR spectroscopy (Figure 5.21 and Figure 5.22). All the peaks corresponding to protons of both the double bonds and nucleobases functionalities were successfully assigned, indicating the successful

synthesis. Moreover, DOSY, HMBC, HMQC, elemental analysis and mass spectrometry were also used to confirm the structures.

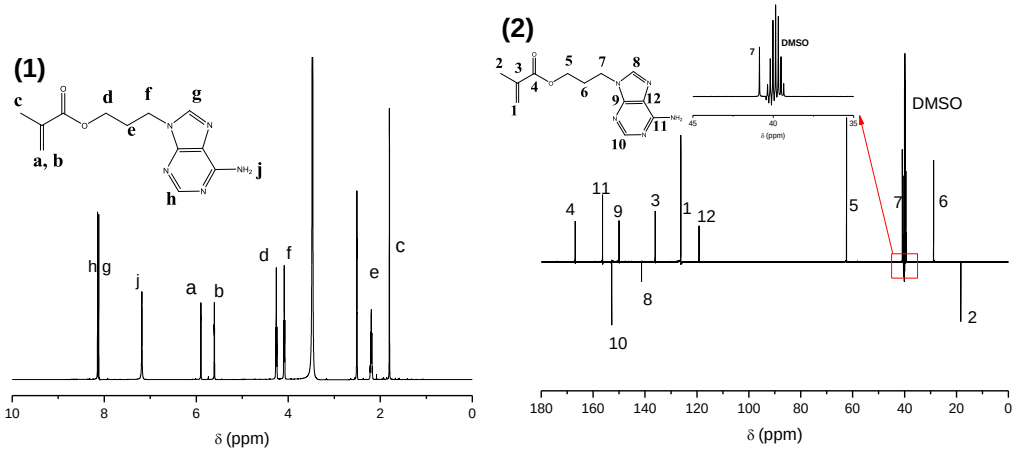

Figure 5.21 ^{1}H NMR and ^{13}C DEPT NMR spectra of AMA2 monomer in DMSO-d_6.

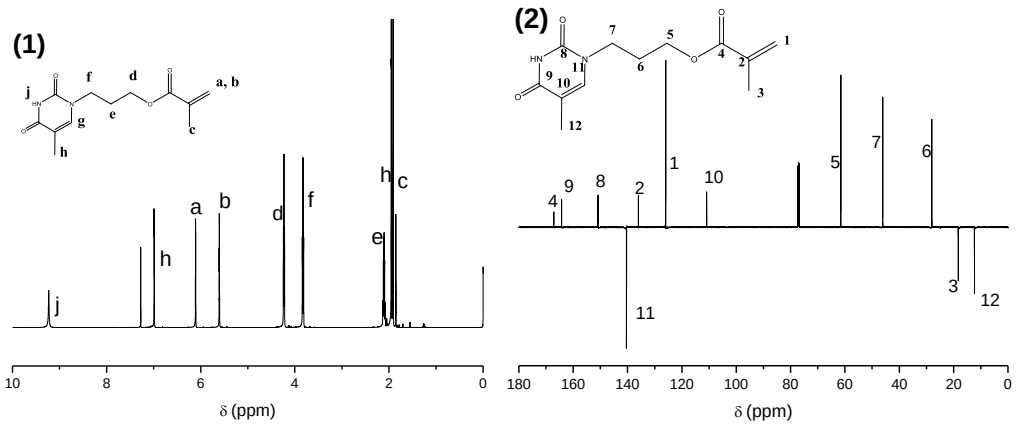

Figure 5.22 ^{1}H NMR and ^{13}C DEPT NMR spectra of TMA2 monomer in $CDCl_3$.

5.3.8 Synthesis of block copolymers using AMA2 and TMA2 monomers, polymers 4 – 6

Block copolymers **4** – **6** using AMA2 and TMA2 as monomers were synthesized in a similar way to polymers **1** – **3** (Scheme 5.4). The polymers were characterized by ^{1}H NMR spectroscopy and SEC analysis (DMF as eluent, PMMA as standards) (Table 5.3 and Figure 5.23). These results suggested the polymers were obtained with comparable molecular weights and monomodel molecular weight distributions. However, it should be noted that the resultant block copolymers have poorer solubility than polymers **1** – **3** in DMF, especially for polymer **5**, POEGMA$_{70}$-*b*-

$PAMA2_{126}$, which was not fully soluble in DMF and thus the SEC analysis of **5** using DMF as eluent was not possible.

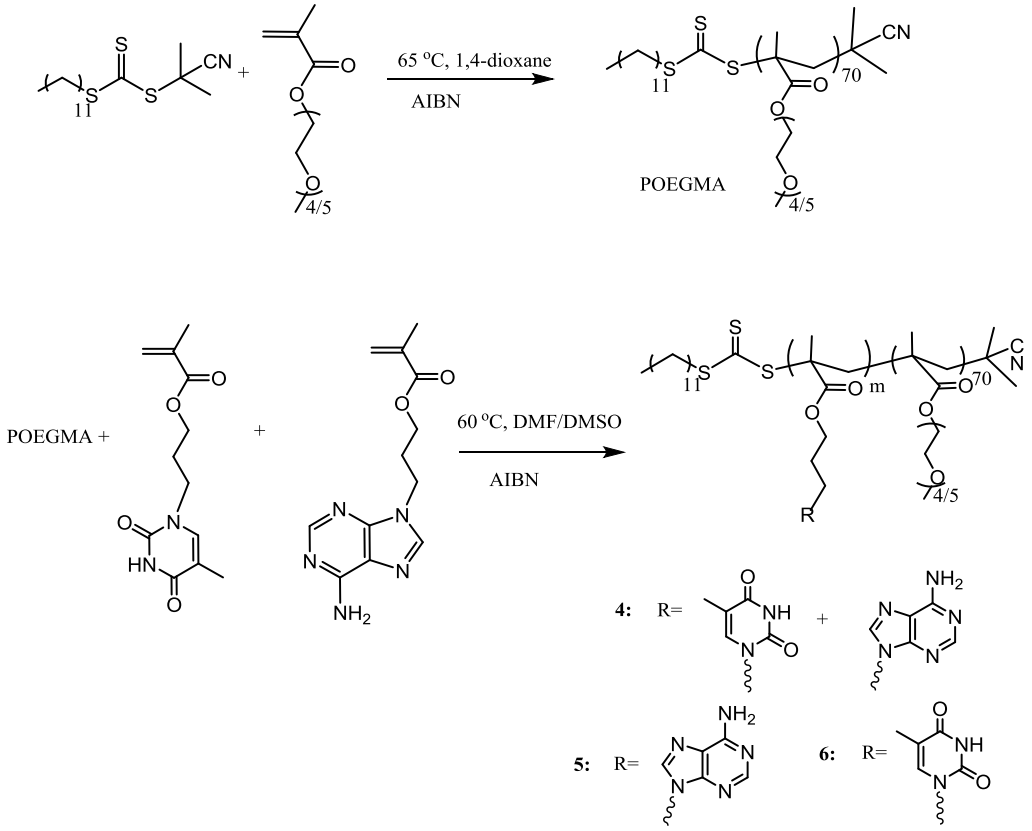

Scheme 5.4 Synthetic route for nucleobase-containing block copolymers, **4 – 6** using AMA2 and TMA2 as monomers.

Table 5.3 Characterization data for block copolymers **4 – 6** using AMA2 and TMA2 as monomers

Polymer	$M_{n,th}$ (kDa)	$M_{n,NMR}$ (kDa)[a]	$M_{n,SEC}$ (kDa)[b]	$Đ_M$	DP of nucleobase[d]	f [e]
$POEGMA_{70}$-*b*-($PAMA2_{0.5}$-*co*-$PTMA2_{0.5})_m$, **4**	46.7	52.3	31.4	1.37	122	0.40
$POEGMA_{70}$-*b*-$PAMA2_m$, **5**	47.1	53.9	--[c]	--[c]	126	0.39
$POEGMA_{70}$-*b*-$PTMA2_m$, **6**	46.2	52.2	34.8	1.41	124	0.40

[a]determined by ^{1}H NMR spectroscopy; [b]determined by SEC analysis (DMF as eluent, PMMA as standards); [c] polymer is not fully soluble in DMF; [d]calculated from $M_{n,NMR}$; [e]POEGMA weight fraction of the polymer using $M_{n,NMR}$.

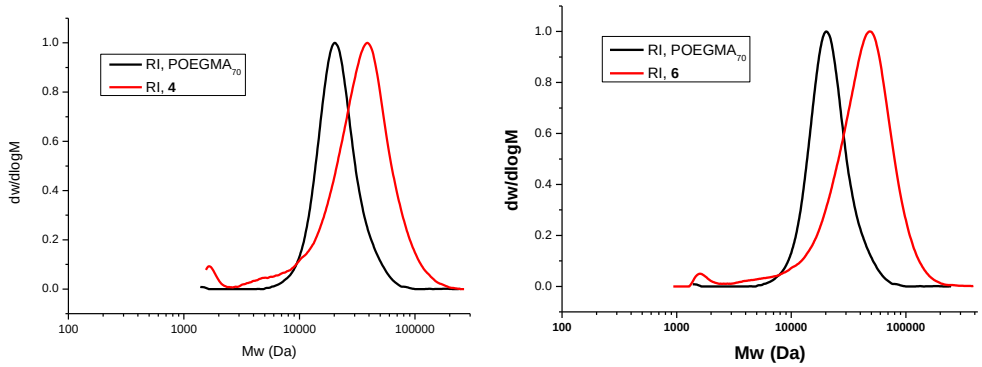

Figure 5.23 SEC traces of $POEGMA_{70}$ and polymers **4** and **6** prepared by RAFT polymerization in DMF using $POEGMA_{70}$ as the macro-CTA (DMF as eluent, PMMA as standards).

5.3.9 Study on stability of polymers 4 – 6 in aqueous environments

Although there is still one ester group present in the new monomers, these monomers and their corresponding polymers are expected to be stable in water in an analogue manner to other methacrylate materials. To show the good stabilities of these polymers in aqueous solutions, polymers **4** – **6** were dissolved in both DMSO-d_6 and a mixture of DMSO-d_6 and H_2O (volume fraction of H_2O is 15% or 20%) and then left at 60 °C for 4 weeks. The solutions were monitored periodically by ^1H NMR spectroscopy and the results are shown in Figure 5.24. Regardless of the solvents used, DMSO-d_6 or a mixture of DMSO-d_6 and H_2O, no obvious extra peaks were observed in all the ^1H NMR spectra of polymers **4** – **6**. These results suggested that the new batch of polymers were much stable in aqueous environments compared to polymers **1** – **3**. Therefore, polymers **4** – **6** were taken forward for further self-assembly studies.

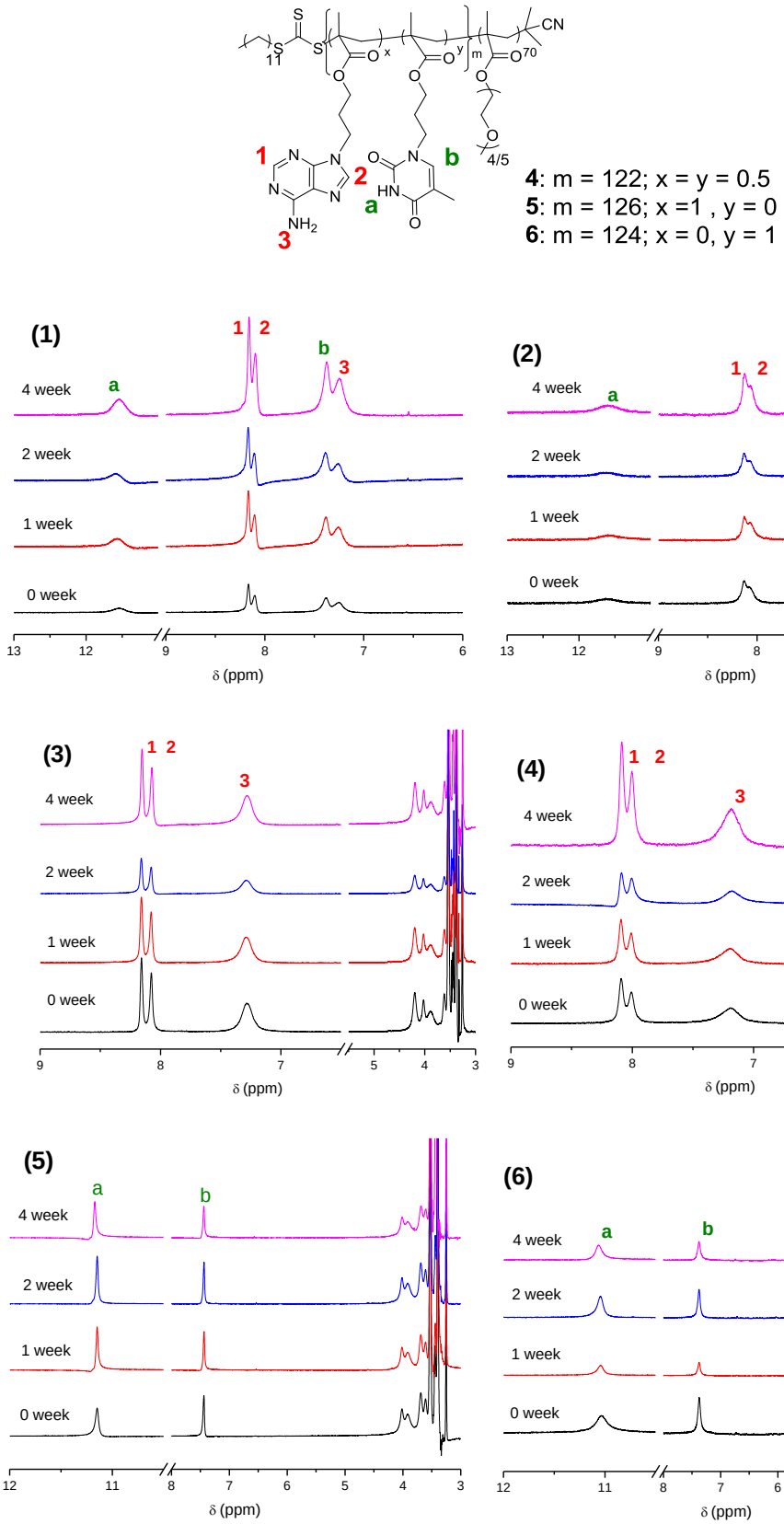

Figure 5.24 Structure of polymers **4 – 6** and ^{1}H NMR spectra of polymers treated at 60 °C with time: (1) polymer **4** in DMSO-d_6; (2) polymer **4** in a mixture of H_2O and DMSO-d_6 (volume fraction of H_2O = 15%); (3) polymer **5** in DMSO-d_6; (4) polymer **5** in a mixture of H_2O and DMSO-d_6 (volume fraction of H_2O = 20%); (5) polymer **6** in DMSO-d_6; (6) polymer **6** in a mixture of H_2O and DMSO-d_6 (volume fraction of H_2O = 20%).

5.3.10 Self-assembly of 4 – 6 by solvent switch using DMF as a common solvent

After the successful synthesis of polymers and demonstration of the polymers' good stabilities against water, the self-assembly behavior of polymers **4** – **6** was studied. According to our above studies on the self-assembly behavior of polymers **1** – **3**, the solvent switch method rather than the direct dissolution method was selected to prepare the self-assemblies. In general, the method to prepare self-assemblies of polymers **4** – **6** was the same as it to assemble polymers **1** – **3**. DMF was firstly investigated as the common solvent. The initial polymer concentration in DMF was kept at 8 mg/mL. Water was added to the solution at a rate of 1 mL/h until the final volume ratio between water and DMF was 8:1. The solution was then dialyzed against water to remove DMF and the final concentration was estimated by measuring the final volume, which were approximately 1 mg/mL.

Self-assemblies prepared from polymers **4**, **5**, **6**, and a 1:1 mixture of **5** and **6** were diluted to 0.2 mg/mL, and characterized by TEM and DLS analysis (**X-DMF**, **X** is the polymer number). Only spherical micelles were observed, the same observation as for polymers **1** – **3** (Figure 5.25, left).

In addition, spherical structures were maintained and no morphology transition was observed after annealing solutions **X-DMF** (Figure 5.25 right, **X-DMF'**, **X** is the polymer number), which was also consistent with the observations of polymers **1** – **3**. Moreover, it was found that the particles obtained after annealing had narrower size distributions determined by DLS analysis, which was constistent with the results observed from polymers **1** – **3**. We proposed that although annealing could relatively increase polymers' mobility, due to the limited core dimension and small aggregation number, spheres were still an energy favorable phase and thus a

morphology transition did not occur. However, owing to the increased mobility of polymer chains and nucleobase interactions, a small rearrangement occurred and thus well-defined particles were attained after annealing.

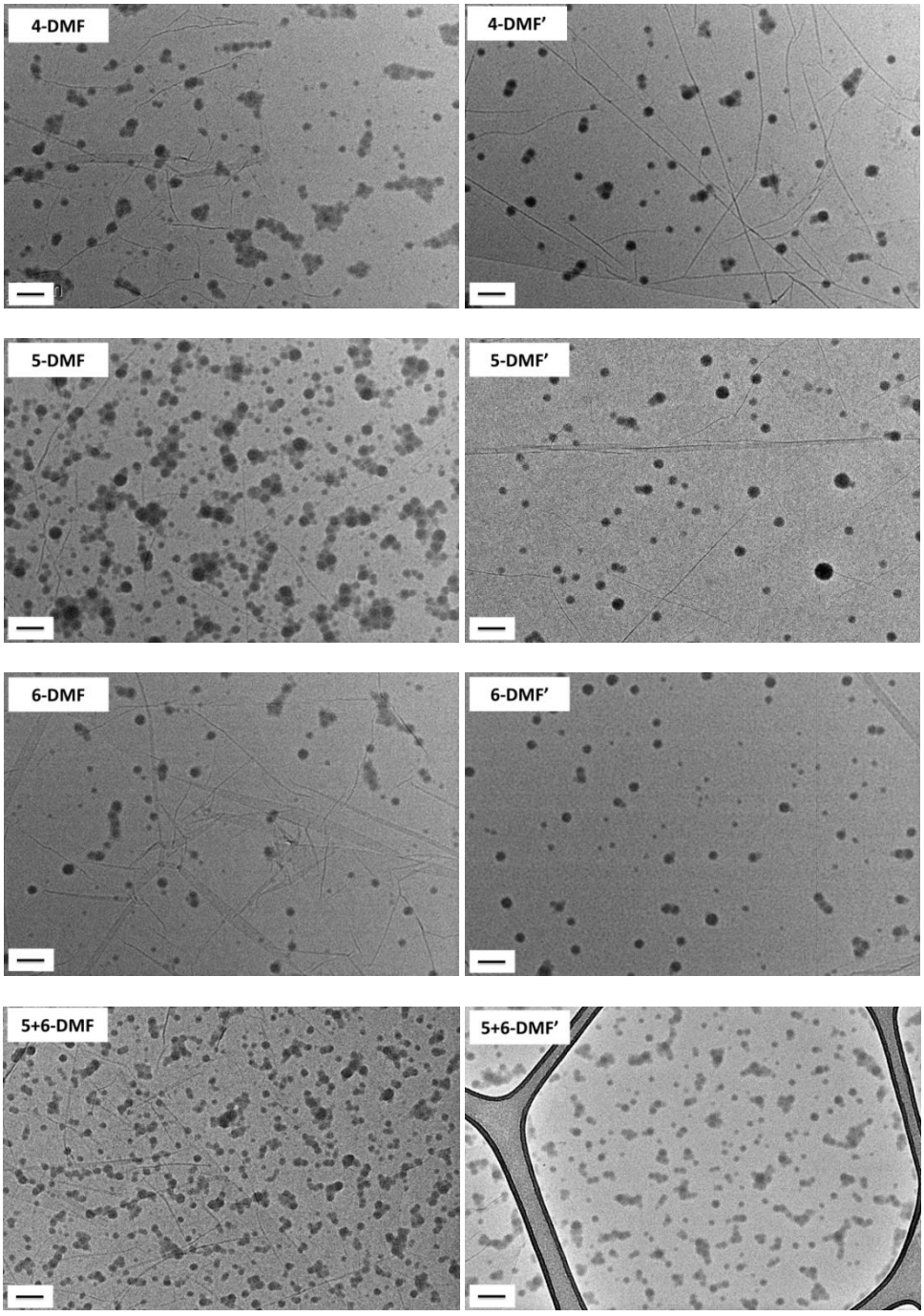

Figure 5.25 Representative TEM images of self-assemlbies **4-DMF**, **5-DMF**, **6-DMF** and **5+6-DMF** and their corresponding anealed self-assemblies **4-DMF'**, **5-DMF'**, **6-DMF'** and **5+6-DMF'** (annealing conditions: 15 – 85°C and then 85 – 15 °C with a rate of 1 °C/min for 3 cycles). Scale bar: 100 nm.

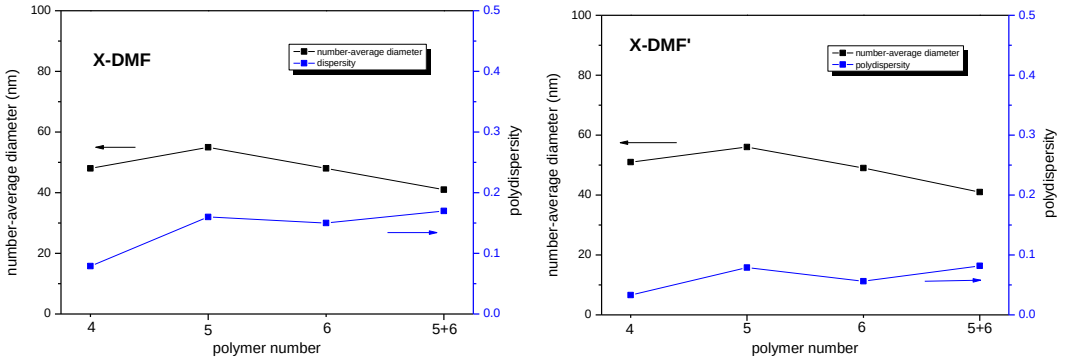

Figure 5.26 DLS analysis of self-assemlbies **4-DMF**, **5-DMF**, **6-DMF**, **5+6-DMF** and their corresponding annealed self-assemblies **4-DMF'**, **5-DMF'**, **6-DMF'** and **5+6-DMF'** (annealing conditions: 15 – 85°C and then 85 – 15 °C with a rate of 1 °C/min for 3 cycles).

5.3.11 Self-assembly of 4 – 6 by solvent switch using DMSO as a common solvent

When DMSO was used as the common solvent, bicontinuous structures were obtained from polymers **1** – **3** and moreover a morphology transition was observed with annealing. However, as mentioned above, polymers **1** – **3** were not stable in the presence of water and with annealing. To eliminate the possibility that the formation of bicontinuous structures and the transition of morphologies were induced by hydrolysis of the polymers, self-assemblies of polymers **4** – **6** were prepared in a similar way to polymers **1** – **3** by the solvent switch method using DMSO as a common solvent. In addition, effects of annealing conditions, polymer concentrations, and water content on the resulting self-assemblies were studied, followed by a kinetic study of the morphology transition with annealing.

5.3.11.1 Self-assembly and effect of annealing

Polymers **4**, **5**, **6** and a 1:1 mixture of **5** and **6** were dissolved in DMSO with a concentration of 8 mg/mL. Water was then added to the solutions at a rate of 1 mL/h until the final volume ratio between water and DMSO was 8:1. The solutions were then dialyzed against water to remove DMSO and the final concentration was estimated by measuring the final volume, which were approximately 1 mg/mL. Self-

assemblies of **4**, **5**, **6** and a 1:1 mixture of **5** and **6** were diluted to 0.05 mg/mL before being characterized by TEM and DLS analysis (Figure 5.27, **X-DMSO**, **X** is the polymer number). All the polymers were fully soluble in DMSO. Upon addition of water to the solution, bicontinous micelles were again observed when using polymer **4**, $POEGMA_{70}$-*b*-($PAMA2_{0.5}$-*co*-$PTMA2_{0.5}$)$_{122}$ (Figure 5.27, **4-DMSO**). However, the size distribution of the particles was slightly broad (PD = 0.29) with two populations by DLS analysis. We assumed that the high initial polymer concentration had an effect on the broad size distribution and therefore the effect of lower initial polymer concentrations is discussed later. When polymer **5,** $POEGMA_{70}$-*b*-$PAMA2_{126}$ was used, precipitation occurred similar to the behavior of polymer **2** and therefore no TEM images were obtained for **5**. Self-assembly of polymer **6**, $POEGMA_{70}$-*b*-$PTMA2_{124}$ led to the formation of clustered structures (Figure 5.27, **6-DMSO**), which unexpectedly possessed a size distribution of 0.24 with one population by DLS analysis. When a 1:1 mixture of **5** and **6** was assembled, bicontinuous micelles were also observed, although they were smaller in size compared to those obtained from polymer **4** (Figure 5.27, **5+6-DMSO**). These particles had a narrow size distribution with only one population (PD = 0.083) by DLS analysis. Compared to the self-assemblies prepared from polymers **1** – **3** using the same method, the resultant morphologies prepared from polymers **4** – **6** were not exactly the same. For copolymers containing both adenine and thymine, polymer **1** and **4**, nanoparticles prepared from **4** (421 nm) had bigger size than it from polymer **1** (180 nm). For adenine-containing polymer, **2** and **5**, precipitation occurred during both assembly processes. When thymine-containing polymers, **3** and **6**, were investigated, well-defined spheres were observed from polymer **3** and clustered micelles were formed from polymer **6**. In the case of a 1:1 mixture of adenine

polymer and thymine polymer, **2+3** and **5+6**, micelles with internal structures were both observed, however particles prepared from **5+6-DMSO** possessed smaller diameter (**5+6-DMSO**: 181 nm; **2+3-DMSO**: 212 nm). These similarity and difference were due to the slight structural variation of the nucleobase-containing blocks. Polymers **4** – **6** were expected not to hydrolyze and moreover possessed shorter linkers between the polymer backbones and nucleobase functionalities, which may lead to less mobile polymer chains.

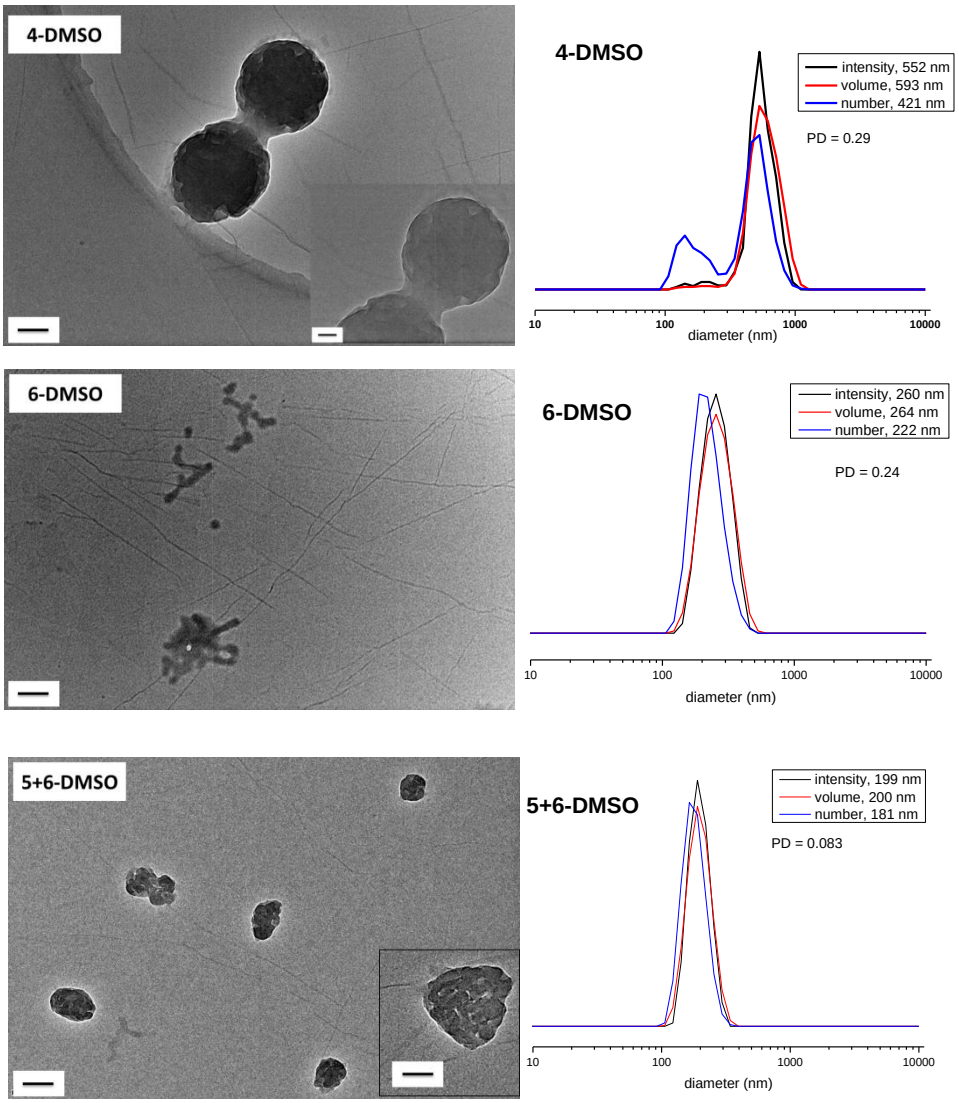

Figure 5.27 Representative TEM and DLS analysis of self-assemblies prepared from polymers **4**, **6**, a 1:1 mixture of **5** and **6** by a solvent-switch method using DMSO as the common solvent: **4-DMSO**, **6-DMSO**, and **5+6-DMSO**. Scale bar: 100 nm (inset 50 nm).

Annealing was then applied to 0.2 mg/mL solutions of **4-DMSO**, **6-DMSO**, and **5+6-DMSO** (named as **X-DMSO'**, **X** is the polymer number). The annealing condition was the same as it for polymers **1** – **3**, where the samples were heated up from 15 °C – 85 °C and then cooled down from 85 °C – 15 °C with a rate of 1 °C/min for 3 cycles. The annealing experiments were performed on a variable-temperature UV-vis spectrometer (λ = 500 nm). The samples were diluted to 0.05 mg/mL before being characterized by TEM and DLS analysis (Figure 5.28). By DLS analysis, it was found that all the annealed samples possessed narrower size distributions than those before annealing. In addition, morphology changes were obtained for all the samples observed by dry-state TEM microscopy. For polymer **4**, hollow structures were observed, some of which appeared with multiple layers (Figure 5.28, **4-DMSO'**). These hollow structures were apparently different from the self-assemblies before annealing (**4-DMSO**) and also seemed more complex than **1-DMSO'** which were obtained from annealed **1-DMSO** prepared from polymer **1**. Vesicles were also observed by annealing **6-DMSO** prepared from polymer **6** (**6-DMSO'**). The self-assemblies after annealing were different but much better-defined than those before annealing. For a 1:1 mixture of **5** and **6**, hollow structures with single or multiple layers were observed, suggesting there was a solid-hollow transition induced by annealing. These observations obtained from polymer **4** – **6** were very similar to those of polymer **1** – **3**, which suggested that the morphology transition observed in polymer **1** – **3** was induced by the annealing itself rather than hydrolysis of the polymers.

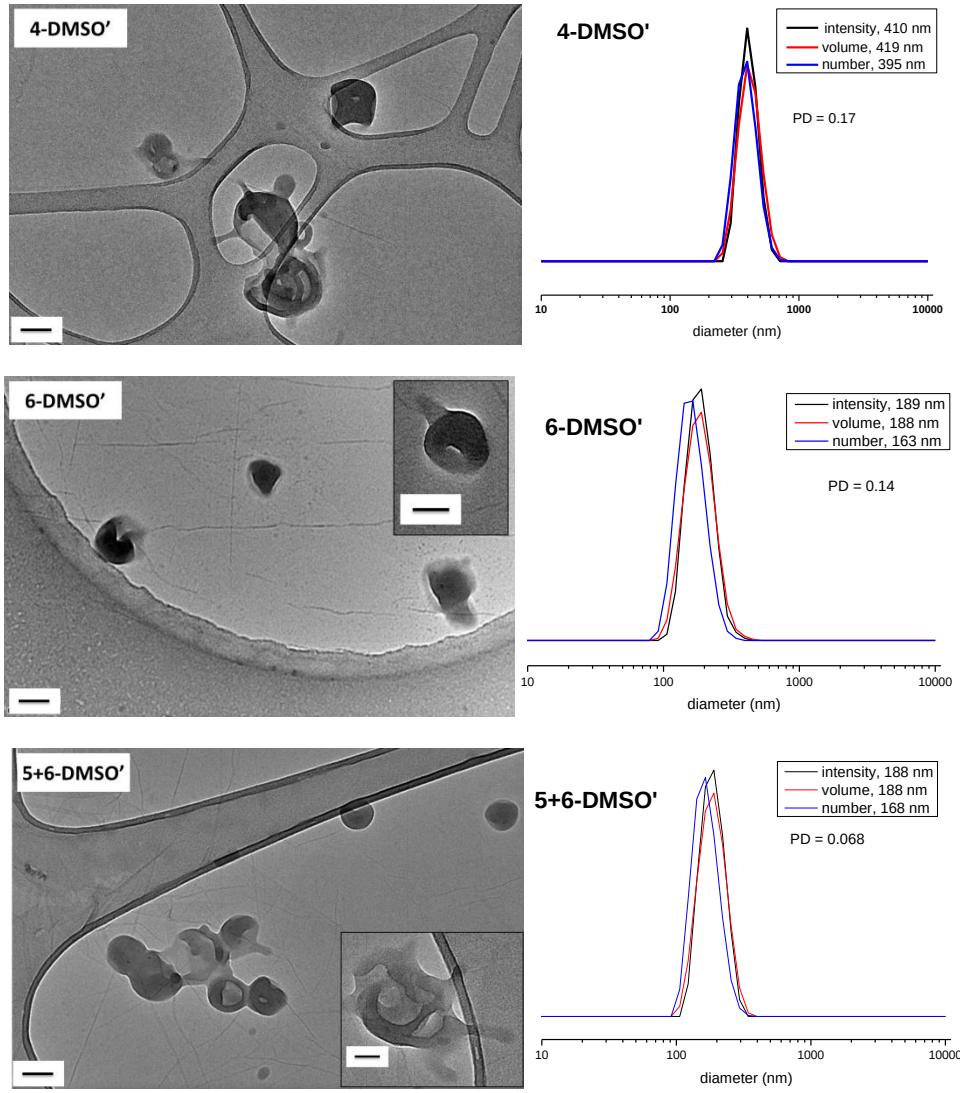

Figure 5.28 Representative TEM and DLS analysis of self-assemblies **4-DMSO'**, **6-DMSO'**, and **5+6-DMSO'** annealed from 0.2 mg/mL solutions of **4-DMSO**, **6-DMSO**, and **5+6-DMSO** (annealing conditions: 15 °C – 85°C and then 85 °C – 15 °C with a rate of 1 °C/min for 3 cycles). Scale bar: 100 nm (inset 50 nm).

Solutions of **4-DMSO** and **4-DMSO'** were also characterized by cryo-TEM to allow access to more details about the structures in a solution state. Bicontinuous micelles with internal hairy structures were clearly observed for **4-DMSO** at different concentration, 1 mg/mL (Figure 5.29a) and 0.2 mg/mL (Figure 5.29b). Self-assemblies appeared to have the same morphology at these two concentrations, showing that dilution had no effect on the morphology. In comparison, onion-like vesicles were observed for annealed solution **4-DMSO'** (Figure 5.29, c and d). The morphologies from cryo-TEM were consistent with the observations by dry-state

TEM, yet more internal details were provided. Self-assemblies **5+6-DMSO** and its annealed solution **5+6-DMSO'** were also characterized by cryo-TEM analysis (Figure 5.29, e and f). These observations further confirmed that a morphology transition occurred with annealing.

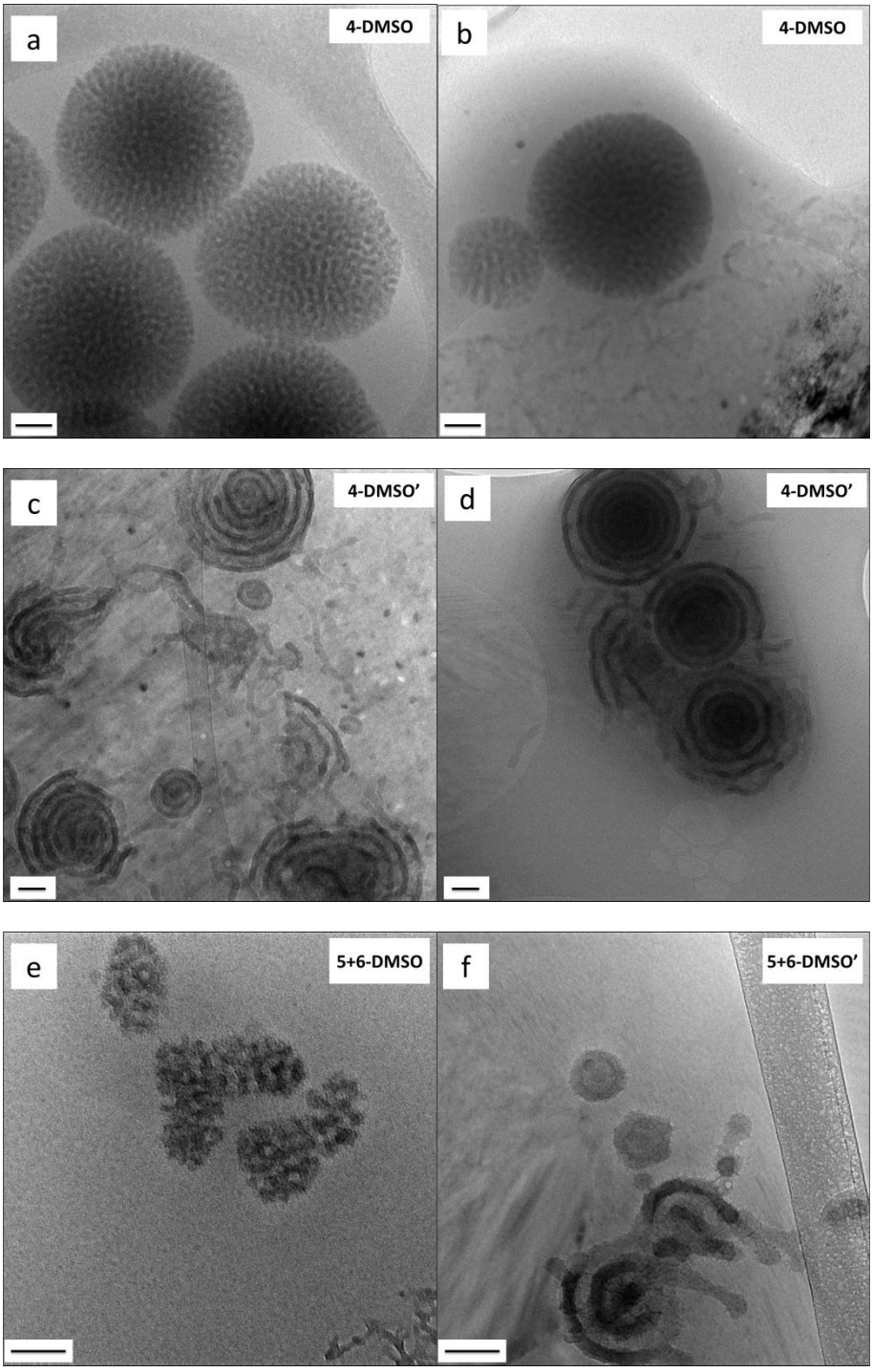

Figure 5.29 Cryo-TEM images of self-assemblies (a) **4-DMSO**, 1mg/mL; (b) **4-DMSO**, 0.2mg/mL and its annealed sample **4-DMSO'** , 0.2 mg/mL (c,d); (e) **5+6-DMSO**, 1 mg/mL; (f) **5+6-DMSO'**, 0.2 mg/mL. Scale bar: 100 nm.

However, compared to polymers **1** – **3**, the self-assembled structures prepared from polymers **4** – **6**, before and after annealing, had a similar trend yet were not identical which might be due to the differences of nucleobase-containing blocks. As mentioned above, nucleobase blocks in polymers **4** – **6** were expected to be more stable in water, less mobile due to the shorter linkers, and possess more nucleobase functionalities in the backbones, which would affect the degrees of stretching of polymer chains and strength of nucleobase interactions among polymers. Holder and Sommerdijk *et al.* reported the formation of bicontinuous micelles and multilamellar vesicles from a block copolymer poly(ethylene oxide)$_{52}$-*b*-poly(*n*-butyl methacrylate)$_{86}$, which may result from the different polymer curvature in THF and 1,4-dioxane.[27] In our study, these two morphologies were also formed from one polymer, (*i.e.*, polymer **4**, POEGMA$_{70}$-*b*-(PAMA2$_{0.5}$-*co*-PTMA2$_{0.5}$)$_{122}$), but induced by annealing rather than the identity of solvent. These observations indicated that the apparent polymer dimensions before and after annealing were altered, leading to different resultant morphologies. We assume that annealing firstly made polymer chains mobile and then resulted in a chain rearrangement, which further altered the apparent polymer curvatures and eventually resulted in the structures observed. Recently, Holder and coworkers further investigated poly(ethylene oxide)-*b*-poly(octadecyl methacrylate) (PEO-*b*-PODMA) system and reported the importance of hydrophilic weight fractions on the types of nanoparticles and sizes of internal pore sizes.[29] From the phase diagram they established, bicontinuous particles were formed from polymers with relatively low PEO content ($f \leq 0.25$), while multi-lamellar morphologies were present with intermediate PEO content ($0.25 \leq f \leq 0.31$).[29] Herein, in our study, the POEGMA weight fraction was *ca.* 0.4, which was a

slight high compared to the diagram, but considering the difference in polymer structure and composition, the results were still reasonable.

Moreover, we think the rearrangement of polymer chains in our case is expected to decrease the total free energy of the system, which is more thermodynamically favorable. In Holder's work, the bicontinuous micelles formed from PEO-*b*-PODMA were both kinetically and thermodynamically stable under the conditions observed, which could be reversibly reformed upon heating and cooling cycles.[26,29,31] In comparison, in our study, the morphology transition was not reversible. We assumed that the bicontinuous micelles obtained in this study were kinetically frozen due to the high water content and poor mobility of nucleobase-containing polymer chains at room temperature. However, the bicontinuous micelles still reflected the thermodynamics at the point where the structures became frozen. We suggest that before the structures were frozen, the aggregates adapted their shape and organization to minimize the surface energy and thus led to the formation of bicontinuous micelles that were thermodynamically stable at that point. Additionally, we hypothesize that nucleobase-containing chains randomly interact with each other at this point. However, with annealing, the polymer chains became mobile and tended to interact in a relatively complementary way, thus more favorable thermodynamic equilibrium had a tendency to be reached, which led to the formation of new morphologies.

Finally, it should be mentioned that self-assembly behavior was different among polymers **4** – **6**. As mentioned above, in this study the presence of adenine-thymine interactions was critical in the formation of bicontinuous nanoparticles, while individual adenine or thymine polymer appeared poor capability of stabilizing particles or driving into well-organized structures. Previously van Hest and

coworkers investigated the self-assembly behavior of PEO_{45}-*b*-poly(adenine)$_{11}$, PEO_{45}-*b*-poly(thymine)$_{14}$ and a mixture of the two. It was found that the mixtures exhibited different self-assembly behavior compared to individual polymers, which possessed a higher critical aggregation concentration (CAC) and one population of self-assembly while the self-assembly of individual polymer had two populations.[6] Owing to the difference in polymer composition, the results were not directly comparable, but the observation that the presence of adenine-thymine interactions affected the self-assembly behavior could be drawn from both their investigation and our study in this Chapter.

5.3.11.2 Study on polymers' stability before and after annealing

In Section 5.3.9, we have shown that the polymers were stable in the presence of water at 60 °C. To prove that the polymers were still stable after self-assembly and annealing, polymer **4**, $POEGMA_{70}$-*b*-$(PAMA2_{0.5}$-*co*-$PTMA2_{0.5})_{122}$ was harvested from **4-DMSO** and **4-DMSO'** and then characterized by both ^{1}H NMR spectroscopy and SEC chromatography.

In order to harvest enough polymer for ^{1}H NMR spectroscopy characterization, **4-DMSO** with a concentration of 1 mg/mL was directly annealed without dilution. No precipitations were observed after 3 cycles of annealing. **4-DMSO'** with a concentration of 1 mg/mL was firstly characterized by TEM to prove the successful annealing (Figure 5.30 (1)). Hollow structures with multiple layers were observed, showing that the concentration of the annealed solution had little effect on the resultant morphologies. Solutions **4-DMSO** and **4-DMSO'** were freeze-dried and the obtained polymers were then characterized by both SEC chromatography (DMF as eluent, PMMA as standards) and ^{1}H NMR spectroscopy. No obvious differences of molecular weight and molecular weight distribution were observed for polymer **4**

before and after annealing (Figure 5.30 (2)), suggesting that the polymers were stable during the annealing procedure. In addition, ^{1}H NMR spectra of polymers harvested before and after annealing were identical to spectra before self-assembly (Figure 5.30 (3) and (4)), indicating that polymers were stable during the whole self-assembly process.

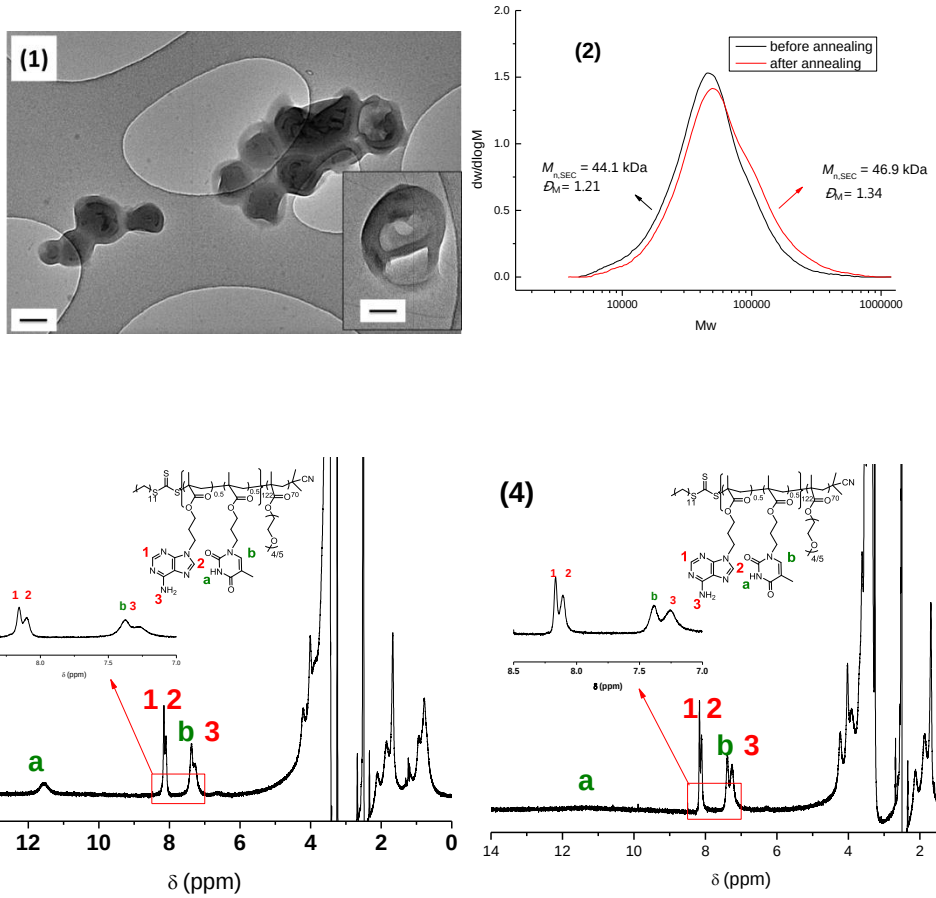

Figure 5.30 Representative TEM image of **4-DMSO'** with a concentration of 1 mg/mL (1); SEC traces of polymer **4** harvested from solution **4-DMSO** and **4-DMSO'** (2); ^{1}H NMR spectra of polymer **4** harvested from solution: **4-DMSO** (3); **4-DMSO'** (4).

5.3.11.3 Effect of annealing conditions

In this Section, annealing conditions and their effects on resultant morphologies were investigated. The annealing condition we used above included 3 heating-cooling cycles, where a solution was heated from 15 °C to 85 °C and then cooled from 85 °C to 15 °C at a rate of 1 °C/min. We assume that the annealing rate and relaxation time affected the resultant morphologies. In other words, a slow annealing rate was

considered as a key parameter for the formation of well-defined structures and morphology transitions, as polymer chains might have enough time to rearrange. To prove this hypothesis, solution **4-DMSO** prepared from polymer **4**, $POEGMA_{70}$-*b*-$(PAMA2_{0.5}$-*co*-$PTMA2_{0.5})_{122}$ with a concentration of 0.2 mg/mL was heated at 85 °C for 45 min and then cooled down slowly to 30 °C in an oil bath for *ca.* 60 min. It was observed that the temperature dropped fast at high temperature range (from 85 °C to 55 °C, *ca.* 20 min) and then slowly. Although both POEGMA and nucleobase blocks were insoluble at 85 °C, due to the low concentration, there was no precipitation by visual inspection, but we assume the structures were metastable. The resultant solution was diluted to 0.05 mg/mL and then characterized by TEM and DLS analysis (Figure 5.31). Poor-defined sheet-like structures were observed rather than bicontinuous micelles or onion-like vesicles. We assume that these structures were mainly caused by the aggregation of POEGMA at 85 °C, although a rearrangement of nucleobase-containing blocks also had an effect. This result suggested that the slow annealing rate and the relaxation time play a key role in the formation of well-defined onion-like structures.

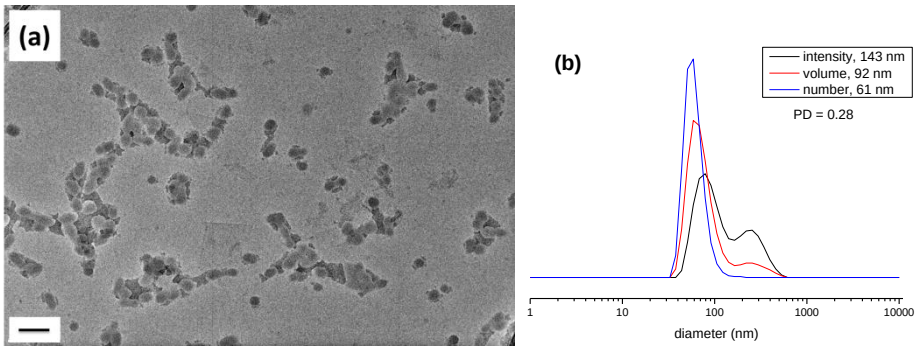

Figure 5.31 Representative TEM image and DLS analysis of **4-DMSO** heated at 85 °C for 45 min and then cool down in an oil bath naturally. Scale bar: 100 nm.

In addition, the effect of temperature was also investigated. As POEGMA had a cloud point around 65 °C, the highest annealing temperature was set to 60 °C for comparison. Herein, solution **4-DMSO** with a concentration of 0.2 mg/mL was

annealled by two methods: (a) the solution was heated at 60 °C for 45 min and then cooled down in an oil bath slowly (*ca*. 50 min, from 60 °C to 30 °C, non-constant rate); (b) the solution was heated from 15 °C – 60 °C and then cooled down from 60 °C – 15 °C at a rate of 1 °C/min, which was repeated 3 times in total. The observed morphology was no longer bicontinuous micelles in samples prepared by both method (a) and method (b), yet onion-like vesicles were also not formed (Figure 5.32). Small aggregations were observed in the sample annealed using method (a) (Figure 5.32 a), indicating the nucleobase-containing blocks become slightly mobile at 60 °C and thus the bicontinuous micelles disassembled. However, the thermodynamic favorable onion-like structures were not formed as the annealing temperature was not high enough. When method (b) was applied where the annealing rate was consistent with previous annealing procedure (1 °C/min), chrysanthemum-like aggregations were observed which possessed a few cylindrical tentacles (Figure 5.32 b). This observation further suggested that bicontinuous micelles were not the most thermodynamically favorable structure and were disassembled with annealing. However, due to the relatively low annealing temperature, the polymer chains were not mobile and stretching enough to form thermodynamic reachable and well-defined onion-like structures.

Based on the above observations, we assume that both annealing temperature and annealing rate are key parameters for the morphology transition from bicontinuous micelles to onion-like vesicles. If optimized annealing rates and temperatures were utilized, well-define structures like onion-like vesicles could be formed as they were more thermodynamically favorable. In addition, these observations further indicate that the bicontinuous structure in our study was metastable.

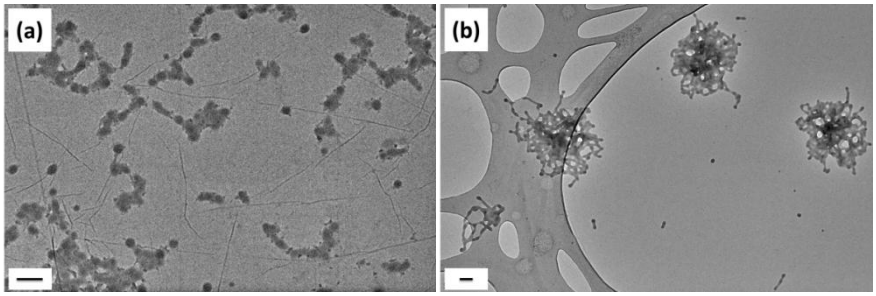

Figure 5.32 Representative TEM images of **4-DMSO** annealed by different methods: (a) sample was heated at 60 °C for 45 min and then cool down in an oil bath naturally; (b) sample was heated from 15 °C – 60 °C and then cooled down from 60 °C – 15 °C at a rate of 1 °C/min, which was repeated 3 times in total. Scale bar: 100 nm.

5.3.11.4 Effect of polymer concentration and water content

Initial polymer concentration was kept at 8 mg/mL in the common solvent in the previous section. Herein, polymer solutions in DMSO with a lower initial concentration (2 mg/mL) were prepared and the effect of concentration and water content on the resultant morphologies was investigated.

Polymers **4**, **5**, **6** and a 1:1 mixture of **5** and **6** were dissolved in DMSO at a concentration of 2 mg/mL. Water was then added to the solution at a rate of 1 mL/h until final volume ratio between water and DMSO was 8:1, which was the same as the preparation method for **X-DMSO**. The resultant solutions were dialyzed to remove DMSO and the final concentrations were estimated to be about 0.2 mg/mL. The solutions (**X-DMSO-2a**, **X** is the polymer number) was then diluted to 0.05 mg/mL and characterized by TEM and DLS analysis (Figure 5.33 and Figure 5.34). In general, similar structures were observed compared to **X-DMSO** which had higher initial polymer concentrations (8 mg/mL). For polymer **4**, $POEGMA_{70}$-*b*-$(PAMA2_{0.5}$-*co*-$PTMA2_{0.5})_{122}$, bicontinuous micelles were observed by TEM analysis (Figure 5.33, **4-DMSO-2a**) although the particles possessed smaller sizes (155 nm) compared to micelles prepared from **4-DMSO** (421 nm). However, the size distribution was not improved significantly. For polymer **5**, $POEGMA_{70}$-*b*-$PAMA2_{126}$ polymers did not obviously precipitate when lower polymer

concentration was used. Spherical micelles were observed by TEM microscopy (Figure 5.33, **5-DMSO-2a**). However, the resultant particles possessed a broad size distribution as observed by both TEM and DLS analysis (PD = 0.41). When polymer **6**, POEGMA$_{70}$-*b*-PTMA2$_{124}$ was studied, clustered structures were again observed (**6-DMSO-2a**), which were very similar to self-assemblies prepared from **6-DMSO**. For a 1:1 mixture of **5** and **6**, bicontinuous micelles with an average diameter of 97 nm were observed (**5+6-DMSO-2a**), which had a similar shape to **5+6-DMSO** yet smaller size (**5+6-DMSO**: 181 nm). These results showed that the initial polymer concentration had little effect on the resultant morphologies but affected the sizes of particles.

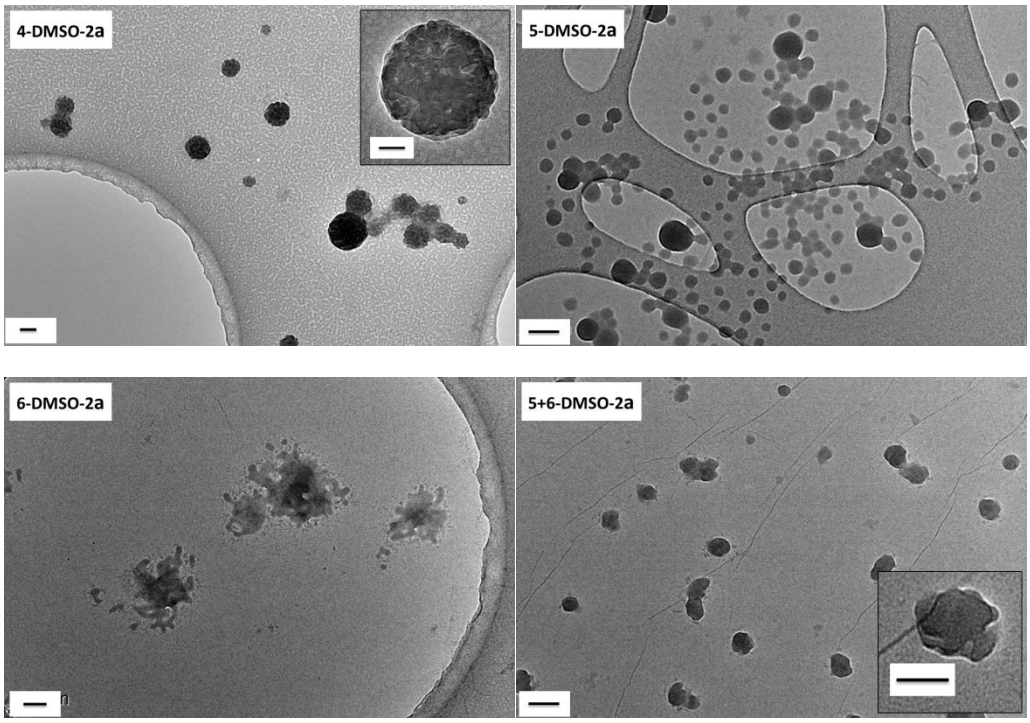

Figure 5.33 Representative TEM analysis of self-assemblies prepared from polymers **4**, **5**, **6**, a 1:1 mixture of **5** and **6** with an initial concentration of 2 mg/mL by solvent-switch method using DMSO as the common solvent: **4-DMSO-2a**, **5-DMSO-2a**, **6-DMSO-2a**, and **5+6-DMSO-2a**. Scale bar: 100 nm (inset 50 nm).

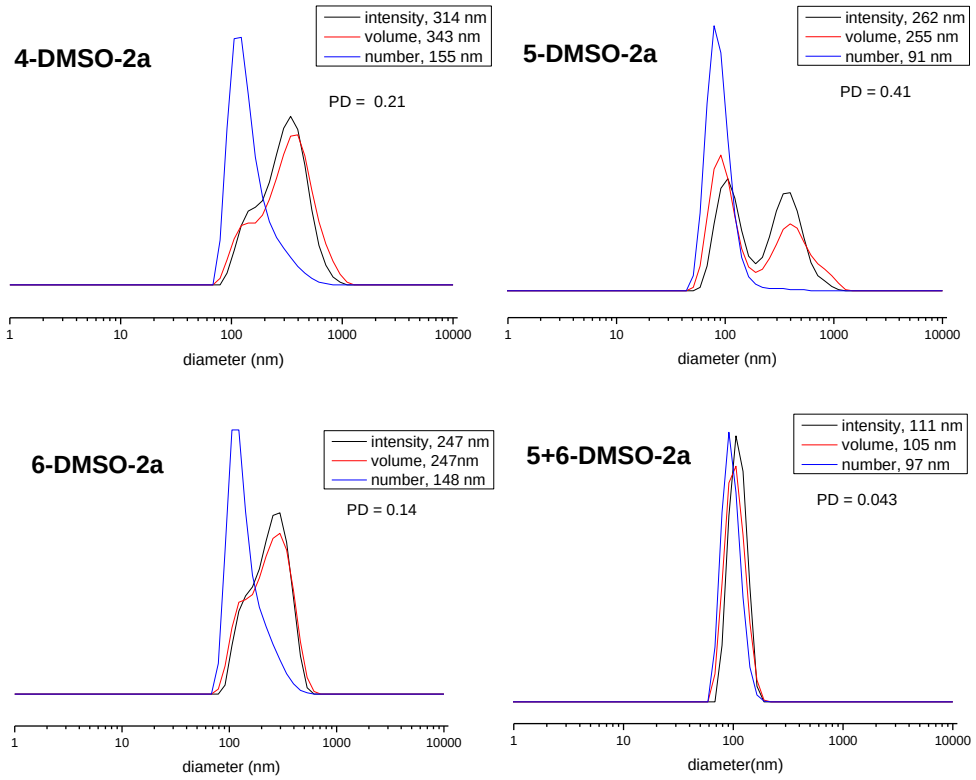

Figure 5.34 DLS analysis of self-assemblies prepared from polymers **4**, **5**, **6**, a 1:1 mixture of **5** and **6** with an initial concentration of 2 mg/mL by solvent-switch method using DMSO as the common solvent: **4-DMSO-2a**, **5-DMSO-2a**, **6-DMSO-2a**, and **5+6-DMSO-2a**.

The above self-assemblies **X-DMSO-2a** at a concentration of 0.2 mg/mL were annealed. The annealing condition used was the same as it for **X-DMSO**, which included 3 heating-cooling cycles with a temperature range from 15 °C to 85 °C (1 °C/min). The annealed samples (**X-DMSO-2a'**) were diluted to 0.05 mg/mL and characterized by TEM and DLS analysis. Similar morphologies were observed compared to **X-DMSO'**. In addition, a solid-hollow transition was observed for polymers **4**, **6**, and a 1:1 mixture of **5** and **6** (Figure 5.35), indicating the occurrence of rearrangement of polymer chains. In comparison, for polymer **5**, micelles were still solid after annealing, as the mobility of PAMA2 was poor and the core dimensions of spheres were limited, thus no morphology transition was observed. In conclusion, we have shown that polymer concentration had little effect on morphologies of self-assemblies but affected their sizes.

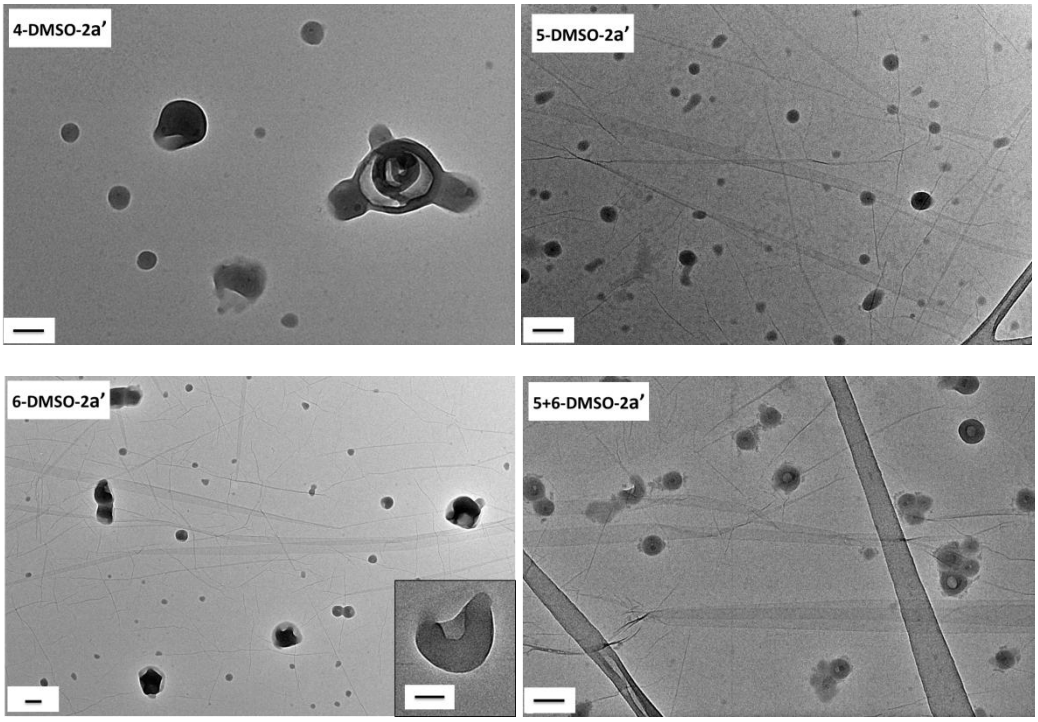

Figure 5.35 Representative TEM analysis of self-assemblies **4-DMSO-2a'**, **5-DMSO-2a'**, **6-DMSO-2a'**, and **5+6-DMSO-2a'** prepared by annealing **4-DMSO-2a**, **5-DMSO-2a**, **6-DMSO-2a**, and **5+6-DMSO-2a**, (annealing conditions: 15 °C – 85°C and then 85 °C – 15 °C with a rate of 1 °C/min for 3 cycles). Scale bar: 100 nm (inset 50 nm).

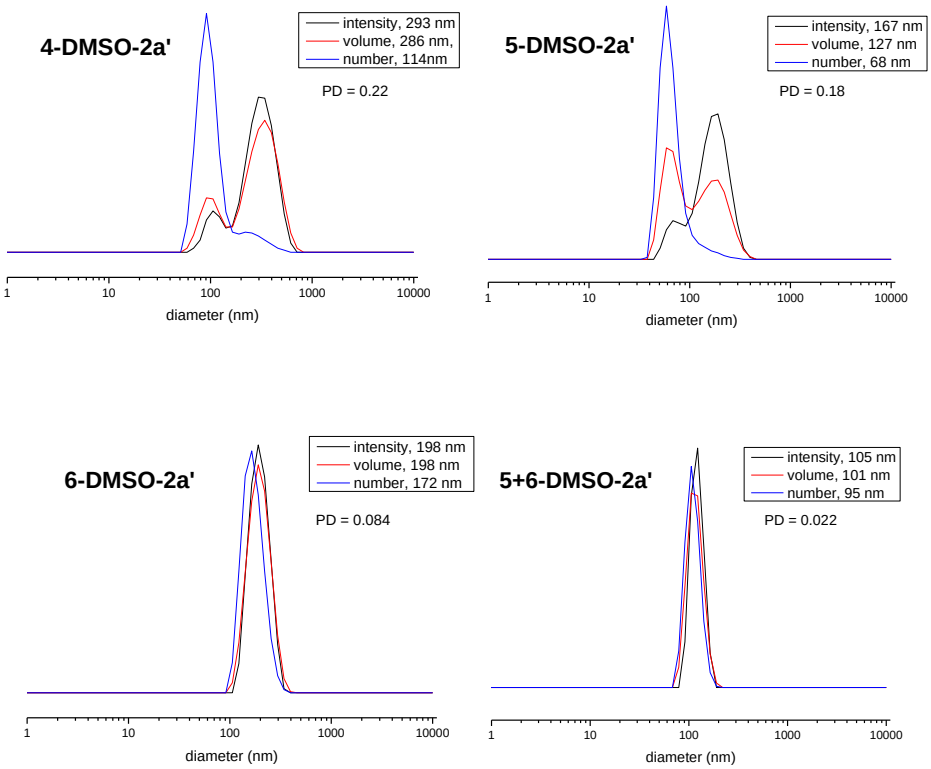

Figure 5.36 DLS analysis of self-assemblies **4-DMSO-2a'**, **5-DMSO-2a'**, **6-DMSO-2a'**, and **5+6-DMSO-2a'** prepared by annealing **4-DMSO-2a**, **5-DMSO-2a**, **6-DMSO-2a**, and **5+6-DMSO-2a**, (annealing conditions: 15 °C – 85°C and then 85 °C – 15 °C with a rate of 1 °C/min for 3 cycles).

Water content which is one of the key factors affecting morphologies was also investigated. Polymer concentration in DMSO was kept at 2 mg/mL. Water was then added to the solutions at a rate of 1 mL/h until the final volume ratio between water and DMSO was 2:1 (previous study was 8:1). The solutions were dialyzed against water to remove DMSO and the final concentration was approximately 0.6 mg/mL. The solutions were diluted to 0.05 mg/mL before being characterized by TEM and DLS analysis. Self-assemblies prepared from polymers **4**, **5**, **6** and a 1:1 mixture of **5** and **6** were investigated (**X-DMSO-2b**, **X** is polymer number). The results were generally consistent with **X-DMSO-2a**, indicating the little effect of water content on the resultant morphologies (Figure 5.37, left). We assume very similar morphologies are observed because the morphologies became kinetically frozen below the final water contents for both **X-DMSO-2a** and **X-DMSO-2b**. Samples **X-DMSO-2b** were subsequently annealed and a similar morphology transition was also observed (Figure 5.37, right, **X-DMSO-2b**').

In addition, cryo-TEM was conducted on **4-DMSO-2b** and its annealed solution **4-DMSO-2b'** to provide more detailed information on the morphologies (Figure 5.38). Bicontinuous micelles with dentritic internal structures were clearly observed from sample **4-DMSO-2b** prepared before annealing (Figure 5.38, 1 and 2), while onion-like structures were observed from sample **4-DMSO-2b'** which was obtained after 3 annealing cycles (Figure 5.38, 3 and 4). However, compared to the morphologies of **4-DMSO** and **4-DMSO'** (polymer concentration: 8 mg/mL; water content: 8:1), the dimensions of the structures were smaller. Moreover, **5+6-DMSO-2b** and its annealed **5+6-DMSO-2b'** were also characterized by cryo-TEM (Figure 5.38, 5 and 6). These studies further prove that a morphology transition was induced by annealing and moreover the studied water contents and polymer concentrations had

little effect on the resultant morphologies yet altered the dimensions of the self-assemblies.

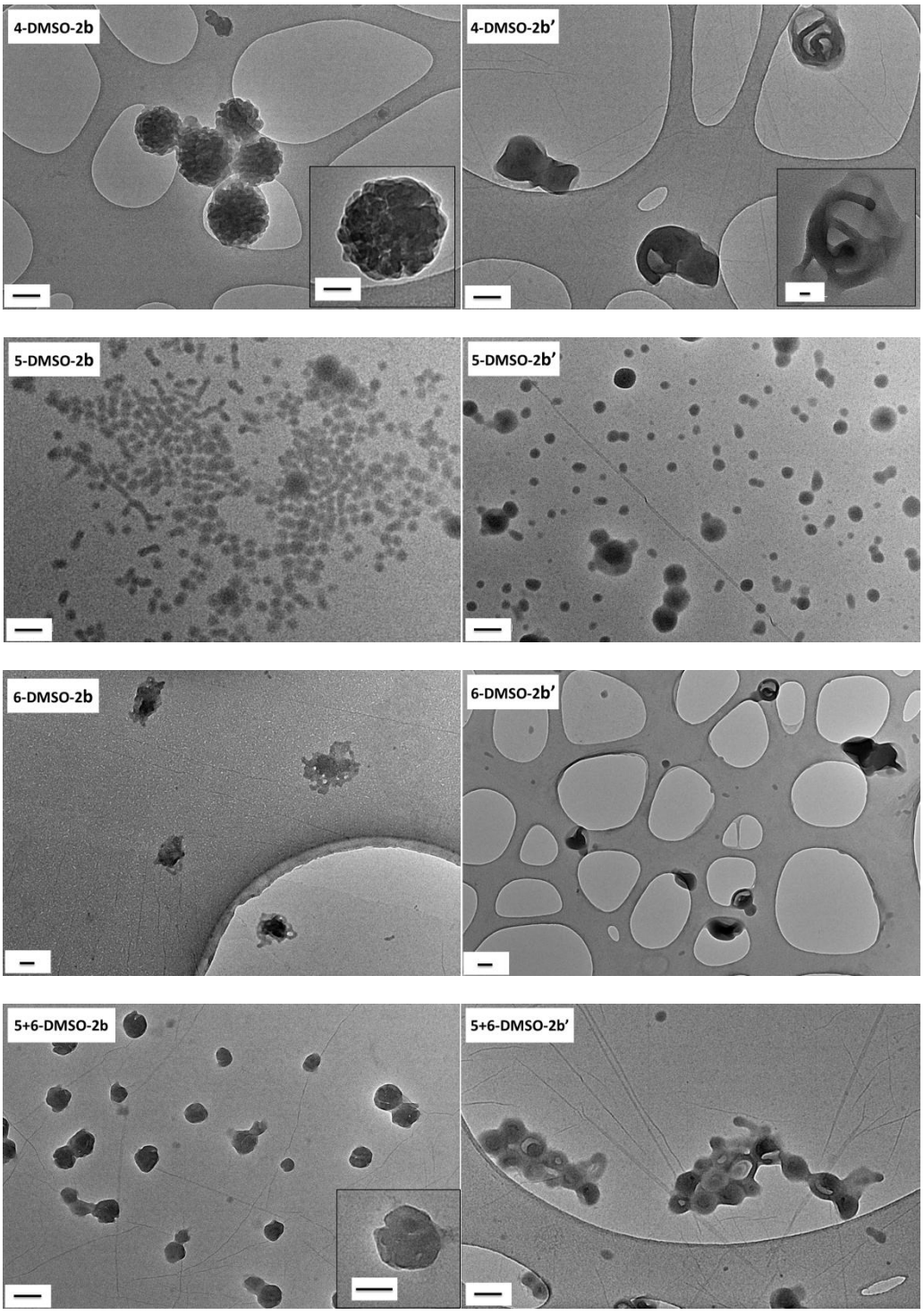

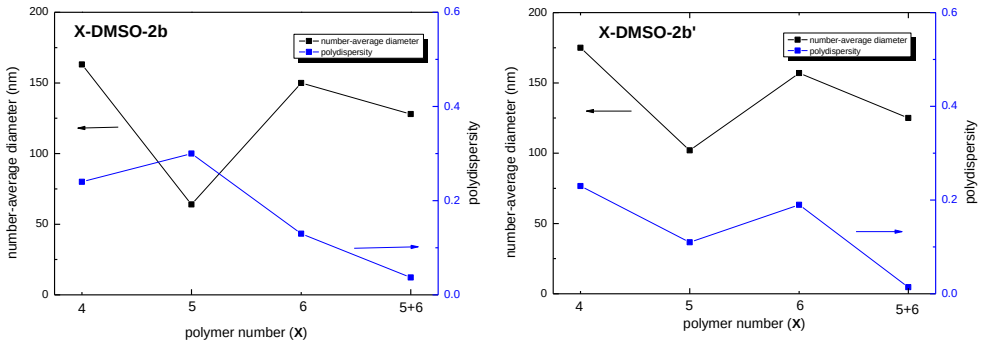

Figure 5.37 Representative TEM images and DLS analysis of self-assemblies **4-DMSO-2b**, **5-DMSO-2b**, **6-DMSO-2b**, and **5+6-DMSO-2b** and their corresponding annealed self-assemblies **4-DMSO-2b'**, **5-DMSO-2b'**, **6-DMSO-2b'**, and **5+6-DMSO-2a'** (annealing conditions: 15 °C – 85°C and then 85 °C – 15 °C with a rate of 1 °C/min for 3 cycles).Scale bar: 100 nm (inset 50 nm).

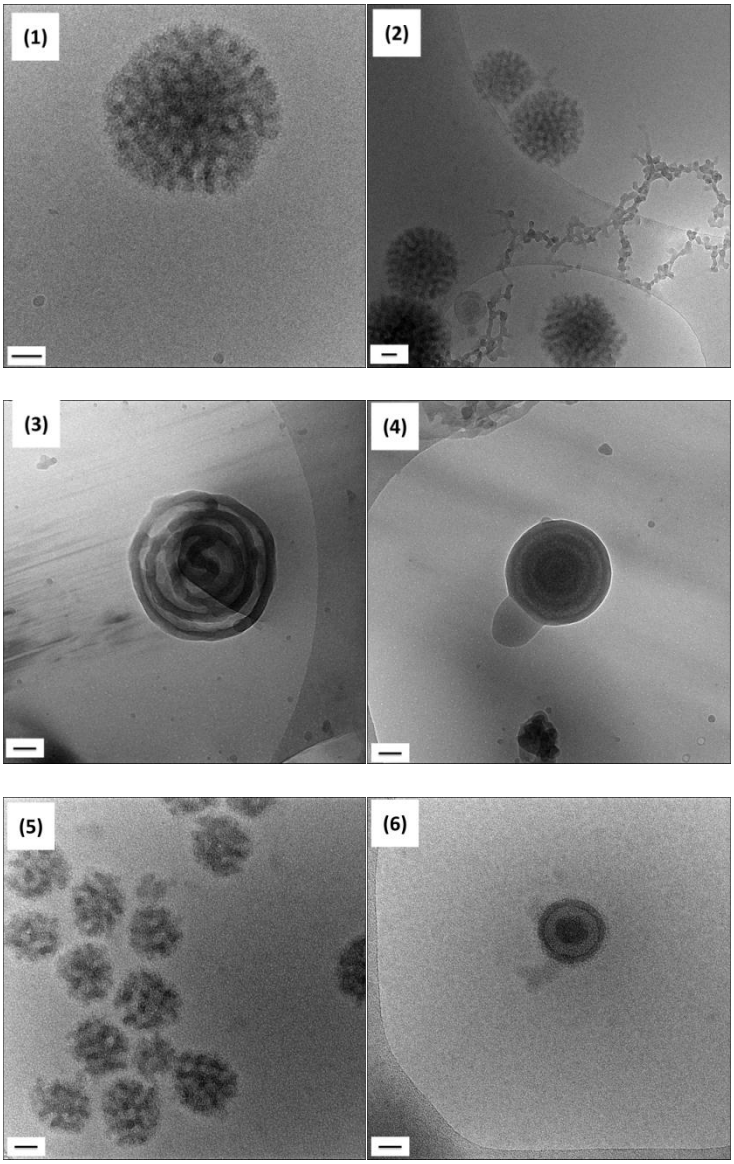

Figure 5.38 Cryo-TEM images of self-assemblies: **4-DMSO-2b** (1) and (2); its annealed sample **4-DMSO-2b'** (3) and (4); **5+6-DMSO-2b** (5); **5+6-DMSO-2b'** (6). Scale bar: 50 nm.

5.3.11.5 Effect of annealing cycles on morphologies

For polymer **4**, annealing cycles were always repeated 3 times to achieve the morphology transition from bicontinuous micelles to onion-like structures. Herein the effect of annealing cycles on morphologies was investigated for solution **4-DMSO-2b** with a concentration of 0.2 mg/mL. The solutions obtained after each annealing cycle were characterized by TEM and DLS analysis (Figure 5.39). It was found that after the first annealing cycle the bicontinuous micelles (Figure 5.39, cycle 0) were rearranged into particles with tentacles (Figure 5.39, cycle 1), indicating the mobility of polymer chains was increased. After the second annealing cycle, the particles were rearranged further and moreover the tentacles started to fuse (Figure 5.39, cycle 2). Finally, vesicle structures with multiple layers were formed after the third annealing cycle (Figure 5.39, cycle 3). If the multilamellar vesicles were annealed for a further 3 cycles (Figure 5.39, cycle 6), no obvious change was observed, indicating that the onion-like structures were thermodynamically favorable. The transition was also characterized by cryo-TEM analysis (Figure 5.40), which was consistent with the results from dry-state TEM analysis. However, more details on the internal structures could be observed by cryo-TEM analysis, which provided insights into understanding the process of this morphology transition.

These observations show that the first three annealing cycles were vital to the formation of onion-like structures. Once the thermodynamic equilibrium was reachable, the transition was accomplished and the structures were retained. In addition, this kinetic study provided insight into understanding the transition from bicontinuous micelles to onion-like structures. As we proposed above, the bicontinuous micelles were induced by nucleobase interactions but kinetically frozen upon addition of water, which was supported by the irreversible morphology

transition observed. With annealing, the polymer chains became relatively mobile and structural rearrangement was induced, which may result in changes the polymer curvature or polymer interactions and thus led to the formation of thermodynamically favorable onion-like structures. However, further investigation is required to confirm this explanation.

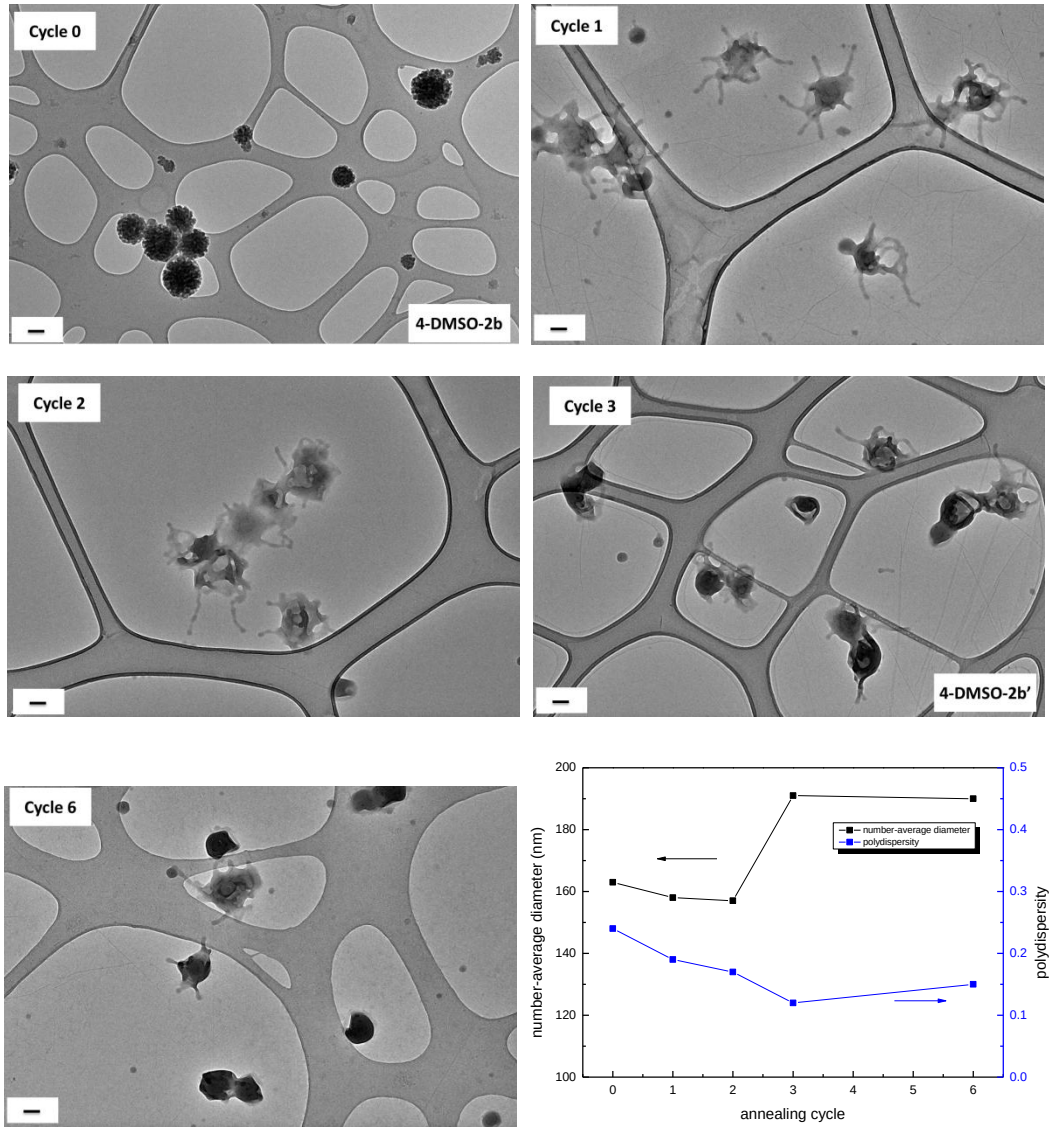

Figure 5.39 Evolution of self-assembly from **4-DMSO-2b** to **4-DMSO-2b'** with annealing cycles characterized by unstained TEM analysis (scale bar = 100 nm) and their number-average diameters and size distributions determined by DLS analysis.

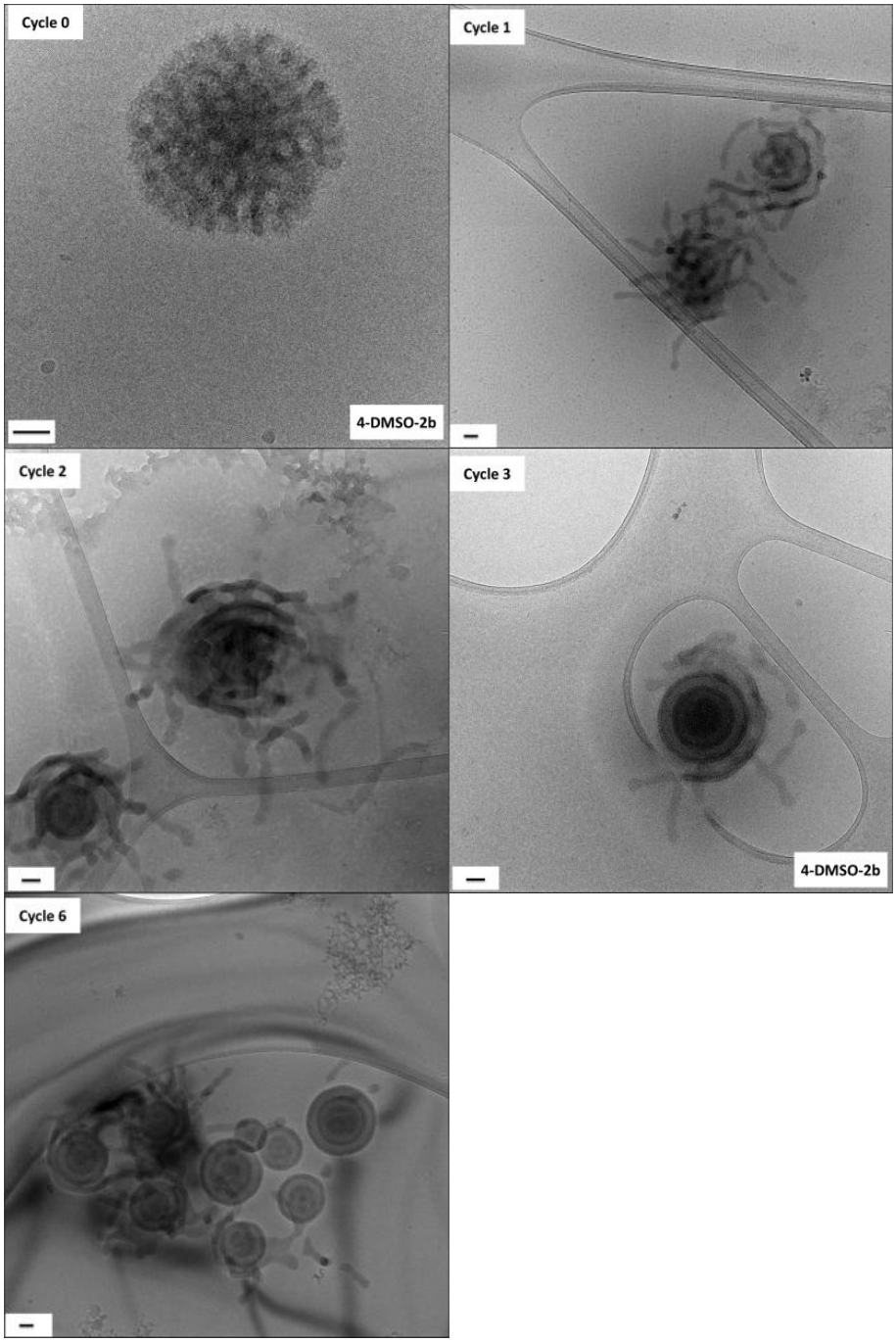

Figure 5.40 Evolution of self-assembly from **4-DMSO-2b** to **4-DMSO-2b'** with annealing cycles characterized by cryo-TEM analysis (scale bar = 50 nm).

5.4 Conclusion

In conclusion, nucleobase-containing block copolymers were successfully synthesized by RAFT polymerizations, in which $POEGMA_{70}$ was used as the hydrophilic block and nucleobase-containing polymers made up the hydrophobic segments. Two types of nucleobase-containing methacrylate monomers with slightly different structures were used as the monomers to prepare the hydrophobic blocks. One type was composed of two ester groups in the structures (AMA and TMA) and the other contained only one ester group in the backbone (AMA2 and TMA2). It was found that polymers synthesized from AMA2 and TMA2 were much more stable in aqueous environments than those made from AMA and TMA.

In addition, self-assemblies were prepared using both direct dissolution and solvent switch method, however better results were obtained from the solvent switch method. Different common solvents, DMF and DMSO, were used when performing the solvent switch method and different morphologies were observed depending on the identity of the common solvent. Spherical micelles and bicontinuous micelles were obtained respectively when DMF and DMSO were used. We proposed the reason for this observation was the difference in polymer curvatures resulting from different polymer solubility in these two common solvents.

Furthermore, this study showed that the type of aggregated formed was directed by the nucleobase interactions rather than the hydrophilic-hydrophobic balance. The presence of adenine-thymine interactions was important for the formation of bicontinuous micelles in this study.

Finally, annealing was demonstrated as a promising way to make better-defined spheres with narrow size distributions or to induce morphology transitions such as a transition from bicontinuous micelles to onion-like structures. These might result

from structural rearrangements induced by annealing, which were aimed at forming thermodynamically favorable systems.

The study in this Chapter not only enriches the preparation of bicontinuous micelles, but provides insight into understanding the properties of nucleobase-containing polymers in water.

5.5 Experimental section

5.5.1 Materials

Oligo(ethylene glycol) methyl ether methacrylate (OEGMA, average M_n = 300) was bought from Aldrich and passed through a column of neutral alumina to remove inhibitor. 2,2-Azo-bis(isobutyronitrile) (AIBN) was purchased from Molekula and recrystallized from methanol. 2-cyano-2-propyldodecyl trithiocarbonate (CPDT) was synthesized according to a previous reference.[58] The synthesis of monomers 2-(2-adenine-9-yl)acetoxyl ethyl methacrylate (AMA) and 2-(2-(thymine-1-yl)acetoxyl) ethyl methacrylate (TMA) is given in chapter 2.[59] The preparation of 3-bromopropyl methacrylate, 3-(adenin-9-yl)propyl methacrylate (AMA2), and 3-(thymin-1-yl)propyl methacrylate (TMA2) is according to previous literature.[57] *N*,*N*-Dimethylformamide (DMF), dimethyl sulfoxide (DMSO), and other solvents were used as received from Fisher. Deuterated solvents were all purchased from Apollo Scientific.

5.5.2 Instrumentation

^{1}H NMR and ^{13}C NMR spectra were recorded on a Bruker DPX-300 or DPX-400 spectrometer with DMSO-d_6 or deuterated chloroform ($CDCl_3$) as the solvent. The chemical shifts of protons were reported relative to tetramethylsilane at δ = 0 ppm when using $CHCl_3$ or solvent residues (DMSO ^{1}H: 2.50 ppm).

Size exclusion chromatography (SEC) was obtained in HPLC grade DMF containing 5 mM NH_4BF_4 at 50 °C, with a flow rate of 1.0 mL per minute, on a set of two PLgel 5 μm Mixed-D columns, plus one guard column. SEC data was analyzed with Cirrus SEC software calibrated using poly(methyl methacrylate)

(PMMA) standards. The SEC was equipped with both refractive index (RI) and UV detectors.

Transmission electron microscopy (TEM) observations were performed on a JEOL 2000FX electron microscopy at an acceleration voltage of 200 kV. All TEM samples were prepared on graphene oxide (GO)-coated carbon grids (Quantifoil R2/2 or lacey carbon) which allows high contrast TEM images to be acquired without staining.[60] Generally, a drop of sample (20 μL) was pipetted onto a grid, blotted immediately and left to air dry.

Cryogenic transimission electron microscopy (cryo-TEM) was performed on a Tecnai G2 12 Twin TEM at an acceleration voltage of 120 kV equipped with a Gatan CCD camera. The temperature of the cryo stage was maintained below -170 °C during imaging. For sample preparation, 5 μL of the sample was deposited onto a lacey carbon grid, blotted immediately and vitrified by plunging into liquid ethane.

Hydrodynamic diameters (D_h) and size distributions of the self-assemblies were determined by dynamic light scattering (DLS). The DLS instrumentation consisted of a Malvern Zetasizer NanoS instrument operating at 25 °C with a 4 mW He-Ne 633-nm laser module. Measurements were made at a detection angle of 173 ° (back scattering), and Malvern Zetasizer 7.03 software was used to analyze the data.

Static light scattering (SLS) measurement was conducted with an ALV CGS3 (λ =632 nm) at 20 °C. The data was collected from 12° up to 30° with an interval of 2° or 30° up to 150° with an interval of 10°, calibrated with filtered toluene and filtered water as backgrounds. The refractive index increment (*dn/dc*) of the polymer self-assembly in water was measured to be 0.13 mL/g.

UV-vis spectroscopy was carried out on a Perkin Elmer Lambda 35 UV/vis spectrometer, equipped with a PTP-1+1 Peltier temperature programmer and stiring system, and a PCB 1500 water system to maintain the desired temperature throughout the experiments. Quartz cuvettes were used for all the experiments.

5.5.3 Polymerization of OEGMA, $POEGMA_{70}$

The typical procedure of RAFT homopolymerization of OEGMA was as follows: OEGMA (x), CPDT (x, 1 eq), and AIBN (x, 0.1 eq) were dissolved in 1,4-dioxane. The mixture was thoroughly degassed *via* 4 freeze-pump-thaw cycles, filled with oxygen free nitrogen and then immersed into an oil bath at 65 °C for 6 hours. The reaction was quenched by putting into a liquid nitrogen bath and exposing to air. The mixture was precipitated in diethyl ether. The yellow polymers were characterized by ^{1}H NMR spectroscopy and DMF SEC (PMMA as standard).

^{1}H NMR (400 MHz, $CDCl_3$, ppm): δ = 4.10 (br, $2H_{backbone}$, $COOCH_2CH_2$), δ = 3.86 – 3.50 (m, $16H_{backbone}$, $COOCH_2CH_2O(CH_2CH_2O)_{3.5}CH_3$), δ = 3.39 – 3.35 (s, $3H_{backbone}$, $COOCH_2CH_2O(CH_2CH_2O)_{3.5}CH_3$), δ = 3.20 (br, $2H_{end\text{-}group}$, $CH_2SC{=}S$), δ = 1.96 – 1.81 (m, $2H_{backbone}$, CH_2CCH_3), δ = 1.51 – 0.60 (m, $18H_{end\text{-}group}$, $SCH_2CH_2(CH_2)_9CH_3$; $3H_{backbone}$, CH_2CCH_3).

5.5.4 Synthesis of block copolymers using $POEGMA_{70}$ as a macro-CTA

The typical procedure as follows: $POEGMA_{70}$ (x, 1 eq), AMA or AMA2(x), TMA or TMA2(x), and AIBN (x, 0.1 eq) were dissolved in DMF or DMSO. The mixture was thoroughly degassed *via* 4 freeze-pump-thaw cycles, filled with oxygen free nitrogen and then immersed into an oil bath at 60 °C. The reaction was quenched by exposing to air and cooling down. The mixture was precipitated in mixture of methanol and diethyl ether (v/v, 1:20) and washed with this mixture several times. The light yellow

polymers were dried in a vacuum oven overnight and characterized by ^{1}H NMR spectroscopy and DMF SEC (PMMA as standards).

^{1}H NMR (400 MHz, DMSO-d_6, ppm) of POEGMA$_{70}$-*b*-(PAMA$_{0.5}$-*co*-PTMA$_{0.5}$)$_{121}$: δ = 11.96 – 11.31 (br, 1H$_{backbone-PTMA}$, N*H*CO), δ = 8.24 – 7.99 (d, 2H$_{backbone-PAMA}$, two NC*H*N of adenine), δ = 7.56 – 7.10 (d, 3H$_{backbone-PTMA+PAMA}$, NC*H*=CCH$_3$ of thymine and N*H*$_2$ of adenine), δ = 5.54 – 4.80 (br, 2H$_{backbone-PAMA}$, NC*H*$_2$COO), δ = 4.60 – 3.82 (m, 10H$_{backbone-PAMA+PTMA}$, OC*H*$_2$C*H*$_2$O of PAMA and OC*H*$_2$C*H*$_2$OCOC*H*$_2$ of PTMA; 2H$_{backbone-POEGMA}$, COOC*H*$_2$CH$_2$), δ = 3.70 – 3.50 (m, 16H$_{backbone}$, COOCH$_2$C*H*$_2$O(C*H*$_2$C*H*$_2$O)$_{3.5}$CH$_3$), δ = 3.28 – 3.23 (s, 3H$_{backbone}$, COOCH$_2$CH$_2$O(CH$_2$CH$_2$O)$_{3.5}$C*H*$_3$), δ = 2.12 – 1.50 (m, 3H$_{backbone-PTMA}$, 2H$_{backbone}$, CH=C(C*H*$_3$) of thymine and C*H*$_2$CCH$_3$ of backbone), δ = 1.50 – 0.60 (m, 18H$_{end-group}$, SCH$_2$CH$_2$(C*H*$_2$)$_9$CH$_3$; 3H$_{backbone}$, CH$_2$CC*H*$_3$).

5.5.5 Self-assembly

Direct dissolution: The polymer was dissolved in water (18.2 MΩ·cm) to give a final concentration of 1 mg/mL and then stirred for 2 days.

Solvent switch: The polymer was dissolved in DMF or DMSO to a concentration of 8 mg/mL or 2 mg/mL and stirred for 2 days. 18.2 MΩ·cm water was added by syringe pump at a rate of 1 mL/h. For samples with a concentration of 8 mg/mL in DMF/DMSO, the final volume ratio between water and organic solvent is 8:1. For samples with a concentration of 2 mg/mL in DMSO, the final volume ratios between water and DMSO are 8:1 or 2:1. The solution was then dialyzed against 18.2 MΩ·cm water, incorporating at least 6 water changes (6 ×1L). The final concentration for the self-assembly was estimated by measuring the final volume.

5.6 References

(1) Khan, A.; Haddleton, D. M.; Hannon, M. J.; Kukulj, D.; Marsh, A. *Macromolecules* **1999**, *32*, 6560.

(2) South, C. R.; Weck, M. *Macromolecules* **2007**, *40*, 1386.

(3) Lo, P. K.; Sleiman, H. F. *J. Am. Chem. Soc.* **2009**, *131*, 4182.

(4) McHale, R.; Patterson, J. P.; Zetterlund, P. B.; O'Reilly, R. K. *Nature Chem.* **2012**, *4*, 491.

(5) Ilhan, F.; Galow, T. H.; Gray, M.; Clavier, G.; Rotello, V. M. *J. Am. Chem. Soc.* **2000**, *122*, 5895.

(6) Spijker, H. J.; Dirks, A. J.; van Hest, J. C. M. *J. Polym. Sci., Part A: Polym. Chem.* **2006**, *44*, 4242.

(7) Bazzi, H. S.; Sleiman, H. F. *Macromolecules* **2002**, *35*, 9617.

(8) Thibault, R. J.; Hotchkiss, P. J.; Gray, M.; Rotello, V. M. *J. Am. Chem. Soc.* **2003**, *125*, 11249.

(9) Sijbesma, R. P.; Beijer, F. H.; Brunsveld, L.; Folmer, B. J. B.; Hirschberg, J. H. K. K.; Lange, R. F. M.; Lowe, J. K. L.; Meijer, E. W. *Science* **1997**, *278*, 1601.

(10) Kang, Y.; Pitto-Barry, A.; Willcock, H.; Quan, W.-D.; Kirby, N.; Sanchez, A. M.; O'Reilly, R. K. *Polym. Chem.* **2015**, *6*, 106.

(11) Thibault, R. J.; Galow, T. H.; Turnberg, E. J.; Gray, M.; Hotchkiss, P. J.; Rotello, V. M. *J. Am. Chem. Soc.* **2002**, *124*, 15249.

(12) Tao, Y.; Yang, Y.; Shi, D.; Chen, M.; Yang, C.; Liu, X. *Polymer* **2012**, *53*, 1551.

(13) Lee, R.-S.; Peng, K.-Y.; Wang, S.-W.; Li, Y.-Z. *Polym. J.* **2014**, *46*, 710.

(14) Kuang, H.; Wu, S.; Xie, Z.; Meng, F.; Jing, X.; Huang, Y.

Biomacromolecules **2012**, *13*, 3004.

(15) Garcia, M.; Beecham, M. P.; Kempe, K.; Haddleton, D. M.; Khan, A.; Marsh, A. *Eur. Polym. J.* **2015**, doi:10.1016/j.eurpolymj.2015.03.014.

(16) Blanazs, A.; Armes, S. P.; Ryan, A. J. *Macromol. Rapid Commun.* **2009**, *30*, 267.

(17) Mai, Y.; Eisenberg, A. *Chem. Soc. Rev.* **2012**, *41*, 5969.

(18) Zhu, J.; Zhang, S.; Zhang, K.; Wang, X.; Mays, J. W.; Wooley, K. L.; Pochan, D. J. *Nat. Commun.* **2013**, *4*.

(19) Li, Z.; Chen, Z.; Cui, H.; Hales, K.; Qi, K.; Wooley, K. L.; Pochan, D. J. *Langmuir* **2005**, *21*, 7533.

(20) Liu, Y.-L.; Chang, Y.-H.; Chen, W.-H. *Macromolecules* **2008**, *41*, 7857.

(21) Pochan, D. J.; Chen, Z.; Cui, H.; Hales, K.; Qi, K.; Wooley, K. L. *Science* **2004**, *306*, 94.

(22) Chen, Z.; Cui, H.; Hales, K.; Li, Z.; Qi, K.; Pochan, D. J.; Wooley, K. L. *J. Am. Chem. Soc.* **2005**, *127*, 8592.

(23) Sommerdijk, N. A. J. M.; Holder, S. J.; Hiorns, R. C.; Jones, R. G.; Nolte, R. J. M. *Macromolecules* **2000**, *33*, 8289.

(24) Cornelissen, J. J. L. M.; Fischer, M.; Sommerdijk, N. A. J. M.; Nolte, R. J. M. *Science* **1998**, *280*, 1427.

(25) Hales, K.; Chen, Z.; Wooley, K. L.; Pochan, D. J. *Nano Lett.* **2008**, *8*, 2023.

(26) McKenzie, B. E.; Nudelman, F.; Bomans, P. H. H.; Holder, S. J.; Sommerdijk, N. A. J. M. *J. Am. Chem. Soc.* **2010**, *132*, 10256.

(27) McKenzie, B. E.; de Visser, J. F.; Friedrich, H.; Wirix, M. J. M.; Bomans, P. H. H.; de With, G.; Holder, S. J.; Sommerdijk, N. A. J. M. *Macromolecules* **2013**, *46*, 9845.

(28) Parry, A. L.; Bomans, P. H. H.; Holder, S. J.; Sommerdijk, N. A. J. M.; Biagini, S. C. G. *Angew. Chem. Int. Ed.* **2008**, *47*, 8859.

(29) McKenzie, B. E.; Friedrich, H.; Wirix, M. J. M.; de Visser, J. F.; Monaghan, O. R.; Bomans, P. H. H.; Nudelman, F.; Holder, S. J.; Sommerdijk, N. A. J. M. *Angew. Chem. Int. Ed.* **2015**, *54*, 2562.

(30) Holder, S. J.; Sommerdijk, N. A. J. M. *Polym. Chem.* **2011**, *2*, 1018.

(31) Holder, S. J.; Woodward, G.; McKenzie, B.; Sommerdijk, N. A. J. M. *RSC Adv.* **2014**, *4*, 26354.

(32) Lutz, J.-F. *J. Polym. Sci., Part A: Polym. Chem.* **2008**, *46*, 3459.

(33) Lutz, J.-F.; Akdemir, Ö.; Hoth, A. *J. Am. Chem. Soc.* **2006**, *128*, 13046.

(34) Han, S.; Hagiwara, M.; Ishizone, T. *Macromolecules* **2003**, *36*, 8312.

(35) Cheng; Zhu; Kang, E. T.; Neoh, K. G. *Langmuir* **2005**, *21*, 7180.

(36) Liu, Y.; Li, M.; Wang, D.; Yao, J.; Shen, J.; Liu, W.; Feng, S.; Tao, L.; Davis, T. P. *Aust. J. Chem.* **2011**, *64*, 1602.

(37) Halperin, A. *Macromolecules* **1990**, *23*, 2724.

(38) Halperin, A.; Tirrell, M.; Lodge, T. P. *Adv. Polym. Sci.* **1992**, *100*, 31.

(39) Zhang, L. F.; Eisenberg, A. *Polym. Adv. Technol.* **1998**, *9*, 677.

(40) Gao, Z.; Varshney, S. K.; Wong, S.; Eisenberg, A. *Macromolecules* **1994**, *27*, 7923.

(41) Lim Soo, P.; Eisenberg, A. *J. Polym. Sci., Part B: Polym. Phys.* **2004**, *42*, 923.

(42) Desbaumes, L.; Eisenberg, A. *Langmuir* **1998**, *15*, 36.

(43) Albert, J. N. L.; Epps Iii, T. H. *Mater. Today* **2010**, *13*, 24.

(44) Darling, S. B. *Prog. Polym. Sci.* **2007**, *32*, 1152.

(45) Mather, B. D.; Baker, M. B.; Beyer, F. L.; Berg, M. A. G.; Green, M. D.;

Long, T. E. *Macromolecules* **2007**, *40*, 6834.

(46) Douglas, S. M.; Dietz, H.; Liedl, T.; Hogberg, B.; Graf, F.; Shih, W. M. *Nature* **2009**, *459*, 414.

(47) Liu, D.; Park, S. H.; Reif, J. H.; LaBean, T. H. *Proc. Natl. Acad. Sci. U. S. A.* **2004**, *101*, 717.

(48) Storhoff, J. J.; Mirkin, C. A. *Chem. Rev.* **1999**, *99*, 1849.

(49) Schmuck, C.; Wienand, W. *J. Am. Chem. Soc.* **2002**, *125*, 452.

(50) Discher, D. E.; Ahmed, F. *Annu. Rev. Biomed. Eng.* **2006**, *8*, 323.

(51) Discher, D. E.; Eisenberg, A. *Science* **2002**, *297*, 967.

(52) Yu, Y.; Zhang, L.; Eisenberg, A. *Macromolecules* **1998**, *31*, 1144.

(53) Vangeyte, P.; Gautier, S.; Jérôme, R. *Colloids and Surfaces A: Physicochem. Eng. Aspects* **2004**, *242*, 203.

(54) Patterson, J. P.; Robin, M. P.; Chassenieux, C.; Colombani, O.; O'Reilly, R. K. *Chem. Soc. Rev.* **2014**, *43*, 2412.

(55) Cotanda, P.; Wright, D. B.; Tyler, M.; O'Reilly, R. K. *J. Polym. Sci., Part A: Polym. Chem.* **2013**, *51*, 3333.

(56) Truong, N. P.; Jia, Z.; Burges, M.; McMillan, N. A. J.; Monteiro, M. J. *Biomacromolecules* **2011**, *12*, 1876.

(57) Spijker, H. J.; Dirks, A. J.; van Hest, J. C. M. *Polymer* **2005**, *46*, 8528.

(58) Chong, Y. K.; Moad, G.; Rizzardo, E.; Thang, S. H. *Macromolecules* **2007**, *40*, 4446.

(59) Kang, Y.; Lu, A.; Ellington, A.; Jewett, M. C.; O'Reilly, R. K. *ACS Macro Lett.* **2013**, *2*, 581.

(60) Patterson, J. P.; Sanchez, A. M.; Petzetakis, N.; Smart, T. P.; Epps III, T. H.; Portman, I.; Wilson, N. R.; O'Reilly, R. K. *Soft Matter* **2012**, *8*, 3322.

Chapter 6. Conclusions and future work

6.1 Conclusions

In conclusion, the synthesis of nucleobase-containing polymers has been explored using RAFT polymerization techniques and the self-assembly behavior of nucleobase polymers has been investigated in both organic solvent and aqueous solution.

In Chapter 2, it was shown that the synthesis of nucleobase-containing polymers could be achieved by RAFT polymerization with good control in terms of molecular weight and molecular weight distributions. Moreover, nucleobase interactions were present in less polar solvent, $CHCl_3$, but absent in DMF, which affected the resultant copolymer composition when an adenine-containing monomer and thymine-containing monomer were copolymerized. It was found that in $CHCl_3$ a modest alternating polymer tended to form, while in DMF a statistical copolymer was most likely obtained.

In Chapter 3, RAFT dispersion polymerizations were utilized to prepare adenine-containing polymers and adenine/thymine containing copolymers and simultaneously provide their corresponding nanostructures. The identity of the polymerization solvent played a key role in the polymerization kinetics and resultant self-assembly morphologies. When $CHCl_3$ was used as the polymerization solvent, only complex spheres were observed with increasing the equivalents of monomer to macro-CTA. In comparison, in 1,4-dioxane, a range of structures including spheres, cylinders, lamella, and knot-like structures were observed. The different observations resulted from the slight difference of polymer solubility and nucleobase interactions in these two solvents.

In Chapter 4, RAFT dispersion polymerization was also applied to polymerize thymine-containing monomer. A variety of polymerization parameters, including

polymerization solvent, the amount of monomer, the length of macro-CTA and the presence of adenine-containing mediator were investigated. It was found that the resultant morphologies were well-defined although the resulting polymers possessed broad molecular weight distributions.

Chapter 5 investigated the self-assembly of nucleobase-containing block copolymers in aqueous solution. The identity of common solvent played a key role in the resultant morphologies when self-assemblies were prepared by a solvent switch method. Only spheres were observed when DMF was used as the common solvent, while bicontinuous micelles could be formed when using DMSO, which resulted from the observation that DMSO was a better solvent for nucleobase-polymers than DMF and thus led to different polymer curvatures in these two solvents. Moreover, a morphology transition from bicontinuous micelles to onion-like vesicles was observed, which was induced by annealing. Finally, the presence of nucleobase interactions affected the self-assembly behavior of nucleobase-containing polymers, where it was found that the presence of adenine-thymine interactions was critical for the formation of bicontinuous nanospheres in our study.

6.2 Future work

In this thesis, we have established procedures for the synthesis and self-assembly of nucleobase-containing polymers. Further work to this research includes full characterization of the complex morphologies (*e.g.* bicontinuous micelles and onion-like structures in Chapter 5) using more advanced techniques, such as cryo-electron tomography and exit wave reconstruction, and to gain greater scientific understanding of the formation of the structures and effect of nucleobase pairs on the resultant morphologies.

As a range of nanostructures can be obtained from the nucleobase-containing diblock copolymers, these nanostructures after end group removal could be adapted to the well-established templating/segregation approach and used as a template or segregation environment to induce the polymerization of complementary monomers. As the size, morphology and internal structure of the nanostructures are controlled and tunable, it may be possible to tune the molecular weight and type of the resultant daughter polymer.

The solubility of nucleobase-containing methacrylate polymers is very limited. Further study could focus on other types of nucleobase-containing polymers, which may possess better solubility or lower T_g values. For example, nucleobase-containing acrylate polymers are expected to have low T_g values, which will make the polymers more flexible. Moreover, by incorporating soluble units into the structure (*e.g.* a short PEG unit) or synthesizing acrylamide monomers, nucleobase-containing polymers are expected to have better solubility particularly in water. Furthermore, by incorporating charged units into the backbone, nucleobase polymers are expected to exhibit additional properties.

It is also of interest to study the binding between nucleobase-containing synthetic polymers and DNA, for which the preparation of water-soluble nucelobase-containing polymers will be necessary. Such a study will help to elucidate the differences between synthetic nucleobase polymers and DNA and provide opportunity to prepare novel DNA-polymer hybrid nanostructures.

Based on these findings and improvements, in future, we hope to achieve DNA-like synthetic nucleobase-containing polymers, which possess specific sequences and can code information in their structures. We propose that such materials could mimic the templating, replication, transcription and precise self-assembly behavior of DNA or RNA, yet would be synthetically easier to prepare, modify, and scale-up as well as be more robust under non-physiological environments. These synthetic nucleobase polymers are expected to have potential applications in biological chemistry and biomedicine, as a probe, sensor or delivery vehicle, etc.